Methods in Molecular Biology 1376

Springer Protocols

Mark G. Waugh *Editor*

Lipid Signaling Protocols

Second Edition

Humana Press

METHODS IN MOLECULAR BIOLOGY

Series Editor
John M. Walker
School of Life and Medical Sciences
University of Hertfordshire
Hatfield, Hertfordshire, AL10 9AB, UK

For further volumes:
http://www.springer.com/series/7651

Lipid Signaling Protocols

Edited by

Mark G. Waugh

University College London, School of Life and Medical Sciences,
London, United Kingdom

Humana Press

Editor
Mark G. Waugh
University College London
School of Life and Medical Sciences
London, United Kingdom

ISSN 1064-3745 ISSN 1940-6029 (electronic)
Methods in Molecular Biology
ISBN 978-1-4939-3169-9 ISBN 978-1-4939-3170-5 (eBook)
DOI 10.1007/978-1-4939-3170-5

Library of Congress Control Number: 2015947784

Springer New York Heidelberg Dordrecht London

Printed on acid-free paper

Humana Press is a brand of Springer
Springer Science+Business Media LLC New York is part of Springer Science+Business Media (www.springer.com)

Preface

Lipids are of central importance in the regulation of many aspects of cell function including receptor signaling, vesicle trafficking, and motility. There are a very large number of therapeutically important G-protein-coupled receptors and receptor tyrosine kinases that activate lipid signaling pathways and a range of diseases including some cancers and neurodegenerative conditions that are associated with defective intracellular lipid metabolism. Furthermore, as our knowledge of the molecular basis of human genetic disease expands so too does the long list of rare but often devastating inherited diseases that arise from mutations in genes encoding enzymes involved in lipid signaling. Therefore, there is a requirement for sensitive, reliable, and quantitative laboratory methods to investigate this medically important area of biochemistry.

However, mainly because of their characteristic insolubility in aqueous buffers, lipids have collectively proven to be more difficult to study than other biomolecules such as proteins and nucleic acids. There are very few off-the-shelf commercially available kits to purify and quantify signaling lipids, such as for example the seven different phosphoinositide species, and compared to other bioscience disciplines there has then been less progress generally in the development of easy to use, inexpensive, and highly selective techniques to measure and detect these molecules in cultured cells. Nevertheless, despite these various hurdles, progress is being made in laboratories across the globe to develop robust protocols to study lipid signaling at the cellular level, and many of these cutting-edge techniques are described in detail in this volume.

In this second edition of Lipid Signaling, tried and tested methods are described to measure the synthesis of lipids such as the phosphoinositides, ceramides, and sphingomyelin, and to molecularly characterize the various kinases and phosphatases that regulate their levels in cells. As lipid signaling occurs within membranes and is known to be sensitive to alterations in membrane environment, there are also all several chapters detailing strategies to isolate, characterize and image receptor-initiated signaling cascades in detergent-resistant membrane domains and cholesterol-rich lipid rafts. These detailed experimental protocols are complemented by review chapters that highlight the technical considerations, challenges, and potential pitfalls associated with using these laboratory-based approaches.

As editor I have been struck by the enthusiasm of the lipid research community to contribute to this book. This completely rewritten second edition of Lipid Signaling has truly been an international project. The finished product represents the combined work of 47 authors from 4 continents and I am very grateful to all of them for their efforts. Finally I would like to thank Prof John Walker, *Methods in Molecular Biology* series editor at Springer, for his editorial guidance during the preparation of this book.

London, UK ***Mark G. Waugh***

Contents

Contributors

Massimo Aureli • *Department of Medical Biotechnology and Translational Medicine, University of Milan, Segrate, Milano, Italy*

Ricarda A. Busse • *Department of Neurobiology, Max-Planck-Institute for Biophysical Chemistry, Göttingen, Germany*

Vinicio Carloni • *Department of Experimental and Clinical Medicine, Center for Research, Transfer and High Education, DENOthe, University of Florence, Florence, Italy*

Wonhwa Cho • *Department of Chemistry, University of Illinois at Chicago, Chicago, IL, USA*

Timothy A. Couttas • *Prince of Wales Clinical School, Faculty of Medicine, University of New South Wales, Sydney, NSW, Australia*

Mindy I. Davis • *Division of Preclinical Innovation, National Center for Advancing Translational Sciences, National Institutes of Health, Rockville, MD, USA*

Anthony S. Don • *Prince of Wales Clinical School, Faculty of Medicine, University of New South Wales, Sydney, NSW, Australia*

Victor Faundez • *Department of Cell Biology, Emory University, Atlanta, GA, USA; Center for Social Translational Neuroscience, Emory University, Atlanta, GA, USA*

Joachim Füllekrug • *Molecular Cell Biology Laboratory, Internal Medicine IV, University of Heidelberg, Heidelberg, Germany*

Matthew C. Gage • *Division of Medicine, Centre for Clinical Pharmacology, University College of London, London, UK*

Christina Anja Gewinner • *Translational Innovation Group, UCL-Eisai Collaborative, University College London, London, UK*

Avanti Gokhale • *Department of Cell Biology, Emory University, Atlanta, GA, USA*

Sara Grassi • *Department of Medical Biotechnology and Translational Medicine, University of Milan, Segrate, Milano, Italy*

Yusi Hu • *Department of Chemistry, University of Illinois at Chicago, Chicago, IL, USA*

Laura Ren Huey Ip • *Research Department of Cancer Biology, UCL Cancer Institute, University College London, London, UK*

Yvon Jaillais • *Laboratoire de Reproduction et Développement des Plantes, CNRS, INRA, ENS Lyon, UCBL, Université de Lyon, Lyon Cedex, France*

Hyunjin Kim • *Department of Chemistry, University of Illinois at Chicago, Chicago, IL, USA*

John G. Koland • *Department of Pharmacology, Carver College of Medicine, The University of Iowa, Iowa City, IA, USA*

Kimberly J. Krager • *Department of Pharmacology, Carver College of Medicine, The University of Iowa, Iowa City, IA, USA; Division of Radiation Health, College of Pharmacy, University of Arkansas for Medical Sciences, Little Rock, AR, USA*

Roswitha Krick • *Institute of Cellular Biochemistry, University Medicine, Georg-August University, Göttingen, Germany*
Karin Kühnel • *Department of Neurobiology, Max-Planck-Institute for Biophysical Chemistry, Göttingen, Germany*
Abasha Lewis • *Cellular Pathobiology Section, IRP, DHHS, NIDA, NIH, Baltimore, MD, USA*
Xin Ying Lim • *Prince of Wales Clinical School, Faculty of Medicine, University of New South Wales, Sydney, NSW, Australia*
Russell Pickford • *Bioanalytical Mass Spectrometry Facility, University of New South Wales, Sydney, NSW, Australia*
Inés Pineda-Torra • *Division of Medicine, Centre for Clinical Pharmacology, University College of London, London, UK*
Matthieu Pierre Platre • *Laboratoire de Reproduction et Développement des Plantes, CNRS, INRA, ENS Lyon, UCBL, Université de Lyon, Lyon Cedex, France*
Margarete Poppelreuther • *Molecular Cell Biology Laboratory Internal Medicine IV, University of Heidelberg, Heidelberg, Germany*
Benoit Pourcet • *Division of Medicine, Centre for Clinical Pharmacology, University College of London, London, UK; UMR INSERM 1011, Institut Pasteur de Lille, Université Lille Nord de France, Université Lille 2, Lille Cedex, France*
Alessandro Prinetti • *Department of Medical Biotechnology and Translational Medicine, University of Milan, Segrate, Milano, Italy*
Lucia E. Rameh • *Department of Medicine, Boston University School of Medicine, Boston, MA, USA*
Neale D. Ridgway • *Department of Pediatrics, Dalhousie University, Halifax, NS, Canada; Department of Biochemistry and Molecular Biology, Dalhousie University, Halifax, NS, Canada*
Krista Rombouts • *Division of Medicine, Institute for Liver and Digestive Health, Royal Free Hospital, University College London (UCL), London, UK*
Pearl V. Ryder • *Department of Cell Biology, Emory University, Atlanta, GA, USA*
Mitul Sarkar • *Department of Pharmacology, Carver College of Medicine, The University of Iowa, Iowa City, IA, USA*
Deborah A. Sarkes • *U.S. Army Research Laboratory, Sensors and Electron Devices Directorate, Adelphi, MD, USA*
Atsuo T. Sasaki • *Department of Internal Medicine, Division of Hematology Oncology UC Cancer Institute, University of Cincinnati, OH, USA; UC Neuroscience Institute, Department of Neurosurgery, Brain Tumor Center, UC Neuroscience Institute, College of Medicine, University of Cincinnati, Cincinnati, OH, USA*
Andreea Scacioc • *Department of Neurobiology, Max-Planck-Institute for Biophysical Chemistry, Göttingen, Germany*
Amanda M. Schalk • *Department of Neurobiology, Max-Planck-Institute for Biophysical Chemistry, Göttingen, Germany; Department of Biochemistry and Molecular Genetics, University of Illinois at Chicago, Chicago, IL, USA*
Anton Simeonov • *Division of Preclinical Innovation, National Center for Advancing Translational Sciences, National Institutes of Health, Rockville, MD, USA*
Sandro Sonnino • *Department of Medical Biotechnology and Translational Medicine, University of Milan, Segrate, Milano, Italy*

Robert V. Stahelin • *Department of Chemistry and Biochemistry, University of Notre Dame, Notre Dame, IN, USA; Department of Biochemistry and Molecular Biology, Indiana University School of Medicine-South Bend, South Bend, IN, USA*

Tsung-Ping Su • *Cellular Pathobiology Section, IRP, DHHS, NIDA, NIH, Baltimore, MD, USA*

Kenichi G.N. Suzuki • *Institute for Integrated Cell-Material Sciences (WPI-iCeMS), Institute for Frontier Medical Sciences, Kyoto University, Kyoto, Japan; Institute for Stem Cell Biology and Regenerative Medicine (inStem), National Centre for Biological Sciences (NCBS), Bangalore, India*

Michael Thumm • *Institute of Cellular Biochemistry, University Medicine, Georg-August University, Göttingen, Germany*

Shang-Yi Tsai • *Cellular Pathobiology Section, IRP, DHHS, NIDA, NIH, Baltimore, MD, USA*

Kathryn Del Vecchio • *Department of Chemistry and Biochemistry, University of Notre Dame, Notre Dame, IN, USA*

Mark G. Waugh • *University College London, School of Life and Medical Sciences, London, United Kingdom*

Stephanie A. Zlatic • *Department of Cell Biology, Emory University, Atlanta, GA, USA*

Chapter 1

Method for Assaying the Lipid Kinase Phosphatidylinositol-5-phosphate 4-kinase α in Quantitative High-Throughput Screening (qHTS) Bioluminescent Format

Mindy I. Davis, Atsuo T. Sasaki, and Anton Simeonov

Abstract

Lipid kinases are important regulators of a variety of cellular processes and their dysregulation causes diseases such as cancer and metabolic diseases. Distinct lipid kinases regulate the seven different phosphorylated forms of phosphatidylinositol (PtdIns). Some lipid kinases utilize long-chain lipid substrates that have limited solubility in aqueous solutions, which can lead to difficulties in developing a robust and miniaturizable biochemical assay. The ability to prepare the lipid substrate and develop assays to identify modulators of lipid kinases is important and is the focus of this methods chapter. Herein, we describe a method to prepare a DMSO-based lipid mixture that enables the 1536-well screening of the lipid kinase phosphatidylinositol-5-phosphate 4-kinase α (PI5P4Kα) utilizing the D-myo-di16-PtIns(5)P substrate in quantitative high-throughput screening (qHTS) format using the ADP-Glo™ technology to couple the production of ADP to a bioluminescent readout.

Key words Quantitative high-throughput screening (qHTS), PI5P4Kα, Kinase, Lipid, Bioluminescence, Luciferase, ADP-Glo, Phosphorylation

1 Introduction

Lipids are important signaling molecules that when dysregulated can contribute to human disease [1]. There are seven derivatives of phosphatidyl inositol lipids that are formed by phosphorylation at the 3-, 4-, and/or 5-positions of the inositol ring. Phosphatidylinositol-5-phosphate 4-kinases (PI5P4Ks or type II PIPKs) are lipid kinases that phosphorylate phosphatidylinositol 5-phosphate (PI-5-P), which is present in cells at very low levels [2], on the 4′ position to produce PI-4,5-P_2 as shown in Fig. 1. There are three isoforms α, β, and γ encoded by the genes *PIP4K2A*, *B* and *C*. An alternate route to PI-4,5-P_2 is by phosphorylation of PI-4-P on the 5′ position by phosphatidylinositol-4-phosphate 5-kinases (PI4P5Ks or type I PIPKs), which also have three isoforms, encoded by *PIP5K1A*, *B*, and *C*. The type I and type II kinases have different cellular

Mark G. Waugh (ed.), *Lipid Signaling Protocols*, Methods in Molecular Biology, vol. 1376,
DOI 10.1007/978-1-4939-3170-5_1,

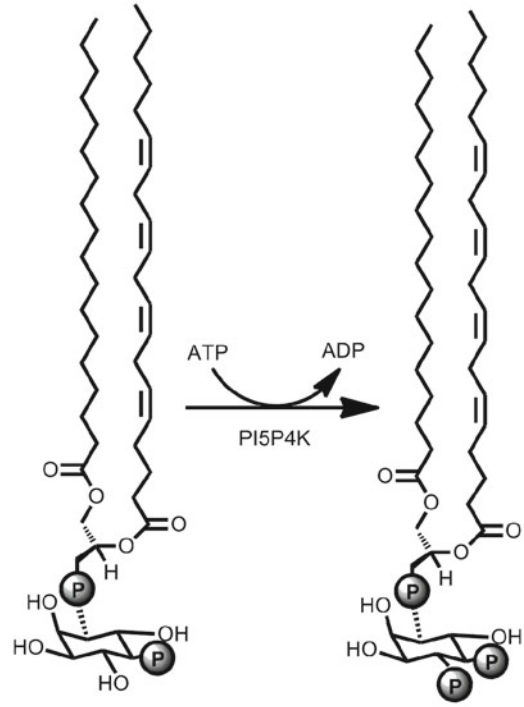

Fig. 1 Schematic representation of the phosphorylation of D-myo-di16-PtIns(5)P by the PI5P4Ks. Reprinted from ref. [13] with permission from PLoS ONE

locations with the type I enzymes located at the plasma membrane and type the II enzymes localized at internal membranes. Recently, the PI5P4K α and β forms, which are upregulated in some breast cancer lines (e.g., BT474), were shown to be important for cell growth in p53-deficient breast cancer cell lines and knockdown lead to increased levels of reaction oxygen species (ROS) and induced cellular senescence [3]. Also it has been shown that the α isoform is highly expressed in acute myeloid leukemia (AML) cell lines and depletion of the α isoform by shRNA decreases cell proliferation, survival, and tumorigenic activity [4].

The knockdown studies described above suggest that developing small molecule inhibitors of the PI5P4K family could be a new avenue for drug development for p53-deficient cancers with upregulated PI5P4K levels. There are a variety of assay formats that have been described previously to investigate compound modulation of kinase enzyme activity, such as HTRF KinEase (Cisbio), Transcreener FP ADP Assay (Bellbrooks), ADP-Glo™ (Promega), and transfer of γ-phosphate from radiolabeled ATP to product [5–8]. To develop a lipid kinase assay, an important consideration is the choice and preparation of the lipid substrate. Lipids are often prepared as liposomes [9], and a report utilizing the D-myo-di16-PtIns(5)P substrate, which has limited aqueous solubility, relied on

commercial lipid vesicle preparation to generate 384-well assays for PI5P4K α and β that was used to screen a kinase-directed library [10]. A recent paper described a time-resolved fluorescence resonance energy transfer (TR-FRET) method for assessing PI5P4Kβ activity in 384-well format utilizing the D-myo-di8-PtIns(5)P substrate, which has a shorter chain length and is soluble in assay buffer [11]. Herein, we describe a DMSO-based method with bioluminescence readout to assay PI5P4Kα activity with D-myo-di16-PtIns(5)P substrate in 1536-well format. The DMSO-based method allows the lipid mixture to be prepared directly at the bench and enabled miniaturization to the 1536-well level for a substrate with limited aqueous solubility. The assay described herein is a coupled assay in which the product ADP from the PI5P4Kα enzyme reaction is coupled through a two-step process to luminescence produced by firefly luciferase (FLuc) (ADP-Glo™), a method that has been utilized for many types of kinases [5, 12].

2 Materials

Unless otherwise noted, prepare reagents using ultrapure water and store reagents at room-temperature.

2.1 D-myo-di16-PtIns(5)P/DPPS Lipid Preparation

1. 1,2-dipalmitoyl-*sn*-glycero-3-phosphoserine (DPPS; Echelon Biosciences) was suspended in DMSO (1 mL DMSO per 3 mg DPPS), sonicated for 1 min and mixed by vortexing for 30 s, forming a solution (*see* **Note 1**).
2. D-myo-phosphatidylinositol 5-phosphate diC16 (D-myo-di16-PtIns(5)P; Echelon Biosciences) was suspended in DMSO, and alternately sonicated and mixed by vortexing for several minutes (333 μL DMSO per 1 mg D-myo-di16-PtIns(5)P). At this stage there is still particulate matter visible.
3. 1000 μL of DPPS was added to 500 μL of D-myo-di16-PtIns(5)P making a 2:1 mixture. 2250 μL of DMSO was added, and the resulting lipid mixture was alternately sonicated and mixed by vortexing for several minutes. The result is a suspension with no visible particulate matter.

2.2 PI5P4Kα qHTS Assay

1. PI5P4Kα/D-myo-di16-PtIns(5)P reagent: 10 nM PI5P4Kα, 31 μM D-myo-di16-PtIns(5)P, 79 μM DPPS, 40 mM Hepes pH 7.4, 0.25 mM EGTA, 0.1 % CHAPS. Protein was expressed and purified as described in ref. [13]. To make this reagent, 500 μL of lipid mix described in Subheading 2.1 was added to 6130 μL of buffer (43 mM Hepes pH 7.4, 0.27 mM EGTA, 0.108 % CHAPS), and the mixture was sonicated and mixed by vortexing. PI5P4Kα (37 μL) was then added and the solution was gently mixed by pipetting. This reagent was stored on wet ice.

2. No PI5P4Kα buffer: 31 μM D-myo-di16-PtIns(5)P, 79 μM DPPS, 40 mM Hepes pH 7.4, 0.25 mM EGTA, 0.1 % CHAPS. Assembled as described in **step 1** but with 50 mM Hepes pH 7.4, 0.1 % CHAPS buffer replacing the enzyme.
3. No D-myo-di16-PtIns(5)P buffer: 10 nM PI5P4Kα, 40 mM Hepes pH 7.4, 0.25 mM EGTA, 0.1 % CHAPS. Assembled as described in **step 1** but with DMSO replacing the lipid mix (*see* **Note 2**).
4. ATP buffer: 15 μM ATP, 20 mM Hepes 7.4, 60 mM $MgCl_2$, 0.1 % CHAPS (*see* **Notes 3–4**).
5. Thaw ADP-Glo™ Reagent (Promega) at room temperature per manufacturer's protocol (*see* **Note 5**).
6. Thaw Kinase Detection Reagent (Promega) at room temperature per manufacturer's protocol and transfer kinase detection buffer to powdered kinase detection reagent making sure the buffer is fully dissolved. If precipitate is present in the buffer, the supernatant can be removed and the precipitate discarded or the solution can be warmed with swirling to 37 °C per the manufacturer's protocol prior to addition to the powdered kinase detection reagent.
7. Assay Plates: 1536-well white solid bottom medium-binding high-base plates from Greiner were used.
8. The assay reagents were dispensed using a BioRAPTR (Beckman Coulter).
9. The Lopac^{1280} (Sigma-Aldrich) library was screened and the control compound was Tyrphostin AG82 (Cayman Chemical Company). Compounds were transferred to the assay plate with a pintool (Kalypsys Systems) (*see* **Note 6**).
10. The assay plate was read on a ViewLux (PerkinElmer) plate reader.

3 Methods

Carry out all procedures at room temperature unless otherwise specified.

3.1 PI5P4Kα qHTS Assay

1. Dispense 2 μL of PI5P4Kα/D-myo-di16-PtIns(5)P enzyme reagent into columns 1, 2, 5–48 of the assay plate with a BioRAPTR.
2. Dispense 2 μL of no D-myo-di16-PtIns(5)P buffer into column 3 as a control for assessment of enzyme uncoupling.
3. Dispense 2 μL of no PI5P4Kα buffer control into column 4 as the control for normalizing.
4. Centrifuge for 10 s at 300 × *g*.

5. Transfer 23 nL of each library compound dissolved in DMSO from a 1536-well clear compound plate arrayed in columns 5–48 and 23 nL of control compounds (DMSO in column 1, 3–4, and Tyrphostin AG82 [13] in duplicate 16-pt dose response in column 2) from a 1536-well compound plate arrayed in columns 1–4 into the assay plate using the pintool (*see* **Note 7**).
6. Incubate the assay plate for 15 min to allow for compound binding.
7. Initiate the enzyme reaction by dispensing 1 μL of ATP buffer to all wells of the assay plate using the BioRAPTR.
8. Cover the plate with a solid gasketed lid that prevents both evaporation and exposure to light.
9. Incubate at room temperature for 1 h.
10. Dispense 2 μL of ADP-Glo™ reagent (*see* **Note 8**).
11. Incubate the lidded plate for 40 min.
12. Dispense 4 μL of Kinase Detection reagent.
13. Incubate the lidded plate for 30 min.
14. Read the luminescence signal (20 s exposure) with a ViewLux.
15. Normalize the data using the DMSO-treated control columns with (maximum signal; column 1) and without (minimum signal, column 4) enzyme. Figure 2 shows the assay statistics for a six-plate qHTS library screen of the Lopac^{1280} library [13] (*see* **Notes 9–11**).

4 Notes

1. Making the lipid reagents in glass vials will minimize sticking that can occur to plastic containers. The DPPS/D-myo-di16-PtIns(5)P lipid mixture can be made ahead of time and stored in glass vials at −20 °C until use. The mixture is stable to at least six freeze–thaw cycles. The lipid mixture can be thawed at room temperature and sonicated prior to use. For the dispensing on the BioRAPTR, a glass vial was placed inside the plastic container and the samples were placed in the glass vial. D-MYO-DI16-PtIns(5)P is minimally soluble in DMSO. Therefore it is recommended to add the DPPS DMSO solution to the D-MYO-DI16-PtIns(5)P followed by sonication to assist the formation of the uniform suspension.
2. Contaminating ATPases in the enzyme preparation can confound the ADP-Glo™ data on your lipid kinase. Testing whether the protein prep has ATPase activity in the absence of substrate can indicate a contaminating ATPase or, particularly in the case of a tyrosine kinase, some autophosphorylation activity.

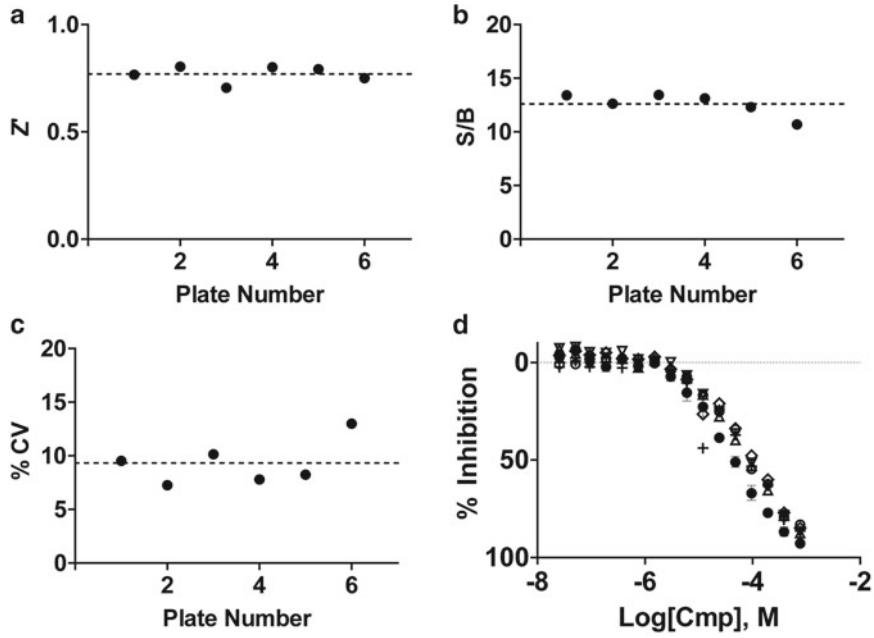

Fig. 2 Performance of the PI5P4Kα Lopac[1280]qHTS screen in 1536-well plates. (**a**) Z' factor, (**b**) signal/background, and (**c**) % column variance as a function of assay plate. (**d**) IC_{50} data for AG-82 control compound from each of six plates displayed with six symbols. Reprinted from ref. [13] with permission from PLoS ONE

3. The Ultra Pure ATP that is included in the ATP-Glo™ kit was used here. It is important to use a source of ATP that contains very low levels of ADP which will interfere with the assay.
4. The assay conditions have ATP present at the K_m which provides maximum sensitivity to identifying all three types of inhibitors (competitive, noncompetitive, and uncompetitive) [14]. This assay format can be modified to determine the mechanism of inhibition with respect to ATP by running the assay at various ATP concentrations spanning from 0.25 to 10× K_m of ATP [13]. Then, by plotting the [ATP]/K_m vs. IC_{50}, the slope of the line will indicate the mechanism of action with respect to ATP: a positive slope indicates competitive, a negative slope indicates noncompetitive, and no slope indicates uncompetitive mode of inhibition.
5. The ADP-Glo™ kit can be used per the manufacturer's protocol for concentrations of ATP up to 1 mM, and it is able to detect picomolar levels of ADP. The final Mg^{2+} concentration in the reaction must be between 0.5 and 50 mM. The kit is able to tolerate up to 5 % DMSO per the manufacturer's protocol and that is the concentration of DMSO utilized in this assay. These ADP-Glo™ reagents can be refrozen and stored at −20 °C for subsequent use. Any particulates present

upon thawing should be removed prior to dispensing on the BioRAPTR.

6. Additional details for preparing the compound plates for qHTS is described in ref. [15].
7. The tolerability of the enzyme assay to DMSO should be tested if the compounds are to be added as a DMSO solution. Here the final reaction DMSO concentration is 5 % and there is no effect of DMSO until >15 % [13].
8. In order to have the total volume of the final coupled reaction fit within the confines of the 1536-well plate (12 μL total volume to completely fill the well; <10.5 μL would be a recommended total volume) while still allowing the initial enzyme reaction to be in a volume amenable to pin transfer of compounds, the volume ratio of the ADP-Glo™ reagents was decreased (3 kinase reaction : 2 ADP-Glo™: 4 Kinase Detection) compared to the manufacturer's protocol, which recommends 1 kinase reaction: 1 ADP-Glo™: 2 Kinase Detection. The linearity of the kit was tested by using admixtures of ATP and ADP that total 5 μM and assessing the linearity of the kit at the decreased ratio of ADP-Glo™ reagents. There was no decrease in assay performance under the conditions described herein upon reduction of the ratio of reagents but this would need to be validated for alternate assay designs. Additionally, a standard curve can be made by testing the various % conversion equivalents of the ATP/ADP mixtures to determine what % conversion the assay is being run at. For the PI5P4Kα under the conditions described herein, the assay is at 20 % conversion. The enzyme concentration should be optimized for each new lot of PI5P4Kα.
9. The signal to background achieved with the DMSO-based method and the lipid vesicle method described in ref. [10] were very similar [13].
10. The plate stats for a 6-plate screen executed against the Lopac^{1280} compound library had $Z' = 0.77$, CV = 9.3 % and S/B = 12.6 [13]. The MSR of the IC_{50} for Tyrphostin AG-82 was 1.29. Data were deposited in PubChem AID 652105, 652103, 743286, and 743285 (detection counterassay).
11. Set up mock reactions without PI5P4Kα kinase but with all other assay components present, including a mixture of ADP and ATP to mimic the kinase reaction results (i.e., 2 μM ADP and 3 μM ATP to mimic 20 % conversion for a 5 μM ATP reaction), to test whether the test compounds interfere with any aspects of the detection system. The ADP-Glo™ kit includes multiple enzyme components, one of which, firefly luciferase, has been shown previously to be subject to modulation by small molecules [16, 17].

Acknowledgement

This work was supported by the Molecular Libraries Common Fund Program of the National Institutes of Health. The content of this publication does not necessarily reflect the views of policies of the Department of Health and Human Services, nor does mention of trade names, commercial products, or organizations imply endorsement by the U.S. Government.

References

1. Wymann MP, Schneiter R (2008) Lipid signalling in disease. Nat Rev Mol Cell Biol 9(2):162–176. doi:10.1038/nrm2335
2. Rameh LE, Tolias KF, Duckworth BC, Cantley LC (1997) A new pathway for synthesis of phosphatidylinositol-4,5-bisphosphate. Nature 390(6656):192–196. doi:10.1038/36621
3. Emerling BM, Hurov JB, Poulogiannis G, Tsukazawa KS, Choo-Wing R, Wulf GM, Bell EL, Shim HS, Lamia KA, Rameh LE, Bellinger G, Sasaki AT, Asara JM, Yuan X, Bullock A, Denicola GM, Song J, Brown V, Signoretti S, Cantley LC (2013) Depletion of a putatively druggable class of phosphatidylinositol kinases inhibits growth of p53-null tumors. Cell 155(4):844–857. doi:10.1016/j.cell.2013.09.057
4. Jude JG, Spencer GJ, Huang X, Somerville TD, Jones DR, Divecha N, Somervaille TC (2014) A targeted knockdown screen of genes coding for phosphoinositide modulators identifies PIP4K2A as required for acute myeloid leukemia cell proliferation and survival. Oncogene. doi:10.1038/onc.2014.77
5. Tanega C, Shen M, Mott BT, Thomas CJ, MacArthur R, Inglese J, Auld DS (2009) Comparison of bioluminescent kinase assays using substrate depletion and product formation. Assay Drug Dev Technol 7(6):606–614. doi:10.1089/adt.2009.0230
6. Harbert C, Marshall J, Soh S, Steger K (2008) Development of a HTRF kinase assay for determination of Syk activity. Curr Chem Genomics 1:20–26. doi:10.2174/1875397300801010020
7. Hastie CJ, McLauchlan HJ, Cohen P (2006) Assay of protein kinases using radiolabeled ATP: a protocol. Nat Protoc 1(2):968–971
8. Kleman-Leyer KM, Klink TA, Kopp AL, Westermeyer TA, Koeff MD, Larson BR, Worzella TJ, Pinchard CA, van de Kar SA, Zaman GJ, Hornberg JJ, Lowery RG (2009) Characterization and optimization of a red-shifted fluorescence polarization ADP detection assay. Assay Drug Dev Technol 7(1):56–67. doi:10.1089/adt.2008.175
9. Szoka F Jr, Papahadjopoulos D (1980) Comparative properties and methods of preparation of lipid vesicles (liposomes). Annu Rev Biophys Bioeng 9:467–508. doi:10.1146/annurev.bb.09.060180.002343
10. Demian DJ, Clugston SL, Foster MM, Rameh L, Sarkes D, Townson SA, Yang L, Zhang M, Charlton ME (2009) High-throughput, cell-free, liposome-based approach for assessing in vitro activity of lipid kinases. J Biomol Screen 14(7):838–844. doi:10.1177/1087057109339205
11. Voss MD, Czechtizky W, Li Z, Rudolph C, Petry S, Brummerhop H, Langer T, Schiffer A, Schaefer HL (2014) Discovery and pharmacological characterization of a novel small molecule inhibitor of phosphatidylinositol-5-phosphate 4-kinase, type II, beta. Biochem Biophys Res Commun 449(3):327–331. doi:10.1016/j.bbrc.2014.05.024
12. Vidugiriene J, Zegzouti H, Goueli SA (2009) Evaluating the utility of a bioluminescent ADP-detecting assay for lipid kinases. Assay Drug Dev Technol 7(6):585–597. doi:10.1089/adt.2009.0223
13. Davis MI, Sasaki AT, Shen M, Emerling BM, Thorne N, Michael S, Pragani R, Boxer M, Sumita K, Takeuchi K, Auld DS, Li Z, Cantley LC, Simeonov A (2013) A homogeneous, high-throughput assay for phosphatidylinositol 5-phosphate 4-kinase with a novel, rapid substrate preparation. PLoS One 8(1):e54127. doi:10.1371/journal.pone.0054127
14. Copeland RA (2005) Evaluation of enzyme inhibitors in drug discovery. A guide for medicinal chemists and pharmacologists. Methods Biochem Anal 46:1–265
15. Yasgar A, Shinn P, Jadhav A, Auld D, Michael S, Zheng W, Austin CP, Inglese J, Simeonov A (2008) Compound management for quantitative high-throughput screening. JALA Charlottesv Va 13(2):79–89. doi:10.1016/j.jala.2007.12.004
16. Auld DS, Southall NT, Jadhav A, Johnson RL, Diller DJ, Simeonov A, Austin CP, Inglese

J (2008) Characterization of chemical libraries for luciferase inhibitory activity. J Med Chem 51(8):2372–2386. doi:10.1021/jm701302v

17. Thorne N, Shen M, Lea WA, Simeonov A, Lovell S, Auld DS, Inglese J (2012) Firefly luciferase in chemical biology: a compendium of inhibitors, mechanistic evaluation of chemotypes, and suggested use as a reporter. Chem Biol 19(8):1060–1072. doi:10.1016/j.chembiol.2012.07.015

Chapter 2

Assaying Ceramide Synthase Activity In Vitro and in Living Cells Using Liquid Chromatography-Mass Spectrometry

Xin Ying Lim, Russell Pickford, and Anthony S. Don

Abstract

Sphingolipids are one the major lipid families in eukaryotes, incorporating a diverse array of structural and signaling lipids such as sphingomyelin and gangliosides. The core lipid component for all complex sphingolipids is ceramide, a diacyl lipid consisting of a variable length fatty acid linked through an amide bond to a long chain base such as sphingosine or dihydrosphingosine. This reaction is catalyzed by a family of six ceramide synthases (CERS1-6), each of which preferentially catalyzes the synthesis of ceramides with different fatty acid chain lengths. Ceramides are themselves potent cellular and physiological signaling molecules heavily implicated in diabetes and neurodegenerative diseases, making it important for researchers to have access to sensitive and accurate assays for ceramide synthase activity. This chapter describes methods for assaying ceramide synthase activity in cell or tissue lysates, or in cultured cells (in situ), using liquid chromatography-tandem mass spectrometry (LC-MS/MS) as the readout. LC-MS/MS is a very sensitive and accurate means for assaying ceramide synthase reaction products.

Key words Ceramide, Ceramide synthase, Assay, Mass spectrometry, LC-MS, Liquid chromatography, CERS

1 Introduction

The importance of ceramides as mediators of physiological and pathological processes is now well established and recent advances in mass spectrometry have enabled researchers to delve into the roles for specific forms of ceramide as mediators of different functions and pathologies [1, 2]. Ceramides appear to be particularly important as mediators of metabolic distress and insulin resistance, and neurodegenerative conditions [3–5]. At the cellular level, ceramides are an integral component of the cell death signaling machinery and play an essential role in cell differentiation [6, 2].

Ceramides are synthesized through the addition of a variable length fatty acid to the amine group of a sphingoid base. In mammalian cells, the sphingoid base used for de novo ceramide synthesis is usually the C18:0 lipid dihydrosphingosine (Fig. 1), formed

Mark G. Waugh (ed.), *Lipid Signaling Protocols*, Methods in Molecular Biology, vol. 1376,
DOI 10.1007/978-1-4939-3170-5_2,

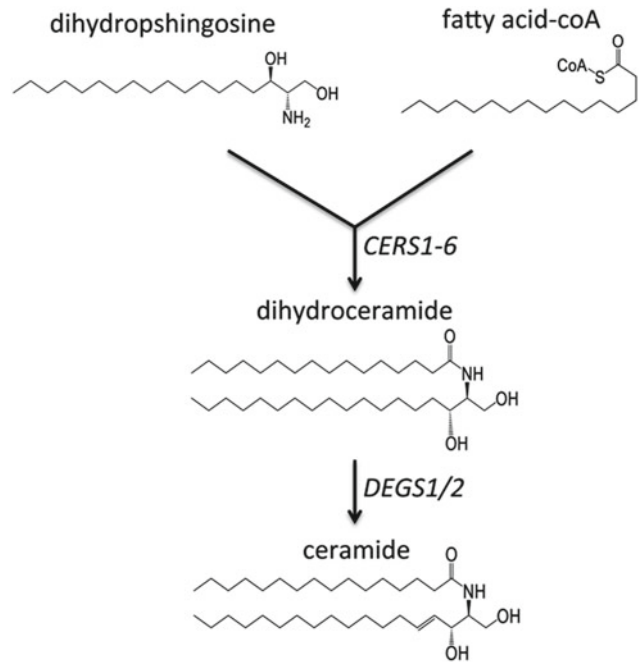

Fig. 1 Diagrammatic illustration of ceramide synthase activity. CERS enzymes catalyze the transfer of a variable length fatty acid, linked to coenzyme A (C16:0 fatty acid is shown), to dihydrosphingosine. In living cells, the dihydroceramides formed are rapidly desaturated by ceramide desaturases (DEGS1/2), forming ceramides. Note that CERS1-6 can use sphingosine as a substrate in place of dihydrosphingosine, directly forming ceramides rather than dihydroceramides

from the condensation of serine and palmitoyl-coenzyme A (C16:0-CoA). C16 or C20 sphingoid bases occur at much lower abundance [7, 8]. Ceramide synthesis is catalyzed by a family of six ceramide synthases (CERS1-6), each of which preferentially transfers fatty acids of different lengths to the amine group of dihydrosphingosine. Thus, CERS1 preferentially catalyzes the transfer of a C18:0 fatty acid, forming C18:0 dihydroceramide (d18:0/18:0 ceramide); CERS2 preferentially transfers very long chain fatty acids (C22–C26); CERS3 transfers even longer chain fatty acids (C26, C28), forming highly hydrophobic ceramides that are a very important part of the water barrier function of skin; CERS4 transfers C18 and C20 fatty acids; CERS5 transfers C16 fatty acids, and potentially also C14 and C18 fatty acids; and CERS6 transfers C14 and C16 fatty acids [1, 9, 10].

To assay CERS activity using LC-MS/MS, crude extracts containing cell membranes are firstly prepared from tissues or cultured cells. These extracts are used as the enzyme source for reactions containing deuterated dihydrosphingosine (or sphingosine) and a fatty acid substrate linked to CoA. The precise product formed is

naturally dependent on the substrates used. For example, C24:1 dihydroceramide (d18:0/24:1 ceramide) is formed in a reaction using dihydrosphingosine (C18:0) and C24:1 fatty acid-coenzyme A (nervonoyl-CoA), whilst C24:0 ceramide (d18:1/24:0 ceramide) is formed from sphingosine (C18:1) and C24:0-CoA (lignoceroyl-CoA). Reactions are stopped with the addition of four volumes of methanol and, after clearing insoluble material, reaction products are quantified directly from this reaction mixture using LC-MS/MS. A standard curve may be prepared from commercially available dihydroceramide standards for absolute quantification.

The method we describe is intended for a triple quadrupole MS, as these instruments are very common and exhibit the greatest dynamic range. Users with different instrumentation would need to adapt the instrument set-up and product detection conditions to their particular MS, but the HPLC conditions should remain constant. Although dihydroceramide reaction products could be detected following direct infusion into the MS electrospray source, the use of an HPLC column provides improved sensitivity, greater confidence in identification of the product, and more accurate quantification based on HPLC peak areas. As shown in Fig. 2, the limit of sensitivity using LC-MS/MS on a Thermo Fisher Scientific Quantum Access triple quadrupole mass spectrometer is <40 fmoles on column, permitting the detection of as little as 0.5 pmoles product formed in a standard 50 μL reaction with 500 pmoles substrate.

Compared to traditional TLC methods for product quantification, LC-MS/MS permits the separation and quantification of closely related but structurally distinct ceramide species. For example, C24:1 dihydroceramide and C24:0 dihydroceramide are easily

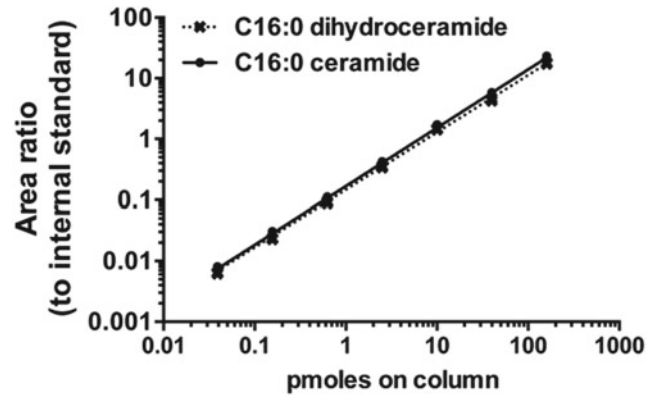

Fig. 2 Linearity of peak areas as a function of pmoles loaded for C16:0 ceramide and C16:0 dihydroceramide. Peak areas are expressed as ratios to 50 pmoles C17:0 ceramide internal standard. The amounts shown (*x*-axis) are pmoles on column (i.e. pmoles/20 μL)

distinguished on the basis of both mass and HPLC elution time. Even ceramide variants with identical mass, such as C24:1 dihydroceramide (d18:0/24:1) and C24:0 ceramide (d18:1/24:0), can be distinguished on the basis of HPLC elution time and differing fragment ions produced under interrogation with tandem mass spectrometry: although both molecules are detected as an ion with mass/charge ratio (m/z) of 650.64, ceramides produce an m/z 264.1 product ion following collision-induced dissociation, whilst the equivalent fragment ion produced by dihydroceramides has m/z 266.1. LC-MS/MS is therefore a very sensitive and accurate approach for quantifying the products of ceramide synthase reactions. Researchers without ready access to LC-MS instrumentation may consider fluorescence-based assays described in Chapter 3, or traditional radioactive methods [11, 12].

This chapter also includes a method for analyzing ceramide synthase activity in cultured cells. In this method, cells are incubated with deuterated (D7) dihydrosphingosine, which is converted in the cells by ceramide synthases to D7-dihydroceramides, and then to D7-ceramides. These cellular lipids are extracted using a method adapted from Bielawski et al. [13], and quantified using LC-MS/MS.

2 Materials

2.1 Cell or Tissue Lysis for In Vitro Assays

1. Phosphate Buffered Saline (PBS). Can be purchased directly from various suppliers.
2. Lysis buffer: 20 mM Hepes, pH 7.4, 10 mM KCl, 1 mM dithiothreitol, complete protease inhibitor cocktail (Roche), and 3 mM β-glycerophosphate (*see* **Note 1**).
3. Total protein assay kit. We use the BCA assay kit.
4. Plastic cell scrapers.

2.2 CERS Reactions

1. Fatty acid-coenzyme A conjugates may be purchased from Sigma-Aldrich or Avanti Polar Lipids. These may be reconstituted at 5 mM with water and stored in aliquots at −20 °C.
2. Deuterated (D7) dihydrosphingosine is purchased from Avanti Polar Lipids, reconstituted at 10 mM in methanol or DMSO, and stored at −20 °C (*see* **Note 2**).
3. C17 ceramide (d18:1/17:0) or C17:0 dihydroceramide (d18:0/17:0) internal standard (available from Avanti Polar Lipids). This is reconstituted at 5 mM in methanol and stored at −20 °C.
4. Reaction buffer: 20 mM Hepes, pH 7.4, 25 mM KCl, 2 mM $MgCl_2$, 0.5 mM DTT, 0.1 % (w/v) fatty acid free BSA

(*see* **Note 3**), 10 μM dihydrosphingosine, and 50 μM of the appropriate fatty acid-CoA (e.g., C16:0-CoA or C24:0-CoA).

5. Eppendorf Thermomixer or similar instrument for agitated incubation of 1.5 mL tubes.
6. Glass HPLC vials with fused inserts and caps. We use screw top glass vials with 0.3 mL fused inserts, and matched rubber caps with PTFE septa.

2.3 Quantification of Dihydroceramide Products Using LC-MS

1. Mass Spectrometer (MS) equipped with autosampler and LC system. We describe settings for a Thermo Fisher Scientific Quantum Access triple quadrupole MS coupled to a Thermo Fisher Scientific Accela UPLC.
2. A C8 or C18 reverse phase chromatography column. Column elution times are shorter with a C8 column (Table 1). The protocol described herein uses an Agilent 3×150 mm XDB-C8 column (5 μM pore size) or an Agilent Poroshell 120, 2.1×150 mm SB-C18 column (2.7 μM pore size).
3. Dihydroceramide standards for quantification (d18:0/16:0, d18:0/18:0, d18:0/24:0, d18:0/24:1), purchased from Avanti Polar Lipids. Stored as 5 mM stock solutions in methanol, at −20 °C.
4. HPLC mobile phase: methanol containing 0.2 % formic acid (v/v) and 1 mM ammonium formate.

2.4 Quantification of CeramideSynthase Activity in Living Cells

1. Cell culture plates (6-well) and growth medium suitable for the cells of interest.
2. 75 % isopropanol/25 % deionized water (v/v) for cell extraction.
3. Ethyl acetate for cell extraction.
4. Borosilicate glass centrifuge tubes with screw caps. We use 15 mL (16×125 mm) tubes from Thermo Fisher Scientific, but 10 mL tubes are also suitable.
5. SpeedVac centrifugal vacuum evaporator system (Thermo Fisher Scientific) or similar.
6. 5 mL borosilicate glass vials (75×12 mm) suitable for use in the SpeedVac or similar system.
7. Glass HPLC vials with fused inserts and caps.

3 Methods

3.1 Lysis of Cells or Tissues for In Vitro Assays

1. We recommend lysing 10–20 mg fresh-frozen tissue or a minimum of 10^6 cells in 0.5 mL lysis buffer. This should yield protein concentrations in the range 1–3 mg/mL. Cells should be washed once with PBS and scraped directly into lysis buffer.

Alternatively, cells can be detached with trypsin/EDTA solution, washed with PBS, then pelleted by centrifugation at 200 × *g* for 5 min prior to lysis.

2. Tissue or cells can be lysed using either a glass Dounce homogenizer or a sonicating bath that is suitable for small volumes. We use a Diagenode Bioruptor set to High intensity, with a 30 s on/30 s off cycle. As the sonicating bath heats very rapidly, the Bioruptor is kept at 4 °C and ice is added to prevent sample heating. For solid tissues, a tissue homogenizer should be used, or the tissue should be ground over dry ice or liquid nitrogen prior to lysis, using Eppendorf micropestles.
3. The homogenate is centrifuged for 10 min at 800 × *g* to pellet nuclei and unbroken cells, and the supernatant is transferred to a new tube.
4. The protein concentration is measured using a BCA assay kit (*see* **Note 4**), and the lysate is stored in aliquots at −80 °C.

3.2 CERS Assay

1. Reactions are run in 1.5 mL tubes. The standard reaction volume is 50 μL, using the reaction buffer described above. Reactions are started with the addition of 10–25 μg lysate protein and run at 37 °C on a thermomixer with vigorous shaking (*see* **Note 5**).
2. Reactions are stopped with the addition of four volumes of methanol that includes 50 pmoles C17 ceramide internal standard, and the tubes are vortexed. The tubes are centrifuged for 20 min at 21,800 × *g* to remove any insoluble material, after which the top 0.2 mL of the supernatant is transferred to glass HPLC vials for MS analysis. The vials may be stored at 4 °C (*see* **Note 6**).
3. It is recommended to set up controls in which no enzyme (i.e., lysate) or no fatty acid-coA substrate is added to the reaction.

3.3 Quantifying Ceramide Products on a Triple Quadrupole MS

1. Selected reaction monitoring mode is employed on the mass spectrometer after positive mode electrospray ionization. Precursor and product ion mass-to-charge ratios (m/z) are as indicated in Table 1. Mass to charge ratios for both precursor and product ions of D7-dihydroceramides are increased by 7 mass units compared to the naturally occurring lipids. We strongly recommend that instrument-specific parameters such as most abundant product ion, collision energy, collision gas pressure, electrospray voltage, electrospray source temperature, source gas flow rates, tube lens/S lens voltage, capillary temperature, and skimmer offset be determined empirically in the laboratory in which the assay is being run. This is done by direct infusion of one or more dihydroceramide standards into the MS source, according to the instrument manufacturer's instructions.

Table 1
Exact mass, column elution times, and precursor and product ion masses [M + H] for commonly studied dihydroceramide and ceramide species

Ceramide[a]	Molecular weight	Precursor *m/z* [M + H][c]	Product *m/z* [M + H][c]	Collision energy (eV)	C8 column elution time (min)	C18 column elution time (min)
Dihydroceramides						
d18:0/16:0	539.53	540.5 (547.5)	522.5 (529.5)	17	3.1	3.3
d18:0/18:0	567.55	568.6 (575.6)	550.6 (557.6)	17	3.6	4.3
d18:0/24:0	651.65	652.7 (659.7)	634.7 (641.7)	17	5.8	10.9
d18:0/24:1	649.64	650.6 (657.6)	632.6 (639.6)	17	5.0	8.0
Ceramides						
d18:1/17:0[b]	551.53	552.5	264.1	30	3.2	3.4
d18:1/16:0	537.51	538.5 (545.5)	264.1 (271.1)	30	3.0	3.0
d18:1/18:0	565.54	566.5 (573.5)	264.1 (271.1)	30	3.4	3.9
d18:1/20:0	593.57	594.6 (601.6)	264.1 (271.1)	30	3.9	5.3
d18:1/22:0	621.61	622.6 (629.6)	264.1 (271.1)	30	4.6	7.2
d18:1/24:0	649.64	650.6 (657.6)	264.1 (271.1)	30	5.5	9.9
d18:1/24:1	647.62	648.6 (655.6)	264.1 (271.1)	30	4.7	7.3

Elution times are given for a 3 × 150 mm Agilent XDB-C8 column (5 μm pore size) and an Agilent Poroshell 120, 2.1 × 150 mm SB-C18 column (2.7 μm pore size). Mass/charge (*m/z*) values in parentheses are for D7-labeled compounds formed in the reactions. Note that triple quadrupole mass spectrometers are generally only accurate to unit mass (whole number) (*see* **Note 9**)

[a]d18:0 forms are commonly referred to as dihydroceramides; d18:1 forms are referred to as ceramides

[b]d18:1/17:0 ceramide is the C17:0 ceramide internal standard

[c]Reactions or cell incubations with D7-dihydrosphingosine result in formation of D7-labeled forms of dihydroceramide and ceramide. The *m/z* values for these are given in parentheses

2. The flow rate is 0.5 mL/min using the HPLC mobile phase described in the Materials section.
3. 20 μL of each sample is resolved on the column, with a total run time of 9 min for the C8 column and 15 min for the C18 column. Different dihydroceramide or ceramide products elute at different times from the HPLC column, as listed in Table 1.
4. An external calibration curve spanning the range 1 nM to 2 μM (0.25–500 pmoles in 250 μL HPLC mobile phase) should be constructed for the dihydroceramide or ceramide reaction product that is being measured. For the standard curve, it is ideal to use the naturally occurring equivalent to the form of D7-dihydroceramide that is generated in the reaction. Each standard curve dilution should contain 50 pmoles C17 ceramide internal standard.

5. Data is analyzed using the vendor software (XCalibur for Thermo MS systems). Peak areas are determined for the D7-dihydroceramide reaction product and expressed as a ratio relative to the C17:0 ceramide internal standard for each sample. Similarly, external standard peak areas are expressed as ratios to the internal standard, and the resulting calibration curve (Fig. 2) is used to calculate the pmoles product formed in the reaction. Figure 3 shows chromatograms for an example reaction assaying C24:1 ceramide synthase activity in mouse liver homogenates. As expected, product formation is inhibited with the well characterized ceramide synthase inhibitor fumonisin B1 [14].

3.4 Assaying CERS Activity of Living Cells

1. Cells are seeded on the preceding day at the desired concentration for the assay. We have found 2.5×10^5 cells per well of a 6-well culture plate to be suitable for this assay.

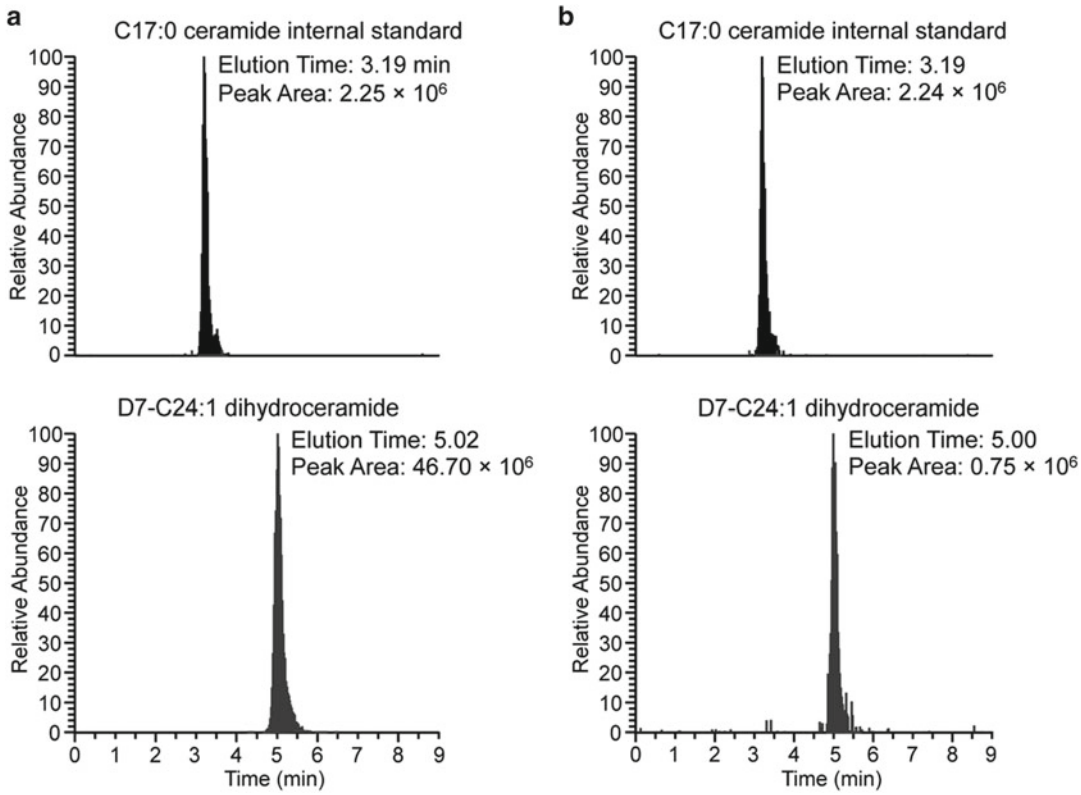

Fig. 3 Chromatograms showing peaks for D7-labeled C24:1 dihydroceramide products. Reactions were set up with 25 μg mouse liver homogenate, and D7-dihydrosphingosine (10 μM) and C24:1-CoA (50 μM) as substrates. Chromatograms shown in (**b**) are for a reaction that included the ceramide synthase inhibitor fumonisin B1 (10 μM), illustrating the inhibition of product (D7-C24:1 dihydroceramide) formation relative to the vehicle control reaction (**a**). Chromatograms for the C17:0 ceramide internal standard are also shown for reference

2. Cells are pretreated with the desired inhibitors or genetic manipulations, then incubated for 1 h with 500 nM D7-dihydrosphingosine.
3. Cells are washed once with PBS to remove serum proteins.
4. The cells are held on ice, and 0.4 mL 75 % isopropanol containing 50 pmoles C17:0 ceramide internal standard is added to each well. A cell scraper is used to collect the cells into the solvent mixture, and the cell extracts are transferred to a 15 mL glass centrifuge tube. The culture wells are then washed with another 0.4 mL 75 % isopropanol, and this extract is combined with the first.
5. Ethyl acetate (1.2 mL) is added to each tube, and the mixture is vortexed, then sonicated for 2 h in a sonicating water bath, with heating to approximately 50 °C (*see* **Note 7**).
6. Cell extracts are centrifuged at 3700 × *g* for 10 min to pellet insoluble debris, and the supernatant is transferred to a 5 mL glass vial.
7. Insoluble debris is re-extracted with another 2 mL ethyl acetate–isopropanol–water (6:3:1, v/v/v) as described above. The supernatants are combined.
8. Cell extracts (i.e., supernatant) are dried down in a SpeedVac or similar vacuum evaporator, or under a stream of nitrogen.
9. Cell extracts are reconstituted with vigorous vortexing in 0.25 mL HPLC mobile phase.
10. Glass tubes are centrifuged at 3700 × *g* for 10 min to pellet any insoluble material, and 0.2 mL of the supernatants are transferred to glass HPLC vials with inserts. Vials are stored at 4 °C pending LC-MS analysis (*see* **Note 6**).
11. Quantify D7-dihydroceramides and D7-ceramides using LC-MS/MS, as described in Subheading 3.3. In cultured cells, the D7-dihydroceramides formed from D7-dihydrosphingosine will be rapidly converted to ceramides by desaturases (*DEGS1* and *DEGS2*). It is therefore important to quantify D7-ceramides as well as D7-dihydroceramides (*see* **Note 9**). Figure 4 shows an example for U251 glioblastoma cells treated with the ceramide synthase inhibitor fumonisin B1.

4 Notes

1. We include the β-glycerophosphate as a protein phosphatase inhibitor. A recent publication has demonstrated that ceramide synthase activity in yeast is regulated by phosphorylation [15].
2. Deuterated (D7) dihydrosphingosine is used as the substrate to avoid any baseline level of dihydroceramide products attrib-

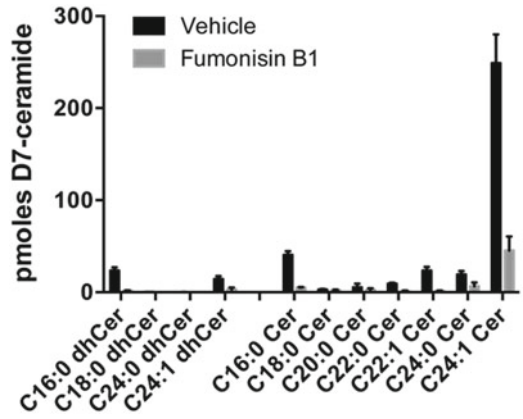

Fig. 4 Formation of D7-ceramides from D7-dihydrosphingosine in cultured cells. U251 glioblastoma cells (2.5×10^6 cells) were pretreated for 1 h with 5 μM fumonisin B1, prior to a 1 h incubation with 500 nM D7-dihydrosphingosine. As expected, the D7-dihydrosphingosine is converted to dihydroceramides and ceramides in the cells, and this is inhibited with fumonisin B1. *Cer* ceramide, *dhCer* dihydroceramide

uted to endogenous dihydroceramides in the cell or tissue extracts. Note that these endogenous dihydroceramides are likely to be low abundance, and it is therefore also feasible to use natural dihydrosphingosine as the substrate in place of the D7 form, provided that control reactions with cell or tissue extract but without dihydrosphingosine substrate are included to assess endogenous levels of dihydroceramides.

3. Fatty acid free BSA, available from a number of common biochemical suppliers, is used as a carrier for the ceramide formed in the reaction. Standard laboratory BSA contains lipids and fatty acids that may interfere with the reaction or quantification of reaction products.
4. Serum proteins will interfere with estimation of protein concentration by BCA or similar protein assay. Protein concentration may also be determined using other common assays.
5. It is recommended for the user to run a test assay confirming that CERS activity is linear with respect to time and/or lysate concentration before picking a single time and lysate protein concentration at which to compare different samples. In our experience, reactions are linear over 30 min, using between 10 and 30 μg lysate protein, but this will obviously depend on the level of CERS activity in the samples of interest.
6. Prolonged storage at 4 °C, or particularly at −20 °C, may result in further precipitate forming. In this case the supernatant should be transferred to new HPLC vials. Care should be taken

to ensure that no precipitate is loaded onto the LC-MS system, as this may clog the injection port or column.

7. It is important not to allow the sonication to cause overheating of the glass tubes, as this will result in solvent spillage into the water bath and a potential inhalation hazard with the ethyl acetate.
8. When considering lipids that are separated in mass by only two mass units, it is important to consider the peaks produced by naturally occurring heavy carbon (^{13}C) isotopes. These represent around 1 % of all carbon atoms. For example, C24:1 ceramide, monitored with m/z 648.6, will also produce a peak with m/z 650.6, albeit with greatly reduced intensity compared to the m/z 648.6 peak. Since m/z 650.6 will also detect C24:1 dihydroceramide and C24:0 ceramide, it is very important in these instances to employ external standards for each lipid of interest, in order to confirm the expected HPLC column elution times. This issue is not particularly problematic when monitoring a single product formed in an in vitro reaction, but is an important consideration when monitoring a complex lipid mixture isolated from cultured cells. We note that the C18 column provides better resolution of very long chain ceramide species (e.g., C24:1 and C24:0 ceramides and dihydroceramides) than does the C8 column.
9. When using a water loss event to monitor for dihydroceramides, as indicated in Table 1 (e.g., C24:1 dihydroceramide precursor ion m/z 650.6; product ion m/z 632.6), it is important to note that this will detect any molecule in the range m/z 650.1–651.1 that loses a water molecule (m/z 18.0) following collision-induced dissociation. This MS event will therefore also detect isobaric ceramide species such as C24:0 ceramide (also detected with m/z 650.6), and heavy carbon forms of C24:1 ceramide as discussed in **Note 8**. In these instances, HPLC column elution time is particularly important for correct lipid identification.

References

1. Park JW, Park WJ, Futerman AH (2014) Ceramide synthases as potential targets for therapeutic intervention in human diseases. Biochim Biophys Acta 1841(5):671–681
2. Hannun YA, Obeid LM (2011) Many ceramides. J Biol Chem 286(32):27855–27862
3. Chavez JA, Summers SA (2012) A ceramide-centric view of insulin resistance. Cell Metab 15(5):585–594
4. Haughey NJ, Bandaru VV, Bae M, Mattson MP (2010) Roles for dysfunctional sphingolipid metabolism in Alzheimer's disease neuropathogenesis. Biochim Biophys Acta 1801(8): 878–886
5. de la Monte SM (2012) Triangulated mal-signaling in Alzheimer's disease: roles of neurotoxic ceramides, ER stress, and insulin resistance reviewed. J Alzheimers Dis 30(Suppl 2):S231–S249
6. Bieberich E (2008) Ceramide signaling in cancer and stem cells. Future Lipidol 3(3): 273–300
7. Narayanaswamy P, Shinde S, Sulc R, Kraut R, Staples G, Thiam CH, Grimm R, Sellergren B, Torta F, Wenk MR (2014) Lipidomic "deep profiling": an enhanced workflow to reveal new molecular species of signaling lipids. Anal Chem 86(6):3043–3047

8. Merrill AH Jr (2011) Sphingolipid and glycosphingolipid metabolic pathways in the era of sphingolipidomics. Chem Rev 111(10): 6387–6422
9. Mizutani Y, Kihara A, Igarashi Y (2005) Mammalian Lass6 and its related family members regulate synthesis of specific ceramides. Biochem J 390(Pt 1):263–271
10. Jennemann R, Rabionet M, Gorgas K, Epstein S, Dalpke A, Rothermel U, Bayerle A, van der Hoeven F, Imgrund S, Kirsch J, Nickel W, Willecke K, Riezman H, Grone HJ, Sandhoff R (2012) Loss of ceramide synthase 3 causes lethal skin barrier disruption. Hum Mol Genet 21(3):586–608
11. Bose R, Kolesnick R (2000) Measurement of ceramide synthase activity. Methods Enzymol 322:378–382
12. Lahiri S, Lee H, Mesicek J, Fuks Z, Haimovitz-Friedman A, Kolesnick RN, Futerman AH (2007) Kinetic characterization of mammalian ceramide synthases: determination of K(m) values towards sphinganine. FEBS Lett 581(27): 5289–5294
13. Bielawski J, Szulc ZM, Hannun YA, Bielawska A (2006) Simultaneous quantitative analysis of bioactive sphingolipids by high-performance liquid chromatography-tandem mass spectrometry. Methods 39(2):82–91
14. Merrill AH Jr, van Echten G, Wang E, Sandhoff K (1993) Fumonisin B1 inhibits sphingosine (sphinganine) N-acyltransferase and de novo sphingolipid biosynthesis in cultured neurons in situ. J Biol Chem 268(36): 27299–27306
15. Muir A, Ramachandran S, Roelants FM, Timmons G, Thorner J (2014) TORC2-dependent protein kinase Ypk1 phosphorylates ceramide synthase to stimulate synthesis of complex sphingolipids. Elife 3:e03779

Chapter 3

Fluorescent Assays for Ceramide Synthase Activity

Timothy A. Couttas and Anthony S. Don

Abstract

Ceramides are the central lipid metabolite of the sphingolipid family, and exert a potent influence over cell polarity, differentiation, and survival through their biophysical properties and their specific interactions with cell signaling proteins. Literature on the importance of ceramides in physiology and pathological conditions continues to grow, with ceramides having been identified as central effectors in major human pathologies such as diabetes and neurodegenerative conditions. In mammals, ceramide synthesis from a sphingoid base and a variable length fatty acid is catalyzed by a family of six ceramide synthases (CERS1-6), whose active sites exhibit differential specificity for different length fatty acids. CERS activity has traditionally been measured using radioactive substrates. More recently mass spectrometry has been used. In this chapter, we describe a fluorescent CERS assay, the results of which can be quantified using thin-layer chromatography (TLC) or high-performance liquid chromatography (HPLC). Methods for quantification with either TLC or HPLC are described.

Key words Ceramide, Ceramide synthase, Fluorescent, Assay

Abbreviations

CERS	Ceramide
HPLC	High-performance liquid chromatography
NBD-dhCer	NBD-dihydroceramide
NBD-dhSph	NBD-dihydrosphingosine
TLC	Thin-layer chromatography

1 Introduction

The importance of ceramides as mediators of physiological and pathological processes is now well established and recent advances in mass spectrometry have enabled researchers to delve into the roles for specific forms of ceramide as effectors of different functions and pathologies [1, 2]. Ceramides appear to be particularly important as mediators of metabolic distress and insulin resistance, as well as neurodegenerative conditions [3–5]. At the cellular level,

Mark G. Waugh (ed.), *Lipid Signaling Protocols*, Methods in Molecular Biology, vol. 1376,
DOI 10.1007/978-1-4939-3170-5_3,

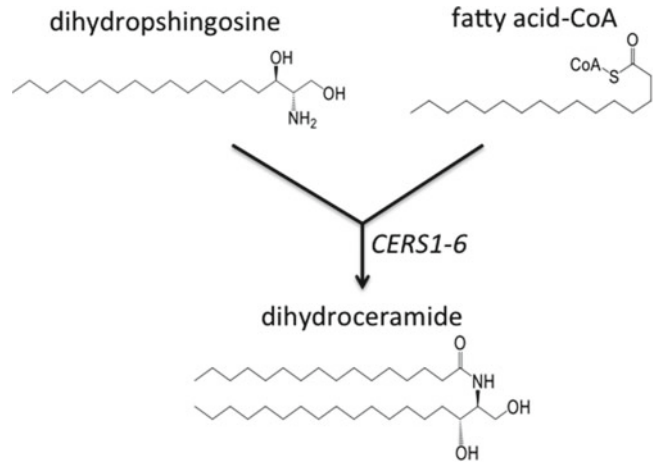

Fig. 1 Ceramide synthases catalyze the condensation of a sphingoid base and a fatty acid substrate. The fatty acid substrate used in the reaction is conjugated to coenzyme A (CoA)

ceramides are an integral component of the cell death signaling machinery and play an essential role in cell differentiation [2, 6].

Ceramides are synthesized through the addition of a variable length fatty acid to the amine group of a sphingoid base. In mammalian cells, the sphingoid base used for de novo ceramide synthesis is usually the C18:0 lipid dihydrosphingosine (Fig. 1), formed from the condensation of serine and palmitoyl-CoA. C16 or C20 sphingoid bases occur at much lower abundance [7, 8]. In mammals, ceramide synthesis is catalyzed by a family of six ceramide synthases (CERS1-6), which exhibit specificity in the length of the fatty acids that they transfer to the amine group of dihydrosphingosine. Thus, CERS1 preferentially catalyzes the transfer of a C18:0 fatty acid, forming C18:0 dihydroceramide (d18:0/18:0 ceramide); CERS2 preferentially transfers very long chain fatty acids (C22–C26); CERS3 transfers even longer chain fatty acids (C26, C28), forming very hydrophobic ceramides that are a very important part of the water barrier function of skin; CERS4 transfers C18 and C20 fatty acids; CERS5 transfers C16 fatty acids, and potentially also C14 and C18 fatty acids; and CERS6 transfers C14 and C16 fatty acids [1, 9, 10].

The study of CERS enzymes has lagged behind the study of ceramide itself. The fluorescent assay methods described herein were designed to improve accessibility of CERS assays to the biomedical community by removing the requirement for radioactive substrates or mass spectrometers. Elimination of radioactivity is an important consideration for many laboratories, particularly isotopes with very long half-lives like ^{3}H and ^{14}C, used for radioactive CERS assays [11, 12]. The only specialized equipment that is

needed is an HPLC system with fluorescent detector or an imaging system with fluorescent camera (for TLC plates). Researchers who have ready access to a mass spectrometer may prefer to use the mass spectrometry-based assay described in Chapter 2.

The fluorescent assay uses commercially available sphingosine or dihydrosphingosine labeled with an NBD (2S,3R)-2-amino-18-((7-nitrobenzo[c][1,2,5]oxadiazol-4-yl)amino)octadecane-1,3-diol) fluorescent group. Depending on the fluorescent substrate used, NBD-sphingosine or NBD-dihydrosphingosine (NBD-dhSph), the product of the reaction will be NBD-ceramide or NBD-dihydroceramide (NBD-dhCer), respectively. Crude tissue or cell homogenates are used as the source of enzyme in reactions containing the NBD-labeled sphingoid base and a fatty acid substrate linked to coenzyme A (CoA). Although specific desaturases rapidly convert dihydroceramides to ceramides inside cells, the in vitro reaction with NBD-dhSph produces NBD-dhCer and not NBD-Cer as the product. Fluorescent dihydroceramides or ceramides formed in the reaction may be detected and quantified using either TLC or HPLC.

Compared to the TLC-based assay, the increased sensitivity afforded by HPLC permits a shortened assay protocol in which 2-phase extraction, drying, and reconstitution of the reaction mixture is not necessary. Instead, reactions may be stopped with the addition of methanol, and the reaction mixture need only be cleared by centrifugation before analysis with HPLC. This considerably shortens the assay protocol and is an advantage with the HPLC approach, compared to TLC. The reproducibility of column retention times from one experiment to the next also increases confidence in correct assignment of products when using HPLC. However, we have found that both assay formats yield robust and reproducible results [13, 14].

2 Materials

2.1 Cell or Tissue Lysis

1. Phosphate Buffered Saline (PBS). Can be purchased directly from various suppliers.
2. Lysis buffer: 20 mM Hepes, pH 7.4, 10 mM KCl, 1 mM dithiothreitol, complete protease inhibitor cocktail (Roche), and 3 mM β-glycerophosphate (*see* **Note 1**).
3. Total protein assay kit. We use a Bicinchoninic Acid (BCA) assay kit.
4. Plastic cell scrapers.

2.2 CERS Reactions

1. Fatty acid-CoA conjugates may be purchased from Sigma-Aldrich or Avanti Polar Lipids. These can be reconstituted with water at 5 mM and stored in aliquots at −20 °C.

2. NBD-dhSph is purchased from Avanti Polar Lipids (*see* **Note 2**).
3. Reaction buffer: 20 mM Hepes, pH 7.4, 25 mM KCl, 2 mM $MgCl_2$, 0.5 mM DTT, 0.1 % (w/v) fatty acid free BSA (*see* **Note 3**), 10 μM NBD-dhSph, and 50 μM of the appropriate fatty acid-CoA (e.g., C16:0-CoA or C24:0-CoA).
4. Eppendorf Thermomixer or similar instrument for agitated incubation of 1.5 mL tubes.

2.3 Quantifying CERS Activity Using TLC

1. An imaging system with fluorescent camera (e.g., Fuji LAS4000 or Bio-Rad ChemiDoc system). Excitation and emission spectra for NBD are variable depending on the solvent and environment (excitation maximum ~466 nM and emission maximum at ~536 nM), but standard green fluorescent filters used for detection of SYBR Safe dye, fluorescein, or green fluorescent protein work well.
2. Analytical grade chloroform and methanol.
3. Silica gel 60 TLC plates, aluminum backed.
4. Glass TLC chamber with lid. If a TLC chamber is not available, a glass beaker covered with aluminum foil may be used.

2.4 Quantifying CERS Activity Using HPLC

1. HPLC system with a fluorescent detector capable of excitation in the range 450–480 nM and detection in the range 530–550 nM. We use a Thermo Scientific Surveyor HPLC, connected to a Shimadzu RF-10AXL fluorescent detector.
2. C8 reverse phase chromatography column. Our protocol uses an Agilent 3 × 150 mm XDB-C8 column with 5 μM pore size.
3. Glass HPLC vials with fused inserts and caps. We use screw top glass vials with 0.3 mL fused inserts, and matched rubber caps with polytetrafluoroethylene (PTFE) septa.
4. HPLC solvent A: deionized water with 0.2 % formic acid and 2 mM ammonium formate.
5. HPLC solvent B: analytical grade methanol with 0.2 % formic acid and 1 mM ammonium formate.
6. C18:0 NBD-ceramide standard from Avanti Polar Lipids may be used to construct standard curves for product quantification and/or as an internal standard for relative quantification.

3 Methods

3.1 Lysis of Cells or Tissues

1. We recommend lysing 10–20 mg fresh-frozen tissue or a minimum of 10^6 cells in 0.5 mL lysis buffer. This should yield protein concentrations in the range 1–3 mg/mL. Cells should be washed once with PBS and scraped directly into lysis buffer. Alternatively, cells can be detached with trypsin/EDTA

solution, washed with PBS, then pelleted by centrifugation at 200 × *g* for 5 min prior to lysis.

2. Tissue or cells can be lysed using either a glass Dounce homogenizer or a sonicating bath that is suitable for small volumes. We use a Diagenode Bioruptor set to high intensity, with a 30 s on/30 s off cycle, for a total of 5 min. As the sonicating bath heats very rapidly, the Bioruptor is kept at 4 °C and ice is added to prevent sample heating. For solid tissues, a tissue homogenizer should be used, or the tissue should be ground over dry ice or liquid nitrogen prior to lysis, using Eppendorf micropestles.
3. The homogenate is centrifuged for 10 min at 800 × *g* to pellet nuclei and unbroken cells, and the supernatant is transferred to a new tube.
4. The protein concentration is measured using a BCA assay kit (*see* **Note 4**), and the lysate is stored in aliquots at −80 °C.

3.2 CERS Reactions

1. Reactions are run in standard 1.5 mL tubes with lids. The standard reaction volume is 50 µL. Reactions are started with the addition of 5–25 µg lysate protein and run for 30 min at 37 °C on a thermomixer with shaking (*see* **Note 5**). Use low laboratory lighting to avoid bleaching of the fluorescence for this and all subsequent steps. Bright fluorescent laboratory lighting may bleach the fluorescence of the NBD-dhSph substrate and reaction products.
2. To ensure that the correct reaction product is being measured, we strongly recommend running negative control reactions in which the enzyme source or fatty acid-CoA substrate is omitted. The user may also wish to perform positive control reactions using lysates of cells overexpressing particular CERS isoforms or control reactions with the CERS inhibitor fumonisin B1, as described in **Notes 6** and 7.
3. If product quantification is to be performed using TLC, reactions are stopped using two volumes of chloroform–methanol (2:1). Follow the instructions in Subheading 3.3.

If HPLC is to be used for product quantification, reactions are stopped with four volumes of methanol. Follow the instructions in Subheading 3.4.

3.3 Quantifying CERS Activity Using TLC

1. Reactions are stopped with the addition of two volumes (i.e., 100 µL per 50 µL reaction) chloroform–methanol (2:1), then vortexed. The tubes are centrifuged for 15 s at 21,800 × *g* to separate the phases, and the lower organic phase, containing the reaction product, is transferred to a 5 mL glass tube. A second extraction of the aqueous layer is performed using

another two volumes chloroform–methanol (2:1), and the organic phase is combined with that from the first extraction.

2. The organic extract is dried in a SpeedVac or similar vacuum desiccator (generally takes only 1 h) or under a stream of nitrogen.
3. Using a pencil, draw a line 2 cm from the base of a Silica Gel 60 TLC plate. Lightly mark the origin for each sample to be resolved along this baseline. The samples should be evenly spaced along the baseline and at-least 2 cm from each edge of the TLC plate (*see* **Note 8**).
4. Reaction products are resuspended with vigorous vortexing in 50 μL methanol. Spot 2.5 μL of each sample on the TLC plate, wait for this to air-dry, then spot another 2.5 μL directly on top.
5. Resolve the TLC plate in chloroform–methanol–water (8:1:0.1 v/v/v). This is done in a fume hood. The TLC plate should be left until the solvent front has migrated between ¾ and all the way to the top of the plate, then removed and briefly air-dried in the fume hood.
6. Fluorescent standards comprising known concentrations of the NBD-dhSph substrate (0.1–100 pmoles) may be spotted directly on to a different TLC plate that is not resolved in a TLC chamber but instead imaged directly. This permits the construction of a standard curve for fluorescent pixel intensity as a function of pmoles substrate on the TLC plate. Since the NBD-dhSph substrate is incorporated to NBD-dhCer product in a 1:1 molar ratio, the pmoles product formed in the reaction may be interpolated directly from this standard curve.
7. The fluorescent bands are visualized on a fluorescent gel or plate imaging system, such as a LAS4000 imaging system with a green fluorescent filter. Many common imaging systems designed to detect green fluorescent dyes in agarose or polyacrylamide gels are suitable. An example is shown in Fig. 2 (*see* **Note 9**).
8. Band intensity is quantified using densitometry. Proprietary vendor software that is specific to the imaging system employed (e.g., ImageQuant software, GE Healthcare) is used for this purpose.

3.4 Quantifying CERS Activity Using HPLC

1. Reactions are stopped with the addition of four volumes (200 μL for a 50 μL reaction) of methanol and vortexed vigorously.
2. Reaction mixtures are microfuged at 21,800 × *g* for 15 min to clear any insoluble material.
3. The supernatants (200 μL) are then transferred to glass HPLC vials and stored at 4 °C until HPLC analysis. We have not

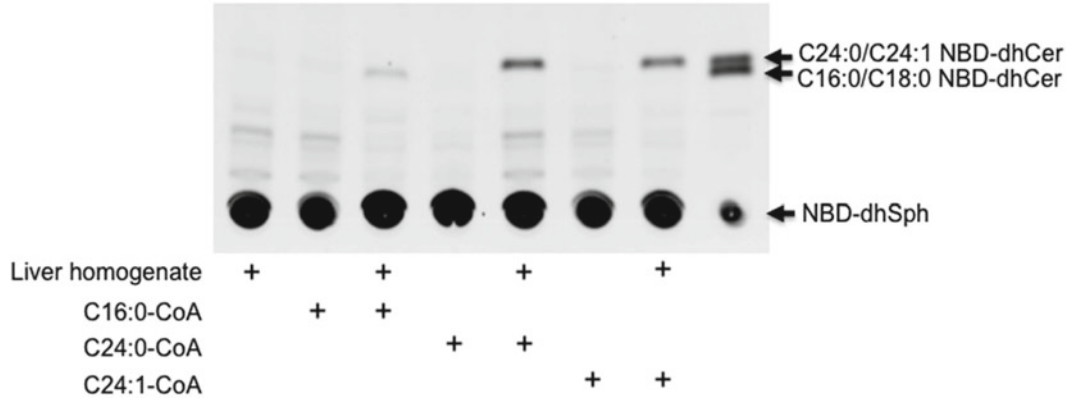

Fig. 2 Example of C16:0, C24:0, and C24:1 NBD-dhCer reaction products resolved on TLC. Reactions were run for 30 min using 20 μg mouse liver homogenate as the enzyme source and C16:0, C24:0, or C24:1 fatty acid-CoA substrate. Reactions with no lysate or no fatty acid-CoA substrate were included as controls, allowing clear discrimination of the product band. The lane on the *right* is a mixture of NBD-dhSph and C16:0, C18:0, C24:0, and C24:1 NBD-dihydroceramides. Image was captured using a Fuji LAS4000 Mini imaging system set to detect SYBR safe dye (green fluorescent filter), and a 2 s exposure time

determined the effects of long-term storage of the samples on NBD-dihydroceramide solubility. It is recommended to analyze the samples as soon as possible.

4. The HPLC system should be set to detect fluorescence with excitation at 466 nM, and emission at 536 nM. Parameters for optimal detection of fluorescence (particularly the gain) should be determined empirically with the user's own HPLC system.
5. 20 μL of each sample is injected onto a C8 column, and separated using the following 12 min gradient. Solvents are as described in Subheading 2.4: Starting at 20:80 A:B (t = 0 min), the gradient is increased to 5:95 A:B over 2 min, then increased from 5:95 A:B to 100 % B between 2 and 8 min. The gradient is held at 100 % B for a further 2 min (t = 10 min), then re-equilibrated to 20:80 A:B for 2 min (t = 12 min). The use of 20:80 A:B as the starting phase permits good separation of NBD-dhCer species and detection of an NBD-dhSph peak, as illustrated in Fig. 3 (*see* **Note 10**).
6. The product is quantified as the peak area, using the software associated with that particular HPLC system. We use a Thermo Scientific Surveyor HPLC system with Xcalibur software.
7. Absolute quantification using an external calibration curve: Peak areas may be converted to pmoles ceramide using a commercially available NBD-ceramide external standard to construct a standard curve. C18:0 NBD-ceramide (d18:1-NBD/18:0 ceramide) from Avanti Lipids may be used for this purpose. Alternatively, the NBD-dhSph substrate,

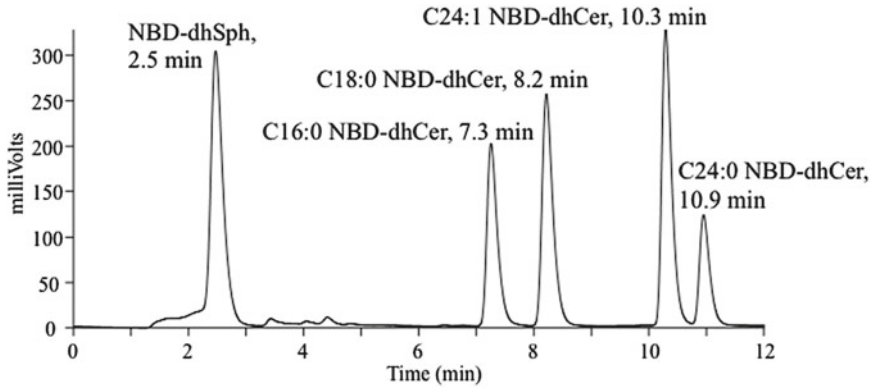

Fig. 3 HPLC chromatogram showing column elution times for NBD-dhSph, as well as C16:0, C18:0, C24:0, and C24:1 NBD-dhCer. Note that these NBD-dhCer standards, with the NBD label on the dihydrosphingosine acyl chain, are not commercially available. Instead, they were prepared in reactions using NBD-dhSph and the appropriate fatty acyl-CoA, as described in [13]

which elutes at 2.5 min (Fig. 3) may be used to construct an external calibration curve (*see* **Note 11**). The external standard curve should span the range 5–500 nM (0.1–10 pmoles on column).

8. Relative quantification: It is not necessary to use an external calibration curve if the intention is simply to compare relative CERS activity between different samples. In this instance, the user may wish to include commercially available C18:0 NBD-ceramide (Avanti Lipids) as an internal standard for normalization of peak areas in each sample. The internal standard (50 pmoles) is added together with the four volumes of methanol used to stop the reactions in **step 3** (i.e., reactions are stopped with 200 μL methanol containing 250 nM C18:0 NBD-ceramide). Peak areas for the product of interest are then normalized to the C18:0 NBD-ceramide internal standard peak area within each sample. The use of this particular internal standard is not feasible if the user wishes to quantify C18:0 CERS activity, due to overlapping peaks.

4 Notes

1. We include the β-glycerophosphate as a protein phosphatase inhibitor. A recent publication has demonstrated that ceramide synthase activity in yeast is regulated by phosphorylation [15].
2. NBD-sphingosine may be used in place of NBD-dhSph as the substrate. In this case, the product of the reaction will be NBD-ceramide rather than NBD-dhCer.

3. Fatty acid free BSA, available from a number of common biochemical suppliers, is used as a carrier for the ceramide formed in the reaction. Standard laboratory BSA contains lipids and fatty acids that may interfere with the reaction or quantification of reaction products.
4. Serum proteins will interfere with estimation of protein concentration by BCA or similar protein assay. Protein concentration may also be determined using other common assays.
5. It is recommended for the user to run a test assay confirming that CERS activity is linear with respect to time and/or lysate concentration before picking a single time and lysate protein concentration at which to compare different samples. In our experience, reactions are linear over 30 min, using between 5 and 30 μg lysate protein, but this will obviously depend on the level of CERS activity in the samples of interest.
6. At the time of writing, the only commercially available NBD-ceramide standard for this assay is C18:0 NBD-ceramide (d18:1-NBD/18:0 ceramide) from Avanti Lipids. The user may wish to verify their reaction product using lysates of cells overexpressing the appropriate CERS isoform. In accordance with the literature, we recommend using CERS1 to produce C18:0 NBD-dhCer, CERS5 or 6 to produce C16:0 NBD-dhCer, and CERS2 to produce C24:0 or C24:1 NBD-dhCer [9, 11, 13]. HEK293 or another high transfection efficiency cell line is transfected with expression plasmids for CERS1, CERS2, or CERS6. At 24 h after transfection, the cells are scraped into lysis buffer and lysed as described in Subheading 3.1. These lysates should yield a strong peak or band corresponding to the desired NBD-dhCer product on HPLC or TLC, respectively. The expression plasmids can be obtained commercially from Origene or a similar supplier of expression-ready cDNA clones. Alternatively the plasmids can be sourced from other academic laboratories.
7. The requirement for CERS activity in a given sample can also be confirmed using the well-characterized CERS inhibitor fumonisin B1 [16]. Fumonisin B1 at 10 μM will inhibit product formation [13, 14].
8. One of the common difficulties encountered with TLC is the "smile" effect, whereby the bands on either side of the plate migrate more quickly than those in the center. It is always advisable to leave 2 cm margins on either side of the TLC plate to offset this effect.
9. Normal phase TLC on standard Silica Gel 60 plates is suitable for quantification of reaction products where there is only expected to be a single reaction product formed. If the user wishes to attain better separation of closely related NBD-dhCer

species, such as separation of C16 and C18, or C22 and C24 NBD-dhCer products, we recommend using either HPLC detection or running reverse phase TLC with C18 TLC plates. See for example [17, 18].

10. We do not recommend running the chromatography without formic acid and ammonium formate. Although this will shorten column elution times for the different lipid species, we have found that the absence of the formate produces inconsistent column elution profiles.
11. One should be aware of the potential problem of a different fluorescent yield between the external calibration standard and the NBD-dhSph used for the reaction. This will impact on absolute quantification but will not affect relative quantification. We have previously found that the fluorescent peak areas obtained with NBD-dhSph are 50–60 % of those obtained with C18:0 NBD-dhCer from Avanti Lipids [14].

References

1. Park JW, Park WJ, Futerman AH (2014) Ceramide synthases as potential targets for therapeutic intervention in human diseases. Biochim Biophys Acta 1841(5):671–681
2. Hannun YA, Obeid LM (2011) Many ceramides. J Biol Chem 286(32):27855–27862
3. Chavez JA, Summers SA (2012) A ceramide-centric view of insulin resistance. Cell Metab 15(5):585–594
4. Haughey NJ, Bandaru VV, Bae M, Mattson MP (2010) Roles for dysfunctional sphingolipid metabolism in Alzheimer's disease neuropathogenesis. Biochim Biophys Acta 1801(8): 878–886
5. de la Monte SM (2012) Triangulated mal-signaling in Alzheimer's disease: roles of neurotoxic ceramides, ER stress, and insulin resistance reviewed. J Alzheimers Dis 30(Suppl 2):S231–S249
6. Bieberich E (2008) Ceramide signaling in cancer and stem cells. Future Lipidol 3(3):273–300
7. Narayanaswamy P, Shinde S, Sulc R, Kraut R, Staples G, Thiam CH, Grimm R, Sellergren B, Torta F, Wenk MR (2014) Lipidomic "deep profiling": an enhanced workflow to reveal new molecular species of signaling lipids. Anal Chem 86(6):3043–3047
8. Merrill AH Jr (2011) Sphingolipid and glycosphingolipid metabolic pathways in the era of sphingolipidomics. Chem Rev 111(10): 6387–6422
9. Mizutani Y, Kihara A, Igarashi Y (2005) Mammalian Lass6 and its related family members regulate synthesis of specific ceramides. Biochem J 390(Pt 1):263–271
10. Jennemann R, Rabionet M, Gorgas K, Epstein S, Dalpke A, Rothermel U, Bayerle A, van der Hoeven F, Imgrund S, Kirsch J, Nickel W, Willecke K, Riezman H, Grone HJ, Sandhoff R (2012) Loss of ceramide synthase 3 causes lethal skin barrier disruption. Hum Mol Genet 21(3):586–608
11. Lahiri S, Lee H, Mesicek J, Fuks Z, Haimovitz-Friedman A, Kolesnick RN, Futerman AH (2007) Kinetic characterization of mammalian ceramide synthases: determination of K(m) values towards sphinganine. FEBS Lett 581(27):5289–5294
12. Bose R, Kolesnick R (2000) Measurement of ceramide synthase activity. Methods Enzymol 322:378–382
13. Kim HJ, Qiao Q, Toop HD, Morris JC, Don AS (2012) A fluorescent assay for ceramide synthase activity. J Lipid Res 53(8): 1701–1707
14. Couttas TA, Lim XY, Don AS (2015) A three-step assay for ceramide synthase activity using a fluorescent substrate and HPLC. Lipids 50:101–109
15. Muir A, Ramachandran S, Roelants FM, Timmons G, Thorner J (2014) TORC2-dependent protein kinase Ypk1 phosphorylates ceramide synthase to stimulate synthesis of complex sphingolipids. Elife 3
16. Merrill AH Jr, van Echten G, Wang E, Sandhoff K (1993) Fumonisin B1 inhibits sphingosine (sphinganine) N-acyltransferase and de novo

sphingolipid biosynthesis in cultured neurons in situ. J Biol Chem 268(36):27299–27306

17. Ohno Y, Suto S, Yamanaka M, Mizutani Y, Mitsutake S, Igarashi Y, Sassa T, Kihara A (2010) ELOVL1 production of C24 acyl-CoAs is linked to C24 sphingolipid synthesis. Proc Natl Acad Sci U S A 107(43): 18439–18444
18. Sassa T, Suto S, Okayasu Y, Kihara A (2012) A shift in sphingolipid composition from C24 to C16 increases susceptibility to apoptosis in HeLa cells. Biochim Biophys Acta 1821(7):1031–1037

Chapter 4

Identification of the Interactome of a Palmitoylated Membrane Protein, Phosphatidylinositol 4-Kinase Type II Alpha

Avanti Gokhale*, Pearl V. Ryder*, Stephanie A. Zlatic*, and Victor Faundez

Abstract

Phosphatidylinositol 4-kinases (PI4K) are enzymes responsible for the production of phosphatidylinositol 4-phosphates, important intermediates in several cell signaling pathways. PI4KIIα is the most abundant membrane-associated kinase in mammalian cells and is involved in a variety of essential cellular functions. However, the precise role(s) of PI4KIIα in the cell is not yet completely deciphered. Here we present an experimental protocol that uses a chemical cross-linker, DSP, combined with immunoprecipitation and immunoaffinity purification to identify novel PI4KIIα interactors. As predicted, PI4KIIα participates in transient, low-affinity interactions that are stabilized by the use of DSP. Using this optimized protocol we have successfully identified actin cytoskeleton regulators—the WASH complex and RhoGEF1, as major novel interactors of PI4KIIα. While this chapter focuses on the PI4KIIα interactome, this protocol can and has been used to generate other membrane interactome networks.

Key words Phosphatidylinositol, Phosphatidylinositol kinase, Phosphoinositide, Phospholipid, Endosome, Interactome, Mass spectrometry, Cross-linking

1 Introduction

Phosphatidylinositol 4-kinases (PI4K) have fundamental roles in lipid signaling and membrane trafficking [1–4]. This kinase family is categorized into type II and III members, which are distinguishable by structure, function, and subcellular localization [5, 6]. The focus of this chapter is on the type II family of PI4K. Yeast, flies, and worms express a single isoform of PI4KII, whereas mammals have two isoforms of type II PI4Ks (PI4KIIα, PI4KIIβ) [2, 4, 7]. PI4KIIα is the most abundant membrane-associated PI4K in mammalian cells and is largely found on the trans-Golgi network and

*These authors contributed equally to this work.

Mark G. Waugh (ed.), *Lipid Signaling Protocols*, Methods in Molecular Biology, vol. 1376,
DOI 10.1007/978-1-4939-3170-5_4,

endosomes [8–15]. Importantly, phosphatidylinositol 4 phosphate is also present in Golgi and endosomal membranes [16]. Biochemical and functional studies have demonstrated that PI4KIIα and β have several diverse functions including, but not limited to, regulating endosomal sorting of specific cargo proteins and recruitment of adaptor proteins, signal transduction, and the regulation of synaptic vesicle biogenesis [7, 11, 12, 15]. Mutations in PI4KIIα are implicated in tumorigenesis and spastic paraplegia suggesting that PI4KIIα is an important molecule in pathogenesis mechanisms and therefore an attractive clinical target [13, 17, 18].

To further dissect the precise role of PI4KIIα in cellular pathways we sought to biochemically identify its molecular interactors [19]. One of the major challenges is that PI4KIIα is associated with membranes and there are technical complications associated with isolating a membrane protein interactome. These complications include (1) a relatively low abundance of PI4KIIα as compared to other membrane proteins; (2) the need for detergent solubilization, which may only partially solubilize PI4KIIα or its in vivo interactions; and (3) we predict that PI4KIIα engages in low affinity interactions in dynamic cellular signaling pathways, which potentially excludes the use of stringent methods for the isolation of PI4KIIα network proteomes [20].

Here we describe a method that uses chemical cross-linkers to allow the selective stabilization of transient interactions, thus circumventing the limitations for biochemical isolation [19–24]. This protocol is applied to cells in culture and uses a homobifunctional membrane permeable cross-linker DSP (dithiobis-(succinimidyl propionate)) with a 12 Å spacer arm [25]. DSP cross-links amine-reactive ester groups to bind primary amines such as lysines or the amino acid terminus of proteins. Under denaturing conditions DSP is cleaved by reduction of a disulfide bond present in the molecule. Cross-linking followed by immunoprecipitation and/or immunoaffinity chromatography of proteins of interest (in this case PI4KIIα) with magnetic beads permits the isolation of protein complexes that otherwise would not be amenable to stringent purification techniques. This protocol is typically compatible with regular immunoblot techniques and it can be scaled up for protein identification by quantitative mass spectrometry.

This protocol has been successfully used to construct network proteomes using various cellular baits [19–24]. In particular, we have effectively isolated PI4KIIα and its novel interactors by quantitative immunoaffinity purification from in vivo cross-linked cell lysates [19]. We found that PI4KIIα interacted with proteins involved in actin cytoskeleton polymerization—primarily the WASH complex and RhoGEF1. These interactions were confirmed by alternate biochemical, genetic, and imaging methods [19]. The interactions between PI4KIIα and WASH are particularly interesting since both molecules have been independently implicated in

onset of the neurodegenerative disorder in mice—spastic paraplegia [13, 26]. This newly discovered molecular interaction between PI4KIIα and the WASH subunits could begin to explain the cellular pathways that ultimately lead to the disease phenotype. The method presented here is applicable to any membrane protein anchored by palmitoyl moieties (Fig. 1).

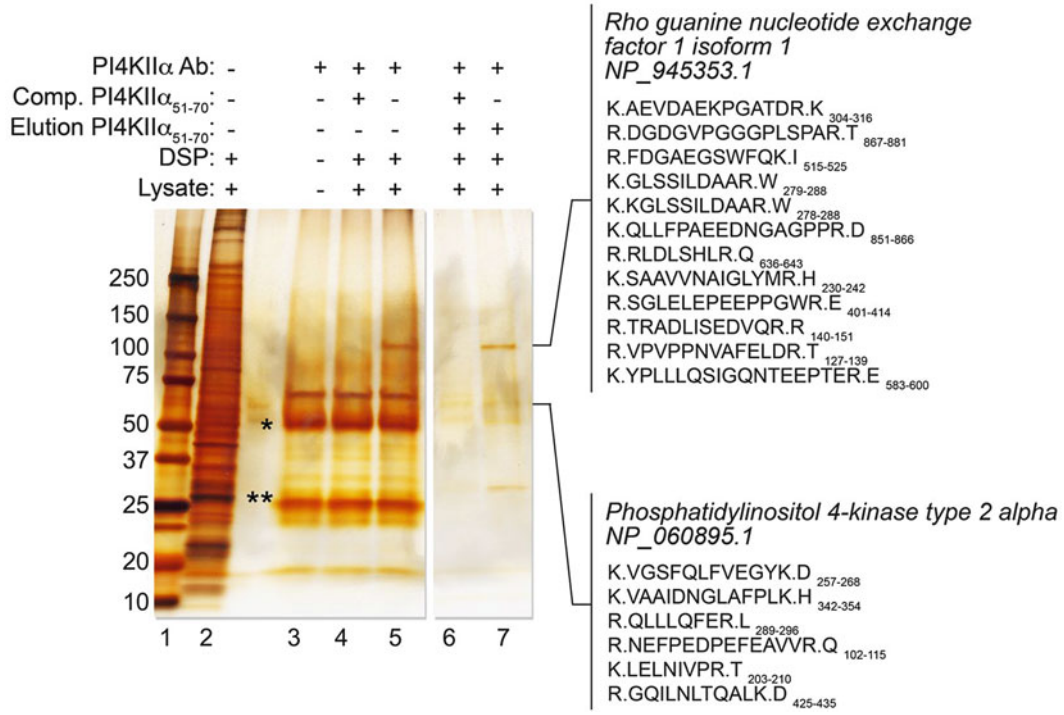

Fig. 1 Silver stain of immunoprecipitation and elution (immunoaffinity precipitation) using PI4KIIα-specific reagents (PI4KIIα antigenic peptide and antibody): **Lane 1**: Molecular weight standard. **Lane 2**: Cross-linked soluble homogenate from SH-SY5Y (ATCC) neuroblastoma cells. **Lane 3**: Immunomagnetic beads incubated only with the PI4KIIα antibody. This negative control predominantly depicts background IgG heavy (**asterisk**) and light (**double asterisk**) bands eluted of the beads when heated with the Laemmli buffer. **Lanes 4** and **5**: Immunoprecipitation with the PI4KIIα antibody. **Lane 4**: Immunoprecipitation with the PI4KIIα antibody in the presence of the excess PI4KIIα peptide. This is an outcompetition control that represents a profile of nonspecific peptides that may bind to the magnetic beads. **Lane 5**: Immunoprecipitation with the PI4KIIα antibody. Note the presence of a prominent band at ~100 kDa in **Lane 5** that is absent from the control **lanes 3** and **4** depicting a putative PI4KIIα specific interactor. Samples in **lanes 4** and **5** and prepared by elution with the Laemmli buffer. **Lanes 6** and **7**: Immunoaffinity purification of PI4KIIα interactors. **Lane 6**: Immunoprecipitation with PI4KIIα with the PI4KIIα antibody in the presence of antigenic peptide for out-competition followed by elution with the excess PI4KIIα peptide. Note the absence of bands in this control. **Lane 7**: Immunoprecipitation followed by elution with the PI4KIIα peptide allowing for selective elution of putative PI4KIIα interacting proteins with low background (compare **lanes 6** and **7** with **lanes 4** and **5**). Note the absence of heavy (**asterisk**) and light (**double asterisk**) IgG chains in **lanes 6** and **7**. MS/MS analysis of the sample in **lane 7** identified highly enriched polypeptides that were absent in all the control samples. The two notable peptides shown here include (a) the PI4KIIα peptide at ~55 kDa as expected and (b) a completely novel PI4KIIα interactor, RhoGEF1, migrating at ~100 kDa seen prominently in **lane 7** as well as **lane 5**

2 Materials

2.1 Cross-Linking and Cell Lysis

1. Phosphate-buffered saline buffer with 0.1 mM $CaCl_2$ and 1 mM $MgCl_2$ (PBS/Ca/Mg). Store at 4 °C (*see* **Note 1**).
2. 10× stock buffer for lysis and immuno-magnetic-precipitation (IP) buffers: 100 mM HEPES, 1.5 M NaCl, 10 mM EGTA, 1 mM MgCl2; pH 7.4. This 10× buffer A solution is diluted to 1× as required.
3. Lysis buffer: 1× Buffer A, 0.5 % Triton X-100 (*see* **Note 2**), Complete Protease Inhibitor Cocktail 4. Stock cross-linking solution: 100 mM solution of DSP. Solution must be prepared fresh every time. Care must be applied to maintain DSP crystal stock free of moisture (*see* **Notes 3-5**).
4. 50× cross-linking quenching solution: 1 M TRIS, pH 7.4. Store at room temperature.

2.2 Immuno-precipitation and Elution (Immunoaffinity Precipitation)

1. Immuno-Magnetic Precipitation Buffer (IP Buffer): 1× Buffer A, 0.1 % Triton X-100. Store at 4 °C.
2. Beads—Dynal magnetic beads.
3. Antibodies and antigenic peptide: PI4KIIα antibody used was raised against the sequence 51-PGHDRERQPLLDRARG AAAQ-70. The antigenic peptide was diluted to a 20 mM stock in 0.5 M MOPS, pH 7.4, and stored at −80 °C. Alternatively, we have used triple FLAG-tagged proteins to purify their interactors [22].
4. Elution buffer: The PI4KIIα peptide was diluted in lysis buffer to a final concentration of 200 μM.

2.3 Analysis of Results

Gel electrophoresis—Samples were resolved by SDS–PAGE electrophoresis, typically using a 4–20 % gel, followed by MS/MS analysis, silver stain, or immunoblotting using the PI4KIIα antibody and antibodies against the identified interacting partners to detect individual proteins (Fig. 1) [19, 22].

3 Methods

3.1 Cross-Linking and Cell Lysis

1. Cells were grown to ~75–90 % confluency and placed directly on ice. The media was aspirated and cells washed twice in ice cold PBS/Ca/Mg buffer.
2. Cells were then incubated either in freshly made DSP cross-linker solution diluted to 1 mM in the PBS/Ca/Mg buffer or a DMSO alone control for 2 h in an ice bath. Gently swirl the solution and ensure all cell monolayer is covered with the DSP solution. Note that there is formation of DSP crystals on the solution yet this is not a concern (*see* **Notes 3-6** below).

3. The cross-linking reaction is quenched by addition of a 25 mM Tris solution for 15 min on ice.
4. Cells were washed twice in ice-cold PBS/Ca/Mg and lysis buffer was added to the cells. Depending on the membrane protein, the lysis buffer may need to be adjusted. Some membrane proteins may need extra salt, ionic detergent, or chaotropic agents. Additionally, sonication of samples may increase the yield of solubilized protein. Cell debris was scraped from the plates and put in Eppendorf tubes and incubated in an end-over-end rotator at 4 °C for 30 min. Lysates were then spun at 16,100 × *g* for 15 min. The supernatant was recovered and diluted to 1 mg/ml for immunoprecipitation.

3.2 Preparation of Beads for Immunoprecipitation

1. 30 μl of the Dynal beads was added to 500 μl of the IP buffer in screw-top microcentrifuge tubes (*see* **Note 7**). To this slurry the PI4KIIα antibody was added to coat the beads. Antibody-free and nonspecific antibody tubes were prepared as negative controls. Additionally PI4KIIα peptide competition controls were included where the PI4KIIα antigenic peptide (final concentration 40 μM) was included in the immunoprecipitation reaction.
2. The tubes were inserted in an end to end rotor for 2 h at room temperature.
3. After 2 h the beads were washed twice in IP buffer.

3.3 Immunoprecipitation and Immunoaffinity Purification

1. 500 μg of the lysate was added to each of the beads coated with antibodies as well as the control beads and the mixture was incubated at 4 °C for 2 h in end to end rotors.
2. After incubation the beads were washed six times for 5 min in the IP buffer. All the washes were done in ice cold conditions with end-over-end rotation at 4 °C.
3. Proteins were then eluted from the beads by heating in Laemmli sample buffer at 75 °C for 5 min (immunoprecipitation, Fig. 1 lane 5). This will elute all IgG from beads and in addition proteins that may bind non-selectively to beads. Elution can also be carried out by incubating with the antigenic peptide for 2 h on ice (immunoaffinity purification, Fig.1 lane 7 compare with lane 5 for the presence of IgGs). In case of the peptide elution the antigenic PI4KIIα peptide was diluted in lysis buffer to a final concentration of 200 μM. This elution protocol completely eliminates bead IgG and non-selectively bound proteins from the sample.
4. Samples were then resolved by SDS-PAGE electrophoresis followed by MS/MS analysis, silver stains, or immunoblotting protocols. We used commercially prepared gels and Laemmli buffer for mass spectrometry studies to minimize contaminants (*see* **Note 8**).

4 Notes

1. The PBS/Ca/Mg buffer should be stored at 4 °C. Calcium and magnesium ions in the PBS buffer are required to maintain adhesion of the cells to the tissue culture plate during the experiment.
2. For preparation of stock 20 % Triton X-100—10 g Triton X-100 is diluted in total volume of 50 ml Milli-Q Water. The stock solution is stored at 4 °C. Do not use and store for more than a month.
3. The DSP cross-linking solution must be made fresh, right before adding it the cells. DSP is highly hydrophobic and is dissolved in DMSO before diluting with warm PBS/Ca/Mg buffer. Warming: PBS/Ca/Mg buffer in a 37 °C water bath prevents precipitation of the DSP crystals [24].
4. Since the cells need to maintain a temperature of 4 °C, the DSP solution should be placed in an ice bath once the DSP is completely solubilized in the warm PBS/Ca/Mg buffer. In the event that DSP is not completely solubilized, significant amounts will precipitate when the solution cools. If this occurs, the solution should be reheated to 37 °C for complete solubilization. If DSP repeatedly precipitates out of solution, fresh DSP solution must be prepared to ensure effective cross-linking. Once DSP is applied to cells in the ice bath it is normal to see the development of a crystalline layer in the wells of DSP treated cells over time. The presence of this layer does not obstruct the cross-linking chemistry in cells [24].
5. 10 μl of the DSP stock solution is added to every 1 ml of warm PBS/Ca/Mg buffer. The DSP stock solution must be added drop wise with repeated mixing until all the DSP has dissolved. A control solution of 10 μl DMSO added to every 1 ml of PBS/Ca/Mg buffer is also used.
6. Volumes required for each plate size.
   (a) 2 ml per well of a 6-well plate.
   (b) 10 ml per plate of a 10 cm plate.
   (c) 20 ml per plate of a 15 cm plate.

   Periodically check if the cells on the plate are fully submerged in the DSP cross-linking solution. If required tap the plate to make sure of even distribution of the cross-linking solution on the plate.
7. Dynal magnetic beads conjugated to sheep anti-rabbit IgG were used to bind the PI4KIIα antibody for isolation of PI4KIIα associated proteins. The use of screw cap microcentrifuge tubes and end-to-end rotators is critical to the protocol.

8. This protocol has been applied to various cell types [19, 21–23]. The number of plates required per experiment is subjective to the goal of the experiment and is dependent upon the yield of total protein the cell type provides. Each standard tube reaction required 500 μg of total protein. Samples from a single tube might be sufficient for identification/confirmation of interactors by western blot analysis. However, for quantitative MS/MS analysis the number of experimental reactions should be increased at least ten times for efficient identification [19, 21–23]. In this latter case the samples are ultimately concentrated to workable volumes by TCA precipitation.

Acknowledgments

This work was supported by grants from the National Institutes of Health (GM077569) and CHOA Children's Center for Neuroscience to V.F. P.V.R. was supported by National Research Service Award Fellowship F31NS0765.

References

1. De Matteis MA, Di Campli A, Godi A (2005) The role of the phosphoinositides at the Golgi complex. Biochim Biophys Acta 1744(3):396–405. doi:10.1016/j.bbamcr.2005.04.013
2. Balla A, Balla T (2006) Phosphatidylinositol 4-kinases: old enzymes with emerging functions. Trends Cell Biol 16(7):351–361
3. Di Paolo G, De Camilli P (2006) Phosphoinositides in cell regulation and membrane dynamics. Nature 443(7112):651–657
4. Tan J, Brill JA (2014) Cinderella story: PI4P goes from precursor to key signaling molecule. Crit Rev Biochem Mol Biol 49(1):33–58. doi:10.3109/10409238.2013.853024
5. Balla T (2013) Phosphoinositides: tiny lipids with giant impact on cell regulation. Physiol Rev 93(3):1019–1137. doi:10.1152/physrev.00028.2012
6. Kim YJ, Hernandez ML, Balla T (2013) Inositol lipid regulation of lipid transfer in specialized membrane domains. Trends Cell Biol 23(6):270–278. doi:10.1016/j.tcb.2013.01.009
7. Wieffer M, Cibrian Uhalte E, Posor Y, Otten C, Branz K, Schutz I, Mossinger J, Schu P, Abdelilah-Seyfried S, Krauss M, Haucke V (2013) PI4K2beta/AP-1-based TGN-endosomal sorting regulates Wnt signaling. Curr Biol 23(21):2185–2190. doi:10.1016/j.cub.2013.09.017
8. Waugh MG, Minogue S, Chotai D, Berditchevski F, Hsuan JJ (2006) Lipid and peptide control of phosphatidylinositol 4-kinase IIalpha activity on Golgi-endosomal Rafts. J Biol Chem 281(7):3757–3763. doi:10.1074/jbc.M506527200
9. Balla A, Tuymetova G, Barshishat M, Geiszt M, Balla T (2002) Characterization of type II phosphatidylinositol 4-kinase isoforms reveals association of the enzymes with endosomal vesicular compartments. J Biol Chem 277(22):20041–20050
10. Barylko B, Gerber SH, Binns DD, Grichine N, Khvotchev M, Sudhof TC, Albanesi JP (2001) A novel family of phosphatidylinositol 4-kinases conserved from yeast to humans. J Biol Chem 276(11):7705–7708
11. Craige B, Salazar G, Faundez V (2008) Phosphatidylinositol-4-kinase type II alpha contains an AP-3 sorting motif and a kinase domain that are both required for endosome traffic. Mol Biol Cell 19:1415–1426
12. Wang YJ, Wang J, Sun HQ, Martinez M, Sun YX, Macia E, Kirchhausen T, Albanesi JP, Roth MG, Yin HL (2003) Phosphatidylinositol 4 phosphate regulates targeting of clathrin adaptor AP-1 complexes to the Golgi. Cell 114(3):299–310
13. Simons JP, Al-Shawi R, Minogue S, Waugh MG, Wiedemann C, Evangelou S, Loesch A, Sihra TS, King R, Warner TT, Hsuan JJ (2009) Loss of phosphatidylinositol 4-kinase 2alpha activity causes late onset degeneration of spinal

cord axons. Proc Natl Acad Sci U S A 106(28):11535–11539. doi:10.1073/pnas.0903011106, 0903011106 [pii]

14. Minogue S, Anderson JS, Waugh MG, dos Santos M, Corless S, Cramer R, Hsuan JJ (2001) Cloning of a human type II phosphatidylinositol 4-kinase reveals a novel lipid kinase family. J Biol Chem 276(20):16635–16640
15. Minogue S, Waugh MG, De Matteis MA, Stephens DJ, Berditchevski F, Hsuan JJ (2006) Phosphatidylinositol 4-kinase is required for endosomal trafficking and degradation of the EGF receptor. J Cell Sci 119(Pt 3):571–581
16. Hammond GR, Machner MP, Balla T (2014) A novel probe for phosphatidylinositol 4-phosphate reveals multiple pools beyond the Golgi. J Cell Biol 205(1):113–126. doi:10.1083/jcb.201312072
17. Li J, Lu Y, Zhang J, Kang H, Qin Z, Chen C (2010) PI4KIIalpha is a novel regulator of tumor growth by its action on angiogenesis and HIF-1alpha regulation. Oncogene 29(17):2550–2559. doi:10.1038/onc.2010.14
18. Qin Y, Li L, Pan W, Wu D (2009) Regulation of phosphatidylinositol kinases and metabolism by Wnt3a and Dvl. J Biol Chem 284(34):22544–22548. doi:10.1074/jbc.M109.014399
19. Ryder PV, Vistein R, Gokhale A, Seaman MN, Puthenveedu M, Faundez V (2013) The WASH complex, an endosomal Arp2/3 activator, interacts with the Hermansky-Pudlak syndrome complex BLOC-1 and its cargo phosphatidylinositol-4-kinase type II alpha. Mol Biol Cell. doi:10.1091/mbc.E13-02-0088
20. Gokhale A, Perez-Cornejo P, Duran C, Hartzell HC, Faundez V (2012) A comprehensive strategy to identify stoichiometric membrane protein interactomes. Cell Logist 2:1–8, doi:http://dx.doi.org/10.4161/cl.22717
21. Gokhale A, Larimore J, Werner E, So L, Moreno-De-Luca A, Lese-Martin C, Lupashin VV, Smith Y, Faundez V (2012) Quantitative proteomic and genetic analyses of the schizophrenia susceptibility factor dysbindin identify novel roles of the biogenesis of lysosome-related organelles complex 1. J Neurosci 32(11):3697–3711. doi:10.1523/JNEUROSCI.5640-11.2012
22. Perez-Cornejo P, Gokhale A, Duran C, Cui Y, Xiao Q, Hartzell HC, Faundez V (2012) Anoctamin 1 (Tmem16A) Ca2+-activated chloride channel stoichiometrically interacts with an ezrin-radixin-moesin network. Proc Natl Acad Sci U S A 109(26):10376–10381. doi:10.1073/pnas.1200174109
23. Salazar G, Zlatic S, Craige B, Peden AA, Pohl J, Faundez V (2009) Hermansky-Pudlak syndrome protein complexes associate with phosphatidylinositol 4-kinase type II alpha in neuronal and non-neuronal cells. J Biol Chem 284(3):1790–1802
24. Zlatic SA, Ryder PV, Salazar G, Faundez V (2010) Isolation of labile multi-protein complexes by in vivo controlled cellular cross-linking and immuno-magnetic affinity chromatography. J Vis Exp 37:1855. doi:10.3791/1855, 1810.3791/1855 [pii]. 1855 [pii]
25. Lomant AJ, Fairbanks G (1976) Chemical probes of extended biological structures: synthesis and properties of the cleavable protein cross-linking reagent [35S]dithiobis(succinimidyl propionate). J Mol Biol 104(1):243–261
26. Blackstone C, O'Kane CJ, Reid E (2011) Hereditary spastic paraplegias: membrane traffic and the motor pathway. Nat Rev Neurosci 12(1):31–42. doi:10.1038/nrn2946, nrn2946 [pii]

Chapter 5

Measurement of Long-Chain Fatty Acyl-CoA Synthetase Activity

Joachim Füllekrug and Margarete Poppelreuther

Abstract

Long-chain fatty acyl-CoA synthetases (ACS) are a family of essential enzymes of lipid metabolism, activating fatty acids by thioesterification with coenzyme A. Fatty acyl-CoA molecules are then readily utilized for the biosynthesis of storage and membrane lipids, or for the generation of energy by ß-oxidation. Acyl-CoAs also function as transcriptional activators, allosteric inhibitors, or precursors for inflammatory mediators. Recent work suggests that ACS enzymes may drive cellular fatty acid uptake by metabolic trapping, and may also regulate the channeling of fatty acids towards specific metabolic pathways. The implication of ACS enzymes in widespread lipid associated diseases like type 2 diabetes has rekindled interest in this protein family. Here, we describe in detail how to measure long-chain fatty acyl-CoA synthetase activity by a straightforward radiometric assay. Cell lysates are incubated with ATP, coenzyme A, Mg^{2+}, and radiolabeled fatty acid bound to BSA. Differential phase partitioning of fatty acids and acyl-CoAs is exploited to quantify the amount of generated acyl-CoA by scintillation counting. The high sensitivity of this assay also allows the analysis of small samples like patient biopsies.

Key words Acyl-CoA synthetase, Fatty acid, Lipid metabolism, Oleic acid, Thioesterification, Fatty acid CoA ligase

1 Introduction

Fatty acyl-CoA synthetases (ACS) are essential enzymes of lipid metabolism found in all organisms throughout the phylogenetic tree of life. The carboxyl group of fatty acids is not very reactive at physiological conditions, but after thioesterification to CoA catalyzed by ACS enzymes it becomes "activated" and enables fatty acid metabolism leading to triglycerides, phospholipids, and other derivatives. The overall reaction is driven forward by the hydrolysis of ATP: $\text{Fatty acid} + \text{ATP} + \text{CoA} \longrightarrow \text{Fatty acyl-CoA} + \text{AMP} + \text{PPi}$. ACS enzymes are commonly subdivided depending on the hydrocarbon chain length of their fatty acid substrates: short chain ACS (ACSS; C2–C4), medium chain ACS (ACSM; C6-C10), long-chain ACS (ACSL; C12-C20), and very long-chain ACS (ACSVL;

Mark G. Waugh (ed.), *Lipid Signaling Protocols*, Methods in Molecular Biology, vol. 1376,
DOI 10.1007/978-1-4939-3170-5_5,

C12–C20, and >C20). ACSL and ACSVL enzymes have been studied widely because their substrates are the physiologically most abundant long-chain fatty acids: C16 (palmitate) and C18 (stearate, oleate, linoleate). "While the systematic name for these ACS enzymes according to the Enzyme Commission is Long-chain-fatty-acid–CoA ligase (EC 6.2.1.3), researchers using mammalian model systems have agreed to use the ACSL nomenclature (e.g., ACSL3 = acyl-CoA synthetase long-chain family member 3); ACSVL enzymes are also called FATP/SLC27A proteins [1–3]. The 13 mammalian long-chain ACS enzymes differ in their tissue expression pattern, transcriptional regulation, substrate specificity, and subcellular localization [4, 5]. Alternative splicing generates further isoforms [6].

Since ACS enzymes are essential for fatty acid and lipid metabolism it is not surprising that they have been implicated in serious and widespread metabolic diseases like type 2 diabetes and atherosclerosis [7]. Fatty acyl-CoAs are metabolic precursors for the biosynthesis of neutral storage lipids and membrane phospholipids as well as for the carnitine esters which are destined for ß-oxidation. Apart from these major metabolic pathways, acyl-CoAs are also regulatory molecules serving as transcriptional regulators and allosteric inhibitors [5, 8]. In addition, arachidonate activating enzymes like ACSL4 are involved in the regulation of eicosanoid biosynthesis [9]. ACS enzymes themselves are under transcriptional regulation especially by nutritional cues [10]; the research on their acute regulation by posttranslational modifications is just beginning [11, 12].

Free fatty acids may traverse membranes either by diffusion or facilitated by proteins [13]; however fatty acyl-CoAs are too polar and therefore membrane-impermeable. Consequently, ACS enzymes have also been implicated in driving cellular fatty acid uptake by metabolic trapping [14–16]. Another intriguing function of ACS enzymes may be the preferential channeling of fatty acids towards a specific metabolic pathway, which would be dependent on the corresponding ACS enzyme and its subcellular localization [5, 17].

To determine the ACS activity for a particular fatty acid, cell lysates (or protein preparations) are incubated together with ATP, coenzyme A, and radiolabeled fatty acid bound to BSA in the presence of the essential cofactor Mg^{2+}. The readout relies on the difference in polarity between the fatty acid substrate and the fatty acyl-CoA product: unreacted fatty acids are extracted with organic solvent, and the remaining fatty acyl-CoA in the aqueous phase is quantified by scintillation counting. Alternative methods appear to be lab specific and have not found widespread use. While the use of radiolabeled reagents is not strictly required, concentrations can be determined with high accuracy and unsurpassed sensitivity. A cell lysate containing 10 µg of total protein corresponding to about 10 ng of ACS enzymes is usually sufficient for one reaction, enabling also the analysis of small unique samples (e.g., patient biopsies).

While some cell types feature a dominant acyl-CoA synthetase, most cells express several ACS enzymes at significant levels at the same time. Therefore the knockout/knockdown of a particular ACS enzyme may not be reflected in the total cellular ACS activity. Vice versa, it may be difficult to assign a change in total cellular enzyme activity to a specific ACS protein. Detailed analysis is feasible by measuring the activity of immunopurified ACS enzymes [11, 18, 19].

Oleate and palmitate are most often used as substrates, based on their nutritional relevance and general abundance. However, it is important to bear in mind that substrate specificities for a particular fatty acid may vary widely between different ACS enzymes. For instance, overexpression of FATP4/ACSVL5 may increase the oleoyl-CoA synthetase activity severalfold but would not significantly change the ACS activity towards arachidonate (J.F., unpublished).

2 Materials

2.1 Assay Master Mix Components

1. 1 M Tris–HCl pH 7.4 buffer: Dissolve 12.1 g of Tris base (Tris(hydroxymethyl)aminomethane) in 50 ml of water and titrate with HCl to pH 7.4. Make up with water to 100 ml.
2. 1 M $MgCl_2$: Dissolve 0.203 g of magnesium chloride hexahydrate in 500 µl of water and make up to 1.0 ml (*see* **Note 1**).
3. 0.1 M DTT: Dissolve 0.154 g of DL-dithiothreitol in 1.0 ml of water; dilute this 1/10 to obtain 0.1 M DTT. Store at –20 °C.
4. 0.1 M ATP: Dissolve 0.551 g of ATP disodium salt in 7 ml of water. Titrate with 1 M NaOH to pH 7.0 (use pH paper) and make up to 10 ml. Store 1 ml aliquots at –20 °C.
5. 10 % [w/v] TX-100: Dissolve 1.0 g of Triton X-100 (TX-100) in water by stirring, adjust to 10 ml and store at 4 °C.
6. 20 mM Coenzyme A stock solution: Dissolve 10 mg of Coenzyme A sodium salt in 650 µl water. Freeze 50 µl aliquots at –20 °C.

2.2 Fatty Acid Labeling Mix

1. TBS: Prepare 100 ml of Tris buffered saline (TBS; 20 mM Tris–HCl pH 7.4, 130 mM NaCl) by adding 2.0 ml 1 M Tris–HCl pH 7.4 (*see* above Subheading 2.1) and 2.6 ml of 5 M NaCl to 90 ml water; make up to 100 ml and store at 4 °C.
2. 200 µM FAF-BSA: Dissolve 0.132 g of fatty acid free BSA in 10 ml of TBS by gentle stirring. Avoid excessive foaming. Freeze 1 ml aliquots at –20 °C. Thaw by gentle shaking at 37 °C.
3. 10 mM NaOH: Mix 10 µl of 1 M NaOH with 990 µl of water.

4a. 2.0 µg/µl (7.1 mM) **oleic acid** stock solution: Oleic acid is stored at –20 °C. Place at RT for 15 min for temperature equilibration and melting of the oleic acid. Dilute 2.4 µl of

oleic acid into 1.0 ml of chloroform (*see* **Note 2**). Overlay with a gentle stream of nitrogen and store at –20 °C (*see* **Note 4**).

4b. 5 mM **arachidonic acid** stock solution: Arachidonic acid is stored at –20 °C. Place at RT for 15 min for temperature equilibration. Dilute 5.4 µl of arachidonic acid into 3.28 ml of ethanol. Overlay with a gentle stream of nitrogen and store at –20 °C.

5a. [**14C**]**oleic acid**: This is 0.1 µCi/µl in ethanol, with a specific activity of 40–60 Ci/mol (*see* **Note 3**). Store at –20 °C. Before opening, let container equilibrate to RT. After withdrawing the required amount, gently overlay with nitrogen and put back at –20 °C (*see* **Note 4**).

5b. [**14C**]**arachidonic acid**: This is 0.1 µCi/µl in ethanol, with a specific activity of 40–60 Ci/mol. Store at –20 °C. Before opening, let container equilibrate to RT. After withdrawing the required amount, gently overlay with nitrogen and put back at –20 °C. Arachidonic acid is especially prone to oxidation. It makes sense to dispense for example 10 % of the total supplied amount into a separate glass vial, and use this as a working aliquot, thus avoiding having to open the original container too often.

2.3 ACS Assay and Scintillation Counting

1. KTx lysis buffer (130 mM KCl, 20 ml Tris–HCl pH 7.4, 1.0 % [w/v] TX-100): Prepare 50 ml by adding 2.17 ml of 3 M KCl, 1.0 ml of 1 M Tris–HCl pH 7.4 (*see* above **step 1** of Subheading 2.1) and 5.0 ml of 10 % [w/v] TX-100 (*see* above **step 5** of Subheading 2.1) to 40 ml of water. Make up to 50 ml and store at 4 °C.
2. Dole's solution: Prepare 510 ml of this reagent by mixing 400 ml isopropanol, 100 ml heptane, and 10 ml of concentrated sulfuric acid (H_2SO_4; *see* **Note 5**).
3. Assay tubes: organic solvent resistant, safe-lock, 2.0 ml tubes.
4. Liquid scintillation cocktail.

3 Methods

3.1 Preparation of the Lysate

Volumes are given for tissue culture cells grown close to confluency on a surface area of 10 cm^2 (one well of a standard 6-well plate), corresponding to approximately one million cells. For tissues *see* **Note 6**.

1. Remove culture medium and wash 2× with phosphate buffered saline (PBS). Add 1.0 ml of ice-cold PBS and scrape cells with a rubber policeman. Transfer cell suspension to a microcentrifuge tube and spin for 5 min at 1000 × *g* and 4 °C. Remove

supernatant and proceed either to **step 2** or freeze the pellet for later analysis at −80 °C.

2. Resuspend cell pellet gently with 200 µl of ice-cold KTx lysis buffer, avoiding excessive foaming. Place on ice for 30 min.
3. Spin for 5 min at 10,000 × *g* and 4 °C, and transfer 180 µl of the supernatant into a fresh tube on ice (*see* **Note 7**).

3.2 Fatty Acid Labeling Mix

The fatty acid labeling mix is fivefold concentrated and contains 100 µM oleate/arachidonic acid bound to 25 µM BSA in TBS; the specific activity is 10 Ci/mol. The following amounts are for six different samples measured in triplicate, including a control without CoA (66 µl of labeling mix are needed for each sample). Efficient solubilization of the fatty acid is essential for the ACS assay (*see* **Note 8**).

1a. [**14C**]**oleate labeling mix**: Pipet 6.5 µl of 7.1 mM oleic acid stock solution and 4.6 µl of [^{14}C]oleic acid into a safe-lock microcentrifuge tube. Evaporate solvents with a gentle stream of nitrogen. Add 5.5 µl of 10 mM NaOH to the residue and pipette up and down until bubbles are forming (*see* **Note 9**). Add 57.8 µl of 200 µM BSA and mix again by pipetting. Add 403 µl of TBS and put at 37 °C with gentle shaking for 30 min.

1b. [**14C**]**arachidonic acid labeling mix**: Saturate BSA and TBS solutions with nitrogen (*see* **Note 10**). Pipet 9.2 µl of 5 mM arachidonic acid stock solution and 4.6 µl of [^{14}C]arachidonic acid into a safe-lock microcentrifuge tube. Evaporate solvents with a gentle stream of nitrogen. Add 57.8 µl of 200 µM BSA and mix thoroughly by pipetting. Add 408 µl of TBS and put at 37 °C with gentle shaking for 30 min.

3.3 ACS Assay Cocktail

The following amounts are for six different samples measured in triplicate, including a control without CoA also measured in triplicate. Reagents are equilibrated to RT first.

1. In a 50 ml polypropylene tube, put 1.09 ml of water. Add sequentially 231 µl of 1 M Tris–HCl pH 7.4, 11.6 µl of 1 M $MgCl_2$, 4.6 µl of 0.1 M DTT, 231 µl of 0.1 m ATP, and 23.1 µl of 10 % [w/v] TX-100. Mix and add the fatty acid labeling mix prepared above. Mix again by pipetting.
2. Remove 3× 89 µl into separate 2 ml safe-lock tubes for the minus CoA controls.
3. Add 21.6 µl of 20 mM CoA to the remaining cocktail. Mix again by pipetting.
4. Remove 3× 20 µl for scintillation counting.
5. Keep at RT until use.

3.4 Acyl-CoA Synthetase Assay

The enzyme reaction is started by adding 90 µl of ACS assay cocktail to 10 µl of cell lysate (*see* **Note 11**), and immediate transfer to a 30 °C heating block. We prefer to process the samples sequentially, with a time window of 15 s between each addition of the assay cocktail to the samples. The standard incubation time at 30 °C is 10 min.

1. For each sample prepared in Subheading 3.1, pipette 3× 10 µl into separate 2 ml safe-lock tubes. Keep on ice.
2. Select three different samples for the minus CoA controls. Add 10 µl of lysate to the first minus CoA control tube (prepared in **step 2** of Subheading 3.3) and place at 30 °C ($t = 0$ s). Add 10 µl of lysate to the second minus CoA control tube and place at 30 °C ($t = 15$ s). Third minus CoA control ($t = 30$ s).
3. Take first sample aliquot (pipetted in **step 1**), add 90 µl of ACS assay cocktail and place immediately at 30 °C ($t = 45$ s). Repeat until all samples are at 30 °C.
4. Take the first tube and stop the reaction by adding 600 µl of Dole's solution ($t = 10{:}00$ min). Remove second tube and add 600 µl of Dole's solution ($t = 10{:}15$ min). Repeat until all samples are done.
5. To each tube, add 250 µl of water and 400 µl of heptane. Mix thoroughly by vortexing. Spin for 1 min with 13,000 × *g* at RT to accelerate phase separation.
6. Remove most of the upper organic phase, but do not aspirate the interphase.
7. Add 600 µl of heptane, vortex vigorously, and spin for 1 min at RT with 13,000 × *g*. Remove the upper organic phase but leave the interphase. Repeat three more times (*see* **Note 12**).
8. Aspirate interphase. Mix 200 µl of the aqueous bottom phase with 4 ml of liquid scintillation cocktail by vigorous vortexing. Put scintillation vials into a liquid scintillation counter and measure cpm together with the three 20 µl aliquots of the ACS assay cocktail (**step 4** of Subheading 3.3).

3.5 Calculation of the Enzyme Activity

1. Protein concentration: The amount of protein present in the cell lysates is determined by the bicinchoninic acid assay (BCA assay). 5 µl of KTx cell lysate is usually sufficient; we use BSA for the calibration curve (*see* **Note 13**). For the calculation below, take the total amount of protein present in the reaction tube (= *b* µg).
2. Fatty acid in the ACS assay cocktail: Each tube receives 90 µl of the assay cocktail which corresponds to 1800 pmol of fatty acid. The radioactivity present in 90 µl of the assay cocktail is calculated based on the three 20 µl aliquots: the cpm values are averaged and multiplied by 4.5 (90 µl /20 µl) to give the total

cpm for each tube. 1800 pmol of fatty acid divided by the total cpm in each tube gives the pmol corresponding to one cpm (= *n* pmol/cpm).

3. Total cpm of the aqueous phase, corresponding to fatty acyl-CoA: The average of the three minus CoA controls is subtracted from the measured cpm values of the samples (200 µl are counted). Multiply this by 3 (because the total aqueous phase is 600 µl; = *x* cpm).
4. Specific fatty acyl-CoA synthetase activity: *n* pmol/cpm × *x* cpm/b µg/10 min. The final units are pmol fatty acyl-CoA/min/µg protein (*see* **Note 14**).
5. The average and the standard deviation (SD) of the triplicate measurements are calculated for each sample separately. With some practice, the SD is less than 5 % of the average value. Measurements should be repeated if the SD is higher than 10 % of the average.
6. Expected values: Oleoyl-CoA synthetase activity ranges from 0.5 to 5.0 pmol/min/µg protein for wildtype tissue culture cells, with hepatoma cells (e.g., HuH-7) showing higher activity than either epithelial (e.g., COS) or epidermal cells (e.g., A431) (*see* **Note 15**).

4 Notes

1. Magnesium 2+ is a cofactor for acyl-CoA synthetases. Therefore, phosphate buffers are avoided throughout the protocol as they would compromise the solubility of Mg^{2+} ions.
2. Chloroform has a boiling point of 61 °C, and significant amounts evaporate at RT. This causes dripping from the pipette tip, which is especially awkward when handling radioactive reagents. To avoid dripping, pipette up and down a few times until the air above the liquid chloroform in the pipette is saturated (or use a reverse pipette). Chloroform is also an efficient solvent: plastic pipette tips and safe-lock tubes are generally fine; however notable exceptions are tissue culture plasticware and Falcon centrifuge tubes which are partially dissolved. Use glassware whenever possible.
3. Reagents containing Carbon-14 do not pose a significant external radiation hazard since the energy of the emitted ß particles is low. Nevertheless, minimize handling and know exactly what you need to do (as always). Follow local regulations concerning work with isotopes and disposal procedures. Fatty acids containing Hydrogen-3 may also be used for the ACS assay. Generally, these are cheaper but emit ß particles of even lower energy than Carbon-14. This does not compromise the

ACS assay but limits applicability for other techniques like thin layer chromatography.

4. Fatty acids containing double bonds are sensitive to oxidation; this increases exponentially with the number of double bonds present. Nitrogen is heavier than oxygen and displaces the air above the reagent. Nitrogen is also dissolved in water and organic solvents, replacing the (invisible) air which is always present. Control the stream of nitrogen carefully to avoid spraying, and do not over-apply since volatile solvents would evaporate.
5. Concentrated sulfuric acid is highly corrosive. Wear protective gloves and clothing, and do not leave any remains anywhere. Heptane and isopropanol are organic solvents; use glassware whenever possible. *See* also **Note 2** above.
6. Tissue samples need to be homogenized by your method of choice so that the lysis buffer efficiently solubilizes the ACS enzymes. Cryostat sections of unfixed tissue worked well in our hands.
7. We did not observe significant differences in ACS enzyme activity when comparing pellets frozen at −80 °C with cells immediately lysed and assayed. However, once the cells have been lysed they cannot be frozen again; likewise prolonged incubation of the lysate at 37 °C would lead to loss of enzyme activity.

   Endogenous or overexpressed mammalian ACS enzymes from tissue culture cells (we thoroughly tested FATP1, FATP4, ACSL1, ACSL3, and ACSL4) are efficiently solubilized by the KTx lysis buffer on ice. If in doubt, the dominant/overexpressed ACS enzyme may be assessed for solubilization by Western blotting. For this, the pellet of detergent-resistant material obtained in Subheading 3.1, **step 3** is washed once with KTx buffer and then boiled in 200 µl of SDS-PAGE sample buffer. The equivalent amount of supernatant is boiled together with half the volume of 4× SDS-PAGE sample buffer (8 % [w/v] SDS, 250 mM Tris–HCl pH 6.8, 40 % [v/v] glycerol, 400 mM ß-mercaptoethanol).

   The concentration of TX-100 may influence the activity of recombinant ACS enzymes [18]. If this is a concern, alternatives to TX-100 solubilization are freeze/thawing (4 cycles of freezing in liquid nitrogen and rapid thawing), or homogenization by shearing (e.g., repeated passage of the cell suspension through a G25 or G27 needle).
8. In the protocol described here, fatty acids are rendered soluble by binding to BSA, mimicking fatty acids in serum. Saturated fatty acids like palmitate may be heated first with NaOH to achieve better solubilization. Cyclodextrins have also been

employed for solubilization, especially for very long-chain fatty acids (e.g., C24:0 lignocerate; [20]). The unbound concentrations of fatty acids (only these are relevant for the ACS enzymes) in the assay cocktail are not known; they are assumed to vary widely between different fatty acids, depending on hydrocarbon chain length and degree of unsaturation. Therefore, ACS activities measured for different fatty acids are not directly comparable.

9. The reaction of NaOH with fatty acids is the classical saponification: the resulting fatty acid anions are amphipathic and have therefore a much higher solubility than the protonated fatty acids, greatly aiding in the binding to BSA. NaOH should not be used for polyunsaturated fatty acids (e.g., arachidonic acid).
10. Saturation of buffers is most efficiently done by first degassing solutions under vacuum, and then using a stream of nitrogen. Avoid excessive foaming of the BSA solution.
11. The final concentrations in the assay tube are: 100 mM Tris–HCl pH 7.4, 5 mM $MgCl_2$, 200 μM DTT, 10 mM ATP, 20 μM fatty acid at 10 Ci/mol bound to 5 μM BSA, 200 μM CoA, 0.2 % [w/v] TX-100 (0.1 % from the ACS assay cocktail, and 0.1 % if 10 μl sample lysate are used). The 10 μl sample lysate also adds 13 mM KCl and 2.5 mM Tris–HCl pH 7.4 (slightly modified based on ref. 19). The recipe for the ACS assay cocktail contains 10 % more volume than actually needed.
12. For the initial assays, it makes sense to monitor the removal of unreacted oleate by measuring the radioactivity of the heptane fractions (the upper organic phase) during the extractions; the last two heptane fractions should contain only 10–20 cpm/100 μl (10 cpm is background environmental radioactivity). If this is fine, aspiration of the upper heptane phase with a sucking device is more convenient than pipetting. Take care that the tubing is compatible with organic solvents, and of course the supernatant qualifies still as radioactive waste.

    For the initial assays, determine the amount of aqueous phase left after the heptane extractions (pipette aqueous phase completely into a fresh tube and balance; differences in weight should not be larger than ±10 %).

    An alternative to the extraction of unreacted fatty acid with organic solvents is the application of thin layer chromatography to separate fatty acids from acyl-CoA. The respective signals may then be quantified with a phosphorimager. However, we found this approach to be less accurate and more laborious. Nevertheless, it is the method of choice for short chain fatty acids which differ not sufficiently in their polarity from the corresponding acyl-CoA.
13. The BCA assay is compatible with detergents, unlike the Bradford assay. Nevertheless, it is mandatory that the BSA

used for calibration has the same ion and detergent concentration as the sample (KTx lysis buffer). Bear in mind that the protein amount determined correlates with proteins which are soluble in *TX-100 on ice* and does not equal the total amount of protein originally present.

14. Fatty acids are together with ATP and CoA the substrates in this enzyme assay. ATP and CoA are water soluble and are at high concentrations, and therefore not limiting. However, if the ACS enzyme activity of the lysate is very high (i.e., too much material), the supplied fatty acid may be limiting. As a rule of thumb, if the cpm obtained in the aqueous phase (fatty acyl-CoA) are more than 25 % of the total cpm (fatty acid supplied), the enzyme activity is going to be underestimated. Dilute your sample and repeat. 5–15 μg of total TX-100 soluble protein is usually sufficient (corresponding to about 50,000 cells).

The cpm values obtained for the minus CoA controls should be less than 30 % of the signal obtained with the real samples. Higher values usually indicate partially degraded and/or oxidized [^{14}C]fatty acids.

15. We have mostly used cell lines which were manipulated for their ACS enzyme content by stable overexpression or RNAi depletion of specific ACS enzymes. Assaying the total cellular lysate is therefore strictly speaking an *indirect* measure of the ACS enzyme in question. It is equally possible if more demanding to purify/enrich specific ACS enzymes, using general membrane protein purification or immunoaffinity techniques [11, 18, 19, 21].

Acknowledgements

This work was supported by DFG Grants FU 340/7-1 (to J.F.) and PO 1767/3-1 (to M.P.). We gratefully acknowledge Ina Feldhoffer and Svenja Sliwinski from our lab who did the cross-reading from a student's perspective.

References

1. Watkins PA, Maiguel D, Jia Z, Pevsner J (2007) Evidence for 26 distinct acyl-coenzyme A synthetase genes in the human genome. J Lipid Res 48(12):2736–2750
2. Mashek DG, Bornfeldt KE, Coleman RA, Berger J, Bernlohr DA, Black P, DiRusso CC, Farber SA, Guo W, Hashimoto N, Khodiyar V, Kuypers FA, Maltais LJ, Nebert DW, Renieri A, Schaffer JE, Stahl A, Watkins PA, Vasiliou V, Yamamoto TT (2004) Revised nomenclature for the mammalian long-chain acyl-CoA synthetase gene family. J Lipid Res 45(10):1958–1961
3. Watkins PA (2008) Very-long-chain acyl-CoA synthetases. J Biol Chem 283(4):1773–1777. doi:10.1074/jbc.R700037200

4. Pérez-Chacón G, Astudillo AM, Balgoma D, Balboa MA, Balsinde J (2009) Control of free arachidonic acid levels by phospholipases A2 and lysophospholipid acyltransferases. Biochim Biophys Acta 1791(12):1103–1113
5. Grevengoed TJ, Klett EL, Coleman RA (2014) Acyl-CoA metabolism and partitioning. Annu Rev Nutr. doi:10.1146/annurev-nutr-071813-105541
6. Soupene E, Kuypers FA (2008) Mammalian long-chain acyl-CoA synthetases. Exp Biol Med 233(5):507–521
7. Li LO, Klett EL, Coleman RA (2009) Acyl-CoA synthesis, lipid metabolism and lipotoxicity. Biochim Biophys Acta 1801(3):246–251
8. Faergeman NJ, Knudsen J (1997) Role of long-chain fatty acyl-CoA esters in the regulation of metabolism and in cell signalling. Biochem J 323(Pt 1):1–12
9. Golej DL, Askari B, Kramer F, Barnhart S, Vivekanandan-Giri A, Pennathur S, Bornfeldt KE (2011) Long-chain acyl-CoA synthetase 4 modulates prostaglandin E2 release from human arterial smooth muscle cells. J Lipid Res 52(4):782–793. doi:10.1194/jlr.M013292
10. Mashek DG, Li LO, Coleman RA (2006) Rat long-chain acyl-CoA synthetase mRNA, protein, and activity vary in tissue distribution and in response to diet. J Lipid Res 47(9):2004–2010
11. Digel M, Staffer S, Ehehalt F, Stremmel W, Ehehalt R, Füllekrug J (2011) FATP4 contributes as an enzyme to the basal and insulin-mediated fatty acid uptake of C2C12 muscle cells. Am J Physiol Endocrinol Metab 301(5):E785–E796
12. Smith ME, Saraceno GE, Capani F, Castilla R (2013) Long-chain acyl-CoA synthetase 4 is regulated by phosphorylation. Biochem Biophys Res Commun 430(1):272–277. doi:10.1016/j.bbrc.2012.10.138, http://dx.doi.org/
13. Kampf JP, Kleinfeld AM (2007) Is membrane transport of FFA mediated by lipid, protein, or both? Physiology (Bethesda) 22:7–14
14. Milger K, Herrmann T, Becker C, Gotthardt D, Zickwolf J, Ehehalt R, Watkins PA, Stremmel W, Füllekrug J (2006) Cellular uptake of fatty acids driven by the ER-localized acyl-CoA synthetase FATP4. J Cell Sci 119(Pt 22):4678–4688
15. Black PN, DiRusso CC (2003) Transmembrane movement of exogenous long-chain fatty acids: proteins, enzymes, and vectorial esterification. Microbiol Mol Biol Rev 67(3):454–472
16. Füllekrug J, Ehehalt R, Poppelreuther M (2012) Outlook: membrane junctions enable the metabolic trapping of fatty acids by intracellular acyl-CoA synthetases. Front Physiol 3:401. doi:10.3389/fphys.2012.00401
17. Digel M, Ehehalt R, Stremmel W, Füllekrug J (2009) Acyl-CoA synthetases: fatty acid uptake and metabolic channeling. Mol Cell Biochem 326(1-2):23–28. doi:10.1007/s11010-008-0003-3
18. Kim J-H, Lewin TM, Coleman RA (2001) Expression and characterization of recombinant rat acyl-CoA synthetases 1, 4, and 5. Selective inhibition by triacsin C and thiazolidinediones. J Biol Chem 276(27):24667–24673
19. Hall AM, Smith AJ, Bernlohr DA (2003) Characterization of the acyl-CoA synthetase activity of purified murine fatty acid transport protein 1. J Biol Chem 278(44):43008–43013
20. Coe NR, Smith AJ, Frohnert BI, Watkins PA, Bernlohr DA (1999) The fatty acid transport protein (FATP1) is a very long chain acyl-CoA synthetase. J Biol Chem 274(51):36300–36304
21. Uchida Y, Kondo N, Orii T, Hashimoto T (1996) Purification and properties of rat liver peroxisomal very-long-chain acyl-CoA synthetase. J Biochem (Tokyo) 119(3):565–571

Chapter 6

Qualitative and Quantitative In Vitro Analysis of Phosphatidylinositol Phosphatase Substrate Specificity

Laura Ren Huey Ip and Christina Anja Gewinner

Abstract

Phosphoinositides compromise a family of eight membrane lipids which play important roles in many cellular signaling pathways. Signaling through phosphoinositides has been shown in a variety of cellular functions such cell proliferation, cell growth, apoptosis, and vesicle trafficking. Phospholipid phosphatases regulate cell signaling by modifying the concentration of phosphoinositides and their dephosphorylated products. To understand the role of individual lipid phosphatases in phosphoinositide turnover and functional signaling, it is crucial to determine the substrate specificity of the lipid phosphatase of interest. In this chapter we describe how the substrate specificity of an individual lipid phosphatase can be qualitatively and quantitatively measured in an in vitro radiometric assay. In addition, we specify the different expression systems and purification methods required to produce the necessary yield and functionality in order to further characterize these enzymes. The outstanding versatility and sensitivity of this assay system are yet unmatched and are therefore currently considered the standard of the field.

Key words Phosphatidylinositol, Inositol-polyphosphate-4-phosphatase type II, PTEN, PI-3 kinase, Lipid phosphatase assay, Cell signaling, Phosphorylation, Enzyme assay, Thin-layer chromatography, Phosphoinositide, GST-pull-down assay, Insect cell culture, Mammalian overexpression system

1 Introduction

Phospholipids play multiple roles in cells such as forming the permeability barrier of the cell membrane and intracellular organelles, as well as providing the supporting matrix and surface for many catalytic processes. In addition, phospholipids actively participate in signaling processes in response to external and internal stimuli. In their function as signal transducers they can be hydrolyzed to produce products that function as second messengers in cellular systems. Besides the classical signaling transduction that occurs at the cell surface, phospholipids also harbor additional functions including regulation of membrane trafficking, the cytoskeleton, permeability and transport functions, as well as nuclear events [1–4].

Mark G. Waugh (ed.), *Lipid Signaling Protocols*, Methods in Molecular Biology, vol. 1376,
DOI 10.1007/978-1-4939-3170-5_6,

Phosphatidylinositol is a class of phospholipid which when phosphorylated results in phosphoinositides. These phosphoinositides initiate various responses that result in cellular growth, cell cycle entry, cell migration, and cell survival. Disruptions of this crucial signaling pathway have been linked to conditions such as cancer, inflammatory disease, obesity, and diabetes [5–7]. Phosphoinositide metabolism is strictly controlled in cells by the action of specific lipid kinases and lipid phosphatases. In general, phosphorylation occurs at two sites within the cell. Mono-phosphorylations of most phosphatidylinositols by Class II phosphoinositol-4-kinase (PI4K) and Class III PI3K occur in endomembranes, such as the endosomes and the Golgi network [8, 9]. Phosphorylation of PI(4)P to PI(4,5)P_2 by phosphatidylinositol-4-phosphate 5-kinase (PIP5K) and further phosphorylation to PIP_3 by class I phosphatidylinositol 3-kinases (PI3Ks) occurs primarily at the plasma membrane [10, 11]. Phosphoinositides have also been found in the nucleus, and their functions encompass many aspects of transcription, chromatin remodeling, and mRNA maturation [8].

The inositol head group of phosphatidylinositol can be reversibly phosphorylated to generate seven different species, which play a fundamental role in mediating membrane-cytosol interactions [12, 13]. Once phosphorylated, phosphoinositides attract specific proteins with a binding domain for phosphatidylinositols [14]. Phosphorylation status of phosphoinositides can be changed by phosphoinositide kinases, phosphoinositide phosphatases and hydrolysis by phosphoinositide-specific phospholipase C enzymes (PLCs) [12, 15–17]. While some of the phosphoinositide phosphatases remove phosphate groups located in a specific position on the inositol ring, others, mainly those that dephosphorylate monophosphorylated phosphoinositides, possess functional specificity related to phosphoinositide localization. In the case of the PI3K/Akt signaling pathway negative regulation is conducted by three major phosphatases, by the catalytic function of the tumor suppressor PTEN, which dephosphorylates PI-3,4,5 P_3 (PIP_3) to PI-4,5 P_2 [18]; the hematopoietic-restricted SH2 containing inositol 5′-phosphatase 1 and 2 (SHIP1/2) which hydrolyze PIP_3 to PI-3,4 P_2 [19]; and the inositol polyphosphate 4-phosphatase type II (INPP4B) which hydrolyzes PI-3,4 P_2, to PI-3 P [20, 21].

Over the last decade, the number of cellular processes known to be directly or indirectly controlled by phospholipids has dramatically expanded. However, due to the large number of phospholipids, their highly active metabolism, and our lack of understanding of protein-lipid specificity, phospholipid signaling remains a challenge to study [22, 23]. The overall complexity of phosphoinositide signaling emphasizes the need for methodology that allows detailed characterization of phospholipid kinases and phosphatases and their regulation of cellular phosphoinositide levels. To determine substrate specificity of individual phospholipid

phosphatases that may otherwise be too challenging to identify in vivo, the protocols described here can be employed to quantify phospholipid phosphatase activity of choice in vitro. In this chapter we additionally describe three overexpression systems used to obtain high yields of functional lipid phosphatases and depict how substrate specificity of lipid phosphatases can be determined and quantified using radiolabeling assays.

2 Materials

All solutions should be prepared with ultrapure water and analytical grade reagents.

2.1 Lipid Phosphatase Protein Expression and Purification Systems

2.1.1 Transient Expression in Mammalian Cells and Enrichment by Immunoprecipitation

1. Cell lysis buffer of choice: A widely used lysis buffer consists of 20 mM Tris–HCl, pH 7.5, 150 mM NaCl, and 1 % Triton-X100. Store lysis buffer at 4 °C. Just before use add Complete protease inhibitors (Roche diagnostics) or add 1 mM benzamidine, 1 μM aprotinin, 1 μM leupeptin, and 1 mM phenylmethylsulfonyl fluoride (200 mM stock in EtOH, stored at −20 °C). Even stronger lysis buffers such as RIPA buffer can be used since they do not interfere with phosphoinositol kinase or lipid phosphatase activity.
2. TNE wash buffer (20 mM Tris–HCl, pH 7.4, 100 mM NaCl), store at 4 °C.
3. 30 mM HEPES, pH 7.4, 0.5 mM EGTA.
4. Specific antibody directed against overexpressed lipid phosphatase or phosphoinositide kinase and antibody-specific beads slurry such as SepharoseA (for rabbit polyclonal antibodies) or IgG beads (usually for mouse monoclonal antibodies) slurry: Alternatively, when the overexpressed phosphoinositide kinase or lipid phosphatase contains a tag, tag-specific beads such as Ni^{2+} (for His-tag) or GST-/Flag (M2) bead slurry may be used. Sepharose bead slurry is generally stored in high-salt storage buffer containing sodium azide. To equilibrate beads slurry to assay buffer conditions the beads should be washed two to three times with assay buffer before use and stored at 4 °C.

2.1.2 Glutathione S-Transferase (GST)-Tagged Protein Expression and Purification

1. *E. coli* BL21(DE3)pLysS cells (Promega).
2. LB-Broth (Sigma). Use for 1 l of deionized water 20 g LB powder and mix. Autoclave for 15 min at 121 °C to sterilize. Allow to cool before addition of antibiotics.
3. Ampicillin or its more stable derivative carbenicillin disodium salt (Sigma) preparation. Dissolve 1 g of sodium ampicillin/carbenicillin in 10 ml deionized water to obtain a final concentration of 100 mg/ml. Sterile filter using a 0.45 or 0.22 μm sterile filter and store aliquots at −20 °C.

4. Glutathione Sepharose4B (GE Healthcare) or GST column cartridge (Bio-Rad). Equilibrate beads slurry with assay buffer by washing beads two to three times with three to five bed volumes assay buffer before use and store at 4 °C. Gently shake or invert tube containing sepharose beads just before use to obtain homogenous slurry.
5. GST-elution buffer: 10 mM L-Glutathione, reduced (Sigma) dissolved in 50 mM Tris–HCl, pH 8.0. Should be made fresh before use.
6. Isopropyl β-D-1-thiogalactopyranoside (IPTG, Thermo Scientific). IPTG induces the transcription from promoters regulated by LacI repressor. Dissolve 1 g in 4196 µl deionized water to make a 1 M solution. Filter sterilize with a syringe and a 0.22 µm filter. Store aliquots at –20 °C.
7. GST-lysis buffer. Mix 1× PBS with 1 % Triton X-100 and store at 4 °C until use.
8. GST-wash buffer 1: GST-lysis buffer with 0.5 % Triton X-100.
9. GST-wash buffer 2: GST-lysis buffer with 0.1 % Triton X-100.
10. Optional: Sarcosyl (Sigma). Dissolve 10 % (w/v) solution in 50 mM Tris–HCl, pH 8.0. Store aliquots at –20 °C.
11. Lysozyme (from chicken egg white, Sigma). Dissolve 10 mg/ml lysozyme in deionized water. Make fresh before use.
12. Protease inhibitor mix tablets (Roche).
13. Tip sonicator.

2.1.3 Protein Expression in Serum-Free Insect Cell Culture

Baculovirus insect cell expression systems have the capacity to produce many recombinant proteins at high levels and provide significant eukaryotic protein processing capabilities [24].

2.1.3.1 Monolayer Culture

T-flasks (25, 75, and 150 cm^2) and plastic roller bottles (Corning).

2.1.3.2 Shaker Culture

1. Equipment consists of orbital shaker with clamps fitted for 100–500 ml Erlenmeyer flasks (LabLine).
2. Disposable Erlenmeyer flasks (Corning).
3. Incubator large enough to house a least two orbital shakers, or a shaking incubator.
4. Fresh complete serum-free media (SFM, such as GIBCO).
5. Optional: Pluronic Polyol F-68, 10 % (GIBCO): Supplement to basal medium. Pluronic F-68 Polyol is a nonionic detergent that protects cells from hydrodynamic damage. Make a 10 % (w/v) solution in insect cell culture medium.
6. Trypan blue stain, 0.4 % (GIBCO) is a widely used method to identify dead cells. Cells with intact membranes can effectively

exclude the dye while dead cells with compromised membranes are stained blue. Use 1:1 with cell suspension. Mix well before introducing in hematocytometer or cell counter.

2.2 Lipid Labeling and Lipid Phosphatase Assay

2.2.1 In Vitro PI-3 Kinase Assay

1. ATP (Sigma): ATP hydrolyzes very quickly and therefore should be always handled on ice and stored at −70 °C. It is good practice to use aliquots only once and remainders should be discarded after first time use. Dissolve ATP in deionized water to a final concentration of 10 mM and aliquot. Store at −70 °C. For a phosphoinositol-labeling reaction use 150–200 μM ATP.
2. Phospholipid preparation: When working with lipids work as fast as possible to avoid evaporation.

   PI (L-α-Phosphatidylinositol in chloroform, Avanti Lipids): Aliquot in brown glass vials. Close vial cap tight and seal with parafilm. Store all vials at −70 °C.

   PI-4P (L-α-Phosphatidylinositol 4-phosphate, bovine brain disodium salt in chloroform, Avanti Polar Lipids): Evaporate chloroform under a stream of nitrogen (*see* **Note 1**), and then dissolve in $CHCl_3$:MeOH (2:1). Aliquot in brown glass vials, at 1 mg/ml. Close vial cap tight and seal with parafilm. Store all vials at −70 °C.

   PI-4,5P_2 (L-α-Phosphatidylinositol 4,5-diphosphate, bovine brain disodium salt in chloroform, Avanti Polar Lipids): Evaporate chloroform under a stream of nitrogen, and then dissolve in $CHCl_3$:MeOH:1 N HCl (2:1:0.01), at 1 mg/ml. Aliquot in brown glass vials. Close vial cap tight and seal with parafilm. Store all vials at −70 °C.

   PS (L-α-Phosphatidyl-L-Serine in chloroform, Avanti Polar Lipids): Dissolve in $CHCl_3$, at 10 mg/ml. Aliquot in brown glass vials. Close vial cap tight and seal with parafilm. All vials are stored at −70 °C.
3. 2 ml sample vials (Baxter) and Teflon-lined caps size 8-425 (Baxter).
4. Thin-layer chromatography (TLC) plates (Silica Gel 60 20×20 cm plates, 250 m layer (Whatman, Fisher)): Pretreatment of TLC plates with oxalate is necessary to visualize PI-3,4,5 P_3 that would otherwise stay at the origin of loading and to enhance overall resolution of phospholipid spots. Prepare fresh TLC pretreatment solution (1 mM EDTA, 1 % (w/v) potassium oxalate (Sigma) in deionized water). Add methanol (chromatography grade, Sigma) to buffer (40:60) and mix carefully. Place plates in a TLC developing tank (Sigma) and add pretreatment solution by slow siphon. The speed should be such that the solvent front runs just ahead of the added solution. Be careful that the plates do not develop air pockets that do not get treated by the pretreatment solution.

Air-dry the plates and then activate plates at 100 °C for 1 h in a baking oven.

5. Baking oven.

2.2.2 In Vitro PI-3Kinase Assay from IP

1. Lipid stocks [2 mg/ml]: PS and PI in $CHCl_3$, PI-4 P and PI-4,5 P2 in $CHCl_3$/MeOH/HCl 1N (2:1:0.1). Refer to Subheading 3.4 for phospholipid preparation and to Table 2 for composition of phospholipid mixture.
2. TLC plate (pre-coated with 1 % potassium oxalate in MeOH). Refer to Subheading 3.4 for pre-treatment of TLC plates with oxalate.
3. 2 M Acetic acid ready to use (Sigma).
4. 1-Propanol (Sigma).
5. Cell lysis buffer (refer to Subheading 2.1.1, **item 1**, for recipe).
6. TNE buffer (20 mM Tris–HCl, pH 7.4, 100 mM NaCl), ice cold. Refer to Subheading 2.1.1, **item 2**, for recipe.
7. HEPES-EGTA buffer: Prepare 30 mM HEPES in deionized water and adjust pH to 7.4 and add 0.5 mM EGTA.
8. 100 mM HEPES, pH 7.4.
9. 500 mM $MgCl_2$.
10. 10 mM ATP (refer to Subheading 3.4 for preparation method).
11. ^{32}P-γ-ATP (PerkinElmer, 3.3 μM, 10 mCi/ml).
12. MeOH:$CHCl_3$ (1:1) mixture. Make fresh before use.
13. 4 N HCl (Add 8.3 ml 36 % concentrated HCl (approx. 12 N) solution to 100 ml deionized water and mix carefully).
14. Screw-cap O-ring tubes (1.5 ml, conical bottom, VWR).
15. Filtered gel loading tips (Starlab).

2.2.3 Lipid Phosphatase Assay

1. 1 M Tris–HCl, pH 8.0. (Dissolve 12.114 g Tris in a glass beaker supplied with 80 ml deionized water. Mix and adjust pH with HCl. Make up to a total volume of 100 ml with deionized water. Store at 4 °C or sterilize at 121 °C for 15 min before storing at room temperature.)
2. 1 M DTT (dissolve 1.5 g of DTT in 8 ml deionized water): Adjust the total volume to 10 ml, dispense in 1 ml aliquots, and store them in the dark at −20 °C. Do not autoclave DTT or solution containing it.
3. Freshly labeled substrate phospholipid(s) (such as PI-3,4,5 P_3 for PTEN or PI-3,4 P_2 for INPP4B) and reference phospholipid(s) (refer to Subheading 3.4 for PI-3 kinase

reaction). Evaporate phospholipid mixture under a stream of nitrogen, and then dissolve in phosphatase assay buffer.

4. 2 μg purified lipid phosphatase, such as PTEN or INPP4B (expressed and purified as described in Subheadings 3.1–3.3).
5. STORM screen: The STORM screen will be exposed to the TLC plate after phospholipid separation to capture γ[^{32}P]-labeled phospholipids.
6. Access to a PhosphorImager for image capture and quantification of phospholipid levels.

3 Methods

3.1 Transient Expression in Mammalian Cells and Protein Enrichment by Immunoprecipitation

Many cell lines are suitable for transient transfection and high-yield protein expression. The protocol below has been described for overexpression of lipid phosphatases in HEK 293 human embryonic kidney cells but can be exchanged with any other cell line that demonstrates high transfection efficiency and high protein expression yields. Depending on the cell line different transfection reagents may be used and therefore the transfection procedure is not described here.

1. Harvest 80–100 % confluent HEK 293 cells 24–72 h post-transfection depending on toxicity and stability of the expressed phospholipid phosphatase protein (*see* **Note 2**).
2. Aspirate growth media and wash HEK 293 cells off the tissue culture plates using 1× PBS (HEK 293 cells show low adherence and therefore can be harvested by washing off the tissue culture plates while other cell lines need to be trypsinized).
3. Pellet HEK 293 cells in tabletop centrifuge at 1000 rpm for 5 min at 4 °C.
4. Remove PBS carefully. Avoid touching the cell pellet.
5. Wash HEK 293 cell pellet once more in ice-cold PBS and treat samples as described in **steps 2** and **3**.
6. Resuspend HEK 293 cell pellet in ice-cold lysis buffer supplemented with protease and phosphatase inhibitors and incubate 5–10 min on ice, vortex the cell lysate occasionally (*see* **Note 3**).
7. Centrifuge cell lysate in a high-speed centrifuge at 16,000 × *g* for 15 min at 4 °C.
8. Carefully transfer the supernatant into a new Eppendorf tube and store on ice. Avoid touching the pellet.
9. Dilute cell lysates to a concentration of approximately 1 mg/ml using cell lysis buffer containing protease and phosphatase inhibitors.

10. Cell lysates containing overexpressed tagged lipid phosphatase such as 6×His or Flag-tag should be purified with tag-specific beads slurry according to manufacturer's recommendation.
11. Untagged lipid phosphatases can be purified by immunoprecipitation (IP) detailed below.
12. Add to the cell lysate the recommended quantity of specific lipid phosphatase antibody (volume of antibody used depends on the quantity of cell extract and affinity of the antibody. Refer to the manufacturer's recommendations).
13. Transfer tubes containing lysates and antibody onto a rotator wheel at 4 °C and incubate for 2 h or overnight depending on the antibody affinity.
14. Add 10–30 μl of specific sepharose bead slurry (IgG or SepharoseA beads depending on the antibody origin) to each IP and incubate for 1 h at 4 °C on a rotator wheel. The amount of beads used depends on quantities of antibody and immunoprecipitated protein.
15. Wash IP samples for phosphatase assay two times in cell lysis buffer containing protease and phosphatase inhibitors, followed by three wash steps using TNE buffer (*see* **Note 3**). For washing, invert tubes containing the IP samples several times or alternatively transfer tubes onto a rotator wheel for 2–5 min at 4 °C. Centrifuge samples at 2000 rpm for 3–5 min at 4 °C to pellet beads.
16. Transfer the IP samples to screw-cap tubes for the last wash. Lipid phosphatase assays can be performed with protein bound "on the beads" or purified by elution.

3.2 Glutathion S-Transferase-Tagged Protein Expression and Purification

Glutathione S-transferase (GST) is a 211-amino acid protein (26 kDa) whose DNA sequence is frequently integrated into expression vectors for production of high yields of functional, recombinant protein of up to 60 kDa in size [25]. Higher molecular proteins (>60 kDa) give rise to low yield and consequently other expression systems should be used. The result of expression from such a vector system is a GST-tagged fusion protein. Because GST rapidly folds into a stable and highly soluble protein upon translation, inclusion of the GST-tag often promotes greater expression and solubility of recombinant proteins than expression without the tag. GST-tagged fusion proteins can be purified or detected based on the ability of GST to bind to its substrate glutathione (GSH) [26].

1. Transform the GST-tagged fusion protein into *E. coli* BL21 bacteria according to the manufacturer's recommendations.
2. Plate transformed bacteria on ampicillin/carbenicillin LB-agar plates and incubate overnight at 37 °C in incubator.

3. The next day inoculate a starter culture. Pick one bacteria colony from the LB-agar plate using a sterile tip and inoculate 20 ml LB medium containing 100 μg/ml ampicillin/carbenicillin.
4. Grow starter culture overnight at 37 °C in an incubated shaker.
5. Start preparative culture by adding 5 ml of starter culture to 200 ml LB-broth medium containing 100 μg/ml ampicillin/carbenicillin.
6. Carefully monitor the growth of the culture by measuring the OD_{600} in regular intervals until an OD_{600} of ~ 0.5 to 0.9 is reached (*see* **Note 4**).
7. Induce expression of culture at OD_{600} ~ 0.5 to 0.9 with 0.1 mM IPTG for 3 h at 28–37 °C in a shaker at 250 rpm (*see* **Note 5**).
8. Pellet cells by spinning for 15 min at 3500 × *g* at 4 °C. All steps should be performed on ice or at 4 °C from this point on.
9. Carefully discard the LB-broth and resuspend cell pellet gently in ice-cold PBS lysis buffer containing protease inhibitors by pipetting up and down slowly. Lysis is more efficient when pellet is fully resuspended.
10. Add lysozyme to 1 mg/ml (from a 50 mg/ml solution in deionized water, store at –20 °C) to the cell lysate and incubate on ice for 30–60 min. Mix occasionally by inverting tubes.
11. Optional: Add sarcosyl to a final concentration of 1 % from a 10 % stock. Mix by inversion (*see* **Note 6**).
12. Sonicate cell lysate on ice using a tip sonicator (3–5 cycles of 10 s followed by 10 s rest) until the lysate becomes fluid and clear (*see* **Note 7**).
13. Spin the sonicated lysate for 15 min at 12,000–15,000 × *g* at 4 °C.
14. Transfer the supernatant to a fresh Falcon tube on ice. Avoid transferring parts of the cell pellet since this can interfere with subsequent purification steps.
15. Load supernatant onto a glutathione-agarose column or slurry previously equilibrated on extraction buffer. As a general rule, use 1 ml GST-agarose per liter of bacterial culture when expressing small fusion proteins or non-fused GST, which usually yield large amounts of protein (*see* **Note 8**).
16. Wash 1: Wash column with 10 bed volumes of GST wash buffer 1 (lysis buffer with 0.5 % Triton X-100 including protease inhibitor mix). For batch purification wash GST-slurry for 15–30 min on a rotator wheel.

17. Wash 2: Wash column with 10 bed volumes of GST wash buffer 2 (lysis buffer with 1 % Triton X-100). For batch purification, wash GST-slurry for 15–30 min on a rotator wheel.
18. Elute GST-fusion protein with 10 bed volumes of lysis buffer including 10 mM glutathione. Collect around 10–12 fractions. The bulk of protein is usually eluted in the first few fractions. For batch purification split elution into several steps of 1–3 bed volumes.
19. Identify elution fractions with the highest GST-fusion protein content by SDS-PAGE and Coomassie Brilliant Blue staining.
20. Pool fractions with the highest GST-fusion content and add glycerol to a final concentration of 40 %. Aliquot and store at −70 °C.

3.3 Protein Expression in Serum-Free Insect Cell Culture

The baculovirus expression vector system is a versatile and powerful platform for protein expression in insect cells. It offers several advantages including high levels of expression as well as similar posttranslational modifications as in mammalian cells (*see* **Note 9**) [27].

3.3.1 Adherent Cultures

Adherent insect cell cultures are slower growing and may be used for small-scale protein expression. Refer to the recommended culture conditions in Table 1.

1. Remove spent growth media and replace with fresh growth media every 3–4 days until cells are ready to subculture (90 % confluency).

Table 1
Recommended culture conditions for insect cell adherent and suspension cultures

	Suspension cultures	Adherent cultures
Cell density	$>2 \times 10^6$ viable cells/ml	>80 % confluent
Culture vessel	125 or 250 ml disposable, sterile Erlenmeyer flask containing 35–50 ml or 75–100 ml total working volume of cell suspension, respectively	T-75 cm^2 to T-175 cm^2 disposable sterile T-flasks. Dilute cells in a total working volume of 15–20 ml for T-75 cm^2 flasks and 40–50 ml for T-175 cm^2 flasks
Seeding density	$3–5 \times 10^5$ viable cells/ml	$2–5 \times 10^4$ viable cells/cm^2
Incubation conditions	28 °C ± 0.5 °C non-humidified, ambient air-regulated incubator or warm room on an orbital shaker platform rotating at 125–150 rpm; loosen caps to allow for oxygenation/aeration	28 °C ± 0.5 °C non-humidified, ambient air-regulated incubator or warm room

2. To subculture insect cells can be easily rinsed off the flask bottom. Remove cell clumps by gently pipetting up and down, then transfer cells into a sterile Falcon tube.
3. Determine cell density and viability of insect cell culture by using a cell counting chamber and the trypan blue exclusion method. Transfer a small aliquot of the cell suspension to a microcentrifuge tube. Mix cell suspension with an equal volume of trypan blue and transfer to the counting chamber. Determine cell density electronically using a cell counter or manually using a hemocytometer chamber. Calculate viable and total cell count.
4. Seed cells at recommended density (refer to Table 1) by diluting in pre-warmed (28 °C) growth medium. Mix cells in growth medium by carefully tilting the flask.
5. Put flasks in incubator with caps loosened to allow for oxygenation/aeration, or in case flasks with filter caps are used tighten cap close.

3.3.2 Suspension Culture

1. Six to ten confluent T-75 cm^2 monolayer flasks are required to initiate a 100 ml suspension culture.
2. Dislodge cells from the bottom of the flasks as described in Subheading 3.3.1, **step 2**.
3. Pool the cell suspension and perform a viable cell count (e.g., Trypan blue exclusion method).
4. Dilute the cell suspension to approximately $3–5 \times 10^5$ viable cells/ml in complete growth media.
5. Incubate spinner vessels at 28 ± 0.5 °C at a constant stirring rate of 50 rpm for spinner cultures and 100 rpm for shake flask cultures (*see* **Note 10**).
6. Initiate subculture when the viable cell count reaches $1–2 \times 10^6$ cells/ml (generally achieved 3–7 days post-passaging). Increase stirring speed by 5 rpm for either spinner or shaker flask cultures. If cell viability drops below 75 % decrease stirring speed by 5 rpm until culture viability recovers above 80 %.
7. In case large cell clumps (>10 cells per clump) occur, let the spinner or shaker flask culture sit a few minutes before subculturing. The big cell clumps will settle to the bottom of the flask and sample for cell counting can be taken from the top third of the suspension culture.
8. It may be necessary that **step 7** needs to be repeated several times until overall large cell clumps in suspension culture are eliminated.

3.3.3 Infection of Serum-Free Cultures with Recombinant Baculovirus

It is important that nutritional or biophysical factors such as pH, oxygen, and temperature are not rate limiting during the infection of insect cells. Cultures should be infected in the mid-logarithmic phase of growth with an established multiplicity of infection (MOI). It is recommended that the culture is infected at a cell density of $2–4 \times 10^6$ cells/ml with an MOI of 0.1–1.0. A maximum of secreted proteins is usually observed 48–72 h post-infection and of non-secreted protein 72–96 h post-infection (*see* **Note 11**).

3.3.4 Monitoring Baculovirus Levels

Infection of insect cells requires monitoring the levels of individual baculovirus in an infected cell culture. The primary means for detecting concentrations of baculovirus DNA within an infected culture is by using polymerase chain reactions (PCR). Individual PCR reactions to detect and quantify levels of baculovirus transgenes are described in Hitchman et al. [28].

3.3.5 Generating Virus Stock Using Monolayer Infection

The protocol described below for generation of baculovirus stock is optimized for 24-well plates, but may be scaled up taking into account the growth area of insect cell culture used.

1. Add to each well in a 24-well plate 0.5 ml of insect cells at 1×10^6 cells/ml.
2. Let the cells attach for 30–60 min at RT.
3. Add 5 μl of baculovirus stock to the insect cells.
4. Incubate insect cells with baculovirus stock for 6 days at 28 °C.
5. Harvest the supernatant of the insect cell culture and spin at 2500 rpm for 5 min at room temperature to remove any cellular contamination. Discard the 24-well plate.
6. Store at 4 °C in the dark. For long-term storage add fetal bovine serum (FBS) or BSA to 10 % and store at −80 °C (*see* **Note 12**).

3.4 Lipid Labeling and Lipid Phosphatase Assay

3.4.1 In Vitro PI3-Kinase Assay from IP

3.4.1.1 Preparation of PI-3 Kinase for Kinase Assay Using Immunoprecipitation

Seed HEK 293 human embryonic kidney cells in 15 cm tissue culture plates. In general, one 15 cm tissue culture plate contains enough endogenous PI-3 kinase for approximately 8–10 PI-3 kinase reactions (*see* **Note 13**).

1. Harvest 80–100 % confluent HEK 293 human embryonic kidney cells by washing HEK 293 cells off the tissue culture plates using ice-cold 1× PBS (HEK 293 cells show low adherence to tissue culture plates and can harvested by washing them off the tissue culture plates). Cell lysates should be handled on ice all times.
2. Pellet HEK 293 cells in table top centrifuge at 1000 rpm for 5 min at 4 °C.
3. Remove PBS carefully. Avoid touching the cell pellet.

4. Wash HEK 293 cell pellet once more in ice-cold PBS and treat samples as described in **steps 2** and **3**.
5. Resuspend HEK 293 cell pellet in lysis buffer on ice and incubate 5–10 min, vortexing the cell lysate occasionally.
6. Centrifuge cell lysate in a high-speed centrifuge at 16,000 × *g* for 15 min at 4 °C.
7. Carefully transfer the supernatant containing the endogenous PI-3 Kinase enzyme into a new pre-labelled Eppendorf tube and store on ice. Avoid touching the pellet since it contains the cell membranes.
8. Dilute cell lysates to a concentration of 1 mg/ml using cell lysis buffer containing protease and phosphatase inhibitors.
9. Set up PI3-kinase IP reaction by adding to the HEK 293 cell lysate 2–5 µl of rabbit anti-PI-3 kinase antibody (volume of antibody used depends on the quantity of cell extract that is being used in the IP; refer to the manufacturer's recommendations.).
10. Transfer tubes containing lysates and antibody onto a rotator wheel at 4 °C and incubator overnight.
11. Add 15–30 µl of SepharoseA bead slurry to each IP and incubate for 1 h at 4 °C on a rotator wheel.
12. Wash IP samples for kinase assay two times in cell lysis buffer containing protease and phosphatase inhibitors, followed by three wash steps using TNE buffer. For washing invert tubes containing the IP samples several times, or alternatively transfer tubes onto a rotator wheel for 2–5 min at 4 °C followed by gentle centrifugation at 2000 rpm for 3–5 min at 4 °C.
13. Divide and transfer the IP samples to screw-cap tubes for the last wash.
14. Aspirate all TNE wash buffer off the SepharoseA beads (do not leave more than approximately 5 µl of wash buffer on top of the bead pellet).
15. Add 65 µl of TNE buffer to reach a final volume of 70 µl (*see* **Note 14**).

3.4.1.2 Preparation of Phospholipids

For each reaction use the lipid substrate composition as shown in Table 2. Mix the substrate phospholipids and dry under gentle nitrogen flow. Add to the dried lipids the prepared HEPES:EGTA assay buffer and sonicate the mixture at room temperature in a cup horn sonicator to form micelles (constant output at 50 % energy, 10 min). Alternatively, a probe tip sonicator can be used (3–5 pulses at 30 % power). The lipid-buffer mixture should have a milky appearance after sonication. Gently vortex the lipid mixture and spin it quickly down. Store the lipid mixture at room temperature until use (*see* **Note 15**).

Table 2
Composition of lipid substrate mixture and "hot" ATP master mix

Lipid substrate mix	Per reaction	"Hot" ATP master mix	Per reaction
PS	4 μg	HEPES (100 mM, pH 7.4)	6.5 μl
PI	2 μg	500 mM $MgCl_2$	2.0 μl
PI-4 P and/or	2 μg	10 mM ATP	0.5 μl
PI-4,5-P_2	2 μg	32-P-γ-ATP	1.0 μl
HEPES/EGTA buffer	20 μl	Total	10.0 μl

3.4.1.3 Preparation of the "Hot" ATP Master Mix

Thaw ^{32}P-γ-ATP and prepare the "hot" ATP master mix for the amount of reactions required as shown in Table 2. Store ATP master mix at room temperature until use.

3.4.1.4 PI-3 Kinase Reaction

1. Equilibrate IP samples to room temperature for 10 min.
2. Add 20 μl of the lipid mix to each sample and preincubate at room temperature for 5–10 min (*see* **Note 16**).
3. To start the kinase reaction, add 10 μl of the "hot" ATP master mix and lipids to each sample. Carefully flick the tube to mix the SepharoseA beads with the ATP master mix. Incubate PI-3 kinase reactions in a heat block which is set to 30 °C. Flick tubes occasionally to allow the SepharoseA beads to mix with the lipids (*see* **Note 17**).
4. Stop the PI-3 kinase reaction exactly after 10 min incubation by adding 50 μl 4 N HCl. To maximize lipid labeling the PI-3 kinase reaction can be extended up to 30 min.

3.4.1.5 Phospholipid Extraction

1. Add 100 μl MeOH:$CHCl_3$ (1:1) mixture to each sample and vortex tubes two times for 30 s (*see* **Note 18**).
2. Spin tubes at 16 x g for 2 min at room temperature.
3. Carefully remove the tubes from the centrifuge without disturbing the chloroform phase.

Each lipid extraction contains three phases: The bottom phase contains the organic chloroform phase and the phospholipids. The middle phase is a thin layer with a white appearance and contains proteins. The top phase is the water-soluble phase.

4. Carefully remove the complete bottom chloroform phase (~50 μl) and transfer it to a new pre-labeled Eppendorf tube. To avoid any traces of the other phases in the pipette tip it is recommended to use the first pressure point of the pipette to enter the bottom chloroform-phospholipid phase, and then carefully increase pressure to the second pressure point of the

pipette, which will exhaust the traces from the other phases before allowing to pipette the chloroform-phospholipid phase (*see* **Note 19**).

3.4.1.6 Spotting Lipids on the TLC Plate

1. Mark guides on the TLC plate with a soft pencil to prevent lipids touching the solvent phase on the bottom of the TLC chamber and to allow enough room for samples to be analyzed. Do not spot the lipids below 1 in. from the bottom of the TLC plate and leave a 1–2 cm gap between the different samples.
2. Bake the TLC plate in the oven at 120 °C for 5 min to remove water vapor prior to use.
3. Use thin, gel-loading tips to spot all of the organic phase onto the TLC plate (*see* **Note 20**).

   When taking up the chloroform-lipid phase immediately tilt the pipette horizontally to prevent dripping of the organic solvent phase. Be careful not to let the solvent reach the filter in the pipette tip. Slowly let the chloroform-lipid phase drip drop by drop onto the TLC plate. The spot should not exceed 5 mm in diameter. If airflow is available dry the spot under gently flow, then proceed with the next drop. Continue in an alternate fashion until the complete sample is spotted. Then continue with the next sample.
4. Transfer the TLC plate into the TLC chamber, and apply vacuum grease on the top of the chamber before closing it with the glass lid to seal it. Add an additional weight to seal it further. Ensure that the TLC plate is not touching the Whatman paper in the TLC chamber. A serological plastic pipette can be used as divider to ensure that contact between the Whatman paper and the TLC plate is avoided.
5. Run the TLC plate overnight (*see* **Note 21**).
6. Air-dry the TLC plate, wrap it in plastic film, and develop in a film cassette using a STORM screen.

3.5 Lipid PhosphataseAssay

Lipid phosphatase assays are an excellent technique to identify and quantify the phospholipid specificity of lipid phosphatases. Radioactive assays are preferred over colorimetric assays due to their higher sensitivity and application to a greater range of phospholipid substrates.

3.5.1 Phosphatase Reaction

1. Dry freshly labeled “hot” phospholipids under gentle nitrogen flow.
2. Add to the dried lipids the phosphatase reaction buffer (100 mM Tris–HCl, pH 8.0, 1 mM DTT). 10 μl of reaction buffer should be added to approx. 4–6 μg radioactive labeled phospholipids (1× PI3 kinase reaction).

3. Sonicate the mixture at room temperature in a cup horn sonicator to form micelles (constant output at 50 % energy, 10 min). Alternatively, a probe tip sonicator can be used (3–5 pulses at 30 % power). The lipid-buffer mixture should have a milky appearance after sonication.
4. Gently vortex the lipid mixture and spin it quickly down. Store the lipid mixture at room temperature until use (*see* **Note 22**).
5. Prepare phosphatase assay by mixing phosphatase reaction buffer (100 mM Tris–HCl, pH 8.0, 1 mM DTT) with 2–4 μg purified lipid phosphatase (phosphatase protein can be used purified or as IP on beads). Start the reaction by addition of 10 μl 'hot' labeled substrate phospholipids in reaction buffer. The final volume of each phosphatase reaction is 50 μl.
6. Incubate phosphatase assay at 37 °C for 1–2 h (for INPP4B phosphatase assay). Occasionally flick the reaction tubes to mix phosphatase reaction (*see* **Note 23**).
7. Stop the PI-3 kinase reaction by adding 50 μl 4 N HCl.
8. Extract phospholipids and spot a TLC plate as described in **steps 6** and **7**, Subheading 3.4.
9. The substrates and products from each phosphatase assay are quantified by Phosphorimager and the percent hydrolysis is calculated (*see* **Note 24**).

3.5.2 Quantification of the Lipid PhosphataseAssay

The quantification of phosphoinositides is generally performed by scanning densitometry using a PhosphorImager. Although phosphorimaging has a lower resolution than X-ray film detection and quantification methods, phosphorimaging has greater sensitivity, faster image development, and an enhanced dynamic range. During the TLC run labeled phosphoinositides are efficiently separated from the radioactivity, remaining near the origin of the run and any radioactive ATP and free phosphate is carried over with the organic phase [29]. The different phosphoinositide classes are separated according to their head groups, with phosphatidylinositol (PI) migrating furthest on the TLC and the more phosphorylated phosphoinositides such as PIP, PIP_2, and PIP_3 migrating slower with increasing phosphorylation state (*see* Fig. 1).

1. After the TLC run air-dry the TLC plate, wrap it in plastic film and develop in a film cassette using a STORM screen.
2. After 3–24 h (depending on the signal strength) analyze STORM screen using a PhosphorImager and quantify the labeled species with the provided quantitation software (*see* **Note 24**).

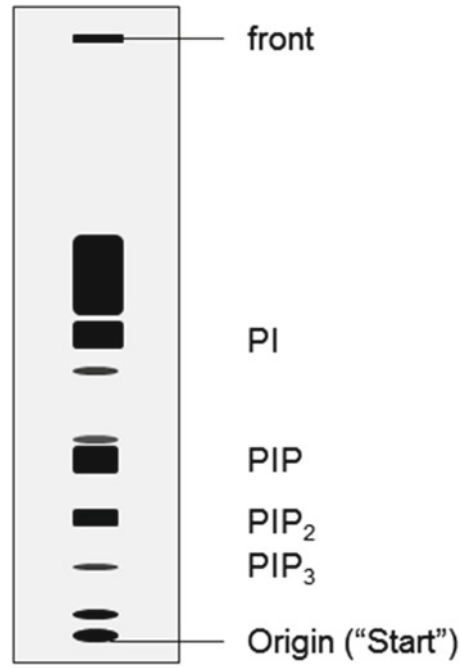

Fig. 1 Schematic of phosphoinositol lipid separation by TLC. Based on their phosphorylation content of the phosphoinositide head group phosphoinositol lipids migrate at different speed. Phospholipids with lowest phosphorylation content migrate fastest while increasing phosphorylation of the head group results in slower migratory speed during the TLC run

4 Notes

1. Drying phospholipids under N2 flow is the best way to avoid oxidation of fatty acids.
2. Protein expression levels of each lipid phosphatase and for each specific cell line should be optimized before a preparative expression and lysis is attempted. In addition, transfection efficiency for each single experiment should be monitored in parallel by using an expression vector for green fluorescence protein (GFP).
3. For INPP4B lipid phosphatase expression and immunoprecipitation experiments no EGTA or EDTA should be added to the lysis buffer, washing buffers or reaction buffer since it interferes with lipid phosphatase activity in the downstream phosphatase assay.
4. Optimal conditions for expression and GST fusion proteins in *E. coli* vary widely, depending on the molecular weight and solubility of the fusion protein, compatibility of the coding

sequence with codon usage of the host bacterial strain, extend of expression induction, and lysis of cells.

5. In case expression of the GST-tagged fusion protein at 37 °C gives rise to inclusion body aggregates, lowering the temperature of culture to 30 °C for 3 h gives rise to considerable amounts of soluble protein.
6. Addition of 0.7–2 % Sarcosyl, 1 % Triton X-100 and 10 mM CHAPS helps to purify natively folded proteins from inclusion bodies [30].
7. The extent of sonication for optimal yields of intact fusion protein must be determined empirically.
8. When making batch instead of column purification, incubate bacterial lysate with GST-slurry for 30–60 min on a rotator wheel.
9. Most insect cell lines (e.g., Sf9, High5) are adapted to growth in serum-free media, however, insect cells also grow well in traditional media supplemented with serum (10 % FBS). Serum-free growth requires a multi-passage adaptation process. For insect cell line adaptation to serum-free growth refer to (27) for a detailed protocol.
10. Growing cells in shaker cultures of 100 ml volume with loosened bottle caps is preferred because oxygen is not rate limited under these conditions. It is recommended that the SFM formulation contain 0.05–0.1 % Pluronic Polyol F-58 or a Polyol equivalent in performance that prevents shearing.
11. It is important to determine the expression kinetics of each recombinant virus product since many proteins are rapidly degraded by cellular proteases. Optimization will allow to establish an ideal time for harvesting the culture. The dynamics of infection and protein expression differs between monolayer and suspension cultures, especially the time to optimal expression, which is always longer when using monolayer cultures.
12. Freezing and storing the baculovirus stock at –70 °C will result in loss of functional virus lowering the overall MOI (multiplicity of infection).
13. This protocol is optimized for in vitro PI-3 Kinase assay from immunoprecipitated, endogenous PI-3 kinase from HEK human embryonic kidney 293 cells. It is quantitative but care should be taken that the assay condition is within the linear range for the amount of kinase assayed. Where the PI-3 kinase assay is used to generate labeled phospholipids for a consecutive lipid phosphatase assay the reaction time of the PI-3 kinase assay can be extended to 30 min to maximize lipid labeling.
14. The main purpose of the TNE buffer washes is to remove any detergents originating from the lysis buffer since the detergent

will interfere with the lipid kinase reaction. O-ring cap tubes are recommended to prevent the leaking of radioactivity during vortexing steps when performing the PI-3 kinase reaction.

15. Do not chill the sonicated lipids as they will precipitate.
16. For a preparative PI-3 kinase reaction several PI-3 kinase reactions can be pooled in one reaction tube as needed for a subsequent lipid phosphatase assay.
17. Start kinase reactions with 15–30 s gaps to allow for timely handling of each sample.
18. Intensive vortexing of samples is key to efficient phospholipid extraction from aqueous reaction mixtures.
19. To avoid dripping of the pipette tip pre-wet the pipette tip by pipetting up and down three times in the MeOH:$CHCl_3$ mix which was added to each PI-3 kinase reaction.
20. Careful pipetting is essential as chloroform drips easily. Prepare a small bottle of chloroform and "wash" the pipette tip in the chloroform by pipetting up and down several times to saturate the tip with chloroform vapor before pipetting the sample.
21. The minimum time for separating phospholipids is approximately 4 h. The longer the separation of the phospholipids the better the resolution. Development of a TLC depends on the amount of "hot" labeled phospholipids and can take from as little as 3 h to overnight.
22. Do not chill the sonicated lipids as they will precipitate.
23. It is good practice to quantify the signal of phosphatase-specific phospholipid with a labeled control phospholipid that will not be affected by the used lipid phosphatase. In doing so, any variation or loss in phospholipid quantities due to sample handling can be accounted for. Furthermore, kinase-dead or tag-only lipid phosphatase controls should be included.
24. Resolution of phospholipids by TLC can only separate phospholipids according to the number of phosphorylation events on the phospholipid head group (e.g., PIP, PIP_2, or PIP_3), but it cannot differentiate between the different phosphorylation states such as PI-3,4 P_2 or PI-4,5 P_2.

References

1. Dowhan W (1997) Molecular basis for membrane phospholipid diversity: why are there so many lipids? Annu Rev Biochem 66:199–232. doi:10.1146/annurev.biochem.66.1.199
2. Clayton EL, Minogue S, Waugh MG (2013) Mammalian phosphatidylinositol 4-kinases as modulators of membrane trafficking and lipid signaling networks. Prog Lipid Res 52: 294–304. doi:10.1016/j.plipres.2013.04.002, S0163-7827(13)00023-4 [pii]
3. Schramp M, Hedman A, Li W, Tan X, Anderson R (2012) PIP kinases from the cell membrane to the nucleus. Subcell Biochem 58:25–59. doi:10.1007/978-94-007-3012-0_2
4. Cantley LC (2002) The phosphoinositide 3-kinase pathway. Science 296:1655–7. doi:10.1126/science.296.5573.1655, 296/5573/1655 [pii]
5. Balla T (2013) Phosphoinositides: tiny lipids with giant impact on cell regulation. Physiol

Rev 93:1019–137. doi:10.1152/physrev.00028.2012, 93/3/1019 [pii]
6. Auger KR, Cantley LC (1991) Novel polyphosphoinositides in cell growth and activation. Cancer Cells 3:263–70
7. Lee JY, Kim YR, Park J, Kim S (2012) Inositol polyphosphate multikinase signaling in the regulation of metabolism. Ann N Y Acad Sci 1271:68–74. doi:10.1111/j.1749-6632.2012.06725.x
8. Shah ZH, Jones DR, Sommer L, Foulger R, Bultsma Y, D'Santos C, Divecha N (2013) Nuclear phosphoinositides and their impact on nuclear functions. FEBS J 280:6295–310. doi:10.1111/febs.12543
9. Jaber N, Zong WX (2013) Class III PI3K Vps34: essential roles in autophagy, endocytosis, and heart and liver function. Ann N Y Acad Sci 1280:48–51. doi:10.1111/nyas.12026
10. Whitman M, Downes CP, Keeler M, Keller T, Cantley L (1988) Type I phosphatidylinositol kinase makes a novel inositol phospholipid, phosphatidylinositol-3-phosphate. Nature 332:644–6. doi:10.1038/332644a0
11. Antal CE, Newton AC (2013) Spatiotemporal dynamics of phosphorylation in lipid second messenger signaling. Mol Cell Proteomics 12:3498–508. doi:10.1074/mcp.R113.029819, doi: R113.029819 [pii]
12. Hakim S, Bertucci MC, Conduit SE, Vuong DL, Mitchell CA (2012) Inositol polyphosphate phosphatases in human disease. Curr Top Microbiol Immunol 362:247–314. doi:10.1007/978-94-007-5025-8_12
13. Maffucci T (2012) An introduction to phosphoinositides. Curr Top Microbiol Immunol 362:1–42. doi:10.1007/978-94-007-5025-8_1
14. Lemmon MA (2007) Pleckstrin homology (PH) domains and phosphoinositides. Biochem Soc Symp:81–93. doi:BSS0740081 [pii] 10.1042/BSS0740081
15. Jean S, Kiger AA (2014) Classes of phosphoinositide 3-kinases at a glance. J Cell Sci 127:923–8. doi:10.1242/jcs.093773, 127/5/923 [pii]
16. Waugh MG (2012) Phosphatidylinositol 4-kinases, phosphatidylinositol 4-phosphate and cancer. Cancer Lett 325:125–31. doi:10.1016/j.canlet.2012.06.009, S0304-3835(12)00375-8 [pii]
17. Vines CM (2012) Phospholipase C. Adv Exp Med Biol 740:235–54. doi:10.1007/978-94-007-2888-2_10
18. Maehama T, Dixon JE (1998) The tumor suppressor, PTEN/MMAC1, dephosphorylates the lipid second messenger, phosphatidylinositol 3,4,5-trisphosphate. J Biol Chem 273:13375–8
19. Damen JE, Liu L, Rosten P, Humphries RK, Jefferson AB, Majerus PW, Krystal G (1996) The 145-kDa protein induced to associate with Shc by multiple cytokines is an inositol tetraphosphate and phosphatidylinositol 3,4,5-triphosphate 5-phosphatase. Proc Natl Acad Sci U S A 93:1689–93
20. Gewinner C, Wang ZC, Richardson A, Teruya-Feldstein J, Etemadmoghadam D, Bowtell D, Barretina J, Lin WM, Rameh L, Salmena L, Pandolfi PP, Cantley LC (2009) Evidence that inositol polyphosphate 4-phosphatase type II is a tumor suppressor that inhibits PI3K signaling. Cancer Cell 16:115–25. doi:10.1016/j.ccr.2009.06.006, S1535-6108(09)00180-9 [pii]
21. Norris FA, Majerus PW (1994) Hydrolysis of phosphatidylinositol 3,4-bisphosphate by inositol polyphosphate 4-phosphatase isolated by affinity elution chromatography. J Biol Chem 269:8716–20
22. Schultz C (2010) Challenges in studying phospholipid signaling. Nat Chem Biol 6:473–5. doi:10.1038/nchembio.389, nchembio.389 [pii]
23. Di Paolo G, De Camilli P (2006) Phosphoinositides in cell regulation and membrane dynamics. Nature 443:651–7. doi:10.1038/nature05185, nature05185 [pii]
24. Jarvis DL (2009) Baculovirus-insect cell expression systems. Methods Enzymol 463:191–222. doi:10.1016/S0076-6879(09)63014-7, S0076-6879(09)63014-7 [pii]
25. Sehgal BU, Dunn R, Hicke L, Godwin HA (2000) High-yield expression and purification of recombinant proteins in bacteria: a versatile vector for glutathione S-transferase fusion proteins containing two protease cleavage sites. Anal Biochem 281:232–4. doi:10.1006/abio.2000.4569, S0003-2697(00)94569-X [pii]
26. Harper S, Speicher DW (2008) Expression and purification of GST fusion proteins. Curr Protoc Protein Sci Chapter 6:Unit 6 6. doi:10.1002/0471140864.ps0606s52
27. Sokolenko S, George S, Wagner A, Tuladhar A, Andrich JM, Aucoin MG (2012) Co-expression vs. co-infection using baculovirus expression vectors in insect cell culture: Benefits and drawbacks. Biotechnol Adv 30:766–81. doi:10.1016/j.biotechadv.2012.01.009, S0734-9750(12)00011-0 [pii]
28. Hitchman RB, Siaterli EA, Nixon CP, King LA (2007) Quantitative real-time PCR for rapid and accurate titration of recombinant baculovi-

rus particles. Biotechnol Bioeng 96:810–4. doi:10.1002/bit.21177

29. van Dongen CJ, Zwiers H, Gispen WH (1985) Microdetermination of phosphoinositides in a single extract. Anal Biochem 144:104–9, 0003-2697(85)90090-9 [pii]

30. Tao H, Liu W, Simmons BN, Harris HK, Cox TC, Massiah MA (2010) Purifying natively folded proteins from inclusion bodies using sarkosyl, Triton X-100, and CHAPS. Biotechniques 48:61–4. doi:10.2144/000113304, 000113304 [pii]

Chapter 7

Luciferase Reporter Assays to Assess Liver X Receptor Transcriptional Activity

Matthew C. Gage, Benoit Pourcet, and Inés Pineda-Torra

Abstract

Luciferase reporter assays are sensitive and accurate tests that enable the analysis of regulatory sequences, the magnitude of transcriptional activity by transcription factors, and the discovery of gene regulatory elements and small-molecule modulators with high levels of precision. This is made possible through detection of bioluminescence produced by luciferase-coding reporters in a wide range of cellular environments. These assays are routinely used to analyze the activity of transcription factors, including the lipid-activated liver X receptor (LXR), in response to different stimuli as well as for the identification of their ligands. In this chapter we describe in detail the assays performed to investigate LXR activity in a macrophage-like cell line (RAW 267.4). These can be easily adapted to other nuclear receptors and transcription factors.

Key words Nuclear receptors, Liver X receptor, Luciferase, Reporter assay, Luminescence, Macrophage, RAW 267.4

1 Introduction

Luciferase reporter assays are generally performed to (a) identify transcriptional regulatory elements (in promoters, enhancers, or untranslated regions), which control the expression of a gene or genes, (b) help identify ligands for ligand-activated nuclear receptors, and (c) examine changes in the activity of a particular transcription factor/nuclear receptor upon treatment with specific stimuli. Reporter assays rely on the regulatory element or region of interest being fused to a reporter gene not usually expressed in the system being tested, which when translated can be assayed or detected accurately. The level of detected reporter protein is thus directly proportional to the level of mRNA transcribed.

Reporter proteins to date have included β-galactosidase, chloramphenyl acetyltransferase, β-glucuronidase, secretory alkaline phosphatase, and a variety of different fluorescent proteins. One of the most widely used reporters is the luciferase gene, which encodes for the enzyme luciferase that oxidizes D-luciferin in the presence

Mark G. Waugh (ed.), *Lipid Signaling Protocols*, Methods in Molecular Biology, vol. 1376,
DOI 10.1007/978-1-4939-3170-5_7,

of ATP, oxygen, and Mg^{2+}, to yield a product that can be quantified by measuring the released light. The luciferase assay has advantages over other reporter assays due to its high sensitivity, wide dynamic range, and relative affordable cost. This assay was first described in 1987 by de Wet et al. [1] and subsequently commercial kits have become widely available.

Liver X receptors (LXRs) belong to the nuclear receptor superfamily of ligand-activated transcription factors. LXRs are expressed as two isoforms: LXRα, which exhibits tissue- and cell- specific expression in liver, adipose, kidney, adrenal tissues, and macrophages and the ubiquitously expressed LXRβ [2]. LXRs heterodimerize with the retinoid X receptor (RXR) to transcriptionally modulate target genes involved in several processes, primarily in lipid metabolism and inflammation in which innate immune cells such as macrophages have been shown to play a key role [2]. We have optimised the luciferase reporter assay to measure nuclear receptor transcriptional activity and have used this technique successfully to examine gene regulation and identify target genes of different nuclear receptors (including LXR) in a variety of cell lines [3–5]. The general strategy is to (a) identify the putative regulatory element in the gene of interest, (b) clone this putative regulatory element or the portion of a promoter/enhancer containing the regulatory element to a reporter gene (luciferase in this case), (c) transfect or incorporate reporter and expression plasmids into cells, (d) activate nuclear receptor with specific ligands, and (e) detect transcriptional activation by quantifying the luminescence with a luminometer.

In this protocol we describe how in less than a week, a researcher is able to transfect their previously cloned and produced plasmid construct (containing putative or already established regulatory elements together with constructs expressing LXR nuclear receptors) into the RAW macrophage cell line and detect the regulation of their putative regulatory elements using the luciferase reporter assay and β-galactosidase assay as a control. These cells represent an interesting option to study the differential effects of LXRα and LXRβ since they only express the beta subtype [6]. Overall, the assay is as follows: (a) cell transfection with luciferase and expression plasmid constructs, (b) cell lysis, (c) addition of luciferase substrate (D-luciferin), and (d) quantification of luminescence.

2 Materials

Prepare all solutions using ultrapure water (prepare by purifying deionised water to attain a sensitivity of 18 MΩ cm at 25 °C) and analytical grade reagents. Prepare and store all reagents at 4 °C

or −20°C as indicated (unless otherwise noted). Diligently follow all local waste disposal regulations when disposing of waste materials.

Store commercially obtained reagents as advised in product manual.

2.1 Cell Culture

1. RAW 267.4 macrophage cell line (established from murine tumours induced by the Abelson leukemia virus, ATCC®, TIB-71™).
2. Cell culture plates (100 × 20 mm) (sterile, wrapped in a sleeve of 10).
3. 24-well cell culture plate (sterile, individually wrapped).
4. Aspiration polysterene pipette (sterile, individually wrapped).
5. Individually wrapped polysterene serological pipettes, 25, 10, 5 mL.
6. Sterile PBS 1× (*see* **Note 1**).
7. Fetal bovine serum, stored at −20 °C.
8. Gentamycin (10 mg/mL stock), stored at 4 °C.
9. Growth medium: DMEM supplemented with 10 % FBS and 20 μg/mL gentamycin, stored at 4 °C.
10. Hemacytometer/cell counter.
11. Cell scraper/lifter with 19 mm blade, sterile and individually wrapped.
12. Gilson single channel pipettes and sterile tips.
13. Repeat pipettor.
14. Repeat pipettor tips, sterile and individually wrapped.
15. Incubator (37 °C, 5 % CO_2).
16. Tissue culture Class II cabinet.
17. 1.5 mL microcentrifuge tubes, sterile.
18. Sterile polypropylene 15 and 50 mL tubes.
19. Vortex.
20. Centrifuge with rotors for 1.5, 15, and 50 mL tubes.
21. LXR activators, i.e., GW3965 [7]/vehicle controls, stored at −20 °C.
22. Ice.
23. Luciferase Reporter Assay Kit including Luciferase substrate and Lysis buffer 5×.
24. Plate rocker. Water bath at 37 °C.

2.2 Luciferase Reporter Constructs and Transfection

1. Transfection reagent (TurboFect, Fermentas #R0531), kept at 4 °C or on ice (*see* **Note 2**).
2. Endotoxin-free preparations of plasmids diluted at required concentration (*see* **Note 3**).
3. OPTI-MEM®I (Gibco, Invitrogen #S1985-026), stored at 4 °C (*see* **Note 4**).
4. Dulbeco's Modified Eagles Medium (DMEM) (*see* **Note 5**).

2.3 β-Galactosidase Assay

1. *o*-Nitrophenyl-beta-D-galactopyranosidase (ONPG) 4 mg/mL^{-1} in Buffer Z pH 7.5, stored at –20 °C and protected from light (*see* **Note 6**).
2. Buffer Z (Na_2HPO_4 0.1 M, KCl 10 mM, $MgSO_4$ 1 mM), filtered and stored at 4 °C.
3. β-Mercaptoethanol.

2.4 Bioluminescence Detection

1. Luciferase reporter gene assay system (*see* **Note 7**).
2. White opaque 96-well microplates for luciferase reading.
3. Clear 96-well microplates for β-galactosidase reading.
4. Luminometer (*see* **Note 8**).

3 Methods

Carry out all procedures at room temperature unless otherwise specified.

3.1 Cell Seeding to 24-Well Plates

To be done 16–24 h before cell transfection under sterile conditions.

1. Wash previously cultured RAW 267.4 cells with 37°C pre-warmed PBS 1× using a serological pipette.
2. Discard PBS 1× with an aspiration pipette attached to a vacuum line.
3. Add 37 °C pre-warmed complete DMEM.
4. Harvest cells by scrapping them off the plates with a cell scraper.
5. Resuspend cells to a single-cell suspension (*see* **Note 9**).
6. Count cells with a hematocytometer to calculate cell density (cells/mL).
7. Calculate volume of cell homogenate required to get 2×10^5 cells/well × number of wells required. Complete with growth medium to total volume calculated as 500 µL per well × total number of wells.

8. Seed 2×10^5 cells (i.e., 500 μL of cell suspension) per well in a 24-well plate (*see* **Note 10**).
9. Incubate cells at 37 °C, 5 % CO_2, overnight.

3.2 Cell Transfection

Perform cell transfection procedure under sterile conditions.

1. Calculate amount of plasmid required to perform assay (*see* **Note 11**). Use 1.5 mL tubes for the DNA mixes, or for more than 3 ml of total volume use 15 mL tubes. All tubes should be sterile.
2. Pre-warm PBS, OPTI-MEM®1 and complete DMEM at 37 °C.
3. For each well, prepare a *DNA mix* as follows (*see* **Note 12**):
4. In 50 μL total volume add all plasmids needed: 3 μL luciferase reporter vector (100 ng/μL), 1 μL LXR expression vector (i.e., pcDNA3-LXRa) at 50 ng/μL (or empty pCDNA3 vector as negative control) and 1 μL pCMV-Bgal (100 ng/μL). Complete with OPTI-MEM® I (45 μL).
5. Mix by briefly vortexing to mix well.
6. Centrifuge briefly to collect sample at the bottom of the tube.
7. For each well, prepare a *TurboFect mix* as follows:
8. Add 1 μL of TurboFect to 49 μL OPTI-MEM®I per well.
9. Mix gently by pipetting mix up and down (do not vortex).
10. Add TurboFect mix *on top of* the DNA mix (*see* **Note 13**).
11. Mix gently by pipetting up and down about 10×.
12. Incubate at room temperature for 20 min.
13. Before addition of the polymer-DNA mix to the cells, wash cells with pre-warmed PBS 1×.
14. Discard PBS 1× with an aspiration pipette attached to a vacuum line.
15. Add 900 μL of pre-warmed growth medium with a pipette repeater to one side of the well avoiding disruption of the cell layer.
16. Add 100 μL of DNA/TurboFect mix in the corresponding well a drop at a time.
17. Mix the growth medium with the added DNA/TurboFect mix by tilting the plate back and forth and left to right about 5–10 times.
18. Incubate cells at 37 °C, 5% CO_2, for 24 h.

3.3 LXR Activation

1. Calculate quantity of LXR activator and control solution required for a final volume of 500 μL per well (*see* **Note 14**).
2. Prepare activation/control solution with pre-warmed growth medium. Mix well.

3. Discard transfection medium with an aspiration pipette attached to a vacuum line.
4. Wash each well with 200 μL of pre-warmed PBS 1× (optional).
5. Add 500 μL of activation/control medium as prepared above with a pipette repeater to one side of the well avoiding disruption of the cell layer.
6. Incubate cells 18 h, 37 °C, 5 % CO_2.

3.4 Luminescence (LXR Activity) Detection

This step no longer needs to be performed under sterile conditions.

Follow the manufacturer's instructions of the specific detection/assay system used. These are some general guidelines.

3.5 Luciferase Assay

1. Take out lysis buffer (usually a 5× or 10× stock stored @ –20 °C) at RT and thaw completely.
2. Prepare enough 1× lysis buffer with 18 MΩ water.
3. Take cell culture plates from the tissue culture incubator to RT.
4. Remove medium from cells with an aspiration pipette attached to a vacuum line (*see* **Note 15**).
5. Wash cells once or twice with 300 μL ice-cold PBS/well using a repeater and pipetting gently to one side of the well avoiding disruption of the cell layer.
6. Remove PBS (*see* **Note 15**).
7. Add 100 μL lysis buffer 1× (kept at 4 °C from 5× stock).
8. Lyse cells directly on the culture plates by placing them on a rocker at RT for 15–30 min (*see* **Note 16**).
9. Prepare luciferin substrate reagent, stock typically kept at –20 °C if not reconstituted.
10. Remaining luciferin substrate reagent can be stored at –80 °C till the next use.
11. Keep cell culture plates with lysed cells on ice for immediate reading or store plate with lysate at 4 °C until detection on the same day. (Alternatively store at –80 °C for detection on a different day).
12. Transfer 10–20 μL lysate from each well of the culture plate onto a white opaque 96-well plate (*see* **Note 17**).
13. Set up luminometer to inject 50 μL/well substrate (*see* **Note 18**).
14. Set detection for 5 s (*see* **Note 18**).
15. *β-Galactosidase assay.*
16. Prepare Buffer Z mix (80 % buffer Z + 20 % ONPG + 3.4 μL β-mercaptoethanol per mL of mix Z).

17. Transfer 20 μL lysate/well to a clear 96-well plate (*see* **Note 19**).
18. Add 200 μL of Buffer Z.
19. Incubate at 37 °C until colour change (yellow) becomes apparent.
20. Measure absorbance at OD 405 nm in a plate reader with the appropriate filter.

The transcriptional activity of LXR is calculated as luminescence units normalized to β-galactosidase reading.

4 Notes

1. Store at RT unopened, and once opened store at 4 °C. Prewarm to 37 °C in a water bath before use.
2. In our experience with transfections in RAW cells, the type of transfection reagent is crucial. We have routinely and successfully used Turbofect, which is not a cationic lipid-based formula but a sterile solution of a cationic polymer in water. This polymer forms positively charged complexes with plasmid DNA that are stable and protect the DNA from degradation, thus facilitating efficient introduction of the plasmids into cells.
3. In our experience, endotoxin-free plasmid preps get transfected at a higher efficiency compared to standard DNA preparations. In order to minimize the volume of DNA over the total transfection volume required, we typically prepare working dilutions of all plasmids at concentrations high enough so that small volumes are used. Typically the plasmid needed are: (1) a luciferase reporter vector with either an LXR response element (LXRE) or a promoter/enhancer containing an LXRE fused to a luciferase cassette, (2) an expression vector with the LXR cDNA cloned, and (3) an expression vector containing β-galactosidase or a different luminescence reporter such as Renilla to be used as a transfection efficiency control. If changes in LXR activity by cofactors are being tested, additional expression vectors for those cofactors would be needed.
4. OPTI-MEM®I is a special Modified Eagle's Medium (MEM)-based media with components that allow for a reduction in FBS supplementation with no change in cell growth rates. It is also recommended for use with some cationic lipid transfection reagents. We typically use the version that contains a stable form of glutamine.
5. Other media such as RPMI can be used instead.
6. ONPG is the preferred colorimetric substrate to examine β-Galactosidase reporter activity. The product formed is soluble

and has a high extinction coefficient at 405 nm. This substrate yields a yellow product that is easily detectable in the visible range. β-Galactosidase reporters are usually driven by a variety of promoters including the cytomegalovirus (CMV) promoter. To be used as a transfection efficiency control researchers will need to ensure that the activity of the promoter used remains unchanged with the experimental conditions (addition of LXR ligands and LXR ectopic expression in this case).

7. We routinely use commercial kits to analyse luciferase activity which typically include (a) a cell lysis buffer that allows luciferase and β-galactosidase or Renilla assays to be performed from the same extract, (b) a substrate solution, and (c) a buffer to dissolve the substrate. These solutions and buffers can also be easily prepared by the researcher.
8. Must be highly sensitive and able to detect a broad dynamic range of bioluminescence. Microplate options are preferable to single tube models if a large quantity of samples need to be assayed.
9. Mix cell suspension gently by pipetting up and down against the bottom of the tissue culture dish approximately ten times, do not vortex, and try to avoid generating bubbles.
10. To avoid pipetting errors this is best done using a repeater pipette.
11. Typically we prepare a mix of plasmid DNA per well as follows: reporter plasmid (100 ng for multiple copies of individual LXREs or 300 ng for promoter fragments containing an LXRE), LXR expression vector (50 ng), and β-galactosidase reporter (100 ng). For these amounts, we normally have the reporters at concentrations of 100 ng/μL and expression vectors at 50 ng/μL. In general, the maximum amount transfected is 500 ng of plasmid DNA per well.
12. To reduce variability within (triplicate) samples that have identical DNA mixes, we usually prepare master mixes for 7 wells, which include wells activated with vehicle or ligand (3 each) and an additional well to allow for pipetting errors.
13. This order is important for the optimal formation of polymer-DNA complexes.
14. We typically use GW3965 at a final concentration of 1 μM from a 10 mM stock diluted in DMSO. Other agonists may need to be prepared at different concentrations and with other solvents. Please refer to the literature available. Those wells that are not activated by LXR agonists should be incubated in media containing the vehicle compound (in this case DMSO) in which the agonist has been dissolved.

15. If a high number of plates are being processed, plates can be inverted over a sink to discard medium or PBS, followed by aspiration with a pipette to remove the last drops before addition of PBS or lysis buffer depending on the step.
16. Cells may or may not detach and form a pellet. Regardless of whether they detach or not cell lysis still occurs. When pipetting for analysis ensure that the cell pellet is not taken which will affect the reading.
17. 5–10 μL of lysate may be enough depending on the strength of signal/ activity, transfection efficiency, and sensitivity of the luminometer.
18. This is a starting point. May be reduced depending on sensitivity of the luminometer employed.
19. Time may be extended if found to be insufficient to generate a reading.

Acknowledgement

The authors would like to thank the support of the Medical Research Council (New Investigator Grant G0801278), International Reintegration Program (Grant PIRG02-GA-2007-224867) and British Heart Foundation (PG/13/10/30000) to IPT.

References

1. De Wet JR, Wood KV, DeLuca M, Helinski DR, Subramani S (1987) Firefly luciferase gene: structure and expression in mammalian cells. Mol Cell Biol 7:725–737
2. Hong C, Tontonoz P (2014) Liver X receptors in lipid metabolism: opportunities for drug discovery. Nat Rev Drug Discov 6:433–444
3. Nwachukwu JC, Li W, Pineda-Torra I, Huang HY, Ruoff R, Shapiro E, Taneja SS, Logan SK, Garabedian MJ (2007) Transcriptional regulation of the androgen receptor cofactor androgen receptor trapped clone-27. Mol Endocrinol 21:2864–2876
4. Pourcet B, Pineda-Torra I, Derudas B, Staels B, Glineur C (2010) SUMOylation of human peroxisome proliferator-activated receptor alpha inhibits its trans-activity through the recruitment of the nuclear corepressor NCoR. J Biol Chem 285:5983–5992
5. Pourcet B, Feig JE, Vengrenyuk Y, Hobbs AJ, Kepka-Lenhart D, Garabedian MJ, Morris SM Jr, Fisher EA, Pineda-Torra I (2011) LXRα regulates macrophage arginase 1 through PU.1 and interferon regulatory factor 8. Circ Res 109:492–501
6. Costet P, Luo Y, Wang N, Tall AR (2000) Sterol-dependent transactivation of the ABC1 promoter by the liver X receptor/retinoid X receptor. J Biol Chem 275: 28240–28245
7. Collins JL, Fivush AM, Watson MA, Galardi CM, Lewis MC, Moore LB, Parks DJ, Wilson JG, Tippin TK, Binz JG, Plunket KD, Morgan DG, Beaudet EJ, Whitney KD, Kliewer SA, Willson TM (2002) Identification of a nonsteroidal liver X receptor agonist through parallel array synthesis of tertiary amines. J Med Chem 45:1963–1966

Chapter 8

Metabolically Biotinylated Reporters for Electron Microscopic Imaging of Cytoplasmic Membrane Microdomains

Kimberly J. Krager and John G. Koland

Abstract

The protein and lipid substituents of cytoplasmic membranes are not in general homogeneously distributed across the membrane surface. Many membrane proteins, including ion channels, receptors, and other signaling molecules, exhibit a profound submicroscopic spatial organization, in some cases clustering in submicron membrane subdomains having a protein and lipid composition distinct from that of the bulk membrane. In the case of membrane-associated signaling molecules, mounting evidence indicates that their nanoscale organization, for example the colocalization of differing signaling molecules in the same membrane microdomains versus their segregation into distinct microdomain species, can significantly impact signal transduction. Biochemical membrane fractionation approaches have been used to characterize membrane subdomains of unique protein and lipid composition, including cholesterol-rich lipid raft structures. However, the intrinsically perturbing nature of fractionation methods makes the interpretation of such characterization subject to question, and indeed the existence and significance of lipid rafts remain controversial. Electron microscopic (EM) imaging of immunogold-labeled proteins in plasma membrane sheets has emerged as a powerful method for visualizing the nanoscale organization and colocalization of membrane proteins, which is not as perturbing of membrane structure as are biochemical approaches. For the purpose of imaging putative lipid raft structures, we recently developed a streamlined EM membrane sheet imaging procedure that employs a unique genetically encoded and metabolically biotinylated reporter that is targeted to membrane inner leaflet lipid rafts. We describe here the principles of this procedure and its application in the imaging of plasma membrane inner leaflet lipid rafts.

Key words Membrane protein, Membrane microdomain, Nanodomain, Lipid raft, Electron microscopy, EM imaging, Avidin-biotin detection, Gold labeling

1 Introduction

The protein and lipid substituents of cellular cytoplasmic membranes show a remarkable degree of structural organization on the submicron scale. Beyond the well-known cell-cell junctional structures of epithelial and other cells, the synaptic structures of neurons, and the more recently characterized immunological synaptic structures [1], a more subtle submicron spatial organization has

Mark G. Waugh (ed.), *Lipid Signaling Protocols*, Methods in Molecular Biology, vol. 1376,
DOI 10.1007/978-1-4939-3170-5_8,

now been seen in the case of diverse membrane proteins including ion channels, receptors and other signaling molecules. The factors underlying the segregation of such proteins within membrane microdomains are unclear. Among mechanisms proposed are the partitioning of certain proteins into preexisting membrane microdomains (such as lipid rafts or caveolae), the nucleation by certain proteins of raft formation from smaller lipid nanodomains, the confinement of proteins within cytoskeletal corrals, and their interactions with intracellular and extracellular matrix components [2–4]. Microdomains in which the lateral diffusion of membrane proteins is restricted have been termed "transient confinement zones," which may or may not be related to lipid raft structures [5]. There is also evidence for the existence of lipid rafts in the inner and outer leaflets of the plasma membrane that are independent (but potentially interacting) structures and of lipid and protein composition differing from the bulk membrane [6, 7].

As one well-studied example, the localization of epidermal growth factor (EGF) receptor molecules within submicroscopic domains of the plasma membrane has been demonstrated by various high-resolution imaging methods [8–11], in addition to biochemical approaches identifying the EGF receptor in lipid raft fractions of the plasma membrane [12–14]. This observed localization of the EGF receptor in microdomains and/or transient confinement zones has been attributed to all of the above-described mechanisms (raft partitioning, confinement, cytoskeletal attachments). We desired in our recent work to examine whether the observed microdomains of EGF receptor localization were in fact lipid raft structures, and sought a strategy that would allow simultaneous imaging of EGF receptor microlocalization and lipid raft entities.

A very practical approach for visualizing the submicron-scale spatial organization of plasma membrane proteins is the imaging by electron microscopy (EM) of immunogold-labeled proteins in plasma membrane sheets [15]. Originally developed by Sanan and Anderson [16], the immuno-EM "membrane sheet" approach has been elegantly exploited in characterizing the plasma membrane microlocalization of Ras signaling proteins [17], various substituents of immuno-receptor signaling systems [18], and also EGF receptor family (HER family) proteins [19]. This technique is of higher resolution than conventional light microscopy methods and can be used to both visualize and quantitatively analyze the two-dimensional spatial organization of membrane proteins. This method has proven to be a powerful complement to other imaging and biochemical methods for the study of membrane protein microlocalization and membrane microdomains [cf. [5, 20]].

In applying the immuno-EM membrane sheet method, cultured cells grown on glass cover slips are first sandwiched between the cover slip and a specially coated EM grid. Removal of the cover

slip leaves torn-off sheets of the cellular plasma membrane adhering to the grid with the intracellular face (inner leaflet) of the membrane exposed. The membrane sheets are then subjected to immunogold labeling of one or more specific membrane proteins and imaged by transmission EM (TEM). The immuno-EM membrane sheet imaging method thus requires that the protein(s) of interest in immobilized plasma membranes can be specifically labeled with a gold particle-conjugated immunochemical reagent. The imaging of lipid rafts in addition requires the identification of a suitable raft marker protein and an antibody for its specific detection [20]. As an alternative and more streamlined strategy, we have devised an approach for the gold labeling of plasma membrane lipid rafts that employs a genetically encoded and metabolically biotinylated lipid raft-targeted reporter, Lck-BAP-GFP [21]. Notably, this reporter can be labeled in a single step with gold particle-conjugated streptavidin reagents.

The design and construction of the Lck-BAP-GFP reporter has been described in detail (*see* Fig. 1a) [21]. The lipid raft-targeting motif of the reporter is a 26-amino acid N-terminal membrane-targeting sequence from the human Lck kinase. We considered this sequence element, which is myristoylated and potentially dually palmitoylated in mammalian cells, to be among the most extensively characterized membrane-targeting motifs [2, 22, 23] and would be most characteristic of motifs having an affinity for putative cholesterol-rich inner leaflet lipid raft entities. The N-terminal Lck motif is followed by a biotin acceptor peptide (BAP) module, which is metabolically biotinylated by endogenous mammalian biotin ligases [24, 25]. Hence, incorporation of this BAP module allows detection of the reporter with avidin-based reagents, including streptavidin-horseradish peroxidase and streptavidin-gold particle conjugates. The reporter lastly contains a green fluorescent protein module for detection of expression and membrane localization in cultured cells by conventional fluorescence microscopy. The reporter cDNA is cloned in a cytomegalovirus promoter-based expression vector, for its convenient expression by cellular transfection. Our previous work indicated that the Lck-BAP-GFP reporter is readily expressed, is plasma membrane-targeted, and is efficiently biotinylated in cultured cells. EM imaging of the gold-labeled reporter showed it clustering in microdomains of 20–50 nm, consistent with its localization in inner leaflet lipid rafts (*see* Fig. 1b–d) [21].

We detail below our methodology for imaging the spatial distribution of inner leaflet lipid raft entities with the aid of this metabolically biotinylated reporter and the application of this method in examining the potential raft localization of an endogenous membrane protein (i.e., the EGF receptor). The quantitative characterization by Ripley's *K* function analysis of the spatial distributions of the reporter and a second labeled protein is also described.

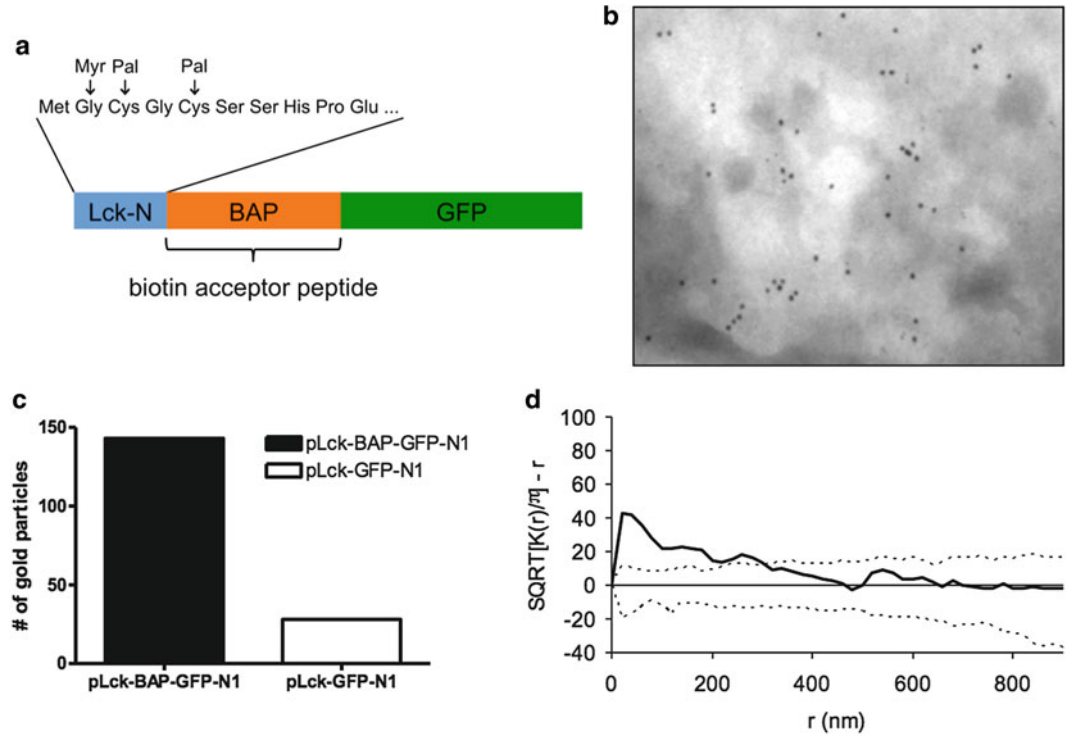

Fig. 1 Design and application of a metabolically biotinylated lipid raft reporter. For the purpose of imaging lipid raft structures in breast cancer cell membranes, we developed a lipid raft-targeted reporter construct (Lck-BAP-GFP) that is metabolically biotinylated and can be detected with avidin reagents, e.g., a streptavidin-gold conjugate for detection by electron microscopy [21]. (**a**) Structure of the Lck-BAP-GFP lipid raft reporter: *Lck-N* lipid raft-targeting sequence from the N-terminus of the Lck kinase with its sites of myristoylation and dual palmitoylation indicated; *BAP* biotin acceptor peptide that is metabolically biotinylated in mammalian cells; *GFP* enhanced green fluorescent protein module for imaging by fluorescence microscopy. (**b**) Representative TEM image of plasma membrane sheets from MDA-MB-468 breast cancer cells expressing the Lck-BAP-GFP lipid raft reporter and labeled with 6 nm gold-conjugated streptavidin. The clustering of the gold-labeled reporter in putative lipid raft structures is evident. (**c**) Graph depicting the number of streptavidin-gold particles from an image of a pLck-BAP-GFP-N1-transfected MDA-MB-468 cell membrane sheet compared to those of negative control pLck-GFP-N1-transfected cells. Streptavidin labeling was significantly higher in the cells expressing the Lck-BAP-GFP reporter, indicating the specificity of the streptavidin-gold labeling. (**d**) Ripley's K-function analysis of the clustering of particles in a TEM image of the gold-labeled Lck-BAP-GFP reporter in an MDA-MB-468 cell membrane sheet. *Solid line* is the statistical function SQRT[K(r)/π] – r evaluated for the particle distribution in *panel* (**b**). *Dashed lines* are the envelopes of positive and negative deviations of the SQRT[K(r)/π] – r function in 99 simulations of random particle distributions. A nonrandom distribution of the Lck-BAP-GFP reporter was evident with clustering in the 20–50 nm range, consistent with the proposed size of lipid raft structures

2 Materials

2.1 Cell Culture and Lck-BAP-GFP Reporter Expression

1. MDA-MB-468 cells: The representative MDA-MB-468 mammary epithelial tumor cell line with high-level EGF receptor expression can be purchased from the American Type Culture Collection and is propagated according to their recommendations.
2. pLck-BAP-GFP plasmid expression vector: The Lck-BAP-GFP reporter cDNA (*see* Fig. 1a) is expressed via transfection of pLck-BAP-GFP [21], a plasmid expression vector derived from pEGFP-N1 (Clontech). The pLck-BAP-GFP plasmid is propagated in *E. coli* DH5α.
3. Transfection reagent: Lipofectamine 2000 (Invitrogen) cationic liposomal transfection reagent used according to manufacturer recommendations.

2.2 Lipid Raft TEM Imaging

See **Note 1** for suppliers of electron microscopy reagents.

1. PBS: Phosphate-buffered saline, calcium and magnesium free.
2. Poly-L-lysine/Formvar/carbon-coated nickel EM grids: Carbon-coated Formvar-filmed nickel EM grids are prepared by standard microscopy procedures or purchased from a supplier. The grids are coated with poly-L-lysine by immersing them in a 1 mg/ml poly-L-lysine solution and allowing them to air-dry after removal of excess solution.
3. 2 % Paraformaldehyde: Aqueous solution from a 16 % stock solution.
4. Blocking buffer: 5 % BSA-C, 0.1 % cold water fish skin gelatin, and 5 % normal goat serum diluted in PBS.
5. Incubation buffer: 0.2 % BSA-C in PBS
6. EGF receptor antibody: Rabbit monoclonal EGF receptor antibody SP9 (Thermo Scientific).
7. Immunogold conjugates: 6 nm gold particle-conjugated streptavidin and 10 nm gold particle-conjugated F(ab′)2 fragment of goat anti-rabbit IgG.
8. 2.5 % Glutaraldehyde: Aqueous solution prepared from a 25 % stock solution.
9. 5 % Uranyl acetate: Aqueous solution prepared from solid uranyl acetate.

2.3 Analysis of Particle Spatial Distribution

1. ImageJ software: The ImageJ2 version of open source image processing software available in the Fiji distribution for biological sciences can be downloaded at http://fiji.sc/Welcome.
2. SPPA software: The Spatial Point Pattern Analysis software package for analysis of gold-particle spatial distributions using the Ripley's *K* function approach was created and generously provided by Dr. Peter Haase.

3 Methods

3.1 Cell Culture and Lck-BAP-GFP Reporter Transfection

1. Cultured mammalian cells to be analyzed (for example MDA-MB-468 mammary epithelial tumor cells) are plated at 70 % confluency on 18-mm glass cover slips in six-well polystyrene tissue culture plates and grown overnight at 37 °C in culture medium [in the case of MDA-MB-468 cells, Leibovitz's L-15 medium with 10 % fetal bovine serum added].
2. The following day, cells in six-well clusters are transfected with pLck-BAP-GFP (1 μg plasmid and 1–5 μl Lipofectamine 2000 transfection reagent mix per well) for 3 h in serum-free medium at 37 °C, and then incubated overnight in serum-supplemented medium at 37 °C (*see* **Note 2**).

3.2 Lipid Raft TEM Imaging

The procedures here are adapted from those previously described (*see* **Note 3**). Unless otherwise noted, they are performed at room temperature.

1. The following day, transfected cells in six-well clusters are was washed two times with PBS.
2. Individual cover slips upon which cells are attached are removed from the second PBS wash, inverted, and lowered (cell side down) upon an arrangement of several poly-L-lysine/formvar/carbon-coated EM grids on a sheet of soft plastic film (e.g., Parafilm-M). (The number of grids used per cover slip will depend upon the need for replicates, for doubling-labeling strategies involving multiple membrane proteins, and/or for optimization of labeling conditions.)
3. Cover slips are pressed down upon the grids with the thumb (10-s gentle pressure), so that cellular membranes adhere to the grid surface.
4. The cover slips are inverted, and the grids, with fragments of plasma membrane attached, are floated off in a small volume of PBS.
5. Grids are then fixed with a 2 % paraformaldehyde solution, washed with PBS, and incubated in blocking buffer for 30 min at room temperature (*see* **Note 4**).
6. Grids are next incubated overnight at 4 °C with 6 nm gold-conjugated streptavidin reagent diluted 50-fold in incubation buffer or, in the case of double-labeling experiments, in the presence of 6 nm gold-conjugated streptavidin and the antibody of choice (e.g., rabbit EGF receptor antibody diluted 50-fold).
7. The following day grids are washed six times with incubation buffer. Double-labeled grids are further incubated with a 10 nm gold-conjugated secondary antibody (e.g., 10 nm gold-

conjugated F(ab′)2 fragment of anti-rabbit-IgG) followed by six additional washes with incubation buffer.

8. Grids are lastly postfixed with 2.5 % glutaraldehyde, washed once with PBS, washed five times with water, then stained with 5 % uranyl acetate, and air-dried.
9. Grids are imaged with a transmission electron microscope (e.g., JEOL JEM 1230) at ~12,000× (*see* **Note 5**).

3.3 Analysis of Gold-Labeled Particle Clustering

TEM images showing the two-dimensional distributions of gold-labeled particles (representing the Lck-BAP-GFP reporter and/or a conventionally immunogold-labeled membrane protein) can be quantitatively analyzed in terms of the extent and size scale of their clustering, as well as their co-clustering in the case of images of double-labeled membranes. In our previous work, the 6 nm gold particle-labeled Lck-BAP-GFP lipid raft marker expressed in MDA-MB-468 breast cancer cell membranes showed a nonrandom spatial distribution and a tendency to cluster on the scale of 20–50 nm, consistent with its presumed existence in submicron lipid raft entities (*see* Fig. 1d), and the 10 nm gold particle-labeled EGF receptor, while itself seen clustering in nanodomains, showed a negligible tendency to co-cluster with the raft reporter [21]. Among alternative statistical methods used to analyze particle clustering in TEM images [20], the Ripley's K function approach is straightforward in its application and yields an intuitively interpretable graphical result (cf. [15, 26]). Here, $K(r)$ is computed using the set of x–y coordinates for all particles in a given image, and the derivative statistical function $\mathrm{SQRT}[K(r)/\pi] - r$ is plotted versus distance (r). This function approximates a constant value of zero for a random particle distribution, and its positive deviation from zero indicates a tendency for the particles in the image to cluster and also the size scale of the clustering [27]. (An analogous bivariate statistical function is used to characterize co-clustering of two different particle types.) The first step in the analysis of the particle spatial distribution is cataloging the x–y coordinates of each gold particle in an image (and creating a separate list of coordinates for each of the two sizes of gold-particles in double-labeling experiments). Ripley's K function analysis of the data is then performed using the SPPA software package developed and generously provided by Dr. Peter Haase [28].

1. Coordinates of the centers of all gold particles in a TEM image are determined by use of automatic particle recognition functions in ImageJ Software supplemented by its manual particle picking function when necessary (*see* **Note 6**).
2. An input data file (in a simple text format) for SPPA is generated with a header line indicating the width and height of the image area in nanometers, the range of distances to be ana-

lyzed (typically 0 to n nanometers, where n is ideally no greater than 1/5 of the image size so as to minimize image edge effects), and the number of random distributions that are to be generated in calculating the confidence interval for deviations from randomness (e.g., 99 for a 99 % confidence interval). Following the header, consecutive lines contain the x and y coordinates of the individual particles in the image given in nanometers. When a bivariate analysis of the co-clustering of two particle types is performed, each coordinate pair is followed by a particle type identifier, either 0 or 1.

3. Plots of SQRT[$K(r)/\pi$] – r versus r generated by SPPA are then inspected to determine if the particle distribution shows clustering (i.e., positive deviations from the envelope of the random distributions, *see* Fig. 1d) and the size-scale upon which the clustering occurs. Particle co-clustering in images of double-labeled membrane specimens (e.g., the Lck-BAP-GFP reporter and an endogenous membrane protein) is similarly indicated by a plot of the bivariate SQRT[$K(r)/\pi$] – r function, again generated by the SPPA software (cf. [21]).

4 Notes

1. The following electron microscopy grade reagents were obtained from Electron Microscopy Sciences: 6 nm gold particle-conjugated streptavidin, 10 nm gold particle-conjugated F(ab′)2 fragment of goat anti-rabbit IgG, normal goat serum, uranyl acetate, and stock solutions of BSA-C (acetylated BSA), cold-water fish skin gelatin, glutaraldehyde, and paraformaldehyde. Other suppliers have not been tested. Gold-conjugated reagents should be examined before use to detect any intrinsic particle aggregation (*see* **Note 6**).
2. The effective transfection of cells and Lck-BAP-GFP reporter expression are readily verified by fluorescence microscopy, with the fluorescence of the GFP module of the reporter being observed.
3. Procedures for immobilizing plasma membrane sheets on EM grids and for immunogold labeling of membrane proteins in membrane sheets have been described in detail by Wilson et al. [29] and Prior et al. [15]. We adapt them here to the streptavidin-gold labeling of a biotinylated membrane species, i.e. the Lck-BAP-GFP lipid raft reporter.
4. This and all other steps in the gold labeling procedure (e.g., fixation, washing, and blocking of the membranes adhering to the grid surface) are performed by floating the grids (membrane side down) on small droplets (e.g., 20 μl) of solution on

a clean sheet of plastic film. Grids are handled throughout with a small forceps. In consecutive treatments, the first solution is wicked away from the grid with a strip of filter paper before the grid is applied to the next solution droplet. While the labeling is performed, the plasma membrane sheets adhering to the grids have their intracellular surface (inner leaflet) exposed, as evidence by the effective immunogold labeling of membrane proteins therein with antibodies recognizing cytoplasmic epitopes and the effective labeling of the cytoplasmically expressed Lck-BAP-GFP reporter.

5. Plasma membrane sheets are identified in initial lower power images, often seen splayed out from broken cell bodies. The membrane sheets themselves show areas of higher and lower contrast, apparently reflecting the differential binding of the uranyl acetate contrast agent to regions of differing lipid/protein composition.
6. Procedures for the use of ImageJ particle discrimination functions are detailed by Prior et al. [15]. Control TEM images of 6 nm gold-conjugated streptavidin and 10 nm gold-conjugated secondary antibody directly applied to an EM grid [*see* Supplemental Material in ref. 21] should indicate that the 6 and 10 nm gold conjugates provided by Electron Microscopy Sciences show essentially non-overlapping size distributions and hence can be readily discriminated. Such control images will also indicate the extent to which gold-conjugated reagents show intrinsic clustering (or aggregation).

Acknowledgement

The authors wish to acknowledge the University of Iowa Central Microscopy Research Facility for their expert technical support and guidance, and for their provision of instrumentation used in TEM imaging.

References

1. Grakoui A, Bromley SK, Sumen C, Davis MM, Shaw AS, Allen PM, Dustin ML (1999) The immunological synapse: a molecular machine controlling T cell activation. Science 285:221–227
2. Chichili GR, Rodgers W (2007) Clustering of membrane raft proteins by the actin cytoskeleton. J Biol Chem 282:36682–36691
3. Lajoie P, Partridge EA, Guay G, Goetz JG, Pawling J, Lagana A, Joshi B, Dennis JW, Nabi IR (2007) Plasma membrane domain organization regulates EGFR signaling in tumor cells. J Cell Biol 179:341–356
4. Nicolau DV Jr, Burrage K, Parton RG, Hancock JF (2006) Identifying optimal lipid raft characteristics required to promote nanoscale protein-protein interactions on the plasma membrane. Mol Cell Biol 26:313–323
5. Lagerholm BC, Weinreb GE, Jacobson K, Thompson NL (2005) Detecting microdomains in intact cell membranes. Annu Rev Phys Chem 56:309–336

6. Pike LJ, Han X, Gross RW (2005) Epidermal growth factor receptors are localized to lipid rafts that contain a balance of inner and outer leaflet lipids: a shotgun lipidomics study. J Biol Chem 280:26796–26804
7. Pyenta PS, Holowka D, Baird B (2001) Cross-correlation analysis of inner-leaflet-anchored green fluorescent protein co-redistributed with IgE receptors and outer leaflet lipid raft components. Biophys J 80:2120–2132
8. Keating E, Nohe A, Petersen NO (2008) Studies of distribution, location and dynamic properties of EGFR on the cell surface measured by image correlation spectroscopy. Eur Biophys J 37:469–481
9. Orr G, Hu D, Ozcelik S, Opresko LK, Wiley HS, Colson SD (2005) Cholesterol dictates the freedom of EGF receptors and HER2 in the plane of the membrane. Biophys J 89:1362–1373
10. Xiao Z, Zhang W, Yang Y, Xu L, Fang X (2008) Single-molecule diffusion study of activated EGFR implicates its endocytic pathway. Biochem Biophys Res Commun 369:730–734
11. Kawashima N, Nakayama K, Itoh K, Itoh T, Ishikawa M, Biju V (2010) Reversible dimerization of EGFR revealed by single-molecule fluorescence imaging using quantum dots. Chemistry 16:1186–1192
12. Waugh MG, Lawson D, Hsuan JJ (1999) Epidermal growth factor receptor activation is localized within low-buoyant density, non-caveolar membrane domains. Biochem J 337: 591–597
13. Ringerike T, Blystad FD, Levy FO, Madshus IH, Stang E (2002) Cholesterol is important in control of EGF receptor kinase activity but EGF receptors are not concentrated in caveolae. J Cell Sci 115:1331–1340
14. Roepstorff K, Thomsen P, Sandvig K, van Deurs B (2002) Sequestration of epidermal growth factor receptors in non-caveolar lipid rafts inhibits ligand binding. J Biol Chem 277:18954–18960
15. Prior IA, Parton RG, Hancock JF (2003) Observing cell surface signaling domains using electron microscopy. Sci STKE 2003:PL9
16. Sanan DA, Anderson RG (1991) Simultaneous visualization of LDL receptor distribution and clathrin lattices on membranes torn from the upper surface of cultured cells. J Histochem Cytochem 39:1017–1024
17. Prior IA, Muncke C, Parton RG, Hancock JF (2003) Direct visualization of Ras proteins in spatially distinct cell surface microdomains. J Cell Biol 160:165–170
18. Wilson BS, Pfeiffer JR, Oliver JM (2002) FcepsilonRI signaling observed from the inside of the mast cell membrane. Mol Immunol 38:1259–1268
19. Yang S, Raymond-Stintz MA, Ying W, Zhang J, Lidke DS, Steinberg SL, Williams L, Oliver JM, Wilson BS (2007) Mapping ErbB receptors on breast cancer cell membranes during signal transduction. J Cell Sci 120:2763–2773
20. Wilson BS, Steinberg SL, Liederman K, Pfeiffer JR, Surviladze Z, Zhang J, Samelson LE, Yang LH, Kotula PG, Oliver JM (2004) Markers for detergent-resistant lipid rafts occupy distinct and dynamic domains in native membranes. Mol Biol Cell 15:2580–2592
21. Krager KJ, Sarkar M, Twait EC, Lill NL, Koland JG (2012) A novel biotinylated lipid raft reporter for electron microscopic imaging of plasma membrane microdomains. J Lipid Res 53:2214–2225
22. Zlatkine P, Mehul B, Magee AI (1997) Retargeting of cytosolic proteins to the plasma membrane by the Lck protein tyrosine kinase dual acylation motif. J Cell Sci 110(Pt 5): 673–679
23. Johnson SA, Stinson BM, Go MS, Carmona LM, Reminick JI, Fang X, Baumgart T (2010) Temperature-dependent phase behavior and protein partitioning in giant plasma membrane vesicles. Biochim Biophys Acta 1798: 1427–1435
24. Parrott MB, Barry MA (2000) Metabolic biotinylation of recombinant proteins in mammalian cells and in mice. Mol Ther 1:96–104
25. Tannous BA, Grimm J, Perry KF, Chen JW, Weissleder R, Breakefield XO (2006) Metabolic biotinylation of cell surface receptors for in vivo imaging. Nat Methods 3:391–396
26. Haase P (2001) Can isotropy vs. anisotropy in the spatial association of plant species reveal physical vs. biotic facilitation? J Veg Sci 12:127–136
27. Kiskowski MA, Hancock JF, Kenworthy AK (2009) On the use of Ripley's K-function and its derivatives to analyze domain size. Biophys J 97:1095–1103
28. Haase P (1995) Spatial pattern analysis in ecology based on Ripley's K-function: introduction and methods of edge correction. J Veg Sci 6:575–582
29. Wilson BS, Pfeiffer JR, Oliver JM (2000) Observing FcepsilonRI signaling from the inside of the mast cell membrane. J Cell Biol 149:1131–1142

Chapter 9

Fluorescence Recovery After Photobleaching Analysis of the Diffusional Mobility of Plasma Membrane Proteins: HER3 Mobility in Breast Cancer Cell Membranes

Mitul Sarkar and John G. Koland

Abstract

The fluorescence recovery after photobleaching (FRAP) method is a straightforward means of assessing the diffusional mobility of membrane-associated proteins that is readily performed with current confocal microscopy instrumentation. We describe here the specific application of the FRAP method in characterizing the lateral diffusion of genetically encoded green fluorescence protein (GFP)-tagged plasma membrane receptor proteins. The method is exemplified in an examination of whether the previously observed segregation of the mammalian HER3 receptor protein in discrete plasma membrane microdomains results from its physical interaction with cellular entities that restrict its mobility. Our FRAP measurements of the diffusional mobility of GFP-tagged HER3 reporters expressed in MCF7 cultured breast cancer cells showed that despite the observed segregation of HER3 receptors within plasma membrane microdomains their diffusion on the macroscopic scale is not spatially restricted. Thus, in FRAP analyses of various HER3 reporters a near-complete recovery of fluorescence after photobleaching was observed, indicating that HER3 receptors are not immobilized by long-lived physical interactions with intracellular species. An examination of HER3 proteins with varying intracellular domain sequence truncations also indicated that a proposed formation of oligomeric HER3 networks, mediated by physical interactions involving specific HER3 intracellular domain sequences, either does not occur or does not significantly reduce HER3 mobility on the macroscopic scale.

Key words HER/ErbB receptor, Membrane microdomain diffusion, Fluorescence recovery after photobleaching (FRAP)

1 Introduction

Epidermal growth factor (EGF) receptor family (HER/ErbB family) members (designated HER1-4 or ErbB1-4) are among cell surface receptors whose signaling activities appear to be modulated by their compartmentalization in plasma membrane microdomains. Whereas initial biochemical analyses suggested the EGF receptor (HER1) was localized in caveolae, ensuing fractionation studies indicated a non-caveolar lipid raft localization [reviewed in ref. 1]. More recent electron microscopic (EM)

Mark G. Waugh (ed.), *Lipid Signaling Protocols*, Methods in Molecular Biology, vol. 1376,
DOI 10.1007/978-1-4939-3170-5_9,

imaging of immunogold-labeled receptors and their associated signaling targets in plasma membrane sheets by Yang et al. indeed showed an elaborate nanoscale organization of EGF receptor and HER2 and HER3 receptor molecules in breast cancer cell membranes, and further indicated that their signaling occurs within discrete nanodomains of the plasma membrane [2]. Using this same methodology, we verified this nanoscale clustering of the EGF receptor in breast cancer cell membranes, and by the additional implementation of a metabolically biotinylated lipid raft reporter construct (see Chapter 8) showed that the domains of EGF receptor clustering were distinct from inner leaflet lipid raft species [1]. The biochemical characteristics of the membrane microdomains in which the EGF receptor resides remain largely unknown.

Uniquely among the four HER family members, the HER3 receptor possesses a significantly impaired protein tyrosine kinase (PTK) activity and thus signals effectively only in the context of a heterodimeric complex with another kinase-competent HER receptor ([3, 4] but see [5, 6]). In comparison with other HER family receptors, HER3 is a particularly robust recruiter and activator of phosphoinositide (PI) 3-kinase (cf. [7]), which likely underlies the marked potentiation by HER3 of the mitogenic and transforming activities of the EGF receptor and HER2. HER3 is an important player in a number of cancer types and is a target of current cancer drug development [8].

The immunogold labeling of receptors in breast cancer cell plasma membrane sheets described by Yang et al. [2] showed that HER3 is concentrated in discrete plasma membrane nanodomains, largely distinct from those of EGF receptor and HER2 localization and which apparently serve as platforms for PI 3-kinase activation in response to activating growth factors. The exact identity and biochemical composition of the membrane microdomain entities in which HER3 resides and the mechanism of its sequestration therein remain unclear. Two possible mechanisms for the clustering of the HER3 protein in nanodomains are its physical interaction with some other entity, for example a cytoskeletal component, and an extended HER3 oligomerization, as has been predicted on the basis of X-ray crystallographic studies of the HER3 structure. Here, Jura et al. [9] identified two independent modes of interaction between pairs of HER3 intracellular domains that can mediate their dimerization, one involving the N-terminal lobes of both PTK domains in a dimer and one involving the C-terminal lobe of the PTK domain in one monomer and a kinase-proximal segment of the CT domain in the other, and further postulated that these two independent modes of interaction could mediate the formation of chains or networks of interacting HER3 receptors in cell membranes. To determine the potential impact of HER3 interactions with other cytosolic entities or with itself in the case of HER3 oligomerization, we analyzed the effect of truncating

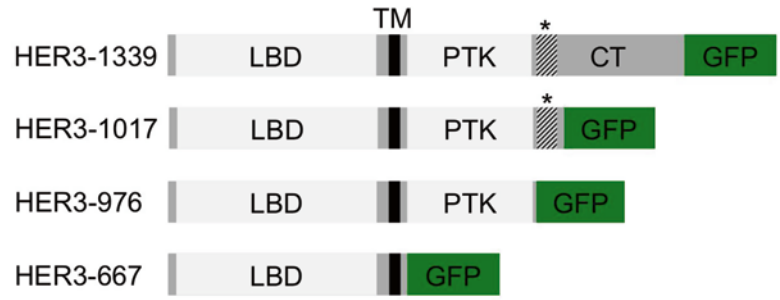

Fig. 1 Fluorescent HER3 reporters with C-terminal intracellular domain truncations. For use in characterizing the diffusional mobility of HER3 receptors in cellular membranes by FRAP, HER3 reporter constructs with varying C-terminal domain truncations and C-terminal monomeric GFP tags were generated. Schematic sequences of the reporters are shown with the locations of the extracellular ligand binding (LBD), transmembrane (TM), protein tyrosine kinase (PTK) and C-terminal phosphorylation (CT) domains, and the monomeric GFP module (GFP) indicated. Also indicated is a putative HER3 oligomerization motif (*) in the kinase-proximal CT domain sequence (residues 982–992 in the rat HER3 precursor protein), which has been postulated to mediate the formation of extended oligomeric networks of HER3 molecules in cellular membranes [9]. The C-terminally complete reporter containing the entire 1339-amino acid sequence of rat HER3 is designated HER3-1339. The HER3-1017, -976, and -667 reporters are truncated after the indicated amino acid residues and thus have progressive deletions of the distal CT domain, the putative HER3 oligomerization motif, and the PTK domain. All retain a positively charged stop-transfer signal immediately following the transmembrane domain, so that they are retained in the cytoplasmic membrane

various segments of the HER3 intracellular domain on the diffusional mobility of the receptor in the plasma membrane by the fluorescence recovery after photobleaching (FRAP) method. To this end, we first generated a panel of recombinant HER3 constructs with varying C-terminal intracellular domain truncations and which were C-terminally tagged with a monomeric GFP (mGFP) module (*see* Fig. 1). We describe here the FRAP methodology used to characterize the lateral diffusional mobility of these mGFP-tagged HER3 constructs in breast cancer cell membranes, a straightforward method that is extensible to investigating the lateral mobility of other plasma membrane-associated proteins. More comprehensive descriptions of FRAP methodology have been presented (e.g., [10, 11]).

2 Materials

2.1 Cell Culture and HER3-mGFP Reporter Expression

1. MCF7 cells: The MCF7 mammary epithelial tumor cell line can be purchased from the American Type Culture Collection and is propagated according to their recommendations.

2. HER3-mGFP plasmid expression vectors: The pcDNA3-HER3-mGFP plasmid is a CMV promoter-based vector (pcDNA3) expressing the full-length rat HER3 protein (1339 residues) fused to the mGFP (monomeric GFP) module, a version of the enhanced GFP protein with an A206K substitution that reduces its dimerization potential. The plasmid was generated by recombinant PCR amplifications of the rat HER3 cDNA sequence in the pcDNA3-HER3 expression vector [12] and the enhanced GFP cassette in the pEGFP-N1 vector, after a mutation effecting the A206K substitution was introduced into the GFP cDNA by site-directed mutagenesis. Again using recombinant PCR, internal deletions were made in the pcDNA3-HER3-mGFP plasmid to truncate the HER3 protein beyond the indicated residues in the HER3-1017, HER3-976 and HER3-667 constructs while retaining the C-terminal mGFP tag (*see* Fig. 1). All amplified sequence elements were validated by DNA sequencing.
3. Transfection reagent: Lipofectamine 2000 (Invitrogen) cationic liposomal transfection reagent used according to the recommendations of the manufacturer.

2.2 FRAP Measurements

1. Glass-bottom culture dishes: FRAP experiments require plastic culture dishes with microscope cover glass bottoms (35 mm diameter).
2. Microscopy instrumentation: FRAP experiments are performed using a conventional inverted laser confocal microscope having built-in functions for photobleaching of a circular region of interest (ROI) (for example bleaching of the mGFP fluorophore in a 5 μm diameter ROI with a 488 nm argon laser beam) and for the time-dependent acquisition of the integrated fluorescence intensities of both circular and irregularly shaped ROIs and which is outfitted with a heated stage.

2.3 FRAP Data Analysis

1. Computer software: Analysis of FRAP kinetic data by the bleached-disk method of Soumpasis [13] is facilitated by the use of nonlinear least squares curve fitting software that allows the incorporation of modified Bessel functions in curve fitting functions, such as Prism 5.0 (GraphPad).

3 Methods

3.1 Cell Culture and HER3-mGFP Reporter Expression

1. Cultured cells to be analyzed (for example MCF7 mammary epithelial tumor cells) are plated in 35 mm glass-bottom culture dishes and grown at 37 °C in culture medium [in the case of MCF7 cells in minimal essential medium (MEM) containing Earle's salts and stabilized glutamine supplement with 10 % fetal bovine serum added].

2. At approximately 40 % confluency cells are transfected with the GFP reporter plasmid DNA expression vector in complex with cationic liposomes (e.g., treated with 0.3–0.5 μg of pcDNA3-HER3-mGFP plasmid using 2–4 μl of Lipofectamine 2000 transfection reagent) for 3 h in serum-free culture medium, and then allowed to recover overnight in normal culture medium at 37 °C.
3. One day prior to FRAP measurements, the cells are incubated overnight in reduced-serum (1.5 % serum in the case of MCF7 cells) culture medium at 37 °C.

3.2 FRAP Measurements

1. FRAP measurements are made typically 48 h after cell transfection, to allow time for adequate GFP reporter expression.
2. When measurements are performed using a microscope with air-exposed stage, the cell culture medium is replaced with Hanks' Balanced Salt Solution immediately prior to FRAP measurements so that physiologic pH is maintained.
3. FRAP experiments can be performed using a conventional inverted confocal microscope (employing a 63× objective and 2× digital zoom in the case of the Zeiss 510 instrument), with a heated stage held at a fixed temperature typically between 30 and 37 °C (*see* **Note 1**). Selection of single cells for FRAP analysis is performed by viewing the GFP fluorescence of the expressed reporter with appropriate excitation and emission settings (e.g., the GFP fluorophore excited by a 488 nm laser line at low power, and the emitted fluorescence captured through a 505–550 nm band-pass filter). The cellular plasma membrane is then placed in the plane of focus.
4. Using built-in software tools of the microscope, a circular ROI of typically 5 μm diameter (the area of photobleaching and primary fluorescence intensity measurements, *see* **Note 2**) is selected, along with a larger, potentially irregularly shaped ROI that surrounds the ROI to be photobleached and is the ROI for control fluorescence intensity measurements (*see* Fig. 2 and **Note 3**).
5. Beginning before photobleaching and continuing throughout the post-photobleaching recovery, a time series of images is captured (typically at 2 s intervals), during which the GFP fluorophore is excited at low intensity, the emitted GFP fluorescence is captured, and time courses of the integrated fluorescence intensities of the measurement (photobleached) and control ROIs are recorded.
6. After recording of the pre-photobleach intensities in the measurement and control ROIs, the circular measurement ROI is rapidly photobleached using programmed photobleaching functions of the microscope (e.g., ten scans of the ROI with a 488 nm laser at 100 % intensity), and the recording of the

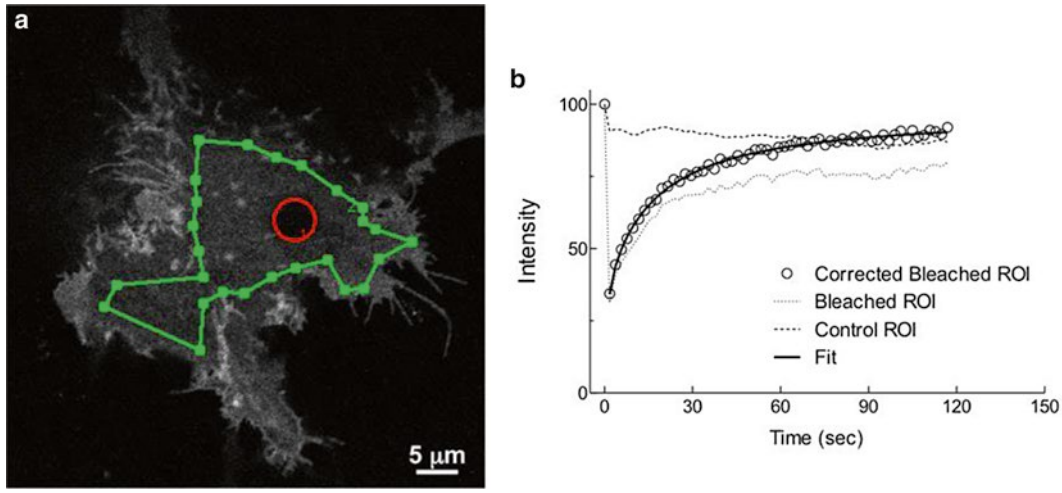

Fig. 2 FRAP analysis of HER3-mGFP lateral diffusion in breast cancer cell membranes. HER3-mGFP reporters of either full-length sequence (HER3-1139) or with progressive C-terminal truncations (HER3-1017, -976, -667) (*see* Fig. 1) were transiently expressed in MCF7 breast cancer cells, and FRAP experiments with samples held at 30 °C performed as described in the text. (**a**) An image from a representative experiment of cellular GFP fluorescence taken immediately following the photobleaching of the measurement ROI (*red circle*), with the larger, irregularly shaped control ROI also indicated (*green polygon*). (**b**) Plots of the recorded integrated fluorescence intensities of the measurement (bleached) and control ROIs (both normalized to a value of 100 at time zero to facilitate their comparison) and the corrected fluorescence intensity (F) in the bleached measurement ROI as functions of time. The corrected intensity data were fit with the analytic equation of Soumpasis as described in the text, and the best fit curve is shown (*solid line*). In this representative experiment in which the full-length HER3-mGFP reporter was examined and in those in which truncated HER3 reporters were examined (*see* Figs. 1 and 3), the recovery of fluorescence after photobleaching was nearly complete. Experiments with multiple reporters thus yielded average mobile fraction values (f_{mobile}) in the range of 0.9–1.0

intensities in the two ROIs resumed and continued throughout the recovery period (1–5-min duration).

7. The intensity versus time data for an individual FRAP experiment (two data sets corresponding to the measurement and control ROIs) are exported from the microscope computer as files that can be imported into standard spreadsheet and scientific graphing programs.

3.3 FRAP Data Analysis

FRAP time course data obtained as described above are analyzed to determine the characteristic diffusion time (τD) of the recovery time course (a time that is dependent upon the diameter of the bleached area), the mobile fraction (f_{mobile}) of the reporter (the fraction of original fluorescence intensity that is regained following the post-photobleaching recovery), and the reporter diffusion coefficient (D).

1. For each experiment, the raw fluorescence intensity (F) versus time (t) data sets corresponding the measurement and control ROIs are imported into a standard spreadsheet program that allows simple mathematical manipulations.

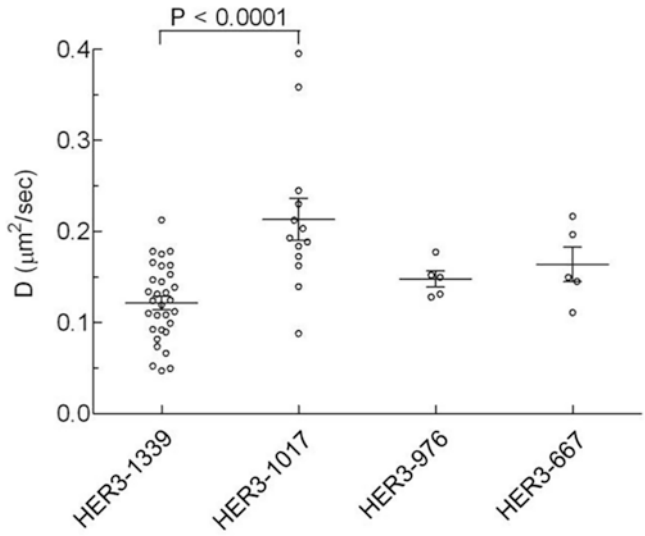

Fig. 3 Effect of HER3 C-terminal truncations on the diffusional mobility of HER3-mGFP reporters in the plasma membrane. FRAP experiments were performed to estimate the diffusion mobility of the full-length HER3-mGFP reporter (HER3-1339) and reporters with the indicated C-terminal intracellular domain truncations (*see* Fig. 1). Fitting of the FRAP data yielded characteristic diffusion times, from which apparent diffusion constant values (corresponding to the 30 °C measurements) were derived as described in the text. Shown here are the results of multiple experiments with the mean of the diffusion constant values indicated. While deletion of the distal HER3 C-terminal domain (compare results for HER3-1017 and HER3-1339) enhanced the diffusional mobility of the receptor, further deletion of either the HER3 sequence between residues 1017 and 976 (which contains the putative HER3 oligomerization motif) or the remaining intracellular domain sequence (compare HER3-976 and HER3-667 to HER3-1017) failed to enhance the mobility of the reporter

2. To correct for measurement-related artifacts (e.g., fluctuations in excitation intensity, slight movement of the cells with respect to the plane of focus, and the gradual photobleaching of the reporter with the repeated scanning of images over the time course of the experiment), a corrected fluorescence intensity value (F') is generated by dividing the intensity of the measurement ROI by that of the control ROI at each time point, and then normalizing the F' values so that they fluctuate around 100 % in the pre-bleach interval. (The numerical average of the F' values in the pre-bleach interval is used in the normalization.) Figure 2 shows representative raw and corrected fluorescence intensity data obtained in a FRAP experiment examining a HER3-mGFP reporter.
3. The F versus t data from the post-bleach recovery interval only are extracted from the data set and the t values numerically adjusted to indicate the time of the midpoint of the individual scans relative to the end of the photobleaching interval.

(If scans were done at 2 s intervals, the first adjusted t value would 2 s plus $(1/2)\Delta t$, where Δt is the time duration of an individual scan.) Time values must all be larger than zero, as the theoretical equation used in fitting the data is not defined at $t=0$ (*see* **Note 4**).

4. Using a graphing program with nonlinear least squares curve fitting functionality (for example GraphPad Prism) the following analytical equation describing the fluorescence recovery in a bleach-disk experiment [13] is fit to the F versus t data:

$$F' = F_0 + (F_\infty - F_0)\exp(-2\tau_D / t)[\mathbf{I}_0(2\tau_D / t) + \mathbf{I}_1(2\tau_D / t)]$$

Here F_0 and F_∞ are the fluorescence intensities at $t=0$ (immediately after photobleaching) and after an infinite time of recovery, respectively, τD is the characteristic diffusion time, and $\mathbf{I}_0$ and $\mathbf{I}_1$ are modified Bessel functions. F_0, F_∞, and τD are adjustable parameters, the values of which are estimated by the curve fitting. Note that F_0 is typically not zero because the photobleaching is not complete. A representative fitting of F versus t data with the theoretical recovery equation is shown in Fig. 2.

5. The determined τD value characterizing the kinetics of the recovery is dependent upon the radius of the bleached area (w). The apparent diffusion constant (D) of the reporter (a value independent of the measurement area) is derived using the formula $D = w^2/4\tau D$. Lastly, the mobile fraction is given by

$$f_{\text{mobile}} = (F_\infty - F_0)/(F_{\text{Pre}} - F_0) = (F_\infty - F_0)/(100 - F_0)$$

where the F_{Pre} is the fluorescence intensity pre-photobleaching, which was set to 100 % in the initial normalization of the F data. The mean values for the diffusion constants of various HER3-mGFP reporters derived from a series of FRAP experiments are presented in Fig. 3.

4 Notes

1. As diffusion is temperature dependent, lower than physiologic temperature can be used to slow the fluorescence recovery time course and increase the accuracy of relative mobility measurements. When reporting measured diffusion coefficients, the temperature of the measurements should always be indicated.
2. A circular ROI is used for the photobleaching (beached-disked FRAP method) so that the fluorescence recovery time course can be appropriately analyzed by fitting of the data with the analytical equation derived by Soumpasis for the bleached-disk scenario [13]. Analytical solutions for bleached ROIs of other geometries (for example square) do not generally exist,

although fitting of the recovery data with exponential decay curves can be used to estimate the recovery time.

3. The control ROI, which surrounds the bleached ROI but is within the cellular perimeter, should be as large as possible so that photobleaching does not significantly alter the total fluorescence intensity in the control ROI.
4. Due to the singularity at $t=0$ in the analytical equation used in the curve fitting analysis described here, the quality of the analysis will suffer if data with time values smaller than $0.05 \cdot \tau D$ are used. Thus data pairs with $t < 0.05 \cdot \tau D$ are generally deleted prior to curve fitting.

Acknowledgement

The authors wish to acknowledge the University of Iowa Central Microscopy Research Facility for their provision of fluorescence confocal microscopy instrumentation.

References

1. Krager KJ, Sarkar M, Twait EC, Lill NL, Koland JG (2012) A novel biotinylated lipid raft reporter for electron microscopic imaging of plasma membrane microdomains. J Lipid Res 53:2214–2225
2. Yang S, Raymond-Stintz MA, Ying W, Zhang J, Lidke DS, Steinberg SL, Williams L, Oliver JM, Wilson BS (2007) Mapping ErbB receptors on breast cancer cell membranes during signal transduction. J Cell Sci 120:2763–2773
3. Guy PM, Platko JV, Cantley LC, Cerione RA, Carraway KL III (1994) Insect cell-expressed $p180^{erbB3}$ possesses an impaired tyrosine kinase activity. Proc Natl Acad Sci U S A 91: 8132–8136
4. Kim HH, Vijapurkar U, Hellyer NJ, Bravo D, Koland JG (1998) Signal transduction by epidermal growth factor and heregulin via the kinase-deficient ErbB3 protein. Biochem J 334(Pt 1):189–195
5. Steinkamp MP, Low-Nam ST, Yang S, Lidke KA, Lidke DS, Wilson BS (2014) erbB3 is an active tyrosine kinase capable of homo- and heterointeractions. Mol Cell Biol 34:965–977
6. Shi F, Telesco SE, Liu Y, Radhakrishnan R, Lemmon MA (2010) ErbB3/HER3 intracellular domain is competent to bind ATP and catalyze autophosphorylation. Proc Natl Acad Sci U S A 107:7692–7697
7. Hellyer NJ, Kim MS, Koland JG (2001) Heregulin-dependent activation of phosphoinositide 3-kinase and Akt via the ErbB2/ErbB3 co-receptor. J Biol Chem 276: 42153–42161
8. Choi BK, Fan X, Deng H, Zhang N, An Z (2012) ERBB3 (HER3) is a key sensor in the regulation of ERBB-mediated signaling in both low and high ERBB2 (HER2) expressing cancer cells. Cancer Med 1:28–38
9. Jura N, Shan Y, Cao X, Shaw DE, Kuriyan J (2009) Structural analysis of the catalytically inactive kinase domain of the human EGF receptor 3. Proc Natl Acad Sci U S A 106:21608–21613
10. González-González IM, Jaskolski F, Goldberg Y, Ashby MC, Henley JM (2012) Chapter six- measuring membrane protein dynamics in neurons using fluorescence recovery after photobleach. In: Conn PM (ed) Methods enzymology. Academic, New York, pp 127–146
11. Day CA, Kraft LJ, Kang M, Kenworthy AK (2012) Analysis of protein and lipid dynamics using confocal fluorescence recovery after photobleaching (FRAP). Curr Protoc Cytom/editorial board, J Paul Robinson, managing editor [et al] Chapter 2:Unit2 19
12. Hellyer NJ, Kim HH, Greaves CH, Sierke SL, Koland JG (1995) Cloning of the rat ErbB3 cDNA and characterization of the recombinant protein. Gene 165:279–284
13. Soumpasis DM (1983) Theoretical analysis of fluorescence photobleaching recovery experiments. Biophys J 41:95–97

Chapter 10

Isolation and Analysis of Detergent-Resistant Membrane Fractions

Massimo Aureli, Sara Grassi, Sandro Sonnino, and Alessandro Prinetti

Abstract

The hypothesis that the Golgi apparatus is capable of sorting proteins and sending them to the plasma membrane through "lipid rafts," membrane lipid domains highly enriched in glycosphingolipids, sphingomyelin, ceramide, and cholesterol, was formulated by van Meer and Simons in 1988 and came to a turning point when it was suggested that lipid rafts could be isolated thanks to their resistance to solubilization by some detergents, namely Triton X-100. An incredible number of papers have described the composition and properties of detergent-resistant membrane fractions. However, the use of this method has also raised the fiercest criticisms. In this chapter, we would like to discuss the most relevant methodological aspects related to the preparation of detergent-resistant membrane fractions, and to discuss the importance of discriminating between what is present on a cell membrane and what we can prepare from cell membranes in a laboratory tube.

Key words Detergent-resistant membrane, Lipid raft, Liquid-ordered phase, Membrane domain, Microdomain, Sphingolipid

1 Introduction

Amphipathic lipids represent the major structural lipids in all cellular membranes in eukaryotes; due to their aggregative properties, they form bilayers that represent the bulk structure of biological membranes, allowing the compartmentalization of the extra- and intra-cellular aqueous environments. Glycerophospholipids (GPL) are by far the major components of biological bilayers, the main bilayer-forming lipid being phosphatidylcholine (PC), which typically accounts for >50 % of all cell membrane GPL. In addition, cellular membranes contain cholesterol and sphingolipids (SL) (in different amounts, depending on the specific membrane, with the highest concentration associated with plasma membranes). Neither cholesterol nor SL are bilayer-forming lipids, however they can be inserted in GPL bilayers through their hydrophobic moieties. Singer and Nicholson [1] proposed that

Mark G. Waugh (ed.), *Lipid Signaling Protocols*, Methods in Molecular Biology, vol. 1376,
DOI 10.1007/978-1-4939-3170-5_10,

the GPL bilayer acts as two-dimensional solvent for the other membrane components, in particular for membrane-associated proteins, allowing in principle the unrestricted freedom of lateral movement of membrane components. Nevertheless, biological membranes are characterized by a high level of lateral order, and membrane components appear to be organized into "membrane domains," i.e., "ordered structures that differ in lipid and/or protein composition from the surrounding membrane" [2]. Lateral heterogeneity in the structure of cellular membranes is strikingly evident in polarized cells (such as epithelial cells, neurons, and oligodendrocytes), however it is present in virtually any cell type, and it is also present in membrane regions lacking a morphologically distinguishable architecture at the micron scale, as revealed by the finding that some membrane components are restricted in their lateral movements and are transiently confined to small domains at the submicron scale ("microdomains") [3]. According to the fluid mosaic model, short- and long range lateral order in biological membranes is due to the creation of a network of protein-driven lateral interactions among membrane components. Considering the wide variety of biologically relevant protein–protein interactions, protein-driven events such as the creation of membrane-associated multiprotein complexes (in some cases, organized by specific proteins able to act as scaffolds [2] such as clathrin, tetraspanins [4], caveolins [5, 6], and flotillins [7]) are undoubtedly major players in the creation and stabilization of membrane domains. A very sophisticated and comprehensive interpretation to protein-driven compartmentalization of membrane components is given by the membrane-skeleton "fence" model [8]. According to this model, limitations in lateral diffusion observed for some membrane-bound proteins might not necessarily imply direct interactions with other membrane components, but might be due to the formation of compartmental boundaries by actin-based membrane skeleton "fences" that are anchored to the membrane by "pickets" consisting of transmembrane proteins. Membrane components are transiently trapped within the compartment. In addition, hydrodynamic friction-like effect at the surface of the immobilized proteins reduces the diffusion rate of membrane components in the adjacent membrane region.

Nevertheless, the collective aggregational properties of membrane lipids might represent a further factor leading to lateral order within membranes. In fact, a series of experiments describing thermal effects on the behavior of lipid mixtures, published almost at the same time of the presentation of the fluid mosaic model, suggested that the limited solubility of lipids in complex lipid mixtures, leading to fluid–fluid phase separation, could be responsible for a certain degree of lateral organization, and could represent a major driving force behind the separation of distinct domains within cell membranes [9–12]. Liquid–liquid phase separation has

been observed in a variety of model systems (reviewed in [13]) and, with some limitations, in biological membranes, for example using fluorescence microscopic and spectroscopic analyses employing order-sensitive probes [14]. In 1982, Karnovsky had already hypothesized that the existence of multiple phases in the membrane lipid environment could drive the "organization of the lipid components of membranes into domains" [15]. However, this notion was applied to an actual cell biology problem only 6 years later, when it was invoked by Simons and van Meer to explain the different lipid composition of the apical and basolateral plasma membrane macrodomains of polarized epithelial cells [16]. Glycosphingolipids (GSL) and cholesterol, which are highly enriched in the apical macrodomain, need to be sorted from the lipids of the basolateral domain (mainly glycerophospholipids) at some intracellular site during their trafficking to the plasma membrane. Van Meer and Simons proposed that the self-associative properties of the apical lipids, leading to the formation of liquid-ordered (l*o*) phase [17–20] domains in intracellular membranes along the trafficking pathway, might be the driving force underlying the differential sorting of apical and basolateral membrane lipid components [21]. These authors introduced the term "lipid rafts" to describe l*o* phase-segregated domains. The concept of lipid rafts became intimately linked with resistance to detergent solubilization in 1992, when Brown and Rose demonstrated that GPI-anchored proteins can be recovered from lysates of epithelial cells in a low-density, detergent-insoluble (Triton X-100-insoluble) form. Detergent-resistant membranes (DRM) enriched in GPI-anchored proteins were also enriched in GSL, but not in basolateral marker proteins [22]. This was regarded as a strong experimental evidence supporting Simons and van Meer's hypothesis regarding the sorting of proteins to the apical domain of polarized cells as a consequence of their association with a GSL-enriched environment, and strongly influenced subsequent research in this field, which became enormously popular when Simons and Ikonen proposed that association with lipid rafts/detergent-resistant membranes might represent a general mechanism for the sorting, targeting and co-localization of membrane-associated proteins, and that lipid rafts might represent functional platforms for the segregation of proteins involved in signal transduction processes [23]. Since 1997, more than 5,000 papers have been published describing the putative structure and functions of lipid rafts (for a few examples, *see* [24–32]), and recently a database specifically dedicated to mammalian lipid raft-associated proteins (RaftProt, http://lipid-raft-database.di.uq.edu.au/) has been developed [33]. A consistent number of these papers relied on the use of resistance to detergent solubilization (based on Brown and Rose's method, sometimes with heavy modifications) for the preparation of fractions representing putative isolated lipid rafts, and many

investigators de facto equated lipid rafts with a membrane fraction characterized by its insolubility in non-ionic aqueous detergents [22]. Alongside enthusiasm, the concept of lipid rafts has elicited fierce criticisms (for an overview *see* [34, 35]), and in particular the notion that detergent-resistance might represent an adequate tool to isolate a fraction enriched in lipid rafts defined as areas of phase separation naturally occurring in biological membrane [2], has been strongly opposed by some authors [35].

In this chapter, we summarize the methodological aspects related to the preparation of detergent-insoluble membrane fractions, and critically review the usefulness of this method as a tool to investigate the supramolecular organization of biological membranes.

2 Preparation of Detergent-Resistant Membrane Fractions

Challenging cells with aqueous solutions containing detergents results in the effective solubilization of most components of the cell membranes (including GPL and intrinsic membrane glycoproteins), as the result of the formation of mixed micelles incorporating detergent and membrane component molecules [36, 37]. This feature has been exploited for the isolation and study of membrane associated proteins. On the other hand, it has been known for a long time that some cellular components are insoluble in non-ionic (Triton X-100) or zwitterionic (Empigin BB) detergents under certain experimental conditions. Indeed, detergent insolubility has been used as an analytical criterion or as a preparative tool long before the lipid raft hypothesis was formulated. The "detergent-insoluble material" (DIM), isolated by sedimentation or centrifugation, was originally shown to be enriched in pericellular matrix proteins (e.g., fibronectin, tenascin, Gp140), in cell attachment site components, including components of cytoskeleton ("detergent-insoluble substrate attachment matrix," DISAM) [38], and in glycosphingolipids, in particular GM1 ganglioside ("detergent-insoluble glycolipid-enriched material," DIG) [39, 40]. Subsequently, it has been shown that detergent-insoluble material was very heterogeneous, being enriched in other sphingolipids, not only gangliosides, (including sphingomyelin, SM, as well) [41–43], cholesterol [42], lipid-anchored proteins (proteins with a glycosylphosphatidylinositol (GPI) or linked with fatty acid residues) [22, 43–48] and other hydrophobic plasma membrane proteins, such as caveolin [49]. Thus, the concept gradually emerged that a peculiar lipid composition leading to the separation of a l*o* phase (the features corresponding to lipid rafts in biological membranes, as hypothesized by van Meer and Simons) could be responsible for the insolubility in aqueous non-ionic detergents, and that DIM is at least in part represented by "detergent-resistant membranes" (DRM), an isolated fraction corresponding to lipid

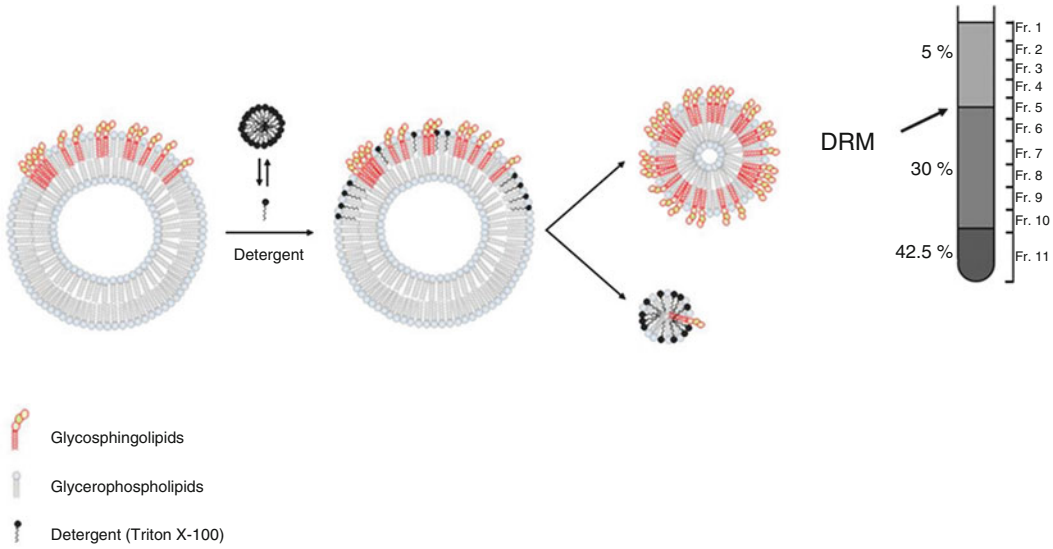

Fig. 1 Detergent insolubility and separation of membrane domains. Detergents in aqueous solutions at concentrations above the critical micellar concentration (CMC) form aggregates such as small micelles. CMC for Triton X-100 is 0.31 mM. Thus, in a 1 % solution, several detergent monomers are present, and can be inserted into the fluid portions of the membrane. Fluid membranes containing Triton X-100 are dissolved and form small mixed micelles enriched in detergent, glycerophospholipids, and proteins. On the other hand detergent is not able to penetrate into membrane areas highly enriched in sphingolipids and cholesterol, due to their high degree of lateral order. This membrane portions form microsome-like structures that can be separated by density gradient centrifugation

rafts, such as those belonging to the apical compartment of polarized epithelial cells (MDCK) or to the caveolar membrane system. Treatment with non-ionic detergent (the most widely used being Triton X-100) at low temperature allows to solubilize lipid components present in the membrane in a liquid-disordered phase (e.g., most glycerophospholipids). These lipids are subtracted from the membrane due to the formation of mixed micelles with the detergent ("solubilization"), while lipid raft components remains laterally organized, excluding detergent monomers ("detergent-insoluble") forming microsome-like or planar structures (Fig. 1). After detergent treatment, the detergent-insoluble membrane fraction can be separated due to its relative low density (buoyancy), likely due to its richness in lipids, i.e., to the high lipid-to-protein ratio [22], using continuous or discontinuous density gradients.

Applying the method originally described by Brown and Rose [22], or its modifications, DRM fractions were isolated from a wide variety of cultured mammalian cells (normal and tumor epithelial cells [22, 49–51], lymphocytes [52, 53] and lymphoid tumor cells [54], neutrophils [55], platelets [56], erythrocytes [57], fibroblasts [50, 58], neurons [59–62] and neuroblastoma

cells [63–65]), and tissues [66–73], plant cells [74, 75], yeast [76, 77], and protozoan [78–80]. We used this procedure to prepare DRM fractions from melanoma [81] and neuroblastoma cells [65], cultured neurons either at different stages of differentiation [59, 82, 83] or challenged with pro-apoptotic stimuli [84], ovarian cancer cells [85, 86], and mouse brain [73].

The original experimental procedure used for the preparation of Triton-insoluble membrane fractions is as follows:

- Cells ($5–8 \times 10^7$, usually corresponding to 4–7 mg cell proteins) are mechanically harvested in phosphate-buffered saline containing 0.4 mM Na_3VO_4, and pelleted.
- Cell pellet is suspended in 1 ml of lysis buffer containing 1 % Triton X-100, 10 mM Tris buffer, pH 7.5, 150 mM NaCl, 5 mM EDTA, 1 mM Na_3VO_4, and protease inhibitors, allowed to stand on ice for 20 min, and homogeneized using a hand-driven tight Dounce homogenizer (ten strokes).
- Cell lysates are centrifuged (5 min at $1300 \times g$) to remove nuclei and large cellular debris.
- The post-nuclear fraction is mixed with an equal volume of 85 % sucrose (w/v) in 10 mM Tris buffer, pH 7.5, 150 mM NaCl, 5 mM EDTA, and 1 mM Na_3VO_4 (the presence of phosphatase and protease inhibitors in the buffers is critical, since the association of certain proteins to the DRM can be modulated by phosphorylation, and DRM represent a site for active and regulated proteolysis).
- The resulting diluent is placed at the bottom of a continuous sucrose concentration gradient (30–5 %) in the same buffer and centrifuged (17 h at $200{,}000 \times g$) at 4 °C.
- The entire procedure is performed at 0–4 °C.
- After ultracentrifugation, the gradient is fractionated, and the white light-scattering band in the low density region of the gradient is regarded as the sphingolipid-enriched fraction (DRM). Fractions can be collected manually or automatically from the top or from the bottom of the gradient without changing the significance of the results.

Two apparently trivial factors deeply influence the reproducibly of the results and the possibility to compare the patterns of DRM-associated molecules reported in different papers. One is represented by the different methods used to collect the fractions. The other is represented by the need to carefully homogenize the compact pellet recovered in the bottom fraction, which contains the majority of sample protein. Substantially overlapping results can be obtained using discontinuous gradients (in our lab, we usually use a two step 5–30 % discontinuous sucrose gradient) or density media other than sucrose (for example, Optiprep).

However, the method has proven to be very sensitive to the specific experimental conditions (where temperature, detergent concentration and detergent-to-cell ratio seem the most critical parameters). Standardization of the experimental procedures is difficult sometime, and the overall composition of DRM fractions or the association of specific molecules with it seem to be affected even by tiny modifications of several conditions, including agents used for membrane disruption (different detergents or different detergent concentration [49, 87–89]), mechanical procedures used to obtain or aid membrane solubilization (sonication, homogeneization) [90], temperature [22, 89, 91, 92], pH, and ratio between detergent and biological material [88].

3 Temperature

As mentioned above, all steps in the DRM preparation should be performed between 0 and +4 °C [22]. Indeed, in our experience incubation at room temperature or at +37 °C before gradient fractionation [92] is one of the best methods to ensure the full solubilization of DRM components. Applying the Triton X-100 extraction procedure to purified myelin at 20 °C led to the formation of two distinct low density fractions [93], both fractions characterized by higher cholesterol/phospholipid and GalCer/phospholipid ratio than the starting myelin preparation. However, the two fractions were characterized by a different content of GM1 ganglioside and by a different enrichment in specific protein markers. Similar discrepancies between the results obtained performing the separation at different temperatures, together with the fact that the low temperature, usually maintained during DRM preparation, can be hardly be extrapolated to those of living cells, has raised serious criticisms about the biological relevance of detergent-insoluble fractions prepared under these experimental conditions. Nevertheless, separation of a l*o* phase in model membranes occurs at 37 °C [94], and DRM in some cases can be prepared from cells and tissues at 20 or 37 °C [88, 89, 91, 93]. In the case of mouse cerebral cortex, the lipid membrane domain markers flotillin, F3, prion protein and alkaline phosphatase were detergent-insoluble at both 4 and 37 °C. Proper adjustment of the ionic composition of the solubilization buffer (e.g., Mg^{+} and K^{+} concentrations similar to those in the intracellular environment and addition of EGTA to chelate Ca^{2+}) allows the preparation at 37 °C of DRMs that have many of the properties of lipid rafts isolated from brain membranes or cultured cells using Triton X-100 or Brij 96 [95]. These “37 °C DRMs” were larger than lipid rafts prepared at low temperature, indicating that some aggregation may have occurred during the purification. This phenomenon can be

avoided by replacing the flotation method for DRM isolation with a magnetic immunopurification procedure, which minimizes the time required for DRM isolation [96].

4 Type of Detergent

As mentioned above, the original method for DRM preparation used Triton X-100 as the detergent, and several papers published afterwards described the composition and feature of Triton X-100 DRM. However, early experiments indicated that similar results can be obtained with other non-ionic or zwitterionic detergents, and in the literature there are several comparative studies performed using a wide range of different detergents [83, 87, 89, 97], aimed at understanding a possible artifactual nature of cellular fractions prepared thanks to their resistance to detergent solubilization. These studies showed that, using detergents with different stringency, it is possible to prepare a DRM fraction enriched in cholesterol and sphingolipids, as well as in certain proteins usually regarded as lipid membrane domain markers, in particular GPI-anchored proteins and acylated proteins. We compared the composition of DRM prepared from differentiated cerebellar neurons in the presence of Triton X-100 or Brij 96 and found a totally overlapping distribution of different lipid classes (DRM being highly enriched in sphingolipids and cholesterol, and depleted of GPL) and of several lipid rafts protein markers, including GPI-anchored proteins (PrP, Thy-1) and Src family kinases [83]. However, the association of other proteins (especially integral membrane proteins) with the DRM fraction is strongly affected by the type of detergent used. We compared the features of DRM prepared using different detergents (Triton X-100 vs. Triton X-114, or Triton X-100 vs. Brij 98) (Fig. 2). All of the different detergent used allowed us to separate a DRM enriched in sphingolipids and cholesterol, and heavily depleted of transferrin receptor (usually regarded as a non-raft marker). However, the association of some proteins, usually regarded as resident in lipid rafts (e.g., uPAR, caveolin-1, integrin receptor subunits), with DRM was deeply affected by the type of detergent used for the separation. For example, uPAR was largely soluble in Triton X-100, but insoluble in Triton X-114, whereas integrin receptor subunits were largely soluble in Triton X-100, and insoluble in Brij 98 (Fig. 2). In general, comparing the behavior of different proteins respect to solubilization with different detergents allows to draw the conclusion that the detergent insolubility of a protein is determined mainly by the intrinsic structural features of the protein, in particular, by the mode of association with the plasma membrane [97], and, thus, detergent-insolubility per se is not a sufficient criterion to establish the association of a protein with a lipid raft. In our

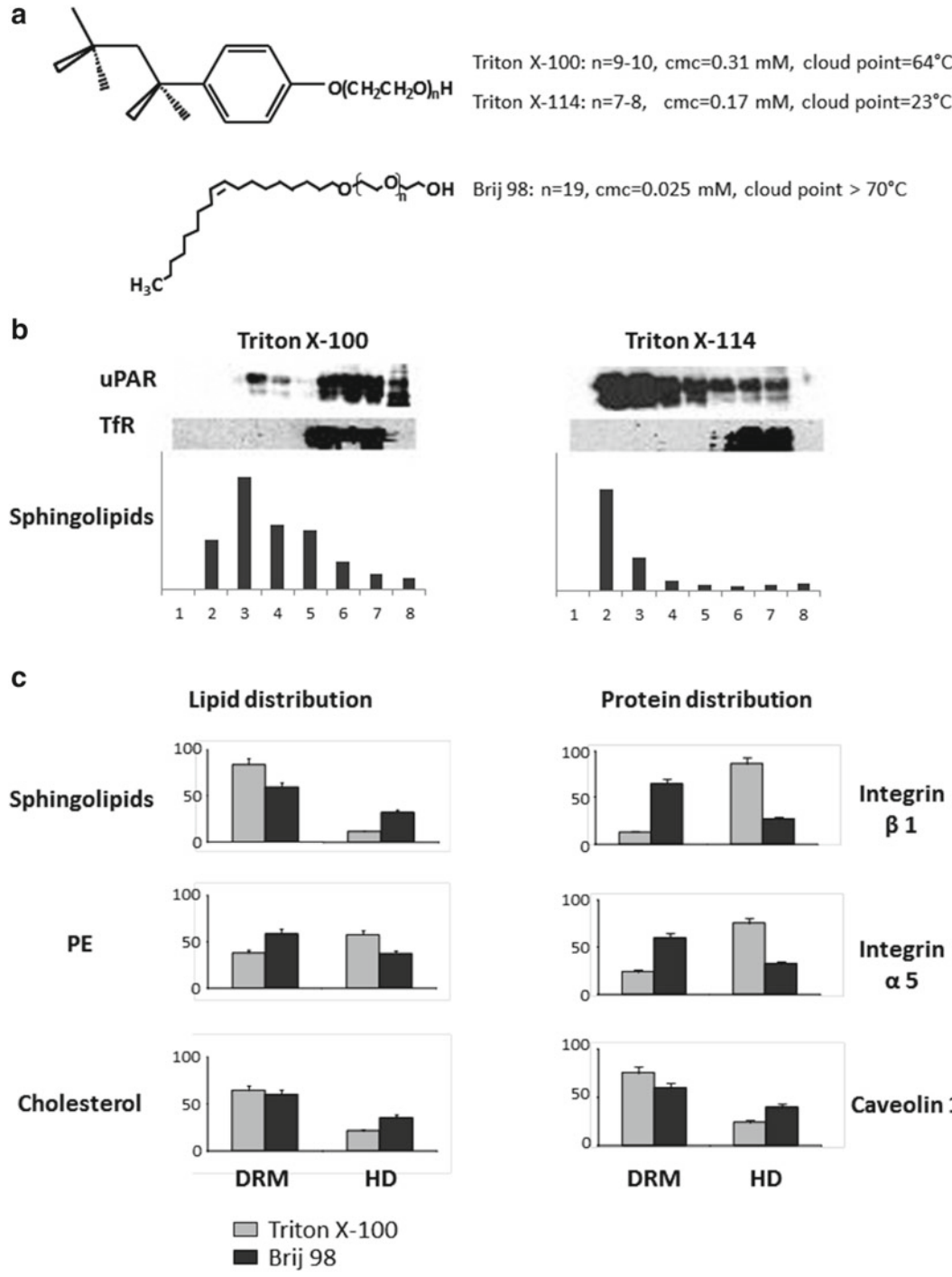

Fig. 2 Lipid and protein composition of DRM prepared using different detergents (Triton X-100 vs. Triton X-114, Triton X-100 vs. Brij 98). Panel (**a**): molecular structures and main physicochemical properties of Triton X-100, Triton X-114 and Brij 98. Panel (**b**): upper panels depict western blot analysis of uPAR (usually regarded as a raft marker), and TfR (usually regarded as a non-raft marker), in fractions prepared by lysis with Triton X-100 or Triton X-114 from HT1080 cells. Lower panels report the sphingolipid distribution along the gradient fractions. Panel (**c**): upper panels depict western blot analysis of integrin receptor subunits β1 and α5 and of caveolin-1 (usually regarded as a raft marker) in fractions prepared by lysis with Triton X-100 or Brij 98 from A2780 ovarian cancer cells. HD, High Density gradient fractions

opinion, the biochemical analysis of the complex environment of the protein, and especially of its lipid composition, remains essential to clarify the protein association with a lipid-rich, laterally organized membrane domain. On the other hand, some structural features that represent putative targeting signals to lipid rafts (in particular, the presence of a GPI anchor or a double fatty acylation) are usually associated with insolubility of the protein in nonionic detergents.

Many authors reported that the detergent-insoluble material obtained in the presence of different detergents floats at different densities, suggesting DRM prepared using different detergents might vary in their lipid composition or in their lipid-to-protein ratio. Again, this seems to point out the artifactual nature of these fractions; a concern further strengthened by the observation that DRM fractions may contain membrane fragments derived from the fusion of distinct lipid membrane domains [87], and that Triton X-100 treatment increased the average domain size by inducing the aggregation of preexisting domains [98] in a model membrane with a composition similar to that of the outer leaflet of plasma membranes. Remarkably, among different detergents Triton X-100 (the paradigmatic detergent used for DRM preparation) seems the one that more markedly alters the lateral organization of biological membranes [99]. Nevertheless, the separation of a l*o* phase in a membrane model was not affected by the treatment with Triton X-100 [98].

On the other hand, at least some studies seem to indicate that the different composition of DRM obtained by using different detergents might actually reflect the existence of biochemically distinct lipid membrane domains within the plasma membrane of the same cell, or the existence of different degrees of lateral order within the same lipid membrane domain [22, 89, 100–103], in agreement with an increasing number of studies indicating the presence of a high heterogeneity in membrane lateral organization in intact cells. In other words, the use of different detergents might represent an adequate tool to dissect the fine structure of membrane domains [89, 104]. For example, differential solubilization by Triton X-100 and Brij 96 has been used to show that two neuronal GPI-anchored proteins, Thy-1 and PrP, belong to structurally different lipid membrane domains characterized by a different degree of order [87]. The presence of two distinct domains characterized by a different detergent solubility has been related to differences in the lipid environment of these proteins [87]. In particular, mass spectrometry analysis of phosphatidylcholine, sphingomyelin and hexosylceramide [104], highlighted an enrichment in saturated fatty acids in the Thy-1 domain and in unsaturated fatty acids in the PrP domain. In addition, the use of different nonionic (Triton X-100, Brij 96, Triton X-102) or zwitterionic (CHAPS) detergents allowed to separate biochemically distinct detergent-specific domains from myelin membrane [89].

5 Protein/Detergent Ratio

Another experimental parameter that is critical in DRM preparation is the ratio between the amount of sample and the amount of detergent. DRM were originally prepared from MDCK cells using about 4 mg of cell protein/1 ml 1 % Triton X-100 [22]. We prepared DRM fractions starting from 0.5 to 6 mg neuronal cell proteins lysed in the same conditions, obtaining a constant composition of the DRM in terms of lipid content and patterns and of selection of proteins associated with this fraction [105]. The amount of lipid and protein material associated with the Triton X-100-insoluble fraction remains constant for a wide range of detergent-to-sample ratios, but it suddenly drops to barely detectable quantities above a certain value, suggesting that for a given type of biological material—cell or tissue—there is a certain threshold value for the detergent-to-sample ratio, above which it is impossible to prepare a low-density DRM fraction simply because the excess of detergent is able to solubilize even membrane domains with a high lateral order, that are normally resistant to detergent solubilization. These results are in agreement with those obtained by Parkin et al. [88, 106], who studied in detail the effect of various protein/Triton X-100 ratios on the isolation of a detergent-resistant fraction from mouse brain. Triton X-100 DRM could be prepared by sucrose gradient centrifugation after solubilization of mouse cerebral cortex with a fixed 1 % Triton X-100 concentration at different protein/detergent ratios, ranging from 15 to 2 mg of protein/ml. This fraction was enriched in two lipid membrane domain marker proteins (alkaline phosphatase and flotillin) regardless form the protein/detergent ratio. However, enrichment of some lipid raft markers (flotillin, prion protein and F3) in the DRM fraction increased when the protein/detergent ratio in the sample was decreased, while the association with this fraction of proteins, usually excluded from the lipid membrane domain, increased at high protein/detergent ratios.

6 Detergent-Free Methods

The fierce criticisms raised by the use of detergents in the isolation of laterally ordered (possibly l*o*) membrane domains stimulated the development of different "detergent-free" methods for the separation of low-density membrane fractions corresponding to lipid rafts. The rationale underlying these methods relies on the principle that resistance to solubilization of highly organized, "rigid," and thermodynamically favored lipid membrane domains should represent a particular aspect of a more general phenomenon, and thus ordered membrane domains should also be resistant to a variety of treatments able to disrupt the structure of less ordered membrane.

The disruption of cells in the presence of high pH or hypertonic sodium carbonate or by mechanical treatments (sonication under carefully controlled conditions, nitrogen cavitation) produces membrane fragments that can be separated by density gradient centrifugation [107–114]. The composition of the detergent-free low-density membrane fractions obtained as described above is very similar, but not identical [49, 59, 61, 65, 81, 90, 91, 115–122], to that of DRM obtained using Triton X-100 or other detergents, suggesting again that any experimental procedure used for membrane disruption alters at some extent the lateral organization of membrane components, while preserving the stable network of interactions underlying the formation of lipid rafts.

7 DRM from Tissues

DRM fractions have been isolated not only from cultured cells but also from various tissues, including chicken smooth muscle [67], mouse [97], rat and human [106, 123] cerebral cortex, mouse [87, 124–128], rat [104, 129–132] and human [133] brain, rat cerebellum [130], bovine and mouse brain myelin [89, 93, 126, 134], rat [135] and mouse [122] brain synaptosomes, rat [136], mouse [125] and rainbow trout [137] liver, rat [138], rabbit [139] and mouse [125] lung, rat lung endothelium [140], pig [88, 97] and mouse kidney [125]. However, as mentioned above, it should be kept in mind that detergent-insoluble material is represented not only by membrane components but also by some extracellular matrix components. Moreover, DRM fractions prepared from tissues originate from heterogeneous cell populations. Thus, the possibility that different lipid membrane domains could artefactually coalesce due to the presence of the detergent is particularly worrying in the case of preparations derived from tissues. Mixing together Triton X-100 DRM fractions obtained from rat and mouse brain resulted in a system where rat and mouse Thy-1 could be immunoprecipitated together, indicating that fusion of distinct lipid membrane domains did occur under these experimental conditions [87]. Nevertheless, we have not observed any fusion of PrP-rich and Thy-1-rich DRM prepared from cultured rat neurons [83]. Treatment of brain tissue sections with low concentrations of Triton X-100 at 4 °C resulted in the extensive redistribution of gangliosides and GPI-anchored proteins [141, 142] Moreover, addition of exogenous gangliosides to mouse brain sections in the presence of Triton X-100 at 4 °C, resulted in the incorporation of ganglioside molecules in white matter areas. Thus, the application of detergent-based methods for the preparation of lipid membrane domains from tissues still requires careful evaluation. In particular, only in a few cases, a partial characterization of the lipid composition of DRM obtained from tissues has been carried out [104, 106, 123].

We analyzed in detail the DRM prepared from mice brain [73]. Using 3–6 mg of proteins in 1 ml 1 % Triton X-100 (thus a protein-detergent ratio in the range usually applied for the preparation of DRM from cultured cells) we obtained a fraction that contained high amounts of Akt protein, that is usually regarded as a non-lipid raft protein marker [82, 143]. In addition, this fraction was highly enriched in lipids with respect to proteins, but did not show any enrichment in sphingolipids and cholesterol with respect to GPL. When we reduced to 1 mg protein the amount of brain subjected to lysis with 1 ml 1 % Triton X-100, all of the membrane were solubilized and no light fraction containing DRM could be separated by sucrose gradient ultracentrifugation. Only using the ratio of 1.3 mg of brain protein/1 ml of 1 % Triton X-100 we could isolate a DRM fraction with lipid and protein enrichments similar to those observed in DRM from neuronal cells in culture. This result suggested that the preparation of DRM from tissues requires careful validation by complex analytical controls, and in particular indicates that the simple use of protein markers to define the quality of a DRM preparation can be misleading, and that it is critical to analyze the enrichment in lipids that (sphingolipids, cholesterol and GPL) must be assessed to confirm the separation of a fraction containing lipid rafts from the bulk membrane.

8 Analysis of DRM Fraction: Importance of Lipid Analysis

Lipid membrane domains are defined on the basis of their peculiar lipid enrichment with respect to the whole cell or cell membranes. Thus, to validate the use of a method for the preparation of a lipid raft-enriched fraction, it is essential to quantitatively analyze the complete cholesterol, glycerolipid and sphingolipid profile of the fraction. Nevertheless, this type of accurate analysis has been performed only in a few papers using detergent insolubility as a tool to isolate lipid rafts, mainly due to the technical difficulties that are faced in the analysis of subcellular fractions with high contents of detergents, sucrose or other density media and salts. Chemical analysis of DRM lipids however usually requires complex purification of the lipid fraction of interest from the total extract, separation by HPTLC followed by colorimetric detection or immunostaining (using anti-glycolipid antibodies or staining with cholera toxin after treatment with bacterial sialidase to identify ganglio-series structures), or mass spectrometry analysis. Most works on DRM simply rely on the use of cholera toxin B subunit, a component of a heat-labile enterotoxin produced by *Vibrio cholerae* to detect GM1 as a putative DRM marker. Nevertheless, it is necessary to recall that GM1 is a very minor component in several cell lines, and that cholera toxin shows similar [144, 145] or higher affinity toward other gangliosides such as Fuc-GM1 [146, 147].

In addition to this, glycoproteins can be also recognized [147]. Thus, the use of cholera toxin alone in a simple immune dot blot identification experiment performed on membrane fractions is inconclusive [147]. In our hands, the most effective way to measure the relative enrichments of different lipid classes in DRM fractions relies on the use of metabolic radiolabeling procedures. Sphingolipids can be metabolically labeled with radioactive serine, palmitate or sphingosine/sphinganine. We have extensively used [1-^{3}H]sphingosine for steady-state metabolic labeling of sphingolipids in a wide variety of cultured cells (including neural and extraneural, normal and transformed, primary cultures and cell lines) [59, 82–86, 92, 148–153]. Using [1-^{3}H]sphingosine allows the simultaneous radiolabelling of phosphatidylethanolamine (PE) (due to the recycling of radioactive ethanolamine formed in the catabolism of [1-^{3}H]sphingosine). Using this procedure, we observed that the DRM fraction contained 50–65 % of the radioactivity associated with sphingolipids in the cell homogenate, and that less than 10 % of radioactive complex sphingolipids was present in the heavy density fraction of the gradient, which contained about 60 % of cell proteins. Radioactive PE, on the other hand, was predominantly recovered in the heavy fractions of the gradient, and only a low amount was detectable in DRM [59]. Thus, metabolic labeling with [1-^{3}H]sphingosine permits the simultaneous analysis of lipid components that are differently enriched in the DRM and non-DRM gradient fractions, representing a valuable analytical tool to check the efficiency of DRM separation under specific experimental conditions. In some cases we have performed a more detailed analysis of the GPL distribution in the gradient by metabolic labeling with [^{32}P]orthophosphate. Using this method, we showed that the DRM fraction from rat cerebellar neurons contained less than 10 % of the total cell GPL. However, about 22 % of PC was present in the DRM, with an enrichment of 13.2, which makes PC the most abundant lipid component of the DRM fraction [59, 82]. Based on our results, all sphingolipids are highly enriched in the DRM fraction (with an enrichment ranging from 30- to 40-fold respect to the cell lysate, depending on the specific sphingolipid). A similar enrichment has been calculated for cholesterol (that can be easily detected by colorimetric procedures after thin layer chromatography separation). In rat cerebellar neurons, the molar ratio between glycerophospholipids, cholesterol, sphingomyelin, ceramide and gangliosides was 41.6:6.1:1.3:0.3:1 in the cell homogenate and 8.3:4.0:1.4:0.2:1 in the DRM [59].

Nevertheless, papers reporting on lipidomics analysis of lipid rafts have recently appeared (and likely their number will greatly increase due to the wide diffusion of high sensitivity lipidomics tools), providing useful comparative sets of data [154, 155]. The analysis of the lipid composition of DRM by mass spectrometry has added very important information on DRM lipids, revealing that

DRM lipids are selected also on the basis of their fatty acid composition, being highly enriched in palmitic acid [82] (confirming the theoretical predictions based on the hypothesis that lipid rafts represent l*o* phase-separated domains), and that different detergent-resistant microenvironments are characterized by a different fatty acid composition: the Thy-1-rich and the PrP-rich microenvironments, separated from rat brain plasma membranes on the basis of their differential detergent solubility, are respectively enriched in saturated and unsaturated fatty acids [104].

9 Immunoseparation of DRM Complexes

In our opinion, the pieces of information discussed so far indicate quite convincingly that detergent membrane fractions contain different subpopulations of particles and supermolecular aggregates, and that some of these aggregates do actually reflect, in their composition and architecture, membrane domains actually existing at the cell surface. However, it is clear that DRM fractions as a whole do not represent isolated lipid rafts. The availability of antibodies toward specific components of DRM (both anti-protein and anti-lipid antibodies) has been sometimes exploited to develop highly specific methods for the immunoisolation of detergent-resistant membrane complexes from a "crude" DRM fraction [61, 81, 116, 118, 156–159]. Caveolin-1, the main structural protein present in *caveolae* and an important molecular organizer for membrane-associated multiprotein complexes [6] is usually highly enriched in lipid rafts (where it closely interacts with sphingolipids). Anti-caveolin-1 antibodies were used to discriminate between caveolar membrane domains and immunoaffinity-purified non-caveolar membrane domains, which seem to represent to distinct lipid raft subpopulations [55, 90, 92, 121, 160–162]. We used anti-caveolin-1 antibody to immunoisolate a multimolecular complex from DRM obtained from ovarian carcinoma cells characterized by high levels of GM3 ganglioside. Caveolin-1 in these cells tightly interacts with gangliosides and integrin receptor subunits, forming a signaling complex able to inhibit cell motility by negatively controlling the activity of Src kinase [85, 86]. We used immunoseparation of a PrP-rich detergent insoluble domain to study the organization of PrP microenvironment and the effect of a modification in membrane lipid composition on the association of PrP to neuronal membranes during apoptosis [83, 84].

Since a high enrichment in glycosphingolipids is a general feature of lipid membrane domains, particularly interesting are the immunoaffinity isolation methods relying on the use of anti-glycolipid antibodies [163]. Anti-GM3 ganglioside monoclonal antibody DH2 was used to immunoisolate GM3-enriched DRM from melanoma [162] and neuroblastoma cells [65]. Anti-GD3

ganglioside monoclonal antibody R24 was used to isolate a DRM fraction from rat cerebellum [129] and from differentiated rat cerebellar neurons [92]. Anti-LacCer monoclonal antibody Huly-m13 was used to isolate LacCer-enriched domains from human neutrophils, demonstrating the functional coupling between LacCer and Lyn [164]. Anti-sulfatide monoclonal antibody O4 was used to isolate lipid rafts from cultured rat immature oligodendrocytes [165].

Immunoisolation of detergent-insoluble complexes has the potential to discriminate between different subpopulations of lipid rafts. Using anti-GM3 ganglioside monoclonal antibody DH2 and anti-caveolin-1 antibody, it was possible to isolate two distinct Triton X-100-resistant membrane subpopulations from B16 melanoma cells by antibody, respectively [162]. Two distinct DRM subpopulations were immunoisolated from mouse brain using two different neuronal GPI-anchored proteins, Thy-1 and PrP, as the target [87]. Immunoprecipitation of two GPI-anchored proteins with different subcellular distribution in polarized epithelial cells allowed to conclude that the microenvironment of the two proteins is characterized by a different enrichment in lipids, and that there is no artificial lipid mixing or domain formation caused by Triton X-100 extraction (that has been shown in whole brain preparations, as discussed in the next paragraph), thus suggesting that the co-immunoprecipitated lipids represent the boundary lipids around each protein [166].

10 Conclusions

Several experimental techniques are currently available for the direct detection of lipid rafts or organized domains in intact cell membranes. These experimental tools were almost completely unavailable when the lipid raft hypothesis was formulated and when Brown and Rose developed the Triton X-100-based method for the preparation of DRM. Nevertheless, the highly diverse experimental methods used for the identification of lipid rafts on the cell surface are all based on the detection of a putative lipid raft marker (which is usually defined on the basis of the marker's enrichment in DRM fractions) and require the use of a physical, chemical, or biological probe whose nature depends on the experimental approach, making it difficult to compare results obtained with different techniques. When applied to the study of cell membrane heterogeneity, these techniques revealed a non-random distribution of cell surface molecules, leading to a highly hierarchical membrane organization that encompasses the existence of microdomains differing in their composition, size, and spatial and temporal dynamics (reviewed in ref. [13]). It is easy to predict that at some point Stimulated Emission Depletion (STED) microscopy shall become the golden standard in this sense. STED has the

potential to overcome the limit imposed by the diffraction barrier, thus scaling the resolution of fluorescence microscopy down to the nano level required for the study of the fine structure of cell membranes and of lipid rafts [167, 168]. STED microscopy demonstrated that putative lipid raft markers, including GPI-anchored proteins, SM, and GM1, were confined to molecular complexes that cover membrane areas with diameters <20 nm. These complexes were transient and had an average life span of 10–20 ms. The complexes appeared to be cholesterol-dependent, as the trapping was reduced upon cholesterol depletion [169, 170]. STED microscopy was also used to demonstrate that CD11b integrin and LacCer are associated with the same "nanodomain" in the membrane of living neutrophils and participate in LacCer-mediated phagocytosis of microorganisms [171].

The biochemical study of detergent-resistant membrane fractions has undoubtedly greatly contributed to our understanding of lateral organization of plasma membranes, and the core concepts elaborated on the basis of the data obtained using this approach have survived the test of modern technologies. It is clear that the association of a certain molecule with DRM does not automatically equate with its presence in lipid raft. DRM fractions represent an average preparation stabilized by the presence of the detergent, while lipid rafts are non-equilibrium entities, dynamic and heterogeneous in time and space. In our opinion, analysis of DRM can still provide useful information, but it is crucial to keep in mind that the methods for DRM preparation require a very tough standardization of the experimental procedures and careful analytical controls.

References

1. Singer SJ, Nicolson GL (1972) The fluid mosaic model of the structure of cell membranes. Science 175:720–731
2. Lindner R, Naim HY (2009) Domains in biological membranes. Exp Cell Res 315: 2871–2878
3. Jacobson K, Sheets ED, Simson R (1995) Revisiting the fluid mosaic model of membranes. Science 268:1441–1442
4. Hemler ME (2005) Tetraspanin functions and associated microdomains. Nat Rev Mol Cell Biol 6:801–811
5. Prinetti A, Prioni S, Loberto N, Aureli M, Chigorno V, Sonnino S (2008) Regulation of tumor phenotypes by caveolin-1 and sphingolipid-controlled membrane signaling complexes. Biochim Biophys Acta 1780: 585–596
6. Sonnino S, Prinetti A (2009) Sphingolipids and membrane environments for caveolin. FEBS Lett 583:597–606
7. Rajendran L, Le Lay S, Illges H (2007) Raft association and lipid droplet targeting of flotillins are independent of caveolin. Biol Chem 388:307–314
8. Kusumi A, Suzuki K (2005) Toward understanding the dynamics of membrane-raft-based molecular interactions. Biochim Biophys Acta 1746:234–251
9. Lee AG, Birdsall NJ, Metcalfe JC, Toon PA, Warren GB (1974) Clusters in lipid bilayers and the interpretation of thermal effects in biological membranes. Biochemistry 13:3699–3705
10. Wunderlich F, Ronai A, Speth V, Seelig J, Blume A (1975) Thermotropic lipid clustering in tetrahymena membranes. Biochemistry 14:3730–3735
11. Wunderlich F, Ronai A (1975) Adaptive lowering of the lipid clustering temperature within Tetrahymena membranes. FEBS Lett 55:237–241

12. Wunderlich F, Kreutz W, Mahler P, Ronai A, Heppeler G (1978) Thermotropic fluid goes to ordered "discontinuous" phase separation in microsomal lipids of Tetrahymena. An X-ray diffraction study. Biochemistry 17:2005–2010
13. Sonnino S, Prinetti A (2012) Membrane domains and the "lipid raft" concept. Curr Med Chem 20:4–21
14. Kaiser HJ, Lingwood D, Levental I, Sampaio JL, Kalvodova L, Rajendran L, Simons K (2009) Order of lipid phases in model and plasma membranes. Proc Natl Acad Sci U S A 106:16645–16650
15. Karnovsky MJ, Kleinfeld AM, Hoover RL, Klausner RD (1982) The concept of lipid domains in membranes. J Cell Biol 94:1–6
16. Simons K, van Meer G (1988) Lipid sorting in epithelial cells. Biochemistry 27:6197–6202
17. Mouritsen OG (2010) The liquid-ordered state comes of age. Biochim Biophys Acta 1798:1286–1288
18. Ipsen JH, Karlstrom G, Mouritsen OG, Wennerstrom H, Zuckermann MJ (1987) Phase equilibria in the phosphatidylcholine-cholesterol system. Biochim Biophys Acta 905:162–172
19. Bagatolli LA, Ipsen JH, Simonsen AC, Mouritsen OG (2010) An outlook on organization of lipids in membranes: searching for a realistic connection with the organization of biological membranes. Prog Lipid Res 49: 378–389
20. Quinn PJ, Wolf C (2009) The liquid-ordered phase in membranes. Biochim Biophys Acta 1788:33–46
21. van Meer G, Simons K (1988) Lipid polarity and sorting in epithelial cells. J Cell Biochem 36:51–58
22. Brown DA, Rose JK (1992) Sorting of GPI-anchored proteins to glycolipid-enriched membrane subdomains during transport to the apical cell surface. Cell 68:533–544
23. Simons K, Ikonen E (1997) Functional rafts in cell membranes. Nature 387:569–572
24. Lajoie P, Partridge EA, Guay G, Goetz JG, Pawling J, Lagana A, Joshi B, Dennis JW, Nabi IR (2007) Plasma membrane domain organization regulates EGFR signaling in tumor cells. J Cell Biol 179:341–356
25. Guirland C, Zheng JQ (2007) Membrane lipid rafts and their role in axon guidance. Adv Exp Med Biol 621:144–155
26. Benarroch EE (2007) Lipid rafts, protein scaffolds, and neurologic disease. Neurology 69:1635–1639
27. Hanzal-Bayer MF, Hancock JF (2007) Lipid rafts and membrane traffic. FEBS Lett 581: 2098–2104
28. Riethmuller J, Riehle A, Grassme H, Gulbins E (2006) Membrane rafts in host-pathogen interactions. Biochim Biophys Acta 1758: 2139–2147
29. Debruin LS, Harauz G (2007) White matter rafting--membrane microdomains in myelin. Neurochem Res 32:213–228
30. Delacour D, Jacob R (2006) Apical protein transport. Cell Mol Life Sci 63:2491–2505
31. Taylor DR, Hooper NM (2006) The prion protein and lipid rafts. Mol Membr Biol 23:89–99
32. Manes S, Viola A (2006) Lipid rafts in lymphocyte activation and migration. Mol Membr Biol 23:59–69
33. Shah A, Chen D, Boda AR, Foster LJ, Davis MJ, Hill MM (2014) RaftProt: mammalian lipid raft proteome database. Nucleic Acids Res 43:D335
34. Sonnino S, Prinetti A (2008) Membrane lipid domains and membrane lipid domain preparations: are they the same thing? Trends Glycosci Glycotechnol 20:315–340
35. Munro S (2003) Lipid rafts: elusive or illusive? Cell 115:377–388
36. Marchesi VT, Andrews EP (1971) Glycoproteins: isolation from cell membranes with lithium diiodosalicylate. Science 174: 1247–1248
37. Helenius A, Simons K (1975) Solubilization of membranes by detergents. Biochim Biophys Acta 415:29–79
38. Carter WG, Hakomor S (1981) A new cell surface, detergent-insoluble glycoprotein matrix of human and hamster fibroblasts. The role of disulfide bonds in stabilization of the matrix. J Biol Chem 256:6953–6960
39. Okada Y, Mugnai G, Bremer EG, Hakomori S (1984) Glycosphingolipids in detergent-insoluble substrate attachment matrix (DISAM) prepared from substrate attachment material (SAM). Their possible role in regulating cell adhesion. Exp Cell Res 155: 448–456
40. Streuli CH, Patel B, Critchley DR (1981) The cholera toxin receptor ganglioside GM remains associated with triton X-100 cytoskeletons of BALB/c-3T3 cells. Exp Cell Res 136:247–254
41. Yu J, Fischman DA, Steck TL (1973) Selective solubilization of proteins and phospholipids from red blood cell membranes by nonionic detergents. J Supramol Struct 1:233–248

42. Davies AA, Wigglesworth NM, Allan D, Owens RJ, Crumpton MJ (1984) Nonidet P-40 extraction of lymphocyte plasma membrane. Characterization of the insoluble residue. Biochem J 219:301–308
43. Mescher MF, Jose MJ, Balk SP (1981) Actin-containing matrix associated with the plasma membrane of murine tumour and lymphoid cells. Nature 289:139–144
44. Vitetta ES, Boyse EA, Uhr JW (1973) Isolation and characterization of a molecular complex containing Thy-1 antigen from the surface of murine thymocytes and T cells. Eur J Immunol 3:446–453
45. Letarte-Muirhead M, Barclay AN, Williams AF (1975) Purification of the Thy-1 molecule, a major cell-surface glycoprotein of rat thymocytes. Biochem J 151:685–697
46. Hoessli D, Rungger-Brandle E (1985) Association of specific cell-surface glycoproteins with a triton X-100-resistant complex of plasma membrane proteins isolated from T-lymphoma cells (P1798). Exp Cell Res 156:239–250
47. Thiele HG, Koch F, Hamann A, Arndt R (1986) Biochemical characterization of the T-cell alloantigen RT-6.2. Immunology 59:195–201
48. Hooper NM, Turner AJ (1988) Ectoenzymes of the kidney microvillar membrane. Differential solubilization by detergents can predict a glycosyl-phosphatidylinositol membrane anchor. Biochem J 250:865–869
49. Sargiacomo M, Sudol M, Tang Z, Lisanti MP (1993) Signal transducing molecules and glycosyl-phosphatidylinositol-linked proteins form a caveolin-rich insoluble complex in MDCK cells. J Cell Biol 122:789–807
50. Chigorno V, Palestini P, Sciannamblo M, Dolo V, Pavan A, Tettamanti G, Sonnino S (2000) Evidence that ganglioside enriched domains are distinct from caveolae in MDCK II and human fibroblast cells in culture. Eur J Biochem 267:4187–4197
51. Zurzolo C, van't Hof W, van Meer G, Rodriguez-Boulan E (1994) VIP21/caveolin, glycosphingolipid clusters and the sorting of glycosylphosphatidylinositol-anchored proteins in epithelial cells. EMBO J 13: 42–53
52. Sorice M, Parolini I, Sansolini T, Garofalo T, Dolo V, Sargiacomo M, Tai T, Peschle C, Torrisi MR, Pavan A (1997) Evidence for the existence of ganglioside-enriched plasma membrane domains in human peripheral lymphocytes. J Lipid Res 38:969–980
53. Garcia-Garcia E, Grayfer L, Stafford JL, Belosevic M (2012) Evidence for the presence of functional lipid rafts in immune cells of ectothermic organisms. Dev Comp Immunol 37:257–269
54. Fra AM, Williamson E, Simons K, Parton RG (1994) Detergent-insoluble glycolipid microdomains in lymphocytes in the absence of caveolae. J Biol Chem 269:30745–30748
55. Iwabuchi K, Nagaoka I (2002) Lactosylceramide-enriched glycosphingolipid signaling domain mediates superoxide generation from human neutrophils. Blood 100:1454–1464
56. Waheed AA, Shimada Y, Heijnen HF, Nakamura M, Inomata M, Hayashi M, Iwashita S, Slot JW, Ohno-Iwashita Y (2001) Selective binding of perfringolysin O derivative to cholesterol-rich membrane microdomains (rafts). Proc Natl Acad Sci U S A 98:4926–4931
57. Samuel BU, Mohandas N, Harrison T, McManus H, Rosse W, Reid M, Haldar K (2001) The role of cholesterol and glycosylphosphatidylinositol-anchored proteins of erythrocyte rafts in regulating raft protein content and malarial infection. J Biol Chem 276:29319–29329
58. Mendez AJ, Lin G, Wade DP, Lawn RM, Oram JF (2001) Membrane lipid domains distinct from cholesterol/sphingomyelin-rich rafts are involved in the ABCA1-mediated lipid secretory pathway. J Biol Chem 276:3158–3166
59. Prinetti A, Chigorno V, Tettamanti G, Sonnino S (2000) Sphingolipid-enriched membrane domains from rat cerebellar granule cells differentiated in culture. A compositional study. J Biol Chem 275:11658–11665
60. Ledesma MD, Simons K, Dotti CG (1998) Neuronal polarity: essential role of protein-lipid complexes in axonal sorting. Proc Natl Acad Sci U S A 95:3966–3971
61. Kasahara K, Watanabe K, Takeuchi K, Kaneko H, Oohira A, Yamamoto T, Sanai Y (2000) Involvement of gangliosides in glycosylphosphatidylinositol-anchored neuronal cell adhesion molecule TAG-1 signaling in lipid rafts. J Biol Chem 275:34701–34709
62. Shogomori H, Futerman AH (2001) Cholera toxin is found in detergent-insoluble rafts/domains at the cell surface of hippocampal neurons but is internalized via a raft-independent mechanism. J Biol Chem 276: 9182–9188
63. Vey M, Pilkuhn S, Wille H, Nixon R, DeArmond SJ, Smart EJ, Anderson RG, Taraboulos A, Prusiner SB (1996) Subcellular colocalization of the cellular and scrapie prion proteins in caveolae-like membranous

domains. Proc Natl Acad Sci U S A 93: 14945–14949

64. Naslavsky N, Stein R, Yanai A, Friedlander G, Taraboulos A (1997) Characterization of detergent-insoluble complexes containing the cellular prion protein and its scrapie isoform. J Biol Chem 272:6324–6331
65. Prinetti A, Iwabuchi K, Hakomori S (1999) Glycosphingolipid-enriched signaling domain in mouse neuroblastoma Neuro2a cells. Mechanism of ganglioside-dependent neuritogenesis. J Biol Chem 274:20916–20924
66. Nixon B, Mitchell LA, Anderson AL, McLaughlin EA, O'Bryan MK, Aitken RJ (2011) Proteomic and functional analysis of human sperm detergent resistant membranes. J Cell Physiol 226:2651–2665
67. Chang WJ, Ying YS, Rothberg KG, Hooper NM, Turner AJ, Gambliel HA, De Gunzburg J, Mumby SM, Gilman AG, Anderson RG (1994) Purification and characterization of smooth muscle cell caveolae. J Cell Biol 126:127–138
68. Celver J, Sharma M, Kovoor A (2012) D(2)-Dopamine receptors target regulator of G protein signaling 9-2 to detergent-resistant membrane fractions. J Neurochem 120: 56–69
69. Suzuki T, Zhang J, Miyazawa S, Liu Q, Farzan MR, Yao WD (2011) Association of membrane rafts and postsynaptic density: proteomics, biochemical, and ultrastructural analyses. J Neurochem 119:64–77
70. Minami SS, Hoe HS, Rebeck GW (2011) Fyn kinase regulates the association between amyloid precursor protein and Dab1 by promoting their localization to detergent-resistant membranes. J Neurochem 118:879–890
71. Florey O, Durgan J, Muller W (2010) Phosphorylation of leukocyte PECAM and its association with detergent-resistant membranes regulate transendothelial migration. J Immunol 185:1878–1886
72. Domingues CC, Ciana A, Buttafava A, Casadei BR, Balduini C, de Paula E, Minetti G (2010) Effect of cholesterol depletion and temperature on the isolation of detergent-resistant membranes from human erythrocytes. J Membr Biol 234:195–205
73. Scandroglio F, Venkata JK, Loberto N, Prioni S, Schuchman EH, Chigorno V, Prinetti A, Sonnino S (2008) Lipid content of brain, brain membrane lipid domains, and neurons from acid sphingomyelinase deficient mice. J Neurochem 107:329–338
74. Carmona-Salazar L, El Hafidi M, Enriquez-Arredondo C, Vazquez-Vazquez C, Gonzalez de la Vara LE, Gavilanes-Ruiz M (2011) Isolation of detergent-resistant membranes from plant photosynthetic and non-photosynthetic tissues. Anal Biochem 417:220–227
75. Fujiwara M, Hamada S, Hiratsuka M, Fukao Y, Kawasaki T, Shimamoto K (2009) Proteome analysis of detergent-resistant membranes (DRMs) associated with OsRac1-mediated innate immunity in rice. Plant Cell Physiol 50:1191–1200
76. Kubler E, Dohlman HG, Lisanti MP (1996) Identification of Triton X-100 insoluble membrane domains in the yeast Saccharomyces cerevisiae. Lipid requirements for targeting of heterotrimeric G-protein subunits. J Biol Chem 271:32975–32980
77. Tanigawa M, Kihara A, Terashima M, Takahara T, Maeda T (2012) Sphingolipids regulate the yeast high-osmolarity glycerol response pathway. Mol Cell Biol 32: 2861–2870
78. Zhang X, Thompson GA Jr (1997) An apparent association between glycosylphosphatidylinositol-anchored proteins and a sphingolipid in Tetrahymena mimbres. Biochem J 323(Pt 1):197–206
79. Parish LA, Colquhoun DR, Ubaida Mohien C, Lyashkov AE, Graham DR, Dinglasan RR (2011) Ookinete-interacting proteins on the microvillar surface are partitioned into detergent resistant membranes of Anopheles gambiae midguts. J Proteome Res 10:5150–5162
80. Obando-Martinez AZ, Curtidor H, Arevalo-Pinzon G, Vanegas M, Vizcaino C, Patarroyo MA, Patarroyo ME (2010) Conserved high activity binding peptides are involved in adhesion of two detergent-resistant membrane-associated merozoite proteins to red blood cells during invasion. J Med Chem 53: 3907–3918
81. Iwabuchi K, Yamamura S, Prinetti A, Handa K, Hakomori S (1998) GM3-enriched microdomain involved in cell adhesion and signal transduction through carbohydrate-carbohydrate interaction in mouse melanoma B16 cells. J Biol Chem 273:9130–9138
82. Prinetti A, Chigorno V, Prioni S, Loberto N, Marano N, Tettamanti G, Sonnino S (2001) Changes in the lipid turnover, composition, and organization, as sphingolipid-enriched membrane domains, in rat cerebellar granule cells developing in vitro. J Biol Chem 276:21136–21145
83. Loberto N, Prioni S, Bettiga A, Chigorno V, Prinetti A, Sonnino S (2005) The membrane environment of endogenous cellular prion

protein in primary rat cerebellar neurons. J Neurochem 95:771–783

84. Rivaroli A, Prioni S, Loberto N, Bettiga A, Chigorno V, Prinetti A, Sonnino S (2007) Reorganization of prion protein membrane environment during low potassium-induced apoptosis in primary rat cerebellar neurons. J Neurochem 103:1954–1967
85. Prinetti A, Aureli M, Illuzzi G, Prioni S, Nocco V, Scandroglio F, Gagliano N, Tredici G, Rodriguez-Menendez V, Chigorno V, Sonnino S (2010) GM3 synthase overexpression results in reduced cell motility and in caveolin-1 upregulation in human ovarian carcinoma cells. Glycobiology 20:62–77
86. Prinetti A, Cao T, Illuzzi G, Prioni S, Aureli M, Gagliano N, Tredici G, Rodriguez-Menendez V, Chigorno V, Sonnino S (2011) A glycosphingolipid/caveolin-1 signaling complex inhibits motility of human ovarian carcinoma cells. J Biol Chem 286:40900–40910
87. Madore N, Smith KL, Graham CH, Jen A, Brady K, Hall S, Morris R (1999) Functionally different GPI proteins are organized in different domains on the neuronal surface. EMBO J 18:6917–6926
88. Parkin ET, Turner AJ, Hooper NM (2001) Differential effects of glycosphingolipids on the detergent-insolubility of the glycosylphosphatidylinositol-anchored membrane dipeptidase. Biochem J 358:209–216
89. Taylor CM, Coetzee T, Pfeiffer SE (2002) Detergent-insoluble glycosphingolipid/cholesterol microdomains of the myelin membrane. J Neurochem 81:993–1004
90. Waugh MG, Lawson D, Hsuan JJ (1999) Epidermal growth factor receptor activation is localized within low-buoyant density, non-caveolar membrane domains. Biochem J 337(Pt 3):591–597
91. Kim KB, Kim SI, Choo HJ, Kim JH, Ko YG (2004) Two-dimensional electrophoretic analysis reveals that lipid rafts are intact at physiological temperature. Proteomics 4:3527–3535
92. Prinetti A, Prioni S, Chigorno V, Karagogeos D, Tettamanti G, Sonnino S (2001) Immunoseparation of sphingolipid-enriched membrane domains enriched in Src family protein tyrosine kinases and in the neuronal adhesion molecule TAG-1 by anti-GD3 ganglioside monoclonal antibody. J Neurochem 78:1162–1167
93. Arvanitis DN, Min W, Gong Y, Heng YM, Boggs JM (2005) Two types of detergent-insoluble, glycosphingolipid/cholesterol-rich membrane domains from isolated myelin. J Neurochem 94:1696–1710
94. Ahmed SN, Brown DA, London E (1997) On the origin of sphingolipid/cholesterol-rich detergent-insoluble cell membranes: physiological concentrations of cholesterol and sphingolipid induce formation of a detergent-insoluble, liquid-ordered lipid phase in model membranes. Biochemistry 36:10944–10953
95. Chen X, Jen A, Warley A, Lawrence MJ, Quinn PJ, Morris RJ (2009) Isolation at physiological temperature of detergent-resistant membranes with properties expected of lipid rafts: the influence of buffer composition. Biochem J 417:525–533
96. Morris RJ, Jen A, Warley A (2011) Isolation of nano-meso scale detergent resistant membrane that has properties expected of lipid 'rafts'. J Neurochem 116:671–677
97. Parkin ET, Turner AJ, Hooper NM (1999) Amyloid precursor protein, although partially detergent-insoluble in mouse cerebral cortex, behaves as an atypical lipid raft protein. Biochem J 344(Pt 1):23–30
98. Pathak P, London E (2011) Measurement of lipid nanodomain (raft) formation and size in sphingomyelin/POPC/cholesterol vesicles shows TX-100 and transmembrane helices increase domain size by coalescing preexisting nanodomains but do not induce domain formation. Biophys J 101:2417–2425
99. Ingelmo-Torres M, Gaus K, Herms A, Gonzalez-Moreno E, Kassan A, Bosch M, Grewal T, Tebar F, Enrich C, Pol A (2009) Triton X-100 promotes a cholesterol-dependent condensation of the plasma membrane. Biochem J 420:373–381
100. Fiedler K, Kobayashi T, Kurzchalia TV, Simons K (1993) Glycosphingolipid-enriched, detergent-insoluble complexes in protein sorting in epithelial cells. Biochemistry 32:6365–6373
101. Kim T, Pfeiffer SE (1999) Myelin glycosphingolipid/cholesterol-enriched microdomains selectively sequester the non-compact myelin proteins CNP and MOG. J Neurocytol 28:281–293
102. Simons M, Kramer EM, Thiele C, Stoffel W, Trotter J (2000) Assembly of myelin by association of proteolipid protein with cholesterol- and galactosylceramide-rich membrane domains. J Cell Biol 151:143–154
103. Roper K, Corbeil D, Huttner WB (2000) Retention of prominin in microvilli reveals distinct cholesterol-based lipid micro-domains in the apical plasma membrane. Nat Cell Biol 2:582–592
104. Brugger B, Graham C, Leibrecht I, Mombelli E, Jen A, Wieland F, Morris R (2004) The

membrane domains occupied by glycosylphosphatidylinositol-anchored prion protein and Thy-1 differ in lipid composition. J Biol Chem 279:7530–7536

105. Scandroglio F, Venkata JK, Loberto N, Prioni S, Schuchman EH, Chigorno V, Prinetti A, Sonnino S (2008) Lipid content of brain, of brain membrane lipid domains, and of neurons from acid sphingomyelinase deficient mice (asmko). J Neurochem 107:329. doi:10.1111/j.1471-4159.2008.05591.x
106. Parkin ET, Hussain I, Karran EH, Turner AJ, Hooper NM (1999) Characterization of detergent-insoluble complexes containing the familial Alzheimer's disease-associated presenilins. J Neurochem 72:1534–1543
107. Rimmerman N, Bradshaw HB, Kozela E, Levy R, Juknat A, Vogel Z (2012) Compartmentalization of endocannabinoids into lipid rafts in a microglial cell line devoid of caveolin-1. Br J Pharmacol 165:2436–2449
108. Song KS, Li S, Okamoto T, Quilliam LA, Sargiacomo M, Lisanti MP (1996) Co-purification and direct interaction of Ras with caveolin, an integral membrane protein of caveolae microdomains. Detergent-free purification of caveolae microdomains. J Biol Chem 271:9690–9697
109. Smart EJ, Ying YS, Mineo C, Anderson RG (1995) A detergent-free method for purifying caveolae membrane from tissue culture cells. Proc Natl Acad Sci U S A 92:10104–10108
110. Kennedy C, Nelson MD, Bamezai AK (2011) Analysis of detergent-free lipid rafts isolated from CD4+ T cell line: interaction with antigen presenting cells promotes coalescing of lipid rafts. Cell Commun Signal 9:31
111. Hummel I, Klappe K, Ercan C, Kok JW (2011) Multidrug resistance-related protein 1 (MRP1) function and localization depend on cortical actin. Mol Pharmacol 79:229–240
112. Persaud-Sawin DA, Lightcap S, Harry GJ (2009) Isolation of rafts from mouse brain tissue by a detergent-free method. J Lipid Res 50:759–767
113. Rimmerman N, Hughes HV, Bradshaw HB, Pazos MX, Mackie K, Prieto AL, Walker JM (2008) Compartmentalization of endocannabinoids into lipid rafts in a dorsal root ganglion cell line. Br J Pharmacol 153:380–389
114. Hofman EG, Ruonala MO, Bader AN, van den Heuvel D, Voortman J, Roovers RC, Verkleij AJ, Gerritsen HC, van Bergen En Henegouwen PM (2008) EGF induces coalescence of different lipid rafts. J Cell Sci 121:2519–2528
115. Liu P, Ying Y, Anderson RG (1997) Platelet-derived growth factor activates mitogen-activated protein kinase in isolated caveolae. Proc Natl Acad Sci U S A 94:13666–13670
116. Wu C, Butz S, Ying Y, Anderson RG (1997) Tyrosine kinase receptors concentrated in caveolae-like domains from neuronal plasma membrane. J Biol Chem 272:3554–3559
117. Couet J, Sargiacomo M, Lisanti MP (1997) Interaction of a receptor tyrosine kinase, EGF-R, with caveolins. Caveolin binding negatively regulates tyrosine and serine/threonine kinase activities. J Biol Chem 272: 30429–30438
118. Bilderback TR, Gazula VR, Lisanti MP, Dobrowsky RT (1999) Caveolin interacts with Trk A and p75(NTR) and regulates neurotrophin signaling pathways. J Biol Chem 274:257–263
119. Silva WI, Maldonado HM, Lisanti MP, Devellis J, Chompre G, Mayol N, Ortiz M, Velazquez G, Maldonado A, Montalvo J (1999) Identification of caveolae and caveolin in C6 glioma cells. Int J Dev Neurosci 17:705–714
120. Bravo-Zehnder M, Orio P, Norambuena A, Wallner M, Meera P, Toro L, Latorre R, Gonzalez A (2000) Apical sorting of a voltage- and Ca2+-activated K+ channel alpha -subunit in Madin-Darby canine kidney cells is independent of N-glycosylation. Proc Natl Acad Sci U S A 97:13114–13119
121. Waugh MG, Lawson D, Tan SK, Hsuan JJ (1998) Phosphatidylinositol 4-phosphate synthesis in immunoisolated caveolae-like vesicles and low buoyant density non-caveolar membranes. J Biol Chem 273:17115–17121
122. Eckert GP, Igbavboa U, Muller WE, Wood WG (2003) Lipid rafts of purified mouse brain synaptosomes prepared with or without detergent reveal different lipid and protein domains. Brain Res 962:144–150
123. Molander-Melin M, Blennow K, Bogdanovic N, Dellheden B, Mansson JE, Fredman P (2005) Structural membrane alterations in Alzheimer brains found to be associated with regional disease development; increased density of gangliosides GM1 and GM2 and loss of cholesterol in detergent-resistant membrane domains. J Neurochem 92:171–182
124. Mukherjee A, Arnaud L, Cooper JA (2003) Lipid-dependent recruitment of neuronal Src to lipid rafts in the brain. J Biol Chem 278:40806–40814
125. Kim KB, Lee JW, Lee CS, Kim BW, Choo HJ, Jung SY, Chi SG, Yoon YS, Yoon G, Ko YG (2006) Oxidation-reduction respiratory chains and ATP synthase complex are localized in detergent-resistant lipid rafts. Proteomics 6:2444–2453

126. Vinson M, Rausch O, Maycox PR, Prinjha RK, Chapman D, Morrow R, Harper AJ, Dingwall C, Walsh FS, Burbidge SA, Riddell DR (2003) Lipid rafts mediate the interaction between myelin-associated glycoprotein (MAG) on myelin and MAG-receptors on neurons. Mol Cell Neurosci 22:344–352
127. Vetrivel KS, Cheng H, Kim SH, Chen Y, Barnes NY, Parent AT, Sisodia SS, Thinakaran G (2005) Spatial segregation of gamma-secretase and substrates in distinct membrane domains. J Biol Chem 280:25892–25900
128. Yu W, Zou K, Gong JS, Ko M, Yanagisawa K, Michikawa M (2005) Oligomerization of amyloid beta-protein occurs during the isolation of lipid rafts. J Neurosci Res 80: 114–119
129. Kasahara K, Watanabe Y, Yamamoto T, Sanai Y (1997) Association of Src family tyrosine kinase Lyn with ganglioside GD3 in rat brain. Possible regulation of Lyn by glycosphingolipid in caveolae-like domains. J Biol Chem 272:29947–29953
130. Chen S, Bawa D, Besshoh S, Gurd JW, Brown IR (2005) Association of heat shock proteins and neuronal membrane components with lipid rafts from the rat brain. J Neurosci Res 81:522–529
131. Rosslenbroich V, Dai L, Franken S, Gehrke M, Junghans U, Gieselmann V, Kappler J (2003) Subcellular localization of collapsin response mediator proteins to lipid rafts. Biochem Biophys Res Commun 305:392–399
132. Maekawa S, Iino S, Miyata S (2003) Molecular characterization of the detergent-insoluble cholesterol-rich membrane microdomain (raft) of the central nervous system. Biochim Biophys Acta 1610:261–270
133. Ledesma MD, Abad-Rodriguez J, Galvan C, Biondi E, Navarro P, Delacourte A, Dingwall C, Dotti CG (2003) Raft disorganization leads to reduced plasmin activity in Alzheimer's disease brains. EMBO Rep 4:1190–1196
134. Arvanitis DN, Yang W, Boggs JM (2002) Myelin proteolipid protein, basic protein, the small isoform of myelin-associated glycoprotein, and p42MAPK are associated in the Triton X-100 extract of central nervous system myelin. J Neurosci Res 70:8–23
135. Besshoh S, Bawa D, Teves L, Wallace MC, Gurd JW (2005) Increased phosphorylation and redistribution of NMDA receptors between synaptic lipid rafts and post-synaptic densities following transient global ischemia in the rat brain. J Neurochem 93:186–194
136. Gebreselassie D, Bowen WD (2004) Sigma-2 receptors are specifically localized to lipid rafts in rat liver membranes. Eur J Pharmacol 493:19–28
137. Zehmer JK, Hazel JR (2003) Plasma membrane rafts of rainbow trout are subject to thermal acclimation. J Exp Biol 206:1657–1667
138. Nanjundan M, Possmayer F (2001) Pulmonary lipid phosphate phosphohydrolase in plasma membrane signalling platforms. Biochem J 358:637–646
139. Palestini P, Calvi C, Conforti E, Daffara R, Botto L, Miserocchi G (2003) Compositional changes in lipid microdomains of air-blood barrier plasma membranes in pulmonary interstitial edema. J Appl Physiol 95: 1446–1452
140. Ramos M, Lame MW, Segall HJ, Wilson DW (2006) The BMP type II receptor is located in lipid rafts, including caveolae, of pulmonary endothelium in vivo and in vitro. Vascul Pharmacol 44:50–59
141. Heffer-Lauc M, Lauc G, Nimrichter L, Fromholt SE, Schnaar RL (2005) Membrane redistribution of gangliosides and glycosylphosphatidylinositol-anchored proteins in brain tissue sections under conditions of lipid raft isolation. Biochim Biophys Acta 1686(3):200–208
142. Heffer-Lauc M, Viljetic B, Vajn K, Schnaar RL, Lauc G (2007) Effects of detergents on the redistribution of gangliosides and GPI-anchored proteins in brain tissue sections. J Histochem Cytochem 55:805–812
143. Baron W, Decker L, Colognato H, ffrench-Constant C (2003) Regulation of integrin growth factor interactions in oligodendrocytes by lipid raft microdomains. Curr Biol 13:151–155
144. Markwell MA, Moss J, Hom BE, Fishman PH, Svennerholm L (1986) Expression of gangliosides as receptors at the cell surface controls infection of NCTC 2071 cells by Sendai virus. Virology 155:356–364
145. Markwell MA, Svennerholm L, Paulson JC (1981) Specific gangliosides function as host cell receptors for Sendai virus. Proc Natl Acad Sci U S A 78:5406–5410
146. Masserini M, Palestini P, Venerando B, Fiorilli A, Acquotti D, Tettamanti G (1988) Interactions of proteins with ganglioside-enriched microdomains on the membrane: the lateral phase separation of molecular species of GD1a ganglioside, having homogeneous long-chain base composition, is recognized by Vibrio cholerae sialidase. Biochemistry 27:7973–7978
147. Yanagisawa M, Ariga T, Yu RK (2006) Cholera toxin B subunit binding does not correlate with GM1 expression: a study using

mouse embryonic neural precursor cells. Glycobiology 16:19G–22G

148. Prinetti A, Basso L, Appierto V, Villani MG, Valsecchi M, Loberto N, Prioni S, Chigorno V, Cavadini E, Formelli F, Sonnino S (2003) Altered sphingolipid metabolism in N-(4-hydroxyphenyl)- retinamide-resistant A2780 human ovarian carcinoma cells. J Biol Chem 278:5574–5583
149. Prioni S, Loberto N, Prinetti A, Chigorno V, Guzzi F, Maggi R, Parenti M, Sonnino S (2002) Sphingolipid metabolism and caveolin expression in gonadotropin-releasing hormone-expressing GN11 and gonadotropin-releasing hormone-secreting GT1-7 neuronal cells. Neurochem Res 27:831–840
150. Loberto N, Prioni S, Prinetti A, Ottico E, Chigorno V, Karagogeos D, Sonnino S (2003) The adhesion protein TAG-1 has a ganglioside environment in the sphingolipid-enriched membrane domains of neuronal cells in culture. J Neurochem 85:224–233
151. Chigorno V, Sciannamblo M, Mikulak J, Prinetti A, Sonnino S (2006) Efflux of sphingolipids metabolically labeled with [1-3H] sphingosine, L-[3-3H]serine and [9,10-3H] palmitic acid from normal cells in culture. Glycoconj J 23:159–165
152. Chigorno V, Giannotta C, Ottico E, Sciannamblo M, Mikulak J, Prinetti A, Sonnino S (2005) Sphingolipid uptake by cultured cells: complex aggregates of cell sphingolipids with serum proteins and lipoproteins are rapidly catabolized. J Biol Chem 280:2668–2675
153. Chigorno V, Riva C, Valsecchi M, Nicolini M, Brocca P, Sonnino S (1997) Metabolic processing of gangliosides by human fibroblasts in culture--formation and recycling of separate pools of sphingosine. Eur J Biochem 250:661–669
154. Brugger B, Glass B, Haberkant P, Leibrecht I, Wieland FT, Krausslich HG (2006) The HIV lipidome: a raft with an unusual composition. Proc Natl Acad Sci U S A 103:2641–2646
155. Valsecchi M, Mauri L, Casellato R, Prioni S, Loberto N, Prinetti A, Chigorno V, Sonnino S (2007) Ceramide and sphingomyelin species of fibroblasts and neurons in culture. J Lipid Res 48:417–424. doi:10.1194/jlr.M600344-JLR200
156. Kawabuchi M, Satomi Y, Takao T, Shimonishi Y, Nada S, Nagai K, Tarakhovsky A, Okada M (2000) Transmembrane phosphoprotein Cbp regulates the activities of Src-family tyrosine kinases. Nature 404:999–1003
157. Yamamura S, Handa K, Hakomori S (1997) A close association of GM3 with c-Src and Rho in GM3-enriched microdomains at the B16 melanoma cell surface membrane: a preliminary note. Biochem Biophys Res Commun 236:218–222
158. Lockwich TP, Liu X, Singh BB, Jadlowiec J, Weiland S, Ambudkar IS (2000) Assembly of Trp1 in a signaling complex associated with caveolin-scaffolding lipid raft domains. J Biol Chem 275:11934–11942
159. Rodgers W, Crise B, Rose JK (1994) Signals determining protein tyrosine kinase and glycosyl-phosphatidylinositol-anchored protein targeting to a glycolipid-enriched membrane fraction. Mol Cell Biol 14:5384–5391
160. Stan RV, Roberts WG, Predescu D, Ihida K, Saucan L, Ghitescu L, Palade GE (1997) Immunoisolation and partial characterization of endothelial plasmalemmal vesicles (caveolae). Mol Biol Cell 8:595–605
161. Oh P, Schnitzer JE (1999) Immunoisolation of caveolae with high affinity antibody binding to the oligomeric caveolin cage. Toward understanding the basis of purification. J Biol Chem 274:23144–23154
162. Iwabuchi K, Handa K, Hakomori S (1998) Separation of "glycosphingolipid signaling domain" from caveolin-containing membrane fraction in mouse melanoma B16 cells and its role in cell adhesion coupled with signaling. J Biol Chem 273:33766–33773
163. Hakomori S, Handa K, Iwabuchi K, Yamamura S, Prinetti A (1998) New insights in glycosphingolipid function: "glycosignaling domain," a cell surface assembly of glycosphingolipids with signal transducer molecules, involved in cell adhesion coupled with signaling. Glycobiology 8:xi–xix
164. Iwabuchi K, Prinetti A, Sonnino S, Mauri L, Kobayashi T, Ishii K, Kaga N, Murayama K, Kurihara H, Nakayama H, Yoshizaki F, Takamori K, Ogawa H, Nagaoka I (2008) Involvement of very long fatty acid-containing lactosylceramide in lactosylceramide-mediated superoxide generation and migration in neutrophils. Glycoconj J 25:357–374
165. Miki T, Kaneda M, Iida K, Hasegawa G, Murakami M, Yamamoto N, Asou H, Kasahara K (2013) An anti-sulfatide antibody O4 immunoprecipitates sulfatide rafts including Fyn, Lyn and the G protein alpha subunit in rat primary immature oligodendrocytes. Glycoconj J 30:819–823
166. Tivodar S, Paladino S, Pillich R, Prinetti A, Chigorno V, van Meer G, Sonnino S, Zurzolo C (2006) Analysis of detergent-resistant membranes associated with apical and basolateral GPI-anchored proteins in polarized epithelial cells. FEBS Lett 580:5705–5712

167. Hell SW (2009) Microscopy and its focal switch. Nat Methods 6:24–32
168. Eggeling C, Mueller V, Ringemann C, Sahl SJ, Leutenegger M, Schwarzmann G, Belov V, Schönle A, Hell SW (2010) Exploring membrane dynamics by fluorescence nanoscopy. Biophys J 98:619a
169. Eggeling C, Ringemann C, Medda R, Hein B, Hell SW (2009) High-resolution far-field fluorescence STED microscopy reveals nanoscale details of molecular membrane dynamics. Biophys J 96:197a
170. Eggeling C, Ringemann C, Medda R, Schwarzmann G, Sandhoff K, Polyakova S, Belov VN, Hein B, von Middendorff C, Schonle A, Hell SW (2009) Direct observation of the nanoscale dynamics of membrane lipids in a living cell. Nature 457:1159–1162
171. Iwabuchi K, Nakayama H, Masuda H, Kina K, Ogawa H, Takamori K (2012) Membrane microdomains in immunity: glycosphingolipid-enriched domain-mediated innate immune responses. Biofactors 38:275. doi:10.1002/biof.1017

Chapter 11

Detection of Isolated Mitochondria-Associated ER Membranes Using the Sigma-1 Receptor

Abasha Lewis, Shang-Yi Tsai, and Tsung-Ping Su

Abstract

The interface between the endoplasmic reticulum (ER) and mitochondria referred to as the MAM (*mitochondria-associated* ER *m*embrane) plays important roles in many physiological functions. A specific marker for this important entity of cellular structure is urgently needed. Thus, we propose in this method chapter that the membrane-bound ER chaperone sigma-1 receptor serves as an ideal marker for the MAM. We describe in detail the preparation and purification of the MAM by using the sigma-1 receptor as the marker and demonstrate the uniqueness of this marker by using a variety of cells, peripheral and neuronal.

Key words Sigma-1 receptor, Chaperone, Endoplasmic reticulum, Mitochondria, MAM, SDS/PAGE electrophoresis, Fractionation

1 Introduction

Since its detection in the 1970s, the specialized area of the ER in physical contact with the outer mitochondrial membrane, termed *m*itochondria-*a*ssociated ER *m*embrane (MAM) [1–7], has emerged as a critical signaling junction within the cell. In fact, the transient contact the MAM provides [8] is used to facilitate critical cellular processes including phospholipid exchange, Ca^{2+} signaling, autophagosome formation, and cellular morphology [9], and has been implicated in several disease models. Just recently, point mutations in the presynaptic protein α-synuclein associated with Parkinson disease was determined to have reduced association with the MAM, in comparison to wild-type α-synuclein, and coincident with a decrease in MAM function and increased fragmentation of mitochondria [10]. Abrogation of MAM functioning has also been implicated in Alzheimer's disease [11–13], diabetes [14–16], and cancer [17].

Due to the increasingly critical implications of MAM localized proteins in the study of neurodegenerative disease, we provide a

Mark G. Waugh (ed.), *Lipid Signaling Protocols*, Methods in Molecular Biology, vol. 1376,
DOI 10.1007/978-1-4939-3170-5_11,

subcellular fractionation assay for the isolation of MAM by taking advantage of differential centrifugation. However, validation of isolated MAM can be problematic. Previous studies have identified several ER-resident proteins enriched at the MAM [9]; however, most of these proteins are also highly detectable in the bulk ER and other cellular compartments. Although phosphatidylethanolamine-N-methyltransferase-2 has emerged as a specific marker for the MAM, it is only reliable in liver and primary hepatocytes [18]. Thus, after careful examination of several MAM-enriched proteins, we show that sigma-1 receptor (Sig-1R) is the most reliable protein marker for this subcellular local in various mammalian cell and tissue types.

2 Materials

2.1 Cell and Tissue Preparation

1. Cell scraper.
2. Phosphate buffered saline (PBS): 13.7 M NaCl, 2.7 mM KCl, 10 mM Na_2HPO_4, 1.8 mM KH_2PO4. Adjust pH to 7.4 and autoclave.
3. Surgeon's scalpel.
4. Hank's balanced salt solution (HBSS) without Ca^{2+} and Mg^{2+}: 13.7 mM NaCl, 5.33 mM KCl, 0.34 mM Na_2HPO_4, 0.44 mM KH_2PO4. Adjust pH to 7.4 and autoclave.

2.2 MAM Isolation Assay

1. Teflon glass homogenizer.
2. Pasteur pipettes, fire-polished.
3. Ultracentrifuge with swinging bucket and fixed angle rotors.
4. Large (16×76 mm) and small (13×51 mm) polycarbonate thick-walled tubes are preferred for use with the rotors.
5. Homogenization buffer (H-B): 10 mM HEPES (4-(2-hydroxyethyl)-1-piperazineethanesulfonic acid), pH 7.4, and 0.25 M sucrose. Store at 4 °C.
6. Isolation medium (I-M): 5 mM HEPES, pH 7.4, 250 mM mannitol, 0.5 mM EGTA. Store at 4 °C.
7. Isolation medium 2 (I-M2): 25 mM HEPES, pH 7.4, 225 mM mannitol, 1 mM EGTA. Store at 4 °C.
8. Percoll medium: 25 mM HEPES, pH 7.4, 225 mM mannitol, 1 mM EGTA, 30 % Percoll (v/v). Make fresh before experiment.
9. SDS-PAGE (sodium dodecyl sulfate–polyacrylamide gel electrophoresis) and western blotting equipment.
10. *Optional*: 10,000 MWCO Centrifugation Filtration Unit.

3 Methods

3.1 Cell and Tissue Preparation

3.1.1 Cell Preparation

1. Culture adherent cells in 15-cm dishes until 90–100 % confluent (*see* **Note 1**).
2. Place cells on ice and wash once with ice-cold PBS.
3. Collect cells in ice-cold PBS by scraping and place into conical tube.
4. Centrifuge cells at 500 × *g* to pellet and discard supernatant. Remove excess supernatant by inverting the tube on a Kimwipes for 30–60 s.

3.1.2 Tissue Preparation

1. Use standard procedures to dissect tissue and place on ice(*see* **Note 2**).
2. Using a surgeon's scalpel, cut the tissue into small pieces and place into conical tube with HBSS.
3. Centrifuge tissue at 500 × *g* to pellet and discard supernatant. Remove excess supernatant by inverting the tube on a Kimwipes for 15–30 s.

3.2 MAM Isolation Assay

To avoid protein degradation during the process, the subcellular fractions should be prepared on ice and centrifuged at 4 °C. Store fractions at −80 °C, if not used immediately.

1. Suspend pelleted cells/tissue in H-B (approximately 9 v/w of wet pellet) and homogenate very slowly with a Teflon glass homogenizer for 20–30 strokes (*see* **Note 3**). Return homogenate to original conical tube.
2. Centrifuge homogenate at 600 × *g* for 5 min. Remove supernatant and place into new conical or eppendorf tube(s). Suspend pellet in H-B and homogenate again (7–15 strokes).
3. Centrifuge homogenate at 600 × *g* for 5 min. Combine resulting supernatant with previous one from **step 2**. Suspend pellet containing cell debris and nuclei in 0.5 ml I-M and store as *P1* fraction.
4. Centrifuge supernatant at 10,300 × *g* for 20 min. Collect supernatant containing microsome and cytosol in large polycarbonate thick-walled tube(s) and place on ice until **step 9**. Thoroughly suspend pellet containing crude mitochondria (mitochondria with intact MAM) in 500 μl of I-M.
5. Layer the crude mitochondria suspension on top of 3 ml of Percoll medium (Fig. 1) in a small polycarbonated thick-walled tube (*see* **Note 4**). Centrifuge at 95,000 × *g* for 30 min using a swinging bucket rotor with deceleration set to zero as not to disturb the gradient.

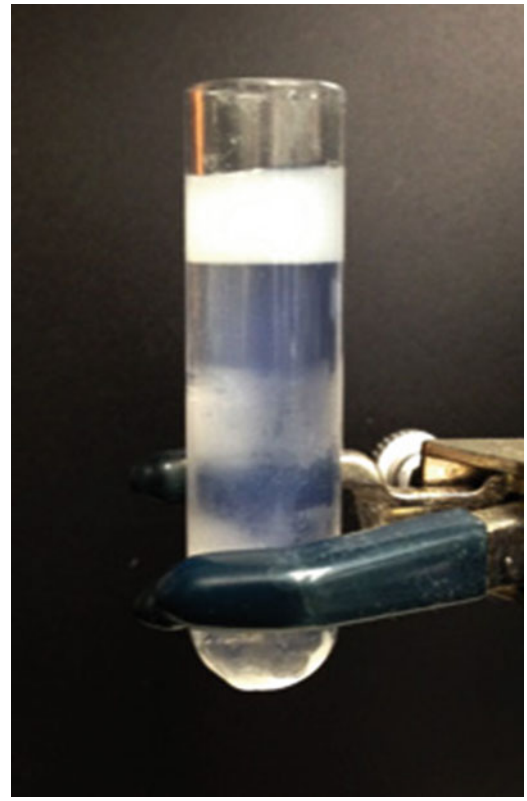

Fig. 1 Crude mitochondrial fraction layered over Percoll medium

6. Collect the MAM and mitochondria (Fig. 2) using fire-polished Pasteur pipettes (*see* **Note 5**). The MAM is observed as a diffuse white layer above the mitochondria. Dense bands containing mitochondria are recovered at approximately $^{3}/_{4}-^{2}/_{3}$ of the way down the tube.
7. Dilute the MAM with five times volume I-M2 and centrifuge at 6300 × *g* for 10 min. Place supernatant containing the MAM into a large polycarbonate thick-walled tube. *Optional*: Resuspend pellet in I-M2 and store as *Crude MAM* (MAM attached to mitochondria or aggregated MAM membranes), otherwise, discard.
8. Centrifuge the MAM and microsome/cytosol from **step 4** at 100,000 × *g* for 1 h using a fixed angle rotor.
9. Dilute mitochondria with five times I-M. Wash three times by centrifugation at 10,500 × *g* for 10 min (*see* **Note 6**). Discard all of the supernatant. Collect pelleted *Mitochondria* fraction by suspending in I-M2 (50–200 μl to obtain 0.5–2 μg/μl protein concentration).

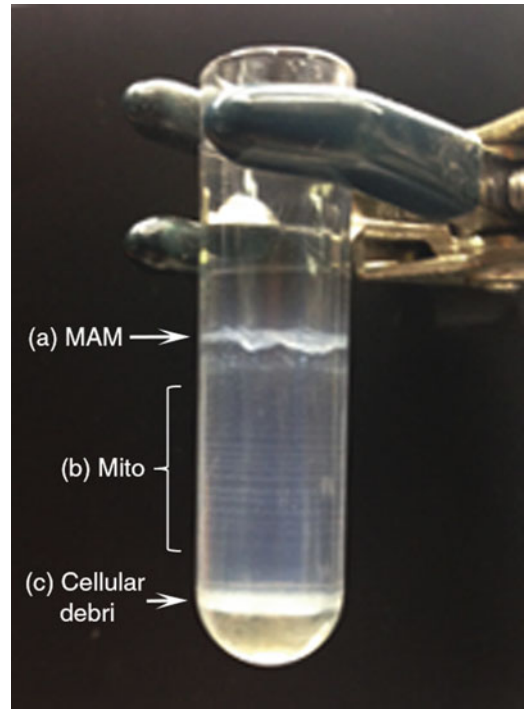

Fig. 2 Ultracentrifugation was used to separate mitochondria and MAM using a Percoll gradient. (**a**) The MAM can be found as a diffuse white band towards the *top* of the tube, while (**b**) mitochondria are found in several dense bands layered *below*. (**c**) Cellular debris collects on the bottom of the tube

10. Collect the MAM: The MAM appears as a loose floating white material (Fig. 3). Gently remove most of the supernatant. Using a fire-polished Pasteur pipette, carefully collect the *MAM* and suspend in H-B (50–200 μl to obtain 0.5–2 μg/μl protein concentration; *see* **Note 7**).
11. Collect microsome and cytosolic fractions: Collect supernatant containing *Cytosolic* fraction (*see* **Note 8**). Add 200 μl of H-B to tube and suspend pelleted *Microsome* fraction by sonicating on ice for 10 s (repeat if necessary).
12. Subcellular fractions (*P1*, *Mito*, *MAM*, *P3*, *Cyto*) are analyzed by SDS-PAGE and western blot analysis (Fig. 4).

4 Notes

1. Four to six 15-cm dishes are recommended to obtain an adequate protein concentration in each fraction; however, the researcher should optimize for the number of cells.
2. Standard dissection procedures can be found in [19].

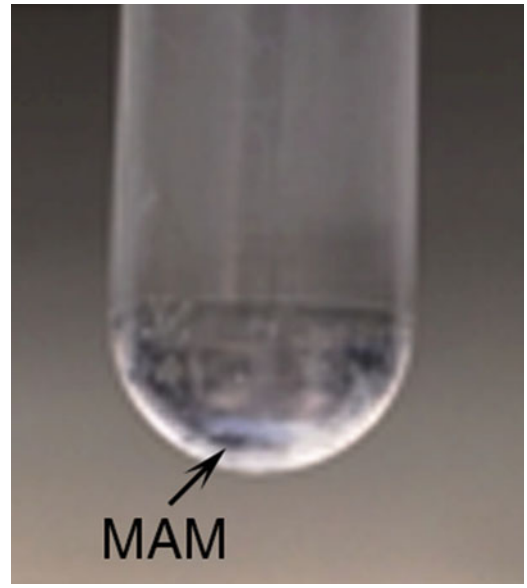

Fig. 3 Ultracentrifugation was used to pellet the purified MAM and is found as a loose white floating material at the bottom of the tube

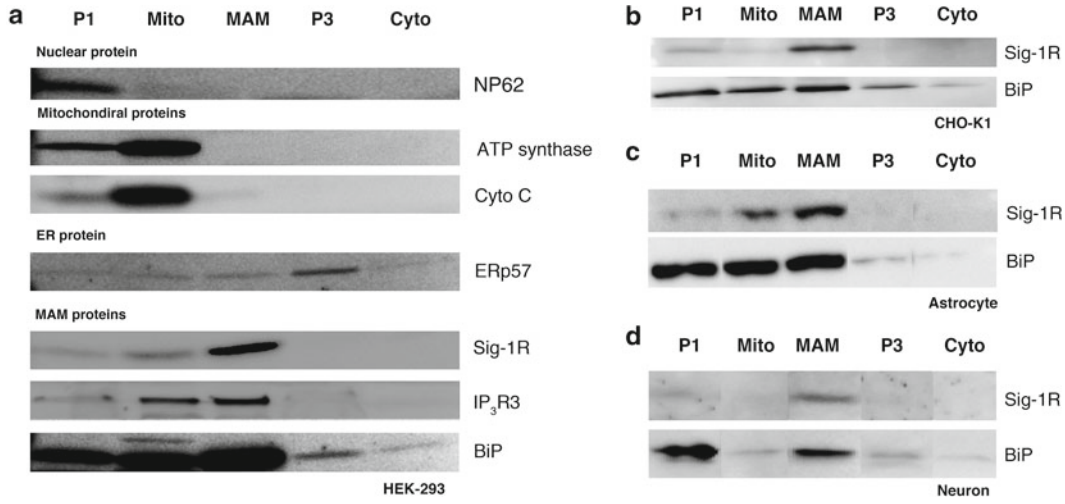

Fig. 4 Western blotting analysis of subcellular fractions collected by the MAM isolation assay protocol in (**a**) HEK cells. Known nuclear (NP62), mitochondrial (ATP synthase, Cytochrome c), MAM-enriched (Sig-1R, BiP, IP_3R3), and ER (ERp57) proteins were used to validate the fractions. Of the MAM-enriched proteins visualized, Sig-1R is the most reliable and is significantly less detectable in other cellular compartments. Cellular distributions of MAM-enriched proteins, Sig-1R and BiP, are also shown for (**b**) CHO cells, (**c**) Astrocytes, and (**d**) Neurons. Overall, Sig-1R was the most reliable protein marker for the MAM when compared to other MAM-enriched proteins

3. Homogenization should be done very slowly and thoroughly as not to destroy the mitochondria and cause dissociation of the MAM. One stroke includes both the up and down movement.
4. Tube size may vary depending on the rotor used. The researcher should optimize the volume of Percoll medium so that it fills approximately $^2/_3$ of the tube. It is also important that the two layers do not significantly mix. Gently layer crude mitochondria on top of Percoll medium so that the interface between the two layers is viewed as a sharp line.
5. Take care when collecting MAM and mitochondria. Place the tip of the fire-polished Pasteur pipette on the wall of the tube and collect from the top of the layer to avoid contamination.
6. This washing step is necessary to remove Percoll medium from the sample. In the presence of Percoll; however, the mitochondrial fraction will not pellet. Thus, after each centrifugation only remove the top $^2/_5 - ^2/_3$ of the supernatant to ensure that mitochondria are retained. Washing is complete when a pellet is visible. All of the supernatant can be removed at this time.
7. Take particular care when collecting the MAM so that only the pellet is recovered. Further dilution of the MAM in H-B may not be necessary. It is up to the research to optimize for desired concentration.
8. *Optional*: The cytosolic fraction can be concentrated using a 10,000 MWCO centrifugal filtration unit.

Acknowledgment

This work is supported by the Intramural Research Program of the National Institute on Drug Abuse, National Institutes of Health, of the Department of Health and Human Services of the United States of America.

References

1. Area-Gomez E, Del Carmen Lara Castillo M, Tambini MD, Guardia-Laguarta C, de Groof AJC, Madra M, Ikenouchi J, Umeda M, Bird TD, Sturley SL, Ea S (2012) Upregulated function of mitochondria-associated ER membranes in Alzheimer disease. EMBO J 31:4106–4123
2. Csordás G, Renken C, V'arnai P, Walter L, Weaver D, Buttle KF, Balla T, Mannella CA, Hajn'oczky G (2006) Structural and functional features and significance of the physical linkage between ER and mitochondria. J Cell Biol 174:915–921
3. Cui Z, Jean E, Chen MH, Voelker DR, Vance DE (1993) Cloning and expression of a novel phosphatidylethanolamine N-methyltransferase. A specific biochemical and cytological marker for a unique membrane fraction in rat liver. J Biol Chem 268:16655–16663
4. Franke WW, Kartenbeck J (1971) Outer mitochondrial membrane continuous with endoplasmic reticulum. Protoplasma 73:35–41
5. Goetz JG, Genty H, St-Pierre P, Dang T, Joshi B, Sauvé R, Vogl W, Nabi IR (2007) Reversible interactions between smooth domains of the

endoplasmic reticulum and mitochondria are regulated by physiological cytosolic Ca^{2+} levels. J Cell Sci 120:3553–3564

6. Guardia-Laguarta C, Area-Gomez E, Rüb C, Liu Y, Jordi M, Becker D, Voos W, Ea S, Przedborski S (2014) α-Synuclein is localized to mitochondria-associated ER membranes. J Neurosci 34:249–259
7. Hayashi T, Su T, Rizzuto R, Hajnoczky G (2009) MAM: more than just a housekeeper. Trends Cell Biol 19:81–88
8. Hedskog L, Moreira C, Filadi R, Rönnbäck A, Hertwig L, Wiehager B (2013) Modulation of the endoplasmic reticulum-mitochondria interface in Alzheimer's disease and related models. Proc Natl Acad Sci U S A 110:7916–7921
9. Ja L, Tata JR (1973) A rapidly sedimenting fraction of rat liver endoplasmic reticulum. J Cell Sci 13:447–459
10. Ca M, Marko M, Penczek P, Barnard D, Frank J (1994) The internal compartmentation of rat-liver mitochondria: tomographic study using the high-voltage transmission electron microscope. Microsc Res Tech 27:278–283
11. Morré DJ, Merritt WD, Ca L (1971) Connections between mitochondria and endoplasmic reticulum in rat liver and onion stem. Protoplasma 73:43–49
12. Pinton P, Giorgi C, Pandolfi PP (2011) The role of PML in the control of apoptotic cell fate: a new key player at ER-mitochondria sites. Cell Death Differ 18:1450–1456
13. Ea S, Area-Gomez E (2013) Mitochondria-associated ER membranes in Alzheimer disease. Mol Cell Neurosci 55:26–36
14. Sebastián D, Hernández-Alvarez MI, Segalés J, Sorianello E, Muñoz JP, Sala D, Waget A, Liesa M, Paz JC, Gopalacharyulu P, Matej O, Pich S, Burcelin R, Palacín M, Zorzano A (2012) Mitofusin 2 (Mfn2) links mitochondrial and endoplasmic reticulum function with insulin signaling and is essential for normal glucose homeostasis. Proc Natl Acad Sci U S A 109: 5523–5528
15. Shore GC, Tata JR (1977) Two fractions of rough endoplasmic reticulum from rat liver. II Cytoplasmic messenger RNA's which code for albumin and mitochondrial proteins are distributed differently between the two fractions. J Cell Biol 72:726–743
16. Spijker S (2011) Dissection of rodent brain regions. In: Li KW (ed) Neuroproteomics. Humana Press, Totowa, NJ, pp 13–26
17. Tubbs E, Theurey P, Vial G, Bendridi N, Bravard A, Chauvin M, Ji-Cao J, Zoulim F, Bartosch B, Ovize M, Vidal H, Rieusset J (2014) Mitochondria-associated endoplasmic reticulum membrane (MAM) integrity is required for insulin signaling and is implicated in hepatic insulin resistance. Diabetes 63:3279–3294
18. Wang HJ, Guay G, Pogan L, Sauvé R, Nabi IR (2000) Calcium regulates the association between mitochondria and a smooth subdomain of the endoplasmic reticulum. J Cell Biol 150:1489–1498
19. Zorzano A, Liesa M, Palacín M (2009) Role of mitochondrial dynamics proteins in the pathophysiology of obesity and type 2 diabetes. Int J Biochem Cell Biol 41:1846–1854

Chapter 12

Using Surface Plasmon Resonance to Quantitatively Assess Lipid–Protein Interactions

Kathryn Del Vecchio and Robert V. Stahelin

Abstract

Surface Plasmon Resonance (SPR) is a quantitative, label-free method for determining molecular interactions in real time. The technology involves fixing a ligand onto a senor chip, measuring a baseline resonance angle, and flowing an analyte in bulk solution over the fixed ligand to measure the subsequent change in resonance angle. The mass of analyte bound to fixed ligand is directly proportional to the resonance angle change and the system is sensitive enough to detect as little as picomolar amounts of analyte in the bulk solution. SPR can be used to determine both the specificity of molecular interactions and the kinetics and affinity of an interaction. This technique has been especially useful in measuring the affinities of lipid-binding proteins to intact liposomes of varying lipid compositions.

Key words Binding affinity, Equilibrium binding, Kinetics, Lipid–protein interactions, Surface plasmon resonance

1 Introduction

A number of techniques have been developed to assess peripheral protein interactions with lipid membranes. Surface plasmon resonance (SPR) is one such technique that has emerged for quantifying protein affinity and specificity for different lipids [1, 2]. Most SPR instruments are based upon the attenuated total reflectance configuration, which relies on the phenomenon of total internal reflection. Total internal reflection is observed when light traveling through an optically dense medium (e.g., glass) reaches an interface between this medium and a medium of lower optical density (e.g., air), and is reflected back. Detection of binding events is possible as an evanescent wave is a component of the incident light that is able to couple with free oscillating electrons (plasmons) in gold film at the interface. A specific angle of incidence (resonance angle) produces a SPR because of energy transfer between the evanescent wave and plasmons on a gold surface. Thus, the SPR signal is sensitive to the mass concentration on the gold surface and is

Mark G. Waugh (ed.), *Lipid Signaling Protocols*, Methods in Molecular Biology, vol. 1376,
DOI 10.1007/978-1-4939-3170-5_12,

expressed in resonance units (RU). The mass change on the surface can be detected in a time dependent manner, which allows for real-time biomolecular interaction analysis.

SPR has been used extensively to observe protein–protein and small molecule–protein interactions, and more recently has been used to explore the interactions of proteins with other biomolecules such as lipids [2–4]. Lipid biochemistry, especially in eukaryotic systems is complex and not wholly understood; membranes may be comprised of over 1000 different lipid species [5], and many cell-signaling pathways are dependent on protein–lipid interactions [6]. As nearly half of proteins are located within or on membranes, it is imperative to characterize the specifics of lipid–protein interactions in order to discern the role these proteins and lipids play on a broader scale. Inherent advantages of SPR include interactions that can be monitored in real-time, neither the ligand nor the analyte require labeling, instruments have high sensitivity, and high throughput of samples can be performed.

Here we discuss how SPR can be used to determine an apparent K_d after approximately 8 h of data collection. We have demonstrated sensitivity of this instrument to detect nanomolar quantities of protein in bulk solution [7]. Additionally, the method can be used to quantify both on- and off-rates and binding affinities of lipid–protein interactions. These applications allow a user to dig deeper into mechanisms regulating peripheral protein association and dissociation from lipid vesicles of varying compositions [3, 4, 8, 9]. This guide details methods that can be used with a BiacoreX system and software.

2 Materials

Prepare all solutions using ultrapure water (18 MΩ resistivity at 25 °C) and analytical grade reagents. It is recommended that you use autoclaved, degassed buffers for both running the instrument and sample preparation. Diligently follow all waste disposal procedures. All solutions are kept at room temperature (25 °C) unless stated otherwise.

2.1 Buffer Preparation

1. *SPR running buffer*: in the most ideal experimental setup, the SPR running buffer should be the same buffer in which the analyte is stored. This will help to minimize any refractive index changes caused by small differences in buffer components (e.g., salt concentration). The running buffer should be free of all detergents as this would destabilize lipid vesicles (*see* **Note 1**). In the case that there is a buffer incompatibility between the analyte storage buffer and the SPR running buffer, a common alternative SPR running buffer is HEPES-KCl (10 mM HEPES, 150 mM KCl, pH = 7.4) (*see* **Note 2**).

2. *50 mM NaOH*: Measure out 0.10 g of NaOH and add to ~25 mL of autoclaved ddH_2O to dissolve the NaOH pellets, followed by dilution to a final volume of 50 mL. Sterile filter this solution through a 0.2 μm filter. Store at room temperature.
3. *20 mM CHAPS detergent*: Measure out 0.614 g CHAPS and add to ~25 mL of autoclaved ddH_2O to dissolve the detergent. Once the detergent is solubilized, dilute to a final volume of 50 mL with autoclaved ddH_2O. Sterile filter this solution through a 0.2 μm sterile syringe filter. Store at room temperature.
4. *40 mM Octyl-β-* d *-Glucopyranoside*: Measure out 0.585 g of Octyl-β-Gluco-Pyranoside and add to ~25 mL of autoclaved ddH_2O to dissolve the detergent. Once the detergent is solubilized, dilute to a final volume of 50 mL with autoclaved ddH_2O. Sterile filter this solution through a 0.2 μm filter. Store at room temperature.
5. *GE L1 Sensor Chip*: Choose a sensor chip that is appropriate for the SPR instrument model you are using. Two common chips are the Sensor Chip L1 and the Series S Sensor Chip L1. The HPA chip can also be used to create a supported bilayer (*see* **Note 3**).

2.2 Lipids and Lipid Vesicle Preparation

It is customary to prepare two samples of lipid vesicles: a control vesicle that contains physiologically relevant compositions of lipids that minimally interact with your analyte, and a second variable component vesicle that contains the same lipids as control vesicles with a single, additional lipid species "spiked" in. Avanti Polar Lipids is the gold standard in terms of lipid purity. Additionally, this setup will help to assess any nonspecific binding of protein analyte to the L1 sensor chip surface.

1. *16:0-18:1 PC*. 1-palmitoyl-2-oleoyl-*sn*-glycero-3-phosphocholine.
2. *16:0-18:1 PE*. 1-palmitoyl-2-oleoyl-*sn*-glycero-3-phosphoethanolamine.
3. *16:0-18:1 PS*. 1-palmitoyl-2-oleoyl-*sn*-glycero-3-phospho-L-SERINE (sodium salt).
4. *Other commonly used lipids*: Lipid–protein SPR can be used to test affinities to lipids other than those listed above. Members of the phosphoinositide (PIP) family [9–11], as well as ceramide-1-phosphate [12, 13] have been used in lipid SPR studies. Most other phospholipids should be amenable to study via this technique (*see* **Note 4**).
5. *Avanti Lipids Mini-Extruder*: https://www.avantilipids.com/index.php?option=com_content&view=article&id=509&Itemid=292&catnumber=610023.
6. *Whatman Filter Membranes*: Whatman Nuclepore Track-Etched Membrane Filtration Product #800309. Specifications: 19 mm diameter, 0.1 μm pore size.

2.3 Protein (Analyte)

1. For the sake of this guide, we discuss proteins as the primary SPR analyte. It is recommended that one follows an established protein purification protocol, keeping in mind that large or bulky tags may interfere with a true SPR signal. In our experience, hexahistidine tags do not seem to cause much issue, but other, larger tags may pose a problem. If your protein is stored in glycerol for increased stability, it is recommended your running buffer contain 5 % glycerol to minimize refractive index changes [14, 15]. It is also advised that proteins remain on ice until just prior to an SPR run.

3 Methods

Carry out all procedures at room temperature unless otherwise specified.

3.1 Preparation of SPR Instrument

1. *Cleaning and Maintenance*: This procedure is recommended as routine maintenance and should be done before starting a new experiment if the SPR has been unused for some time. It is important that any buffers or solutions injected into the instrument are degassed and filter- sterilized. Running buffers should be freshly prepared and detergent-free. Run the following cleaning steps with a blank sensor chip (a "Maintenance" Chip) docked in the instrument to avoid permanently damaging a good Sensor Chip.

   Ensure the buffer intake for the SPR is placed in fresh, degassed, and detergent-free running buffer. Run *Desorb*, using BIAdesorb Solution 1 (0.5 % w/v SDS in pure water) and BIAdesorb Solution 2 (50 mM glycine-NaOH pH 9.5) as per the instrument prompts. Follow the desorb procedure with the *Sanitize* (10 % bleach solution) procedure according to the BIA instrument handbook and as per the instrument prompts. Allow the instrument to run on the *Continue* setting or at a low, continuous flow rate until it is time to run an experiment. It is recommended to dock a proper L1 Sensor Chip at least 12 h prior to running an experiment so that the chip can become equilibrated with the running buffer.

3.2 Preparation of Lipids/LUVs

1. *Control Vesicles*: A standard ratio of lipids in control vesicles is 100 mol% POPC or 80:20 mole percent POPC:POPE. These lipid control compositions work well for protein analytes that bind anionic lipids. Prepare 0.5 mL of 0.5 mM lipid mixture. It will be necessary to calculate the proper volume of stock lipid (in organic solvent) to create the mixture. The formula is as follows: $V = [(M)(TV)(c)(P)]/(C)$

Where *M* is Molecular Weight of Stock Lipid, in g/mol; *TV* is Target Volume, in mL; *c* is Target Concentration, in mM; *P* is Target Mole Percentage, as a decimal value of 1 (e.g., 60 % noted as 0.6); *C* is Concentration of Stock Lipid, in mg/mL.

Measure out each volume of stock lipid precisely with a gastight Hamilton glass syringe. Then dry lipid mixtures under N_2 gas (*see* **Note 5**). Alternatively, a rotary evaporator can be used. Resuspend lipid mixture in the predetermined amount of SPR Running Buffer (component *TV* in the equation above) by vortexing the sample for 10 s. Extrude this lipid mixture as per the protocol provided by Avanti Polar Lipids, Inc. (https://www.avantilipids.com/index.php?option=com_content&view=article&id=1600&Itemid=381). It is recommended to extrude lipids 41 times, i.e., so that the lipid mixture passes through the inner membrane filter 41 times. An odd number of extrusions are necessary so as to collect the lipid vesicles on the opposite side of filter membrane from which the extrusion is started. Take note that vesicles used in SPR are generally 0.1 μm, it is advised to use a proper sized filter accordingly. Store vesicles in a 1.5 mL tube at room temperature (*see* **Note 6**). Vesicles of this size are stable for approximately 36–48 h. Dynamic light scattering can be used to assess the mean vesicle diameter.

2. *Variable Component Vesicles*: A standard ratio of lipids in variable component vesicles will add in a physiologically relevant percentage of your new lipid species, and account for this mole percent addition by subtracting from the total mole percent of POPC. (Ex. Preparing 80:20 POPC:POPE control vesicles and comparing to 60:20:20 POPC:POPE:POPS vesicles). Prepare these vesicles as described in **step 1** (*see* **Note 7**).

3.3 Preparation of the Sensor Surface

1. *CHAPS and Octyl Glucoside washes*: Begin a new sensorgram with access to both flow channels and a flow rate of 30 μL/min. Inject 50 μL of 20 mM CHAPS. On the sensorgram, press the "inject" button, and input the injected volume as 25 μL (*see* **Note 8**). Follow this with an injection of 50 μL of 40 mM Octyl Glucoside (Octyl-β-D-Glucopyranoside). On the sensorgram inject window, input the injected volume as 25 μL. After both injections, exit the sensorgram and prime the system by selecting Tools → Working Tools → Prime. Set the SPR to continue or a low (5 μL/min), continuous flow rate until ready to coat the chip with lipids.
2. *Coating the chip with variable-component liposomes*: Begin a new sensorgram with access only to flow channel 2 (FC2) at a flow rate of 5 μL/min (*see* **Note 9**). Allow the baseline to equilibrate for 2–3 min. Set a baseline for both curves. Pipet up 105 μL of variable component vesicles (made in Subheading

3.2, **step 2**). Then add 5 μL of air by dialing the pipet up to 110 μL, ensuring the tip is exposed to the air. Then add 5 μL of sample by dialing the pipet up to 115 μL, ensuring the tip is submerged in the sample tube. Then add one final 5 μL of air. Inject all 120 μL of volume into the SPR. On the sensorgram inject window, input the injected volume as 80 μL. After the lipid injection, change the flow rate to 50 μL/min. Inject 50 μL of 50 mM NaOH. On the sensorgram inject window, input the injected volume as 10 μL. After the injection, change the flow rate back to 5 μL/min and keep the sensorgram running. Make note of both the absolute response value and the relative response value in resonance units (*see* **Note 10**).

3. *Coating the chip with control liposomes*: In the same sensorgram window, ensure the flow rate is 5 μL/min. Change the flow channel from Flow Channel 2 (FC2) to Flow Channel 1 (FC1) by using Command → Flow Cell → Flow Cell 1 (*see* **Note 11**). Prepare the injection of control vesicles as above: 105 μL liposomes, 5 μL air, 5 μL liposomes, 5 μL air. Inject all 120 μL into the injection port. On the sensorgram inject window, switch the Injection Type dropdown to "Manual Mode" → Continue. Input volume as 80 μL. Pause the injection when the relative response level of FC1 matches FC2, keeping in mind that some of the FC1 coating will come off with the NaOH wash, so erring slightly on overshooting is a good strategy. Once FC1 sufficiently matches FC2, exit the manual injection; any leftover liposomes will be diverted to waste. After the lipid injection, change the flow rate to 50 μL/min. Inject 50 μL of 50 mM NaOH. On the sensorgram inject window, input the injected volume as 10 μL. Repeat this cycle of NaOH injections two more times as necessary (i.e. if both flow channels match after two washes, stop there). After the three NaOH injections, change the flow rate back to 5 μL/min. Keep the sensorgram running. Make note of both the absolute response value and the relative response value in resonance units for both channels (*see* **Note 12**). Stop this sensorgram; it is recommended to save the sensorgram as "Lipid Coat," for reference. Before starting a new sensorgram, prime the system twice by using Tools → Working Tools → Prime.

3.4 Collecting SPR Data of Protein–Lipid Interactions

1. *Initial blocking with BSA*: It is often necessary to block any exposed surfaces of the chip with a stable but unreactive protein (*see* **Note 13**). Bovine Serum Albumen (BSA) is often a good choice for this as it does not specifically bind to most lipids that would be used in the SPR. This is also a good test of assessing the coating efficiency of the L1 sensor chip. Begin a new sensorgram with access to both FC1 and FC2 at a flow rate of 5 μL/min. Allow the baseline to equilibrate for 2–3 min

before setting a baseline for both flow channels. Prepare a 150 μL sample of 0.1 mg/mL BSA (*see* **Note 14**). Pipet up 105 μL of protein, 5 μL of air, 5 μL of protein, and 5 μL of air. Inject all 120 μL into the SPR. On the sensorgram inject window, input the injected volume as 80 μL. After the lipid injection, change the flow rate to 50 μL/min. Inject 50 μL of 50 mM NaOH. On the sensorgram inject window, input the injected volume as 10 μL. After the injection, change the flow rate back to 5 μL/min. Repeat this process as necessary to get the relative response value as close to the baseline as possible (*see* **Note 15**). Make note of both the absolute response value and the relative response value in resonance units for both channels. This is the "new" baseline coating that will be used to collect all protein injection data.

2. *Injections of protein over the sensor surface*: For each protein injection, wait to prepare the dilution until just prior to the injection. Collect a separate sensorgram for each protein injection to better organize the data sets. It is also advised to use fresh, active protein, and to prior to use, spin the stock sample of protein at 50,000 × *g* for 20 min to remove any precipitated protein. Plan the protein dilutions that will be tested over the sensor surface. It is a good idea to go as low as tenfold below the predicted K_d and tenfold above the predicted K_d. A curve should have no fewer than six points, and eight or more points usually comprise a good data set for curve fitting with 12 being an optimal number of data points for fitting. Measurements should be taken from the lowest concentration of protein to the highest concentration (*see* **Note 16**).

   Begin a new sensorgram with access to both FC1 and FC2 at a flow rate of 5 μL/min. Allow the baseline to equilibrate for 2–3 min before setting a baseline for both flow channels. Prepare a 150 μL sample of dilute protein (*see* **Note 17**). Pipet up 105 μL of sample, 5 μL of air, 5 μL of sample, and 5 μL of air. Inject all 120 μL into the SPR. On the sensorgram inject window, input the injected volume as 80 μL and set a delay for washing of 200 s (*see* **Note 18**). Make note of the absolute response value and the relative response value of each channel. After the lipid injection, change the flow rate to 50 μL/min. Inject 50 μL of 50 mM NaOH. On the sensorgram inject window, input the injected volume as 10 μL. After the injection, change the flow rate back to 5 μL/min. Repeat this process as necessary to get the relative response value as close to the baseline as possible. Make note of both the absolute response value and the relative response value for both channels, noting especially if there is any minimal protein remaining on the chip. Proceed with a new sensorgram for each new injection. Once all injections are collected, continue with "Preparing the Sensor Chip for storage" (*see* **Note 19**).

3.5 Preparing the Sensor Chip for Storage

1. *CHAPS and octyl glucoside washes*: After all protein–lipid binding measurements have been made, the chip should have all liposomes removed before storage. In a sensorgram with access to both FC1 and FC2 at a flow rate of 30 μL/min, inject 50 μL of 20 mM CHAPS. On the sensorgram, press the "inject" button, and input the injected volume as 25 μL. Follow this with an injection of 50 μL of 40 mM Octyl Glucoside (Octyl-β-D-GLUCOPYRANOSIDE). On the sensorgram inject window, input the injected volume as 25 μL. After both injections, exit the sensorgram.
2. *Undock L1 chip and store at 4 °C*: Undock the L1 chip by navigating to Command → Undock. Take out the L1 chip and store in a 50 mL conical tube containing approximately 200 μL of running buffer at the bottom to ensure slightly damp storage conditions. To reduce oxidation, a stream of N_2 or argon gas can be used to displace the air in the conical tube prior to storage. Store the sealed tube at 4 °C. Place a maintenance chip in the SPR and dock it. Leave the instrument running on continue or at a low (5 μL/min), continuous flow rate until it is time to run another experiment. Ensure that the running buffer does not run out. Should the system not be needed for use in 3 days, perform a shutdown procedure can be run according to the manufacturer's instructions.

3.6 Data Analysis

This guide describes how to process the data collected using BIAevaluation and KaleidaGraph software.

1. *Quantify Δresonance Unit (ΔRU) for each injection*: In BIAevaluation software, open the first protein injection. This will open the data files for both FC1 and FC2. Select both of these curves and display them using the chart button. Right click and drag to select a small section prior to the time of injection and select Y-Transform → Zero at Average of Selection → Replace Original. Then select X-Transform → Curve Alignment → Next. Zoom in to the area just prior to the injection. Move the cross-hatches for each curve from the leftmost edge of the screen to the point of the injection. Select Accept/OK and this will align the curves at the same X-position. From the Curve: dropdown, select the second of the two curves being analyzed. In the Y-Transform window, select "Curve—Curve 2 (Blank Run Subtraction)" and select the first curve in the pair → Replace Original. Delete off the NaOH washes by right clicking with the mouse and dragging to just before the NaOH washes begin and selecting Edit → Cut. Note the response unit value at the point of saturation on the curve. Repeat this process for all remaining injections, making a table of protein concentration vs. ΔRU value at saturation. It is not necessary to keep the "odd" curves (the zeroed curves)

in the analysis—one can plot all of the "even" curves together to obtain a saturation profile (*see* **Note 20**).

2. *KaleidaGraph curve analysis of SPR data*: Open KaleidaGraph and plot protein concentration in Column A, ΔRU Responses in Column B. Select Gallery → Linear → Scatter. Select Protein Concentration as X and ΔRU as Y. Select Curve Fit → General → Fit1 → Define $(m0 \times m1)/(m0 + m2)$; $m1 = 1100$; $m2 = 1$. Check the "ΔRU" box. The m2 value that appears on the graph is the apparent K_d of the interaction based on the data from Columns A and B. Other graphing programs can be used according to user familiarity and preference.

4 Notes

1. One drawback to the absence of detergents in SPR buffers is that the instrument should be cleaned more frequently (every 2–3 days) as protein will be lost to the inner tube walls of the SPR during experimentation. Additionally, it is recommended that an SPR instrument is cleaned with the desorb procedure approximately every 2 days when working with lipid vesicles to minimize any contamination effects on the lipid surface.
2. It is best to make a 1 L solution of SPR running buffer, autoclave it, and degas immediately before use using a water bath sonicator or vacuum filter prior to use. Keep the SPR running buffer covered with Parafilm or capped with a lid at all times.
3. A variety of methods have been utilized to capture lipids on the sensor surface of SPR instrumentation. The most popular and standardized methods are the supported bilayer (HPA chip) or intact lipid vesicles (L1 chip). The HPA chip utilizes hydrophobic interactions between alkanethiol groups on the gold sensor surface, which will capture the hydrophobic tails of lipid molecules injected into the instrument. This forms a lipid monolayer on the alkanethiol referred to as a supported bilayer. The L1 chip captures intact lipid vesicles injected into the instrument using proprietary hydrophobic groups on the gold carboxymethyldextran sensor surface. In our experience both systems work well for coating and lipid-binding experiments with the L1 chip providing more reproducibility and a longer lifetime of the sensor surface. On the other hand, the HPA chip is better served for proteins that may or are known to cause vesicle fusion as these interactions can change the appearance of the vesicles on the L1 chip surface.
4. For phosphoinositides (PIP) it is recommended that concentrations in the 1–3 mol% range be used in a phosphatidylcholine (PC) vesicle. This way phosphatidylcholine can be used as

a control to directly compare binding of the protein to PC or PC:PIP (97:3) vesicles.

5. Lipid solutions that are prepared in glass amber vials can be dried down under N_2 gas and stored at −20 °C for up to 6 months. It is recommended to wrap the junction between the cap and vial in Parafilm.
6. An odd number of extrusions are necessary so as to collect the lipid vesicles on the opposite side of filter membrane from which the extrusion is started. Take note that vesicles used in SPR are generally 0.1 μm, it is advised to use a proper sized filter accordingly. Vesicles of this size are stable for approximately 36–48 h and dynamic light scattering can be used to assess the mean vesicle diameter.
7. The variable component vesicles should be extruded after control vesicles, so that there is no risk of contaminating the control lipids with any of the variable lipid species.
8. It is always a good idea to inject a higher volume of solution into the SPR to minimize the accidental introduction of air bubbles into the system. The SPR will inject the volume that is input in the program and will divert any leftover solution into the waste—in this way, there is always more than enough liquid in the system and air introduction is minimized.
9. Flow rates faster than 5 μL/min will not robustly support sufficient and timely coating of liposomes on the L1 sensor chip surface.
10. The relative response value is just the Δresponse unit (ΔRU) change in absolute response units relative to the baseline of that particular sensorgram. Absolute response units can be compared from one sensorgram to another.
11. Preparing flow cell 1 as the control and flow cell 2 as the active surface will prevent migration and sample loss of some lipids from flow cell 1 to flow cell 2. In our experience, this is necessary to obtain reproducible data over the course of 1 or 2 days of experimentation with a lipid surface.
12. It is best to have relative response levels to be within 3–5 % between the channels so as not to bias data collection one-way or the other. The closer the channels match, the better.
13. How the lipid vesicles form on the L1 surface is still under debate with most studies suggesting that vesicles are retained intact on the L1 chip surface. One studied suggested the vesicles fuse and form a lipid bilayer [16], while several others using imaging and dye leakage assessment have strong evidence that the lipid vesicles are intact on the sensor surface [4]. The type of surface that forms may be specific to the types and origins of the lipids and lipid mixtures employed as well as the

pH and osmolarity of the running buffer. Either way vesicles anchored to the L1 chip adopt a structure that is relevant for examining lipid–protein interactions.

14. The significance of lipid-coating can be verified by injecting 0.1 mg/mL BSA as less than 100 RU of BSA should bind to a well coated surface while >1000 RU of BSA will bind to an uncoated or poorly coated lipid surface. We've demonstrated that BSA left on the sensor surface will not influence lipid-binding parameters and under some conditions can reduce nonspecific binding to the L1 chip should the protein of interest nonspecifically associate with the carboxylmethyldextran layer.
15. If the relative response value goes down to a certain point but does not completely reach baseline, this is the BSA that has "blocked" the exposed hydrophobic portions of the chip. This often does not take more than 3–5 NaOH washes. Typically, BSA response will be less than 100 resonance units for a sufficiently lipid coated L1 sensor chip.
16. Start with low protein concentration first in case protein binds or sticks to chip or is hard to remove from the lipid vesicles.
17. Only prepare protein sample dilutions right before you are going to inject them into the SPR.
18. It is advised to add a 200+ second delay so that washing of the injection port, which ensues immediately following an injection, does not significantly influence the SPR signal stability. Washing of the injection port can contribute to noise in the SPR signal. When performing saturation (equilibrium binding) measurements a short delay of 200 s or so is sufficient to avoid these issues. Should a user wish to perform detailed kinetic analysis of the off-rate, it is advised to use a longer delay in washing so as to monitor the off-rate as long as possible. This will provide more data points for analysis without noise in signal that comes from the SPR wash step.
19. SPR is also a technique that should receive dedication once a system is working and reproducible. The lifetime of a lipid surface on a L1 chip can last from 12 to 48 h so we recommend dedication, organization, and experimental planning during these times for lab members to collect robust reproducible data over a period of 1–2 days.
20. Kinetic analysis of SPR data can be quite cumbersome and requires careful consideration before publishing results. In brief, the rate of adsorption and desorption are dependent on intrinsic kinetics and mass transport of the system. Diffusion through the boundary layer is usually much slower than the intrinsic adsorption kinetics and is, therefore, the rate determining factor. The best method of detecting a mass transport

limitation is to vary the flow rate of the system, and calculate rate constants under these varying conditions. If mass transport is not rate limiting then rate constants will be consistent over a broad range of flow rates. This holds true because diffusion kinetics are dependent on the flow rate while intrinsic kinetics are not. To eliminate potential mass transport effects, the rate of diffusion must be increased and the rate of binding reduced. Thus, increasing the flow rate and decreasing the ligand density so as to reduce the number of available binding sites are two ways of minimizing the mass transport limitations of a system.

Acknowledgement

The NIH (AI081077) and NSF (1122068) have supported lipid–protein interaction work in the Stahelin lab using SPR. K.D. is funded by a CBBI NIH T32 Predoctoral fellowship (NIH T32GM075762).

References

1. Narayan K, Lemmon MA (2006) Determining selectivity of phosphoinositide-binding domains. Methods 39(2):122–133. doi:10.1016/j.ymeth.2006.05.006
2. Stahelin RV (2013) Surface plasmon resonance: a useful technique for cell biologists to characterize biomolecular interactions. Mol Biol Cell 24(7):883–886. doi:10.1091/mbc.E12-10-0713
3. Stahelin RV, Cho W (2001) Roles of calcium ions in the membrane binding of C2 domains. Biochem J 359(Pt 3):679–685
4. Stahelin RV, Cho W (2001) Differential roles of ionic, aliphatic, and aromatic residues in membrane-protein interactions: a surface plasmon resonance study on phospholipases A2. Biochemistry 40(15):4672–4678
5. van Meer G, Voelker DR, Feigenson GW (2008) Membrane lipids: where they are and how they behave. Nat Rev Mol Cell Biol 9(2):112–124. doi:10.1038/nrm2330
6. Moravcevic K, Oxley CL, Lemmon MA (2012) Conditional peripheral membrane proteins: facing up to limited specificity. Structure 20(1):15–27. doi:10.1016/j.str.2011.11.012
7. Soni SP, Adu-Gyamfi E, Yong SS, Jee CS, Stahelin RV (2013) The Ebola virus matrix protein deeply penetrates the plasma membrane: an important step in viral egress. Biophys J 104(9):1940–1949. doi:10.1016/j.bpj.2013.03.021
8. Bittova L, Stahelin RV, Cho W (2001) Roles of ionic residues of the C1 domain in protein kinase C-alpha activation and the origin of phosphatidylserine specificity. J Biol Chem 276(6):4218–4226. doi:10.1074/jbc.M008491200
9. Stahelin RV, Long F, Diraviyam K, Bruzik KS, Murray D, Cho W (2002) Phosphatidylinositol 3-phosphate induces the membrane penetration of the FYVE domains of Vps27p and Hrs. J Biol Chem 277(29):26379–26388. doi:10.1074/jbc.M201106200
10. Blatner NR, Stahelin RV, Diraviyam K, Hawkins PT, Hong W, Murray D, Cho W (2004) The molecular basis of the differential subcellular localization of FYVE domains. J Biol Chem 279(51):53818–53827. doi:10.1074/jbc.M408408200
11. Stahelin RV, Karathanassis D, Murray D, Williams RL, Cho W (2007) Structural and membrane binding analysis of the Phox homology domain of Bem1p: basis of phosphatidylinositol 4-phosphate specificity. J Biol Chem 282(35):25737–25747. doi:10.1074/jbc.M702861200
12. Stahelin RV, Subramanian P, Vora M, Cho W, Chalfant CE (2007) Ceramide-1-phosphate binds group IVA cytosolic phospholipase a2 via a novel site in the C2 domain. J Biol Chem 282(28):20467–20474. doi:10.1074/jbc.M701396200

13. Ward KE, Bhardwaj N, Vora M, Chalfant CE, Lu H, Stahelin RV (2013) The molecular basis of ceramide-1-phosphate recognition by C2 domains. J Lipid Res 54(3):636–648. doi:10.1194/jlr.M031088
14. Stahelin RV, Digman MA, Medkova M, Ananthanarayanan B, Rafter JD, Melowic HR, Cho W (2004) Mechanism of diacylglycerol-induced membrane targeting and activation of protein kinase Cdelta. J Biol Chem 279(28):29501–29512. doi:10.1074/jbc.M403191200
15. Stahelin RV, Digman MA, Medkova M, Ananthanarayanan B, Melowic HR, Rafter JD, Cho W (2005) Diacylglycerol-induced membrane targeting and activation of protein kinase Cepsilon: mechanistic differences between protein kinases Cdelta and Cepsilon. J Biol Chem 280(20):19784–19793. doi:10.1074/jbc.M411285200
16. Erb EM, Chen X, Allen S, Roberts CJ, Tendler SJ, Davies MC, Forsen S (2000) Characterization of the surfaces generated by liposome binding to the modified dextran matrix of a surface plasmon resonance sensor chip. Anal Biochem 280(1):29–35. doi:10.1006/abio.1999.4469

Chapter 13

Analyzing Protein–Phosphoinositide Interactions with Liposome Flotation Assays

Ricarda A. Busse, Andreea Scacioc, Amanda M. Schalk, Roswitha Krick, Michael Thumm, and Karin Kühnel

Abstract

Liposome flotation assays are a convenient tool to study protein–phosphoinositide interactions. Working with liposomes resembles physiological conditions more than protein–lipid overlay assays, which makes this method less prone to detect false positive interactions. However, liposome lipid composition must be well-considered in order to prevent nonspecific binding of the protein through electrostatic interactions with negatively charged lipids like phosphatidylserine. In this protocol we use the PROPPIN Hsv2 (homologous with swollen vacuole phenotype 2) as an example to demonstrate the influence of liposome lipid composition on binding and show how phosphoinositide binding specificities of a protein can be characterized with this method.

Key words Analytical ultracentrifuge, Small unilamellar vesicles, Protein–lipid overlay assay, PROPPIN, Hsv2

1 Introduction

Phosphoinositide (PIP) binding of proteins can be analyzed with a variety of techniques. Among them are surface plasmon resonance [1–3], reflectometric interference spectroscopy [4], fluorescence resonance energy transfer (FRET) based liposome binding assays [5], stopped-flow FRET measurements [6, 7], and isothermal titration calorimetry [8]. These methods also allow quantification of PIP binding, but not every laboratory has access to the required equipment.

The easiest method to probe protein–lipid interactions are protein–lipid overlay assays, where lipids are spotted on a membrane. These membranes are then incubated with the protein of interest and binding is detected through immunoblotting. The commercially available PIP strips (Echelon Biosciences Incorporated, Salt Lake City USA) contain the seven natural occurring phosphoinositides. The major disadvantage of protein–lipid overlay assays is that

Mark G. Waugh (ed.), *Lipid Signaling Protocols*, Methods in Molecular Biology, vol. 1376,
DOI 10.1007/978-1-4939-3170-5_13,

frequently interactions are found, which are not detected when using other methods. An explanation for these observations is that pure lipids are present at very high local concentrations on nitrocellulose or polyvinylidenfluorid membranes, which is very different from physiological conditions, where phosphoinositides are present at low concentrations in lipid bilayers with 1 % at most [9, 10]. In a genome wide analysis of *Saccharomyces cerevisiae* pleckstrin homology (PH) domain containing proteins, 27 of 33 proteins interacted with PIPs in dot blot assays [11]. However, phosphoinositide binding was confirmed for only ten of these proteins by other methods. More recently, a systematic screen for protein–lipid interactions in *S. cerevisiae* with lipid-arrays yielded 530 interactions among 124 proteins and 30 lipids [12]. The fraction of true interactions was extrapolated as 61.4 % in this study. Thus, interactions detected in protein–lipid overlay assays need to be verified by at least one other method.

Here we describe liposome flotation assays as a convenient tool to analyze protein–phosphoinositide interactions. These experiments require an analytical ultracentrifuge. We perform liposome flotation assays with small unilamellar vesicles (SUVs), which have an average radius of 18 nm [8, 13, 14]. SUVs and the protein of interest are mixed and overlaid with a Nycodenz gradient. After ultracentrifugation the liposomes will float on top of the gradient. If the protein binds to liposomes it will be also present in the top fractions; otherwise, it is localized in the middle and bottom fractions.

In this protocol we use *Kluyveromyces lactis*Hsv2 (homologous with swollen vacuole phenotype 2) as a test case and demonstrate the importance of liposome lipid composition in order to avoid detecting nonspecific interactions. Hsv2 belongs to the PROPPIN (β-propeller that bind polyphosphoinositides) family [2, 15]. PROPPINs have two PIP binding sites [4, 5, 16]. The conserved FRRG motif, which is part of the two PIP binding sites, is essential for PIP binding of PROPPINs [2, 17, 18].

PIP strip analysis shows that *K. lactis*Hsv2 appears to bind phosphatidylinositol-3,5-bisphosphate (PtdIns(3,5)P_2) with a much larger preference than phosphatidylinositol-3-phosphate (PtdIns3P) (Fig. 1). However, a FRET-based liposome binding assay showed that *K. lactis* Hsv2 binds both PtdIns(3,5)P_2 and PtdIns3P-containing liposomes with a submicromolar affinity [5]. Consistent with these results we demonstrate that *K. lactis* Hsv2 specifically interacts with PtdIns3P and PtdIns(3,5)P_2 but not with other phosphoinositides using liposome flotation assays.

2 Materials

An analytical ultracentrifuge is required for liposome flotation assays. We use a Sorvall Discovery M150 SE analytical ultracentrifuge with a S55-S swinging-bucket rotor (Thermo Scientific, Waltham, MA, USA).

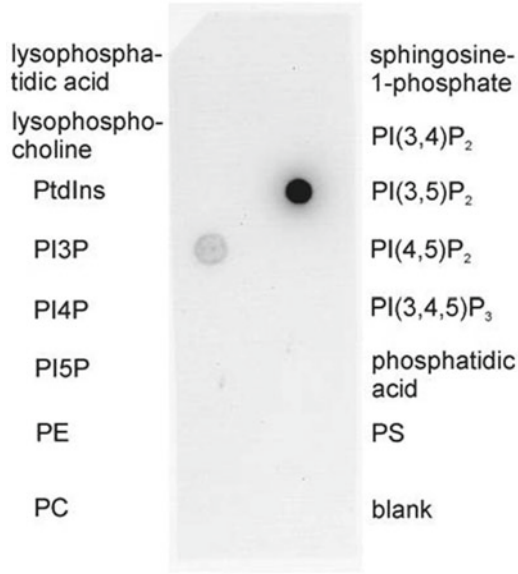

Fig. 1 Protein–lipid overlay assay with *Kluyveromyces lactis*Hsv2. The protein was expressed and purified as described previously [4]. The PIP strip was incubated with 2 μg/mL Hsv2 in 0.15 M NaCl, 20 mM NaH_2PO_4, 2 mM $MgCl_2$ pH 7.3 supplemented with 1 % (w/v) milk powder for 1 h at room temperature. Binding was detected with Penta-His HRP conjugate antibody (Qiagen, Hilden, Germany) in a 1:2000 dilution

All preparatory steps are carried out at room temperature. When disposing of chloroform, follow the local waste disposal regulations for halogenated hydrocarbon compounds.

1. Prepare lipid stock solutions with chloroform (*see* **Note 1**). l-α-phosphatidylcholine (PC), l-α-phosphatidylethanolamine (PE), and 1,2-dioleoyl-*sn*-glycero-3-phospho-l-serine (PS) are dissolved at a concentration of 25 mg/mL. Phosphoinositide stock solutions have a concentration of 1 mg/mL: 1,2-dioleoyl-sn-glycero-3-phospho-(1′-myo-inositol-3′-phosphate) (PtdIns3P) l-α-phosphatidylinositol-4-phosphate (PtdIns4P) 1,2-dioleoyl-*sn*-glycero-3-phospho-(1′-myo-inositol-5′-phosphate) (PtdIns5P), 1,2-dioleoyl-*sn*-glycero-3-phospho-(1′-myo-inositol-3′,5′-bisphosphate) ($PtdIns(3,5)P_2$), 1,2-dioleoyl-*sn*-glycero-3-phospho-(1′-myo-inositol-4′,5′-bisphosphate)($PtdIns(4,5)P_2$),1,2-dioleoyl-*sn*-glycero-3-phospho-(1′-myo-inositol-3′,4′,5′-trisphosphate) ($PtdIns(3,4,5)P_3$). Prepare a 1 mg/mL stock solution of Texas-Red-1,2-dihexadecanoyl-*sn*-glycero-3-phosphoethanolamine (TR-PE), which colors the liposomes pink.

   Store lipid stock solutions in 2 mL screw top amber glass vials (Supelco 27000).

2. Prepare 500 mL HP150 buffer composed of 150 mM KCl, 20 mM HEPES pH 7.4 by dissolving 5.59 g KCl and 2.38 g

HEPES in 450 mL water. Adjust the pH to 7.4 with NaOH and fill up to 500 mL with water.

3. For 3 % (w/v) sodium cholate in HP150 buffer dissolve 1.5 g sodium cholate in 50 mL HP150.
4. Prepare 30 % (w/v) and 80 % (w/v) Nycodenz stock solutions in HP150 buffer (*see* **Note 2**).

3 Methods

3.1 Preparation of Liposomes

Since phosphoinositide-binding proteins can also bind to liposomes containing negatively charged lipids like PS through nonspecific electrostatic interactions, care needs to be taken with the liposome lipid composition [10]. Here we tested different liposomes for binding of *K. lactis*Hsv2. The PIP binding deficient Hsv2^{FTTG} mutant was used as a negative control. Indeed, increasing amounts of PS enhanced nonspecific binding of *K. lactis* Hsv2 to liposomes (Fig. 2a). Neutral liposomes composed of PC:PE:TR-PE (75:23:2, weight ratio) did not interact with wild-type protein and the FTTG mutant. When 1–2 % PIP was added to neutral liposomes, only specific PIP binding of the wild-type protein was observed (Fig. 2a). Liposomes composed of PIP:PE:TR-PE (1:74:23:2) were then used for analyzing the PIP binding specificity of *K. lactis* Hsv2. Liposome flotation assays show that the protein interacts specifically with PtdIns3P and PtdIns(3,5)P_2 (Fig. 2b).

1. Prepare 1 mg of lipid mixture by pipetting the corresponding amounts of the individual lipids. We add 2 % (w/v) TR-PE to all preparations to stain the liposomes. For example, to prepare liposomes composed of PtdIns3P:PC:PE:TR-PE (1:74:23:2, weight ratio) add 10 µL 1 mg/mL PtdIns3P, 29.6 µL 25 mg/mL PC, 9.2 µL 25 mg/mL PE, and 20 µL 1 mg/mL TR-PE into a 2 mL Eppendorf tube. Air-dry through evaporation for approximately 2 h. The dried lipid pellet is purple (*see* **Note 1**).
2. Resuspend the dried lipid pellet in 150 µL 3 % (w/v) sodium cholate in HP150. The sample can be vortexed.
3. The lipid mixture is then run through a self-packed gel-filtration column to remove the sodium cholate causing liposome formation. For one column, resuspend 0.5 g Sephadex G-50 in 10 mL HP150. The slurry is then filled into the column, for example a Bio-Rad 0.5 cm × 15 cm Econo-Column with an attached stopcock, and left to settle. HP150 is also used as the running buffer. Evenly pipet 150 µL of the resuspended lipid mix across the gel bed. After it has entered the gel bed, carefully add 200 µL HP150 and then 4 mL HP150 buffer. Take care not to disturb the lipid layer when pipetting buffer onto the column. The lipids can be followed visually as the

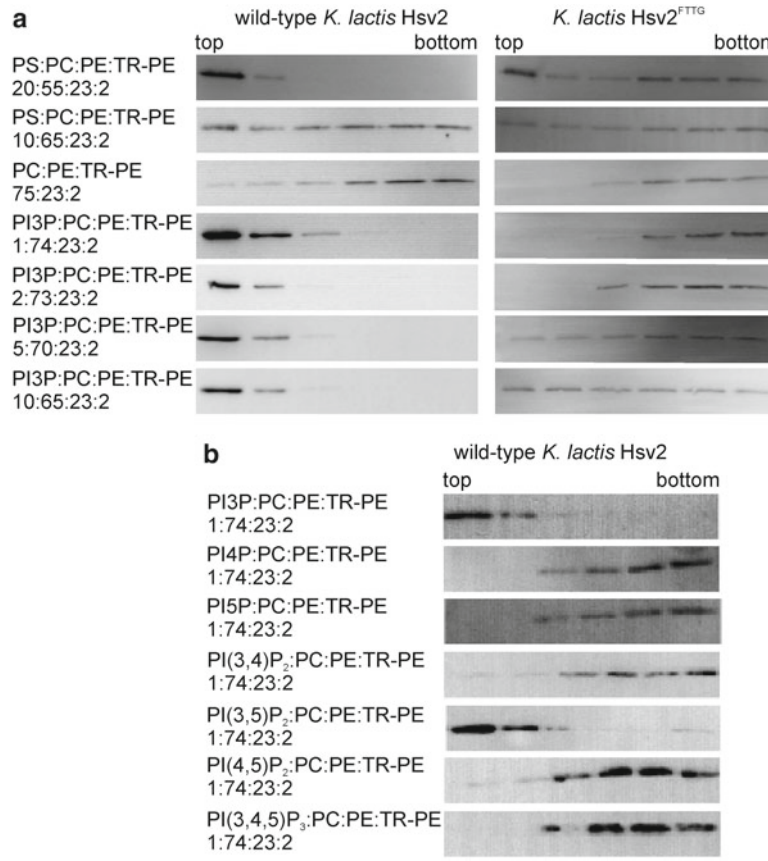

Fig. 2 Liposome flotation assays with wild-type *K. lactis*Hsv2 and *K. lactis* Hsv2^{FTTG}. The FTTG mutant is deficient in PIP binding and serves as a negative control for detecting nonspecific binding. When a protein binds to liposomes it is found in the top two fractions. In contrast, if there are no interactions the protein is localized in the bottom four fractions. (**a**) Increasing amounts of PS increase nonspecific binding of wild-type and *K. lactis* Hsv2^{FTTG}. Neutral liposomes composed of PC:PE:TR-PE (75:23:2) do not bind to wild-type protein and the FTTG mutant. At 5 and 10 % PtdIns3P, nonspecific binding to liposomes is also observed. *K. lactis* Hsv2^{FTTG} was expressed with an N-terminal His-tag from the pACE vector [19] and purified like the wild-type protein. (**b**) Liposome flotation assays to analyze PIP binding specificities of *K. lactis* Hsv2. Liposomes contained 1 % of the respective PIP. *K. lactis* Hsv2 specifically interacts with PtdIns3P and PtdIns(3,5)P_2

pink band. Collect fractions in Eppendorf tubes and pool those that are pink and thus contain small unilamellar vesicles (SUVs). Liposomes can be stored for several days at 4 °C. Do not freeze liposomes.

3.2 Liposome Flotation Assays

1. Proteins are diluted with HP150 buffer to a concentration of 2 μM. 5 μL of 2 μM protein is mixed with 45 μL of liposomes and incubated at room temperature for 10–30 min.

2. 50 μL of the incubated protein–liposome sample is transferred into a 230 μL polycarbonate thick-walled tube and thoroughly mixed with 50 μL of 80 % (w/v) Nycodenz in HP150 by pipetting it up and down ten times.
3. 50 μL of 30 % (w/v) Nycodenz in HP150 is then gently added on top without mixing (*see* **Note 3**).
4. Finally 30 μL HP150 is pipetted as top layer onto the Nycodenz gradient. The bottom layer is pink, whereas the 30 % Nycodenz and top HP150 layers are colorless.
5. Place centrifugation tubes into adaptors for the S55-S swinging-bucket rotor, which allows four samples to run at a time. Spin at 55,000 rpm (260,000 × *g*) for 90 min at 4 °C in a Sorvall Discovery M150 SE analytical ultracentrifuge.
6. Prepare six 1.5 mL Eppendorf tubes, each containing 15 μL 3× concentrated sample loading buffer. Carefully remove buckets from the rotor and take out the tubes. Liposomes form a pink rim on top of the gradient. Take six 30 μL fractions from the gradient and use a fresh tip for each pipetting step. Heat Eppendorf tubes for 3 min at 95 °C (*see* **Note 4**).
7. Analyze samples by Western blotting. The top two fractions of the gradient contain protein bound to liposomes and the bottom four fractions show the unbound protein.

4 Notes

1. Chloroform has a high vapor pressure. To ensure accurate pipetting first pre-wet the tip with chloroform by pipetting chloroform up and down ten times when either preparing lipid stock solutions or pipetting chloroform containing solutions.
2. Nycodenz is a non-ionic tri-iodinated derivative of benzoic acid. It is a nontoxic and very water-soluble compound. To prepare a 80 % (w/v) stock solution weigh 4 g Nycodenz, transfer it into a 15 mL Falcon tube and add 2 mL of HP150 buffer. Put the Falcon tube onto a rotating wheel. After it has dissolved, fill to a final volume of 5 mL. For a 30 % (w/v) Nycodenz stock solution, use 1.5 g with a final volume of 5 mL.
3. A small ball of modeling clay can be used as a support to hold the tube in an approx. 45° tilted angle when pipetting the gradient. Gently pipette solution onto the tube wall and let it run down to the liquid surface.
4. For pipetting off the gradient fractions, first use 200 μL tips to pipette the top layer from the rim of the gradient. This step is repeated once and yields samples 1 and 2. Next use thin 200 μL gel loading tips to pipette samples 3–6 starting from the very

bottom of the centrifugation tube. In this scheme sample 3 corresponds to the very bottom of the gradient. Load samples in the order 1, 2, 6, 5, 4, 3 on a gel to show the gradient starting from top to bottom. TR-PE will be visible as a pink band at the bottom of the SDS PAGE gel for the first two fractions.

Acknowledgements

We thank Geert van den Bogaart for advice and discussions. This work was supported by a SFB860 grant to M.T. and K.K.

References

1. Kelly BT, McCoy AJ, Spate K, Miller SE, Evans PR, Honing S, Owen DJ (2008) A structural explanation for the binding of endocytic dileucine motifs by the AP2 complex. Nature 456(7224):976–979. doi:10.1038/nature07422
2. Dove SK, Piper RC, McEwen RK, Yu JW, King MC, Hughes DC, Thuring J, Holmes AB, Cooke FT, Michell RH, Parker PJ, Lemmon MA (2004) Svp1p defines a family of phosphatidylinositol 3,5-bisphosphate effectors. EMBO J 23(9):1922–1933. doi:10.1038/sj.emboj.7600203
3. Yu JW, Lemmon MA (2001) All phox homology (PX) domains from *Saccharomyces cerevisiae* specifically recognize phosphatidylinositol 3-phosphate. J Biol Chem 276(47):44179–44184. doi:10.1074/jbc.M108811200
4. Krick R, Busse RA, Scacioc A, Stephan M, Janshoff A, Thumm M, Kühnel K (2012) Structural and functional characterization of the two phosphoinositide binding sites of PROPPINs, a beta-propeller protein family. Proc Natl Acad Sci U S A 109(30):E2042–E2049. doi:10.1073/pnas.1205128109
5. Baskaran S, Ragusa MJ, Boura E, Hurley JH (2012) Two-site recognition of phosphatidylinositol 3-phosphate by PROPPINs in autophagy. Mol Cell 47(3):339–348. doi:10.1016/j.molcel.2012.05.027
6. Corbin JA, Evans JH, Landgraf KE, Falke JJ (2007) Mechanism of specific membrane targeting by C2 domains: localized pools of target lipids enhance Ca^{2+} affinity. Biochemistry 46(14):4322–4336. doi:10.1021/bi062140c
7. Perez-Lara A, Egea-Jimenez AL, Ausili A, Corbalan-Garcia S, Gomez-Fernandez JC (2012) The membrane binding kinetics of full-length PKCalpha is determined by membrane lipid composition. Biochim Biophys Acta 1821(11):1434–1442. doi:10.1016/j.bbalip.2012.06.012
8. Busse RA, Scacioc A, Hernandez JM, Krick R, Stephan M, Janshoff A, Thumm M, Kühnel K (2013) Qualitative and quantitative characterization of protein-phosphoinositide interactions with liposome-based methods. Autophagy 9(5):770–777. doi:10.4161/auto.23978
9. Lemmon MA (2008) Membrane recognition by phospholipid-binding domains. Nat Rev Mol Cell Biol 9(2):99–111. doi:10.1038/nrm2328
10. Narayan K, Lemmon MA (2006) Determining selectivity of phosphoinositide-binding domains. Methods 39(2):122–133. doi:10.1016/j.ymeth.2006.05.006
11. Yu JW, Mendrola JM, Audhya A, Singh S, Keleti D, DeWald DB, Murray D, Emr SD, Lemmon MA (2004) Genome-wide analysis of membrane targeting by *S. cerevisiae* pleckstrin homology domains. Mol Cell 13(5):677–688
12. Gallego O, Betts MJ, Gvozdenovic-Jeremic J, Maeda K, Matetzki C, Aguilar-Gurrieri C, Beltran-Alvarez P, Bonn S, Fernandez-Tornero C, Jensen LJ, Kuhn M, Trott J, Rybin V, Muller CW, Bork P, Kaksonen M, Russell RB, Gavin AC (2010) A systematic screen for protein-lipid interactions in *Saccharomyces cerevisiae*. Mol Syst Biol 6:430. doi:10.1038/msb.2010.87
13. van den Bogaart G, Holt MG, Bunt G, Riedel D, Wouters FS, Jahn R (2010) One SNARE complex is sufficient for membrane fusion. Nat Struct Mol Biol 17(3):358–364. doi:10.1038/nsmb.1748
14. Schuette CG, Hatsuzawa K, Margittai M, Stein A, Riedel D, Kuster P, Konig M, Seidel C, Jahn R (2004) Determinants of liposome fusion mediated by synaptic SNARE proteins. Proc

Natl Acad Sci U S A 101(9):2858–2863. doi:10.1073/pnas.0400044101

15. Dove SK, Dong K, Kobayashi T, Williams FK, Michell RH (2009) Phosphatidylinositol 3,5-bisphosphate and Fab1p/PIKfyve underP-PIn endo-lysosome function. Biochem J 419(1):1–13. doi:10.1042/BJ20081950
16. Watanabe Y, Kobayashi T, Yamamoto H, Hoshida H, Akada R, Inagaki F, Ohsumi Y, Noda NN (2012) Structure-based analyses reveal distinct binding sites for Atg2 and phosphoinositides in Atg18. J Biol Chem 287(38):31681–31690. doi:10.1074/jbc.M112.397570
17. Krick R, Tolstrup J, Appelles A, Henke S, Thumm M (2006) The relevance of the phosphatidylinositolphosphat-binding motif FRRGT of Atg18 and Atg21 for the Cvt pathway and autophagy. FEBS Lett 580(19):4632–4638. doi:10.1016/j.febslet.2006.07.041
18. Stromhaug PE, Reggiori F, Guan J, Wang CW, Klionsky DJ (2004) Atg21 is a phosphoinositide binding protein required for efficient lipidation and localization of Atg8 during uptake of aminopeptidase I by selective autophagy. Mol Biol Cell 15(8):3553–3566. doi:10.1091/mbc.E04-02-0147
19. Bieniossek C, Nie Y, Frey D, Olieric N, Schaffitzel C, Collinson I, Romier C, Berger P, Richmond TJ, Steinmetz MO, Berger I (2009) Automated unrestricted multigene recombineering for multiprotein complex production. Nat Methods 6(6):447–450. doi:10.1038/nmeth.1326

Chapter 14

High-Throughput Fluorometric Assay for Membrane–Protein Interaction

Wonhwa Cho, Hyunjin Kim, and Yusi Hu

Abstract

Membrane–protein interaction plays key roles in a wide variety of biological processes. To facilitate rapid and sensitive measurement of membrane binding of soluble proteins, we developed a fluorescence-based quantitative assay that is universally applicable to all proteins. This fluorescence-quenching assay employs fluorescence protein (FP)-tagged proteins whose fluorescence intensity is greatly decreased when they bind vesicles containing synthetic lipid dark quenchers, such as N-dimethylaminoazobenzenesulfonylphosphatidylethanolamine (dabsyl-PE). This simple assay can be performed with either a spectrofluorometer or a plate reader and optimized for different proteins with various combinations of FPs and quenching lipids. The assay allows rapid, sensitive, and accurate determination of lipid specificity and affinity for various lipid binding domains and proteins, and also high-throughput screening of small molecules that modulate membrane binding of proteins.

Key words Membrane–protein binding, Lipid specificity, high-throughput fluorescence assay, Membrane binding inhibitors, Dark quenchers, Fluorescence proteins

Abbreviations

Dabsyl-PE	Dimethylaminoazobenzenesulfonyl-phosphatidylethanolamine
DMSO	Dimethylsulfoxide
EGFP	Enhanced green fluorescence protein
FP	Fluorescence protein
PC	Phosphatidylcholine
POPC	1-palmitoyl-2-oleoyl-*sn*-glycero-3-phosphocholine
POPE	1-palmitoyl-2-oleoyl-*sn*-glycero-3-phosphoethanolamine
POPS	1-palmitoyl-2-oleoyl-*sn*-glycero-3-phosphoserine
PS	Phosphatidylserine
PtdIns	Phosphatidylinositol
PtdIns(3,4,5)P_3	Phosphatidylinositol-3,4,5-trisphosphate
PtdIns*P*	Phosphoinositides
SPR	Surface plasmon resonance
YFP	Yellow fluorescence protein

Mark G. Waugh (ed.), *Lipid Signaling Protocols*, Methods in Molecular Biology, vol. 1376,
DOI 10.1007/978-1-4939-3170-5_14,

1 Introduction

Membrane lipids regulate a wide variety of biological processes, including cell signaling, membrane trafficking, blood coagulation, and viral infection, by recruiting diverse soluble proteins to cell membranes both intracellularly and extracellularly [1–4]. Most of membrane binding proteins contain lipid-binding domains or motifs that mediate membrane binding either through specific recognition of lipid headgroups or by nonspecific electrostatic and/or hydrophobic interactions with membrane lipids [1, 2, 4]. Recent genome-scale computation and characterization of cellular proteins have shown that a large number of previously unsuspected proteins, including protein interaction domains such as PDZ domains, directly interact with membrane lipids [5–11]. A rapid, sensitive, and universally applicable assay for membrane–protein interaction is therefore necessary for identification and characterization of a rapidly growing number of diverse membrane binding proteins and for identification of small molecules that can modulate their membrane interaction.

Membrane binding of soluble and/or peripheral proteins has been measured by various biochemical and biophysical methods [12, 13]. The lipid overlay assay has been popular due to its ease of use but it suffers from low sensitivity, poor reliability and an inability to yield quantitative information [14]. The sedimentation assay using lipid vesicles has also been routinely used to assess membrane binding of proteins [15]. However, its relatively qualitative nature and variable pelleting efficiency associated with different lipid vesicles have limited its utility. The SPR analysis allows robust quantitative analysis of membrane–protein interactions and has thus been a mainstay in biophysical characterization of membrane binding proteins [12, 13]. Although this assay offers many advantages, including high sensitivity, no requirement for protein labeling, and an ability to provide kinetic information, it also has drawbacks, including the necessity of expensive instrumentation and rigorous controls to eliminate nonspecific binding, uncertainty about the physical nature of lipids coated on the sensor chip, and binding measurements under nonequilibrium conditions. Due to their high sensitivity, various fluorescence techniques have been extensively employed to monitor membrane–protein interaction. Most commonly, an increase [16], quenching [17], or fluorescence resonance energy transfer [18, 19] of Trp fluorescence is monitored during membrane–protein binding. Although rapid and convenient, these methods are not generally applicable to all proteins because many proteins do not have Trp on their membrane-binding surfaces. Although Trp can be genetically introduced to the membrane binding surface to a protein, this can dramatically change its membrane binding property [20]. Alternatively, the protein can be

labeled with an organic fluorophore but this approach is limited by experimental inconvenience and the relative low yield of chemical modification [21]. Fluorescence anisotropy [22] and fluorescence correlation spectroscopy analyses [23] have been also used to measure membrane–protein interaction but with limited applications.

Most important, none of these methods allow sensitive, robust, and universal high-throughput analysis. To overcome these technical limitations and obstacles, we have developed a high-throughput membrane binding assay that is based on fluorescence quenching of fluorescence proteins (FPs), such as enhanced green FP (EGFP), fused to a membrane-binding protein by a dark quencher-containing lipid, such as N-dimethylaminoazobenzenesulfonyl-phosphatidylethanolamine (dabsyl-PE), incorporated in lipid vesicles [24]. Since FPs do not have affinity for membrane lipids [24], a FP tag does not affect the membrane binding of a diverse group of proteins tested so far. Furthermore, FPs offer an additional advantage of stabilizing the fused protein or domain (*see* **Note 1**). Through the custom selection of a FP and a dark quencher from widely available collections, this simple and rapid assay can be optimized for sensitive, accurate, and reproducible quantitative determination of lipid affinity and specificity of diverse proteins as well as for high-throughput screening of small molecules that can modulate their membrane binding.

2 Materials

2.1 Lipid Stock Solutions

1. Regular lipids: Dissolve 1-palmitoyl-2-oleoyl-*sn*-glycero-3-phosphocholine (POPC), 1-palmitoyl-2-oleoyl-*sn*-glycero-3-phosphoethanolamine (POPE), 1-palmitoyl-2-oleoyl-*sn*-glycero-3-phosphoserine (POPS), or soy phosphatidylinositol (PtdIns) (all from Avanti Polar Lipids) in the highest grade oxygen-free chloroform to yield 10 mg/ml stock solutions. Store them in Teflon-sealed vials at −20 °C.
2. Phosphoinositides (PtdIns*Ps*): Dissolve 1,2-dipalmitoyl derivatives of PtdIns*Ps* (Cayman Chemical), including phosphatidylinositol-3,4,5-trisphosphate (PtdIns(3,4,5)P_3), in the highest grade oxygen-free chloroform/methanol/water (3:3:1 v/v/v) to yield 0.5 mg/ml solutions. Store them in Teflon-sealed vials at −20 °C.

2.2 Dark Quencher-Containing Lipids (See Note 2)

1. Dabsyl-PE: Dissolve POPE (50 mg) in chloroform (2 ml) and add it to a solution of dabsyl chloride (22.6 mg) and triethylamine (0.2 ml) in chloroform (5 ml). Stir the solution for 6 h at room temperature in the dark and remove the solvent under reduced pressure. Dissolve the residue in dichloromethane/methanol (9:1) and purify it by silica column chromatography

eluted with the same solvent mixture. Evaporate the solvent in vacuo to afford dabsyl-PE as an orange solid. Prepare 10 mg/ml stock solution in chloroform and store it in a Teflon-sealed vial at −20 °C.

2. BHQ1-PE and QSY7-PE: Mix 8 mg of POPE and 5 mg of QSY7 carboxylic acid succinimidyl ester (Life Technologies) or BHQ1 carboxylic acid succinimidyl ester (Biosearch Technologies) in 800 μl of chloroform and 200 μl of triethylamine. Carry out the reaction and purification as described for dabsyl-PE to obtain BHQ1-PE and QSY7-PE. Prepare 10 mg/ml stock solutions in chloroform and store them in Teflon-sealed vials at −20 °C.

2.3 Lipid Vesicles (See Note 3)

1. Large unilamellar vesicles (LUV: 100-nm diameter): Mix the lipid solutions in chloroform according to the final lipid composition (e.g., POPC/dabsyl-PE/PtdIns(3,4,5)P_3 = 92:5:3) (*see* **Note 4**) and evaporate the solvent under the gentle stream of nitrogen gas. Add 20 mM Tris buffer, pH 7.4, containing 0.16 M NaCl to the lipid film to adjust the final lipid concentration, vortex the mixture for 1 min, and sonicate it in a sonicating bath for 1 min to break multilamellar vesicles. Prepare large unilamellar vesicles by multiple extrusion through a 100-nm polycarbonate filter using a Mini-Extruder (Avanti).
2. Small unilamellar vesicles (SUV: 15-nm diameter): Mix the lipid solutions in chloroform according to the final lipid composition and evaporate the solvent under the gentle stream of nitrogen gas. Add 20 mM Tris buffer, pH 7.4, containing 0.16 M NaCl to the lipid film to adjust the final lipid concentration, vortex the mixture for 1 min, and sonicate it using a Branson Sonifier until the solution becomes clear.

2.4 Protein Expression and Purification

1. The pRSETb-EGFP vectors: Subclone the EGFP sequence into the pRSETb vector to express the protein as either a N-terminal or C-terminal EGFP-fusion protein (*see* **Note 1**), and with the N-terminal His_6 tag. Subclone a lipid binding domain/protein into the pRSETb-EGFP vector to prepare a N-terminal or C-terminus EGFP-fusion protein and transform the vector into BL21 RIL cells for protein expression.
2. Lysis buffer: 50 mM Tris–HCl, 300 mM NaCl, 10 mM imidazole, and 10 % (v/v) glycerol, pH 7.9.
3. Ni-NTA agarose column elution buffers: 50 mM Tris buffer-HCl, pH 7.4, containing 20 mM, 40 mM, and 300 mM imidazole, respectively.

2.5 Binding and Inhibition Assays

1. Assay buffer: 20 mM Tris–HCl buffer, pH 7.4, containing 0.16 M NaCl.

2. Protein stock solutions: Dilute the protein solution in the assay buffer to 20–60 μM.
3. Lipid stock solutions: see above.
4. Inhibitor stock solutions: Dissolve inhibitors in dimethylsulfoxide (DMSO) to prepare 5 mM solutions.

3 Methods

3.1 Protein Expression

1. Inoculate 500 ml of Luria broth containing 50 μg/ml kanamycin or 100 μg/ml ampicillin with BL21 RIL colonies expressing each protein construct.
2. Allow cells to grow in the medium at 37 °C until an absorbance at 600 nm reaches 0.6.
3. Induce protein expression with the addition of 100 μM isopropyl 1-thio-β-d-galactopyranoside, and move the cells to a 25 °C shaker for 14 h incubation.
4. Harvest cells by centrifugation (2500 × *g* for 10 min at 4 °C), and resuspend the pellet in 20 ml of the lysis buffer.
5. Sonicate the solution for 5 min with 30 s interval and centrifuge the mixture for 30 min (39,000 × *g* at 4 °C). Transfer the supernatant to a 50-ml Falcon tube and add 1 ml of Ni-NTA agarose (Qiagen) to it.
6. Allow the supernatant to equilibrate with the resin for 30 min at 4 °C with gentle mixing.
7. Pour the supernatant onto a column, and wash the resin with 50 ml of 50 mM Tris buffer, pH 7.4, containing 20 mM imidazole and another 50 ml of 50 mM Tris buffer, pH 7.4, containing 40 mM imidazole. Elute the protein using 50 mM Tris buffer, pH 7.4, with 300 mM imidazole.
8. Check the purity of the eluted protein by sodium-dodecylsulfate gel electrophoresis using 18 % polyacrylamide gel, and determine the concentration using the Bradford reagents. Freeze the protein in liquid nitrogen and store it at –20 °C.

3.2 Plate Reader-Based Quantitative Lipid Specificity Assay (See Note 5)

1. Add a fixed concentration of protein (e.g., 100 nM) to each well of a non-treated black polystyrene 96-well plate (Corning).
2. To each row, add vesicles with varying lipid composition (e.g., POPC/dabsyl-PE/L_1 (95-x:5:x) (L_1 = any signaling lipid such as PtdIns*P*, phosphatidic acid; x = 0–10 mol%)) (*see* **Note 6**). Keep the total lipid concentration constant (e.g., 10 μM) and adjust the final volume of the mixture in the assay buffer to 200 μl.
3. Fill other rows with different lipid mixtures (e.g., POPC/dabsyl-PE/L_2 (95-x:5:x), POPC/dabsyl-PE/L_3 (95-x:5:x)) (*see* **Note 6**).

4. Select one row for background correction for nonspecific binding and quenching with the same protein and POPC/dabsyl-PE (95:5) vesicles.
5. Incubate the plate at 25 °C with extremely gentle shaking for 5 min.
6. Monitor the decrease in EGFP fluorescence intensity at 509 nm with excitation set at 488 nm using a fluorescence plate reader.

3.3 Plate Reader-Based Membrane Binding Affinity Assay (See Note 7)

1. To each well of a given row of a 96-well plate add a fixed concentration of protein (e.g., 100 nM) and an increasing concentration of lipid vesicles with fixed composition (e.g., 0–150 μM of POPC/PtdIns(3,4,5)P_3/dabsyl-PE (92:3:5) vesicles). Adjust the final volume of the assay mixture to 200 μl.
2. Fill multiple (i.e., ≥ triplicate) rows with the same protein and lipid mixtures for multiplex determination.
3. Select one row for background correction for nonspecific binding and quenching with the same protein and dabsyl-PE vesicles (e.g., POPC/dabsyl-PE (95:5) vesicles).
4. Incubate the plate at 25 °C with extremely gentle shaking for 5 min.
5. Monitor the decrease in EGFP fluorescence intensity at 509 nm with excitation set at 488 nm using a fluorescence plate reader.

3.4 Spectrofl uorometric Membrane Binding Affinity Assay (See Note 8)

1. Add 10–20 μl of the protein stock solution to 2 ml of the assay buffer equilibrated at 25 °C to the final concentration (typically 100 nM) depending on the K_d value for the protein and the particular vesicles (e.g., POPC/PtdIns(3,4,5)P_3/dabsyl-PE (92:3:5) vesicles). Transfer the protein solution to a 3-ml quartz cuvette in a thermostated (25 °C) spectrofluorometer.
2. Monitor the equilibrated value of EGFP fluorescence emission intensity at 509 nm with excitation set at 488 nm after 5 μl incremental addition of the lipid vesicle solution.
3. Continue lipid addition until binding reaches saturation.
4. Repeat the same experiment with dabsyl-PE vesicles (e.g., POPC/dabsyl-PE (95:5) vesicles) for background correction for nonspecific binding and quenching.

3.5 High-Throughput Screening of Membrane Binding Inhibitors

1. Add fixed concentrations of a protein and a lipid vesicle in 200 μl of the assay buffer to each well of the plate. Typically, the protein concentration is 100 nM and the lipid vesicle concentration is adjusted to give ≈80 % of maximal FP quenching.
2. Add a fixed concentration of different inhibitors to each well. Minimize the volume of DMSO (i.e., ≤2 % v/v) to avoid protein denaturation. The inhibitor concentration is typically set

at 20 μM for initial screening and is gradually lowered for the following rounds of screening to increase the detection threshold.

3. For background correction for each row, run the assay without lipid vesicles in the mixture in the next row.
4. Incubate the plate at 25 °C with extremely gentle shaking for 10 min.
5. Monitor the increase in EGFP fluorescence intensity at 509 nm with excitation set at 488 nm.

3.6 Determination of Inhibition Parameters

1. Add fixed concentrations of a protein and a lipid vesicle in 200 μl of the assay buffer to each well of the plate. Typically, the protein concentration is 100 nM and the lipid vesicle concentration is adjusted to give ≈80 % of maximal FP quenching.
2. Add an increasing concentration of an inhibitor to each well of a given row. Keep the total volume of DMSO (i.e., ≤2 % v/v) constant for all wells.
3. Incubate the plate at 25 °C with extremely gentle shaking for 10 min.
4. Monitor the increase in EGFP fluorescence emission intensity of each well at 509 nm with excitation set at 488 nm.
5. For background correction for each row, run the assay without lipid vesicles in the mixture in the next row.

3.7 Specificity Data Analysis

1. Subtract the background fluorescence values from binding data.
2. Analyze resulting membrane binding data of proteins using the equation: $\Delta F/\Delta F_{max} = 1/(1 + [L]_{\%}/K)$. ΔF and ΔF_{max} indicate the fluorescence quenching and the maximal quenching, respectively, and $[L]_{\%}$ and K are mole% of a particular lipid and the $[L]_{\%}$ value causing half-maximal quenching, respectively.

3.8 Binding Data Analysis

1. Subtract the background fluorescence values from binding data.
2. Analyze resulting membrane binding isotherms of proteins assuming each protein binds independently to a site on the vesicle surface composed of n lipids with dissociation constant K_d [12] (*see* **Note 9**).
3. Determine values of n and K_d by nonlinear least-squares analysis of the $[P]_b/[P]_o$ vs. $[L]_o$ plot using equation 1 [12]:

$$\Delta F / \Delta F_{max} = [P]_b / [P]_0 = \frac{[P]_o + K_d + [L]_o / n - \sqrt{\left([P]_o + K_d + [L]_o / n\right)^2 - 4[P]_o[L]_o / n}}{2[P]_o} \quad (1)$$

where $[L]_o$, $[P]_o$ and $[P]_b$ are total lipid, total protein and bound protein concentrations, respectively and ΔF and ΔF_{max} indicate the fluorescence quenching and the maximal quenching, respectively.

3.9 Inhibition Data Analysis

1. Subtract the background fluorescence values from inhibition data.
2. Analyze inhibition of membrane binding of a protein by an inhibitor using an equation: $\Delta F = \Delta F_0/(1+[I]/K_i)$ [25]. ΔF and ΔF_0 indicate the fluorescence intensity decrease of EGFP by dabsyl-PE-containing vesicles in the presence and the absence of a given concentration of inhibitor, respectively. [I] and K_i are the free inhibitor concentration and the inhibition constant.

4 Notes

1. For most proteins, N-terminal and C-terminal EGFP tags have essentially the same effect: i.e., they improved the protein expression yield without affecting membrane binding properties of the fused proteins. Depending on the structure of the protein, the location of the N- and C-termini in particular, the efficiency of EGFP quenching by quenching lipids can vary significantly. The location of the EGFP tag and the sequence and length of the linker between EGFP and the tagged protein should thus be adjusted to maximize the EGFP quenching efficiency.
2. Dabsyl-PE is a preferred quenching lipid for routine use because it is easy and inexpensive to prepare in large quantities. Because its absorption spectrum significantly overlaps with the excitation spectrum of EGFP, however, it is not ideal for the assay employing EGFP-fusion proteins. That is, excitation of EGFP at 488 nm also significantly excites the dabsyl group, limiting its capacity to quench EGFP emission. For high quenching efficiency and assay sensitivity, one can substitute BHQ1-PE or QSY7-PE for dabsyl-PE as a quenching lipid. BHQ1-PE (absorption maximum at $\approx$550 nm) has a lower degree of spectral overlap with EGFP and typical fluorescent small molecules ($\lambda_{ex} < 500$ nm). The EFGP quenching can be measured with $\lambda_{ex} = 488$ nm and $\lambda_{em} = 515$ nm. BHQ1-PE typically allows >50 % improvement over dabsyl-PE in EGFP quenching efficiency. QSY7-PE (absorption maximum at $\approx$570 nm) is better suited for YFP ($\lambda_{ex} = 514$ nm; $\lambda_{em} = 527$ nm) and YFP quenching can be measured with $\lambda_{ex} = 510$ nm and $\lambda_{em} = 540$ nm. Despite their superior spectral properties, how-

ever, general use of BHQ1-PE and QSY7-PE is limited because they are expensive to prepare in large quantities.

3. LUVs are more uniform and stable than SUVs and they are thus more suitable for accurate binding measurements. The uniformity of vesicles is also important for quenching efficiency because the presence of vesicles devoid of quenching lipids would lower the overall quenching efficiency by sequestering EGFP-tagged proteins. However, it takes much longer to prepare LUVs through extrusion, which becomes a major limiting factor for high-throughput screening that requires a large amount of vesicles. It is therefore recommended to use SUVs for high-throughput screening. Due to their instability, SUVs should be used within a few hours of preparation.
4. The lipid composition of vesicles and the mole% of a quenching lipid can be adjusted according to the purpose of the assay. All quenching lipids are anionic lipids and might nonspecifically increase the vesicle binding of proteins with cationic membrane binding surfaces. For accurate determination of membrane binding affinity (or specificity) of a protein under physiologically relevant conditions, the concentration of a quenching lipid must be thus kept as low as possible (i.e., just high enough to allow robust quenching). Typically, 40 % of FP quenching is sufficient for accurate and reproducible binding analysis. For initial assessment of membrane binding affinity of a large number of proteins and high-throughput screening of small molecule, one can increase the concentration of the quenching lipid to maximize the FP quenching efficiency. For all cases, background correction with lipid vesicles containing primarily the quenching lipid is recommended. For example, for PtdIns(3,4,5)P_3-binding proteins that are assayed with POPC/dabsyl-PE/PtdIns(3,4,5)P_3 (92:5:3) vesicles, background correction with POPC/dabsyl-PE (95:5) is appropriate. Here POPC is used as a bulk lipid because most proteins do not bind PC.
5. The lipid specificity (such as phosphoinositide specificity) can be determined by simply comparing the quenching efficiency in the same column (i.e., at the same mole% of L_1, L_2, L_3, etc.). More preferably, the lipid specificity is determined by comparing the lipid mole% values giving rise to half-maximal quenching. This is a much more accurate and quantitative way to determine the lipid specificity than other commonly used assays, such as lipid overlay assay and vesicle pelleting assay. Also, our assay allows for determination of lipid acyl chain specificity as well as headgroup specificity.
6. Many membrane-binding proteins interact with both bulk lipids and a signaling lipid coincidently [2]. For example, most of

pleckstrin homology (PH) domains bind multiple anionic lipid molecules, most notably phosphatidylserine (PS), and a PtdIns*P* molecule [26–29]. For accurate, physiological relevant determination of lipid specificity, a two-step assay is thus recommended: (1) First with POPC/dabsyl-PE/L_1 (95-*x*:5:*x*) (L_1 = PS, PtdIns, cholesterol, etc.; *x* = 0–30 mol%) vesicles to detect any requirement for a bulk lipid and (2) with POPC/dabsyl-PE/L_1/L_2 (75-*x*:5:20:*x*) (L_2 = PtdIns*P*, phosphatidic acid, ceramide, diacylglycerol etc.; *x* = 0–10 mol%; 20 mol% is an arbitrary concentration for a bulk lipid) vesicles to determine signaling lipid specificity. This assay is preferred to a single-step assay employing e.g., POPC/dabsyl-PE/*L* (70:5:25) (*L* = all lipids) because it is not physiologically meaningful to directly compare bulk lipids, such as PS, with signaling lipids, such as PtdIns(3,4,5)P_3, which exist in such different concentrations in cell membranes.

7. Once lipid specificity of a protein is known, its affinity for the favorite lipid vesicles, such as POPC/POPS/PtdIns(3,4,5)P_3/dabsyl-PE (72:20:3:5), is determined by varying the total concentration of the same lipid vesicles with a fixed concentration of the protein. An alternative way is to employ the fixed total concentration of lipid vesicles and varying concentrations of the protein. This approach is useful when the nonspecific quenching becomes significant because of low quenching efficiency of specific binding. In this case, a control row containing only varying concentrations of the protein will be used to calculate the degree of quenching and the equation 1 will be used for curve fitting with $[P]_o$ as a variable.
8. The cuvette-based spectrofluorometric assay is recommended when accurate and robust quantification of membrane affinity of proteins is required for biophysical analysis (e.g., binding energy calculation).
9. In this binding formalism, nK_d instead of K_d corresponds to the lipid or protein concentration that causes half-maximal binding. Alternatively, the binding isotherms can be analyzed by a simple 1:1 Langmuir-type binding equation (i.e., substituting $[L]_o$ for $[L]_o/n$ in equation 1) or assuming partition of a protein between the bulk and the membrane [30].

Acknowledgements

The work is supported by national Institutes of Health grants GM68849 and GM110128. We thank Prof. Daesung Lee for assisting in dark quencher lipid synthesis and Charles Delisle for preliminary work on high-throughput screening.

References

1. DiNitto JP, Cronin TC, Lambright DG (2003) Membrane recognition and targeting by lipid-binding domains. Sci STKE 2003:re16
2. Cho W, Stahelin RV (2005) Membrane-protein interactions in cell signaling and membrane trafficking. Annu Rev Biophys Biomol Struct 34:119–151
3. Cho W (2006) Building signaling complexes at the membrane. Sci STKE 2006:pe7
4. Lemmon MA (2008) Membrane recognition by phospholipid-binding domains. Nat Rev Mol Cell Biol 9:99–111
5. Bhardwaj N, Stahelin RV, Langlois RE, Cho W, Lu H (2006) Structural bioinformatics prediction of membrane-binding proteins. J Mol Biol 359:486–495
6. Silkov A, Yoon Y, Lee H, Gokhale N, Adu-Gyamfi E, Stahelin RV, Cho W, Murray D (2011) Genome-wide structural analysis reveals novel membrane binding properties of AP180 N-terminal homology (ANTH) domains. J Biol Chem 286:34155–34163
7. Zimmermann P (1761) The prevalence and significance of PDZ domain-phosphoinositide interactions. Biochim Biophys Acta 2006: 947–956
8. Feng W, Zhang M (2009) Organization and dynamics of PDZ-domain-related supramodules in the postsynaptic density. Nat Rev Neurosci 10:87–99
9. Chen Y, Sheng R, Kallberg M, Silkov A, Tun MP, Bhardwaj N, Kurilova S, Hall RA, Honig B, Lu H, Cho W (2012) Genome-wide functional annotation of dual-specificity protein- and lipid-binding modules that regulate protein interactions. Mol Cell 46:226–237
10. Sheng R, Chen Y, Yung Gee H, Stec E, Melowic HR, Blatner NR, Tun MP, Kim Y, Kallberg M, Fujiwara TK, Hye Hong J, Pyo Kim K, Lu H, Kusumi A, Goo Lee M, Cho W (2012) Cholesterol modulates cell signaling and protein networking by specifically interacting with PDZ domain-containing scaffold proteins. Nat Commun 3:1249
11. Sheng R, Kim H, Lee H, Xin Y, Chen Y, Tian W, Cui Y, Choi JC, Doh J, Han JK, Cho W (2014) Cholesterol selectively activates canonical Wnt signalling over non-canonical Wnt signalling. Nat Commun 5:4393
12. Cho W, Bittova L, Stahelin RV (2001) Membrane binding assays for peripheral proteins. Anal Biochem 296:153–161
13. Narayan K, Lemmon MA (2006) Determining selectivity of phosphoinositide-binding domains. Methods 39:122–133
14. Dowler S, Kular G, Alessi DR (2002) Protein lipid overlay assay. Sci STKE 2002:pl6
15. Rebecchi M, Peterson A, McLaughlin S (1992) Phosphoinositide-specific phospholipase C-delta 1 binds with high affinity to phospholipid vesicles containing phosphatidylinositol 4,5-bisphosphate. Biochemistry 31:12742–12747
16. Kraft CA, Garrido JL, Leiva-Vega L, Romero G (2009) Quantitative analysis of protein-lipid interactions using tryptophan fluorescence. Sci Signal 2:p14
17. Dua R, Wu SK, Cho W (1995) A structure-function study of bovine pancreatic phospholipase A2 using polymerized mixed liposomes. J Biol Chem 270:263–268
18. Bazzi MD, Nelsestuen GL (1987) Association of protein kinase C with phospholipid vesicles. Biochemistry 26:115–122
19. Nalefski EA, Slazas MM, Falke JJ (1997) Ca^{2+}-signaling cycle of a membrane-docking C2 domain. Biochemistry 36:12011–12018
20. Sumandea M, Das S, Sumandea C, Cho W (1999) Roles of aromatic residues in high interfacial activity of Naja naja atra phospholipase A2. Biochemistry 38:16290–16297
21. Yoon Y, Lee PJ, Kurilova S, Cho W (2011) In situ quantitative imaging of cellular lipids using molecular sensors. Nat Chem 3:868–874
22. Miao B, Skidan I, Yang J, Lugovskoy A, Reibarkh M, Long K, Brazell T, Durugkar KA, Maki J, Ramana CV, Schaffhausen B, Wagner G, Torchilin V, Yuan J, Degterev A (2010) Small molecule inhibition of phosphatidylinositol-3,4,5-triphosphate (PIP3) binding to pleckstrin homology domains. Proc Natl Acad Sci U S A 107:20126–20131
23. Rusu L, Gambhir A, McLaughlin S, Radler J (2004) Fluorescence correlation spectroscopy studies of Peptide and protein binding to phospholipid vesicles. Biophys J 87:1044–1053
24. Kim H, Afsari HS, Cho W (2013) High-throughput fluorescence assay for quantifying membrane-protein interaction and screening inhibitors for membrane-protein interaction. J Lipid Res 54:3531–3538
25. Dua R, Cho W (1994) Inhibition of human secretory class II phospholipase A2 by heparin. Eur J Biochem 221:481–490
26. Lucas N, Cho W (2011) Phosphatidylserine binding is essential for plasma membrane recruitment and signaling function of 3-phosphoinositide-dependent kinase-1. J Biol Chem 286:41265–41272

27. Stahelin RV, Long F, Peter BJ, Murray D, De Camilli P, McMahon HT, Cho W (2003) Contrasting membrane interaction mechanisms of AP180 N-terminal homology (ANTH) and epsin N-terminal homology (ENTH) domains. J Biol Chem 278:28993–28999
28. Manna D, Albanese A, Park WS, Cho W (2007) Mechanistic basis of differential cellular responses of phosphatidylinositol 3,4-bisphosphate- and phosphatidylinositol 3,4,5-trisphosphate-binding pleckstrin homology domains. J Biol Chem 282: 32093–32105
29. Manna D, Bhardwaj N, Vora MS, Stahelin RV, Lu H, Cho W (2008) Differential roles of phosphatidylserine, PtdIns(4,5)P2, and PtdIns(3,4,5)P3 in plasma membrane targeting of C2 domains. Molecular dynamics simulation, membrane binding, and cell translocation studies of the PKCalpha C2 domain. J Biol Chem 283:26047–26058
30. White SH, Wimley WC, Ladokhin AS, Hristova K (1998) Protein folding in membranes: determining energetics of peptide-bilayer interactions. Methods Enzymol 295:62–87

Chapter 15

Guidelines for the Use of Protein Domains in Acidic Phospholipid Imaging

Matthieu Pierre Platre and Yvon Jaillais

Abstract

Acidic phospholipids are minor membrane lipids but critically important for signaling events. The main acidic phospholipids are phosphatidylinositol phosphates (PIPs also known as phosphoinositides), phosphatidylserine (PS), and phosphatidic acid (PA). Acidic phospholipids are precursors of second messengers of key signaling cascades or are second messengers themselves. They regulate the localization and activation of many proteins, and are involved in virtually all membrane trafficking events. As such, it is crucial to understand the subcellular localization and dynamics of each of these lipids within the cell. Over the years, several techniques have emerged in either fixed or live cells to analyze the subcellular localization and dynamics of acidic phospholipids. In this chapter, we review one of them: the use of genetically encoded biosensors that are based on the expression of specific lipid binding domains (LBDs) fused to fluorescent proteins. We discuss how to design such sensors, including the criteria for selecting the lipid binding domains of interest and to validate them. We also emphasize the care that must be taken during data analysis as well as the main limitations and advantages of this approach.

Key words Biosensor, Phosphatidylinositol phosphate, Phosphatidic acid, Phosphatidylserine, Genetically encoded probes, Lipid binding domain, Live imaging, PtdIns, Lipid signaling, Phospholipase

1 Introduction

Anionic phospholipids have a negatively charged head group, which gives them specific properties, notably in terms of protein–lipid interactions. The main acidic phospholipids are phosphatidylserine (PS), phosphatidic acid (PA), and phosphatidylinositol (PI and PIPs). In erythrocytes, the PS/PA/PI proportions (by weight) are approximately 8.5 %, 1.5 %, and 1.0 %, respectively, but these may vary according to species or cell types [1].

Phosphatidylinositolphosphates (PIPs) are minor phospholipids, accounting less than 1 % of total membrane lipids, yet they are of disproportionate importance for many membrane-associated signaling events: (1) PIPs can be precursors of various second messengers (e.g., Inositol-3-Phosphate, Diacylglycerol), (2) they

Mark G. Waugh (ed.), *Lipid Signaling Protocols*, Methods in Molecular Biology, vol. 1376,
DOI 10.1007/978-1-4939-3170-5_15,

can activate many ion channels and enzymes, (3) they are involved in membrane trafficking and, (4) they can recruit proteins to the plasma membrane or intracellular compartments through several structured interaction domains (e.g., Pleckstrin Homology domain (PH), Phox homology domain (PX), Fab1/YOTB/Vac1/EEA1 domain (FYVE)) [1–4]. PIPs can be phosphorylated at different positions of the inositol head group, which can generate up to seven different PIP species that include three phosphatidylinositol monophosphates [PI3P, PI4P, and PI5P], three phosphatidylinositol biphosphate [$PI(3,4)P_2$, $PI(3,5)P_2$, and $PI(4,5)P_2$] and one phosphatidylinositol triphosphate [$PI(3,4,5)P_3$]. PIP kinases and phosphatases modify the phosphorylation state of the inositol head group, and phospholipases hydrolyze PIPs to release the soluble head group into the cytosol [1, 4]. The combined action of these enzymes produces the PIP signature of a cell, where certain membrane compartments are enriched or depleted of specific PIPs, contributing to their functional identity [1, 3, 4].

Phosphatidylserine (PS) is an important constituent of eukaryotic membranes and the most abundant acidic phospholipid (up to 10 % of biological membrane) [1, 5–7]. PS is involved in many signaling pathways, as it can recruit and/or activate proteins, notably through their stereospecific PS-binding domain and by regulating membrane surface charges [1, 5, 6, 8]. One particularity of PS is its role as a lipid landmark in both extracellular and intracellular membranes leaflets. For instance, extracellular PS (exposed on the outer leaflet of the plasma membrane) serves as an "eat me" signal for the clearance of apoptotic cells [7, 9]. Intracellular PS regulates a number of signaling pathways involving kinases, small GTPases, and fusogenic proteins [5, 8].

Phosphatidic acid (PA) is a precursor for the biosynthesis of many lipids [10, 11]. Indeed, various enzymes add different chemical group on PA, such as Choline, Ethanolamine, Serine or Inositol to produce phosphatidylcholine (PC), phosphatidylethanolamine (PE), phosphatidylserine (PS) and phosphatidylinositol (PI). PA is also the substrate of Phospholipase D, which produces diacylglycerol, a second messenger involved in many signaling pathways [12]. Furthermore, the biophysical characteristics of PA influence membrane properties such as membrane curvature or membrane fusion [1, 13, 14]. In addition, PA itself recruits various proteins to membranes and PA-protein interaction activates many enzymes. As such, PA can be considered a *bona fide* lipid second messenger.

2 Subcellular Localization of Anionic Phospholipids at a Glance

The localization of the various acidic phospholipid species has been an intense area of research [4, 15, 16]. Functional studies, together with biochemical and live-cell imaging, have built a

relatively clear picture of the precise location of most acidic phospholipids in yeast (Fig. 1a), cultured mammalian cell lines (Fig. 1b), and plants (Fig. 1c).

In animal cells, PI3P mainly resides in early endosomes, where it controls endosome maturation, cargo protein degradation/recycling and cell signaling notably through its interplay with Rab5 GTPases [3] (Fig. 1b). During autophagy induction in animal (e.g., triggered by amino acid starvation), PI3P is transiently produced at the Endoplasmic Reticulum (ER) membrane by the PI3-kinase VPS34 [17] (Fig. 1b). PI3P production in the ER supports the formation of the omegasome a specialized ER domain at the origin of the formation of the autophagophore (also known as the isolation membrane), that itself elongates to form the autophagosome (i.e., double membrane vesicles) [17, 18].

In yeast and animals, PI4P is located in at least two different pools in the cell, one at the Golgi apparatus and the other one at the plasma membrane [19–21] (Fig. 1a, b). Each pool of PI4P has separate and diverse functions. The main function of PI4P at the Golgi is to control membrane trafficking events, in particular, the sorting of proteins toward the plasma membrane or endosomes [3, 22–24]. PI4P, together with other PIPs, recruits strong cationic proteins to the plasma membrane [25]. In yeast, the plasma membrane pool of PI4P controls ER-to-plasma membrane tethering sites that regulate cell signaling and ER morphology [26–28] (Fig. 1a). Furthermore, plasma membrane-localized PI4P is a source of $PI(4,5)P_2$ in animal cells [23, 29]. A pool of PI4P has been recently described in late endosomes/lysosomes in animal cells but the function of PI4P in these compartments remains to be fully elucidated [20] (Fig. 1b).

In mammals, the rare phosphoinositide, PI5P, accumulates in the nucleus and at the plasma membrane under certain stimuli, or during infection by certain pathogens such as the bacterium *Shigella flexneri* [30–34] (Fig. 1b). Furthermore, it has been recently showed that PI5P transiently accumulates at the ER during autophagy induction and can substitute PI3P at the omegasome [35] (Fig. 1b).

In both animal and yeast, $PI(3,5)P_2$ is thought to reside in late endosomes, where it regulates lysosome/vacuole biogenesis [36–38] (Fig. 1a, b). In every eukaryotes, $PI(4,5)P_2$ is localized at the plasma membrane where it has a large spectra of action such as anchoring signaling and membrane trafficking proteins [2, 4, 25, 39–41] (Fig. 1a–c). In addition, $PI(4,5)P_2$ controls ion channel activation and is a substrate of Phospholipase C, which triggers synthesis of the second messengers inositol 1,4,5-trisphosphate and diacylglycerol [2, 4, 42]. $PI(4,5)P_2$ is the source of $PI(3,4,5)P_3$, which together with $PI(3,4)P_2$, accumulate at the plasma membrane but only when specific signaling pathways are activated (e.g., growth factor signaling) [2, 4] (Fig. 1b). $PI(3,4)P_2$ also controls

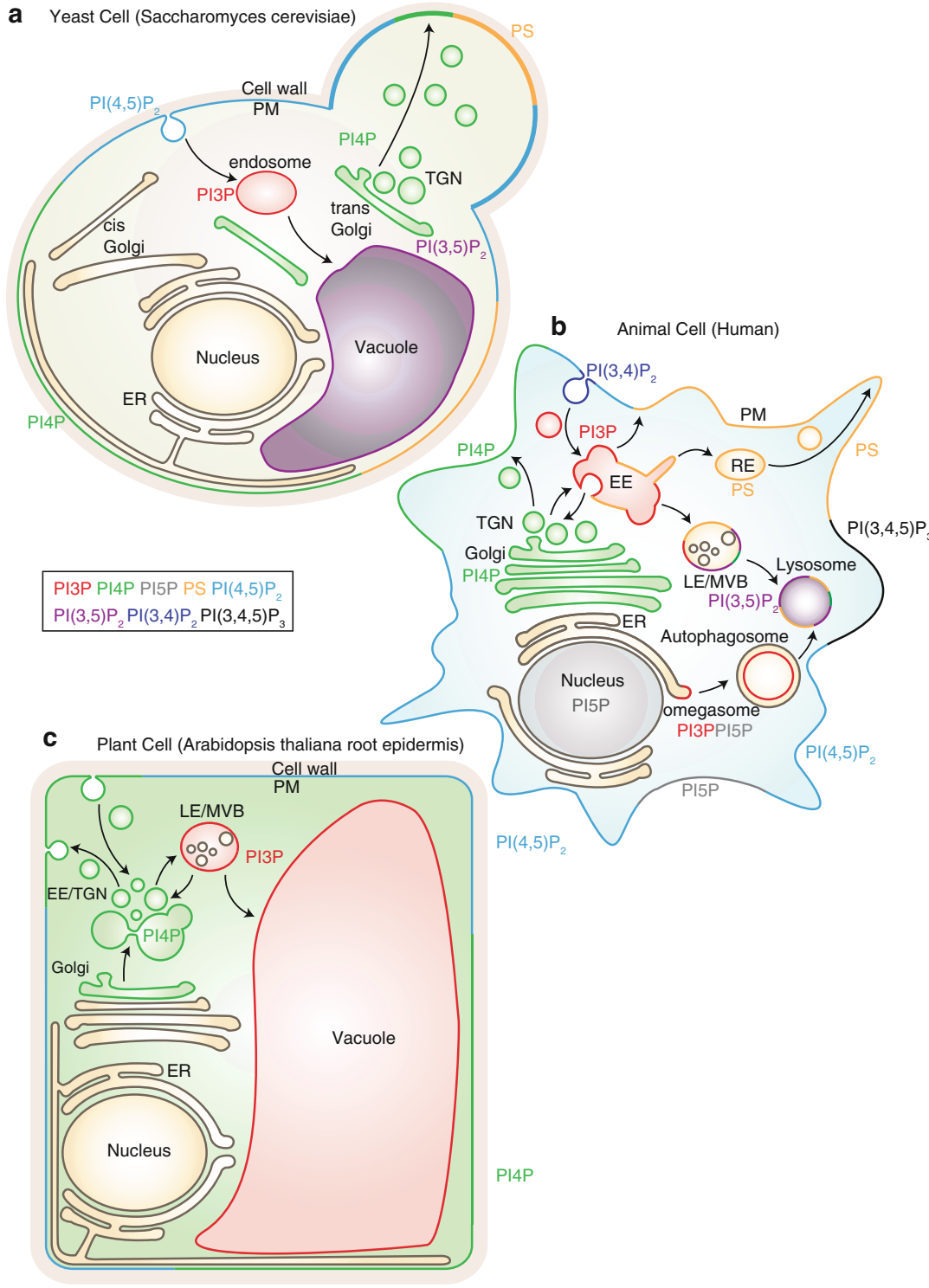

Fig. 1 Summary of the subcellular localization of anionic phospholipids in yeast (**a**), animal (**b**), and plant (**c**) cells. Note that the reported localization are not exhaustive and might vary depending on cell types or signaling activities. The cartoon representing the cell in panel (**b**) is adapted from Jean and Kiger 2012

late-stage clathrin-coated pit formation, independent of PI(3,4,5)P_3 [41, 43].

PS is synthesized in the ER lumen and reaches the cytosolic leaflet through the action of P4-ATPases flippases [7, 9]. Depending on the species, this translocation occurs either at the *trans*-Golgi Network (TGN) and/or at the plasma membrane. This asymmetric PS distribution can be used as a signaling device by the regulated activation of scramblases, which rapidly exposes PS on the extracellular leaflet of the plasma membrane and plays important roles in blood clotting and apoptosis [7, 16], as abovementioned. On the cytosolic leaflet, PS mainly accumulates at the plasma membrane in yeast (Fig. 1a), while it is present both at the plasma membrane and throughout the endosomal system in animal cells (Fig. 1b) [5, 8, 44].

Like PS, PA is synthetized in the ER in all eukaryotic cells [10, 11]. PA can also be synthesized de novo in other organelles such as for example mitochondria or chloroplasts [10]. However, the main pool of PA that is facing the cytosol is likely localized at the plasma membrane. This pool is locally produced by Phospholipase D and Diacylglycerol kinases [12].

3 Detection of Acidic Phospholipidsby Lipid Binding Domains

Anionic lipids such as phosphoinositides are markers of organelle identity. Moreover, because they act as second messengers, their quantity varies rapidly (i.e., within minutes) upon stimulation of various signaling pathways. It is therefore key to be able to track the amount of these lipids in real time and at subcellular resolution. However, the investigation of lipid subcellular localization has proven to be difficult for various reasons. First, it is obviously not possible to label lipids by direct tagging with fluorescent proteins (FPs). Second, common methods of cell or tissue fixation do not fix lipids and are therefore not compatible with the study of lipid subcellular localization. Yet many techniques have been used over the years to uncover the subcellular localization of acidic phospholipids and their respective dynamics upon various stimulations. These techniques were used either in fixed cells, such as for example immuno-labeling with anti-PIP antibodies [19] or live cells, such as for example direct labeling of lipid molecules or the use of genetically encoded biosensors [45]. The later method has been extensively used to indirectly reveal the localization and dynamics of PIPs in intact living cells and, currently, is probably the most widespread technique used to localize acidic phospholipid species [4, 40, 45]. Importantly, this method is directly amenable to live imaging techniques. Genetically encoded biosensors consist of lipid-binding domains (LBDs) that interact specifically with known lipid species in vitro (Fig. 2a, b). These domains

localize in the cell compartments that accumulate the targeted PIPs and can be easily traced when fused with a fluorescent protein (Fig. 2a, b). LBDs are globular domains that mostly bind to acidic phospholipids such as PIPs and PS [1, 46]. Broadly, they fall into two categories: nonspecific LBDs and stereospecific LBDs. Nonspecific LBDs recognize general membrane properties, such as curvature, lipid packing defects, or charges [1, 14]. Examples of nonspecific LBDs include the BAR domain that recognizes membranes with a specific curvature or the KA1 domain that binds highly electronegative membrane [1, 47]. Stereospecific LBDs bind particular acidic lipids with sometime exquisite specificity. PH, PX, FYVE, and some C2 domains belong to this category [1, 46]. To date most LBDs that have been used to report on lipid localization are stereospecific LBDs, yet in recent years nonspecific LBDs have also been exploited to probe some basic properties of the cytosolic leaflet of membrane compartments. For example, the KA1 domain has been used as a reporter of membrane surface charges in human cells [25].

4 Design of Genetically Encoded Acidic Phospholipid Probes

4.1 Construct Strategy

To visualize a certain lipid species, the strategy is to fuse the LBD of interest with a fluorescent protein (FP) (Fig. 2a). Most LBDs can be fused either to their N-terminal or C-terminal end without affecting their binding properties since they are derived from multidomain proteins. To maximize the chances to obtain a stable and functional fusion protein, we usually place the LBD where it would be in its original protein context and separates it from the fluorescent protein by a short flexible linker (e.g., SAGGSAGG or GAGARS linkers). For example the PX domain of the $p40^{phox}$ protein is localized at its N-terminus. We therefore replaced the C-terminal part of this protein with fluorescent proteins, giving PX^{p40}-FP constructs (Fig. 2a). A fluorescent protein is usually sufficient to report each lipid, however methods based on Förster Resonance Energy Transfert (FRET) have also been used [48–51] (Fig. 2c).

Most genetically encoded lipid sensors are soluble proteins and therefore are designed to report only the lipid species that are facing the cytosol. However, addition of a signal peptide to the probe has been generated to secrete the LBD and to follow the accumulation of its cognate lipid along the secretory pathway, such as for example its presence in the ER lumen [9]. However, because of the resolution limits of conventional light microscope, this approach requires Transmission Electron Microscopy (TEM) to distinguish between membrane-bound LBDs and soluble LBDs in the organelle's lumen.

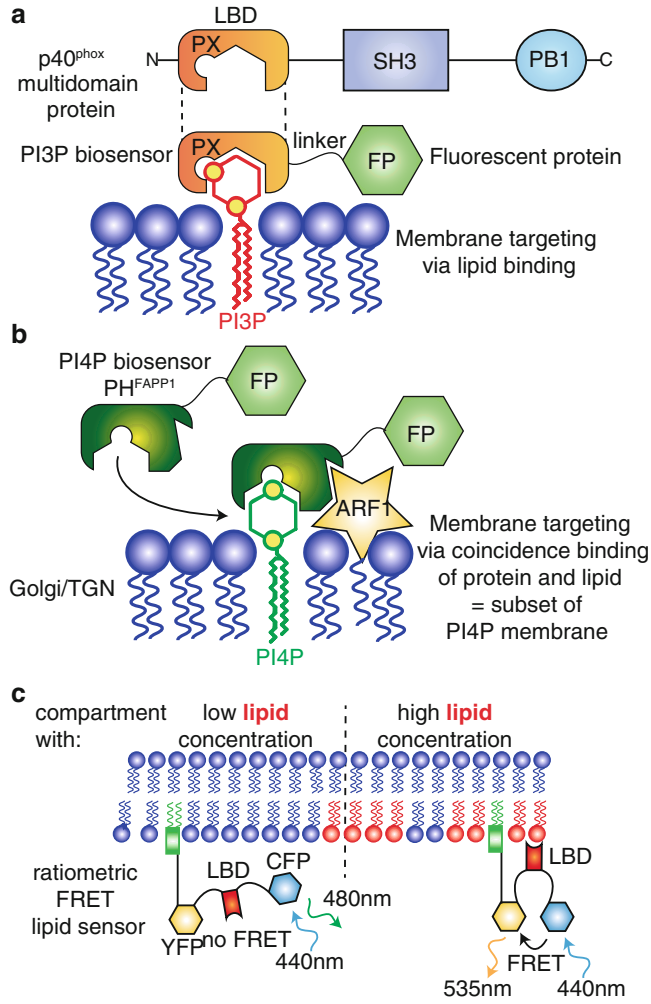

Fig. 2 General principle of genetically encoded lipid biosensors. (**a**) A lipid-binding domain (LBD) from a multidomain protein ($p40^{phox}$ in this example) is fused with a fluorescent protein (FP). This protein fusion acts as a biosensor for PI3P. (**b**) Some LBDs require binding to both a lipid and another molecules (i.e., Ca^{2+}, proteins). This coincidence binding specifies the localization of the corresponding biosensor to a subset of the lipid-enriched membrane, which also contains the target protein. In this example, the PH domain of FAPP1 binds PI4P and ARF1, thereby restricting its localization to the Golgi/TGN. (**c**) Ratiometric FRET sensors are targeted to membranes independently of lipid binding (e.g., via a lipid anchor or a transmembrane segment) and report on the presence of the lipid based on the conformational changes induced in the sensor when the LBD binds its lipid (which increases or decreases the proximity between the two FPs and therefore their FRET ratio)

4.2 Choosing the Appropriate LBD, Consideration on LBD Specificity

The most critical aspect in the design a genetically encoded sensor for a given lipid is to take into account binding specificity and affinity of the LBDs. If one wants to report the localization of a given lipid, the ideal probe should be highly specific for this lipid. However, very few, if any, LBDs are completely specific for only one lipid. Most of the time, their affinity is greater for a lipid than for the others, yet this is enough to confer a specificity of recognition in vivo. Nonetheless, this should be verified, if possible by several in vitro lipid-binding assays. Such assays include qualitative methods (e.g., lipid–protein overlay assays) and more quantitative techniques such as liposome-binding assays, surface plasmon resonance, or isothermal titration calorimetry. Finally, the structure of the LBD-lipid complex (e.g., by X-ray crystallography or NMR spectroscopy) might help to rationalize how the domain specifically recognizes a particular phospholipid headgroup [1].

Moreover, it is common that LBDs require the coincidence detection of a given lipid together with another molecule to promote membrane binding. The most widespread examples are LBDs that bind their target lipid in a calcium-dependent manner (e.g., most C2 domain binds their lipids, mostly PS, only in the presence of Ca^{2+}) [1]. Some LBDs also require the coincidence binding of another protein [1] (Fig. 2b). For example, the PH domain of FAPP1 (and to a lesser extend the PH domain of OSBP) interacts with PI4P preferentially in the presence of the small GTPase ARF1 [21] (Fig. 2b). This requirement for coincidence binding can lead to confounding results that are sometime difficult to evaluate. For example, the PH domain of FAPP1 is capable of binding PI4P alone, but in vivo membrane binding is enhanced by the presence of ARF1 [21]. Because ARF1 mainly localizes at the Golgi and TGN, two compartments that are enriched in PI4P, the PH domain of FAPP1 (and OSBP) preferentially localizes to these two compartments, although PI4P is also present at the plasma membrane [21] (Fig. 1). This particular result led to the long-lasting belief that PI4P is mainly localized at the Golgi and TGN. Therefore, the PH domains of FAPP1 and OSBP are not optimum to report PI4P in all membranes. However, because PI4P association is required for membrane binding of these LBDs, they are suitable PI4P reporters in the Golgi and TGN and have been successfully used to this aim [52] (Fig. 2b). When available, the use of probes that do not require coincidence binding with other molecules should be favored. Alternatively, if such LBD has not been characterized yet, the use of LBD requiring coincidence binding should not be discarded entirely, but the results should be interpreted accordingly.

4.3 Choosing the Appropriate LBD, Consideration on LBD Affinity

The second parameter that one should take into account is the relative binding affinity of the LBD for its target lipid. This is also an important parameter, since difference in relative affinity might result in different subcellular localization of the probe. The first

obvious caveat is when the binding affinity is too weak, which leads to mostly or exclusively soluble localization of the probe (their localization by default, in the absence of binding, being soluble in the cytosol). For example, a single PI3P-binding FYVE domain is soluble when express in mammalian cells and only a tandem dimer construct (2×FYVE domain) is localized to early endosomes, where PI3P accumulates [53]. This leads to the second caveat, which is when binding affinities are too high and high-affinity LBDs might outcompete the lipid binding of endogenous proteins, leading to toxicity upon expression of the probe. However, because any given cell expresses hundreds of proteins harboring LBDs at the same time, it is unlikely that transgenic expression of LBDs will outcompete all the other lipid-binding proteins. It is however common that expression of acidic phospholipid probes affects some signaling pathways. It is therefore advisable to test the toxicity due to the expression of the probe and to favor cells or transgenic organisms with relatively weak expression of the probe (for example by using promoters that confer mild expression).

One should choose LBDs that have affinity ranging in between the two extreme scenarios discussed above. Because there is no way to predict in silico how a LBD will behave in vivo in a particular system, it is preferable to use, when available, several probes to report on the same lipid species. Because of slight changes in either binding affinity or specificity, we often observed that several reporters for the same lipid might harbor different, although overlapping, localization [40]. For example in Arabidopsis root, a 2×FYVE PI3P reporter is localized to late endosomes (where PI3P accumulates in plants, Fig. 1c), while the PX domain of the $p40^{phox}$ protein, also a well characterized PI3P binding domain, localizes to both late endosomes and tonoplast (the membrane of the plant cell vacuole) [40] (Fig. 1c). Although it is not entirely understood how these differences in localization might be explained, these results are useful for several reasons. First, both probes localize to late endosomes, providing confirmation that PI3P is likely to accumulate in this compartment in plants. Second, because the PX domain also localizes to the tonoplast, this raised the possibility that PI3P might localized to this compartment. Although this conclusion should be taken with care, since it was confirmed with only one of the two LBD, it provided us with a new testable hypothesis. One way to explain the dissimilar localization of the FYVE and PX domains is to consider their difference in relative binding affinity. In fact, high affinity LBDs are expected to localize more specifically to the membrane compartment that accumulates the most its cognate lipid, while lower affinity LBDs are more likely to have a broader localization domain (Fig. 3). Low affinity sensors are less efficient in discriminating between two membranes with two different concentrations of their targeted lipid species and as a result they might be targeted to both of these membranes (Fig. 3a). By contrast, high affinity sensors will have increased dwell time at the

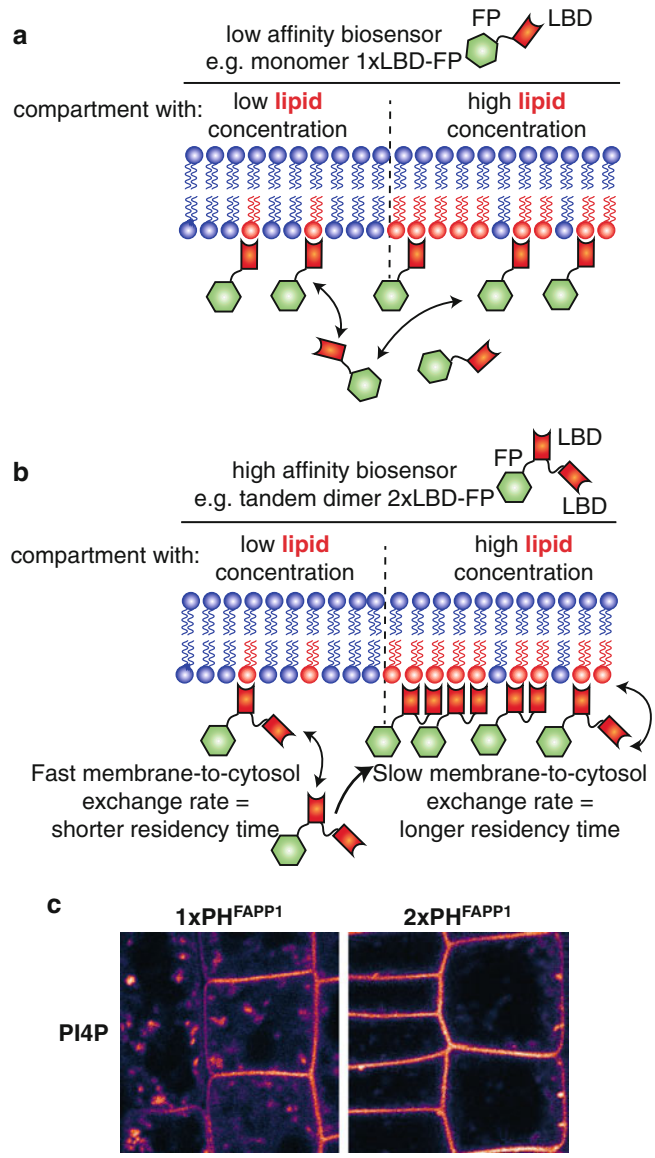

Fig. 3 LBD affinities influence the subcellular localization of the sensors. When several pools of the same lipid exist within the cell, low or high affinity sensors will behave differently with respect to these pools. (**a**) A low affinity sensor (e.g., 1 × LBD) will localize to both membranes with slightly more sensor molecules at the compartment with the highest lipid concentration, while (**b**) a high affinity sensor (e.g., 2 × LBD) will localize preferentially to the compartment with the highest lipid concentration. (**c**) Example of low (1 × PH^{FAPP1}) and high (2 × PH^{FAPP1}) affinity sensor localization in Arabidopsis root cell (image from Simon et al., 2014 Plant Journal)

membrane that is the most enriched in the targeted lipid and they will accumulate preferentially in this compartment (Fig. 3b). In other words, high affinity sensors work like a "Velcro fastener": they will grab more strongly to a surface with more spikes (in this case the spikes being an acidic lipid) (Fig. 3b). Therefore, it is possible that the high affinity 2×FYVE probe mainly localizes to late endosomes because this could be the cell compartment where PI3P accumulates the most, while the PX-based probe localizes also to the tonoplast because this compartment might also have PI3P but to a lesser extent than late endosomes. This is further exemplified when comparing the localization of single versus tandem dimer LBDs. For example in Arabidopsis, we found that the high affinity PI4P sensor $2\times PH^{FAPP1}$ was more strongly localized to the plasma membrane and less to endomembrane compartments than the low affinity sensor $1\times PH^{FAPP1}$ [40] (Fig. 3c). When kept in mind, these variations in localization can actually be exploited to address the relative concentration of a given lipid in several membranes. For example, the results presented in Fig. 3c suggest that the concentration of PI4P is greater at the plasma membrane than in intracellular compartments in plants [40].

5 Validation of Acidic Phospholipid Sensors

As mentioned in the previous section, it is important to test the in vitro binding specificity of a particular LBD. However, this apparent in vitro specificity does not necessarily reflect its localization in vivo or the localization of its cognate lipid in cells. In fact, a comprehensive study on all yeast PH domain suggest that in vitro binding specificity is not a good indicator of the localization of this domain in vivo and does not always predict whether the LBD will be a useful lipid probe or not [54]. Expression of each LBD has to be tested in vivo and if possible validated. A first screen will rapidly discard domains that do not properly accumulate, do not localizes to any membrane compartment or induce strong phenotypes [40]. It is then important to check whether the localization of the probe is in fact dependent on the presence of its cognate lipid. Among other approaches, this could be achieved by pharmacological or genetic inhibition of the lipid biosynthetic enzymes (e.g., phosphatidylinositol kinases, phosphatidylinositol phosphatases, phospholipases). For example, a loss-of-function mutation in *mss4*, the yeast PI4P 5-kinase, leads to a soluble localization of a $2\times PH^{PLC}$ probe that normally highlights $PI(4,5)P_2$ at the yeast plasma membrane [21]. An elegant approach is also the targeted recruitment of lipid kinases or phosphatases to a specific compartment using small molecules or light, because these approaches mediate rapid lipid modifications that are spatially restricted [20, 25, 39, 42, 55–59]. The localization of an ideal lipid reporter should be dependent on

its cognate lipid in both loss- and gain-of-function experiment but not dependent on the production/loss of unrelated lipids. In other words, the probe should leave its endogenous membrane compartment upon loss of its cognate lipid at that membrane. Conversely, it should be recruited to a new membrane compartment upon production of its cognate lipid in this organelle. To date, very few probes have been tested extensively with such gain- and loss-of-function experiments. Besides, they are rarely so versatile, probably because of their requirement on coincidence binding to other molecules (see above the section on the design of genetically encoded acidic phospholipid probes). However, the recent characterization of the P4M PI4P reporter is a must read as an example on how to validate an acidic phospholipid sensor in vivo [20].

In order to validate the localization of a lipid sensor and therefore the cellular localization of a particular lipid, it is important to accumulate several lines of evidence to confirm this localization, such as for example the use of alternate techniques (immunolocalization, direct lipid labeling, …), the similar localization of independent LBDs known to bind the same lipid and/or the colocalization of the probe with endogenous lipid binding proteins.

6 Well-Characterized Acidic Phospholipid Sensors

Several LBDs have been used over the years in different systems and have been shown to behave robustly. In this section we briefly describe these well characterized genetically encoded lipid sensors and, if applicable, point out their respective advantages and limitations. It is nonetheless important to consider the controls described above when using one of these reporters in a new biological context (e.g., new species, new cell type).

7 Phosphoinositide Sensors

7.1 PI3P

The most widely used probe for PI3P are derived from the PX domain of the $p40^{phox}$ protein and the tandem dimer of the FYVE domains (2×FYVE) from the HRS or EEA1 proteins [1, 46, 53, 60, 61]. These domains have been extensively used over the years and are well-accepted PI3P reporters. In animal cells, they mainly report the localization of PI3P in early endosomes [53], but plasma membrane localization has been observed in certain conditions (e.g., insulin treatment [62, 63]). However, they do not highlight the pool of PI3P at the ER upon autophagy induction.

7.2 PI4P

As discussed above (*see* Subheading 4.2), the PH domain of FAPP1 and OSBP report on the localization of PI4P at the Golgi/TGN but not in other membrane compartments due to their requirement for ARF1 binding [21]. The PH domain of the yeast

OSBP-like protein OSH2 is not dependent on ARF1 binding [64]. It is localized both at the Golgi and plasma membrane in yeast but it is localized mainly at the plasma membrane and only weakly at the Golgi in mammalian cells [20, 64]. Therefore, PH^{OSH2} seems to be a better reporter of plasma membrane PI4P than PH^{FAPP1} or PH^{OSBP}. The exact reasons for the plasma membrane preference of PH^{OSH2} are unknown, but might be due to residual $PI(4,5)P_2$ binding [20, 64]. The newly described PI4P reporter, called P4M, seems to be able to report both Golgi and plasma membrane PI4P localization in animal cells and it detects as well a previously uncharacterized pool of PI4P in late endosomes [20]. This reporter seems to be superior to the PH domains of FAPP1, OSBP and OSH2 since it is very specific to PI4P and does not require coincidence binding with other proteins. However, because it has been described fairly recently, it is not yet clear whether this probe will behave similarly in a broad range of cellular contexts.

7.3 PI5P

Few PI5P-binding domains have been characterized, including the PH domains of Dok-1 and Dok-2 [34, 32] and the PHD domain of ING2. A triple repeat of this domain ($3\times PHD^{ING2}$) has been used as a sensor of PI5P localization. It mainly localizes to the nucleus in animal cells [30, 32]. However, immunolocalization and mass spectrometry methods suggest that PI5P localizes in membrane compartments such as the plasma membrane or endosomes [32, 65]. $3\times PHD^{ING2}$ has been recently found to accumulate in omegasomes during autophagy induction by glucose starvation [35]. However, $3\times PHD^{ING2}$ has not extensively been used over the years, perhaps because its expression inhibits PI5P-dependent processes [32]. Therefore, this reporter should be used with caution.

7.4 PI(4,5)P_2

The PH domain of PLCdelta1 (hereafter referred to as PLC) was one of the first LBD to be used as a lipid biosensor [4, 45, 66]. It has an exquisite selectivity for $PI(4,5)P_2$ and has been robustly expressed in many different cellular systems including yeast, mammalian and plant cells [4, 21, 32, 40, 66]. It allowed for example to monitor the reversible $PI(4,5)P_2$ hydrolysis triggered upon PLC activation, i.e., relocalization of membrane-bound PH^{PLC} into the cytosol upon PLC activation by agonists [66]. The C-terminal domain of the TUBBY protein has also been used as a $PI(4,5)P_2$ reporter [40, 67–69]; however, this protein domain binds $PI(3,4)P_2$ in vitro in addition to $PI(4,5)P_2$ [69]. Both reporters are localized exclusively to the plasma membrane, while $PI(4,5)P_2$ has been found in Golgi and ER membrane. This point out to a possible limitation of these probes or simply to the fact that the concentration of $PI(4,5)P_2$ in these compartments is not sufficient to trigger membrane binding at these sites. It is also possible that the physicochemical properties of these compartments (such as their

packing or curvature) are not compatible with binding of these domains. Finally, we cannot exclude that both LBD actually rely on coincidence binding of $PI(4,5)P_2$ and a plasma membrane-resident protein. However, the fact that both reporters behave similarly in many different cellular contexts and species argues against this hypothesis. Altogether, $PH^{PLC\delta1}$ and TUBBY-C are robust reporters of $PI(4,5)P_2$ dynamics at the plasma membrane but might not reflect the possible pool of this lipid in other membrane compartments.

7.5 $PI(3,5)P_2$

The ENTH domains of the yeast proteins Ent3p and Ent5p as well as the PROPPIN domains of Svp1p protein binds to $PI(3,5)P_2$ in vitro [36, 37, 70]. These proteins localize to the membrane of the yeast vacuole suggesting that $PI(3,5)P_2$ accumulates in this compartment [36, 37, 70], but expression of the isolated ENTH or PROPPIN domains does not give consistent results when express in heterologous systems such as animal cells or plants (personal communication). Recently, the cytoplasmic phosphoinositide-interacting domain (ML1N) of the transient receptor potential Mucolipin 1 (TRPML1) has been described to bind $PI(3,5)P_2$ in vitro in the nanomolecular range [38]. A $2\times$ML1N construct was used successfully to report on the localization of $PI(3,5)P_2$ in late endosomes and lysosomes in animal cells [38]. Yet this new tool remains to be tested in additional cellular contexts.

7.6 $PI(3,4)P_2$

Some PX and PH domains are binding $PI(3,4)P_2$ in vitro (e.g., the PX domain of p47 and the PH domains of TAPP1 and TAPP2) [60, 71]. Mainly, PH^{TAPP1} has been used as a read-out of $PI(3,4)P_2$ in vivo and revealed that this lipid mainly accumulates at the plasma membrane [43, 72].

7.7 $PI(3,4,5)P_3$

The PH domain of AKT recognizes both $PI(3,4)P_2$ and $PI(3,4,5)P_3$ and has been extensively used as a read out of type I PI3-kinase activity [4, 45]. Several PH domains have also been described to recognize specifically $PI(3,4,5)P_3$ but not $PI(3,4)P_2$, such as the PH domains from BTK, GRP1, ARNO, or cytohesin1 [1, 4, 45, 46]. $PI(3,4,5)P_3$ does not accumulate at the plasma membrane in the absence of specific stimulus but is synthetized upon stimulation by growth factor or insulin. For example, PH^{BTK} has been used to detect $PI(3,4,5)P_3$ generation at the plasma membrane upon stimulation of fibroblasts by EGF or PDGF [73].

7.8 PS

PS-binding C2 domains have been characterized early on, but in many cases, lipid binding occurs only in the presence of calcium [1]. This restricted the use of these domains to study PS localization in vivo. Nonetheless, the recombinant purified C2 domain of Annexin A5 has been used to detect the presence of PS on the plasma membrane outer leaflet, but this assay requires the presence

of exogenous calcium and is not compatible with live imaging of intracellular events [8]. However, the C2 domain of Lactadherin Synthase 1 (LactC2) was shown to bind specifically PS in the absence of calcium and turned out to be an excellent PS reporter in many systems, including yeast and animal cells [8, 9, 15, 74, 75]. The PH domain of EVECTIN2, a protein localized to the recycling endosomes and involved in membrane traffic, was also shown to specifically bind PS in vitro and to report PS localization in vivo in human cells [44].

7.9 PA

To date, only PA-binding linear motifs but no PA-binding domains have been found and characterized [1]. These short stretches of sequences do not seem to have a particular globular structure and are often rich in basic amino acids. As such, these PA-binding motifs are relatively poorly stereospecific and are able to bind, although with various affinities, other acidic phospholipids [1, 13]. Biosensors using these PA-binding motifs rather than LBDs have been used, such as the PA-binding sequence of the yeast SNARE protein, spo20p, or the yeast protein kinase, Raf1 [76]. Because of the questionable specificity of these motifs for PA, results obtained with these probes should be cautiously interpreted. Their use has nonetheless been instrumental to address some aspects of PA localization and dynamics [76–78].

8 Special Care and Caveat of the Approach

We have highlighted some of the limitations and important controls that must be carried out while analyzing results deduced from genetically encoded lipid biosensors throughout this chapter. However, there are additional potential pitfalls of this approach that should also be considered. We have already covered potential problems due to toxicity. This toxicity might arise, in part, because of competition between endogenous protein and transgenically expressed LBDs for binding the same lipid. This situation is likely to occur when the transgene is overexpressed by strong constitutive promoters and we advocate for the use of mild promoters and/or for the selection of cells or organisms that express weak-to-intermediate level of the reporters. Another strategy is to use inducible expression systems and to study the localization of the lipid sensor at the onset of expression following transgene induction. Furthermore, overexpression of LBDs might induce feedback regulation on the synthesis of the lipid, leading to over-accumulation of this lipid. Systems for mild expression, or better, inducible expression, will reduce these potential feedbacks. It is likely that this lipid over-accumulation is involved in some of the toxicity, which can be observed upon LBD overexpression, possibly by displacing endogenous proteins to new pool of lipids. In addition, it

is important to keep in mind that in some cases, phosphoinositide binding LBDs are able to recognize both the membrane bound lipid and its soluble inositol phosphate counterpart, which could influence membrane association. Lastly, it is unlikely that all phosphoinositides are freely available for LBDs binding. Rather, some lipid species might be synthesized locally and readily engage interactions with endogenous lipid binding proteins as they are being synthesized. For example $PI(4,5)P_2$ is a very important lipid involved in clathrin mediated endocytosis (CME) and several proteins involved in this process are known to binds to this lipid, yet a PH^{PLC} reporter does not localize to clathrin coated pits (CCP) [79]. It is fully conceivable that $PI(4,5)P_2$ in CCPs are bound by the CME machinery and therefore not labeled by the PH^{PLC} probe.

Altogether, it is important to keep in mind that the absence of labeling by a lipid reporter is by no mean a proof of the absence of this lipid. However, the detection of a certain lipid pool by a LBD reporter, if controlled adequately (*see* Subheading 5) is a useful tool, directly amenable to live imaging and dynamic studies.

Acknowledgement

We thank Mathilde Simon, Marie-Cécile Caillaud, and Marlene Dreux for commenting the manuscript. Y.J. has received funding from the European Research Council—ERC Grant Agreement no. [3363360-APPL] and from the Marie Curie Action—CIG Grant Agreement no. [PCIG-GA-2011-303601] under the European Union's Seventh Framework Programme (FP/2007-2013).

References

1. Lemmon MA (2008) Membrane recognition by phospholipid-binding domains. Nat Rev Mol Cell Biol 9(2):99–111. doi:10.1038/nrm2328
2. McLaughlin S, Murray D (2005) Plasma membrane phosphoinositide organization by protein electrostatics. Nature 438(7068):605–611. doi:10.1038/nature04398
3. Jean S, Kiger AA (2012) Coordination between RAB GTPase and phosphoinositide regulation and functions. Nat Rev Mol Cell Biol 13(7):463–470. doi:10.1038/nrm3379
4. Balla T (2013) Phosphoinositides: tiny lipids with giant impact on cell regulation. Physiol Rev 93(3):1019–1137. doi:10.1152/physrev.00028.2012
5. Kay JG, Grinstein S (2013) Phosphatidylserine-mediated cellular signaling. Adv Exp Med Biol 991:177–193. doi:10.1007/978-94-007-6331-9_10
6. Kay JG, Koivusalo M, Ma X, Wohland T, Grinstein S (2012) Phosphatidylserine dynamics in cellular membranes. Mol Biol Cell 23(11):2198–2212. doi:10.1091/mbc.E11-11-0936
7. Hankins HM, Baldridge RD, Xu P, Graham TR (2015) Role of flippases, scramblases and transfer proteins in phosphatidylserine subcellular distribution. Traffic 16(1):35–47. doi:10.1111/tra.12233
8. Yeung T, Gilbert GE, Shi J, Silvius J, Kapus A, Grinstein S (2008) Membrane phosphatidylserine regulates surface charge and protein localization. Science 319(5860):210–213. doi:10.1126/science.1152066
9. Fairn GD, Schieber NL, Ariotti N, Murphy S, Kuerschner L, Webb RI, Grinstein S, Parton RG (2011) High-resolution mapping reveals topologically distinct cellular pools of phosphatidylserine. J Cell Biol 194(2):257–275. doi:10.1083/jcb.201012028

10. van Meer G, Voelker DR, Feigenson GW (2008) Membrane lipids: where they are and how they behave. Nat Rev Mol Cell Biol 9(2):112–124. doi:10.1038/nrm2330
11. Athenstaedt K, Daum G (1999) Phosphatidic acid, a key intermediate in lipid metabolism. Eur J Biochem 266(1):1–16
12. Cazzolli R, Shemon AN, Fang MQ, Hughes WE (2006) Phospholipid signalling through phospholipase D and phosphatidic acid. IUBMB Life 58(8):457–461. doi:10.1080/15216540600871142
13. Horchani H, de Saint-Jean M, Barelli H, Antonny B (2014) Interaction of the Spo20 membrane-sensor motif with phosphatidic acid and other anionic lipids, and influence of the membrane environment. PLoS One 9(11):e113484. doi:10.1371/journal.pone.0113484
14. Bigay J, Antonny B (2012) Curvature, lipid packing, and electrostatics of membrane organelles: defining cellular territories in determining specificity. Dev Cell 23(5):886–895. doi:10.1016/j.devcel.2012.10.009
15. Kay JG, Grinstein S (2011) Sensing phosphatidylserine in cellular membranes. Sensors (Basel) 11(2):1744–1755. doi:10.3390/s110201744
16. Leventis PA, Grinstein S (2010) The distribution and function of phosphatidylserine in cellular membranes. Annu Rev Biophys 39:407–427. doi:10.1146/annurev.biophys.093008.131234
17. Dall'Armi C, Devereaux KA, Di Paolo G (2013) The role of lipids in the control of autophagy. Curr Biol 23(1):R33–R45. doi:10.1016/j.cub.2012.10.041
18. Axe EL, Walker SA, Manifava M, Chandra P, Roderick HL, Habermann A, Griffiths G, Ktistakis NT (2008) Autophagosome formation from membrane compartments enriched in phosphatidylinositol 3-phosphate and dynamically connected to the endoplasmic reticulum. J Cell Biol 182(4):685–701. doi:10.1083/jcb.200803137
19. Hammond GR, Schiavo G, Irvine RF (2009) Immunocytochemical techniques reveal multiple, distinct cellular pools of PtdIns4P and PtdIns(4,5)P(2). Biochem J 422(1):23–35. doi:10.1042/BJ20090428
20. Hammond GR, Machner MP, Balla T (2014) A novel probe for phosphatidylinositol 4-phosphate reveals multiple pools beyond the Golgi. J Cell Biol 205(1):113–126. doi:10.1083/jcb.201312072
21. Levine TP, Munro S (2002) Targeting of Golgi-specific pleckstrin homology domains involves both PtdIns 4-kinase-dependent and -independent components. Curr Biol 12(9):695–704
22. Cruz-Garcia D, Ortega-Bellido M, Scarpa M, Villeneuve J, Jovic M, Porzner M, Balla T, Seufferlein T, Malhotra V (2013) Recruitment of arfaptins to the trans-Golgi network by PI(4)P and their involvement in cargo export. EMBO J 32(12):1717–1729. doi:10.1038/emboj.2013.116
23. Szentpetery Z, Varnai P, Balla T (2010) Acute manipulation of Golgi phosphoinositides to assess their importance in cellular trafficking and signaling. Proc Natl Acad Sci U S A 107(18):8225–8230. doi:10.1073/pnas.1000157107
24. Daboussi L, Costaguta G, Payne GS (2012) Phosphoinositide-mediated clathrin adaptor progression at the trans-Golgi network. Nat Cell Biol 14(3):239–248. doi:10.1038/ncb2427
25. Hammond GR, Fischer MJ, Anderson KE, Holdich J, Koteci A, Balla T, Irvine RF (2012) PI4P and PI(4,5)P2 are essential but independent lipid determinants of membrane identity. Science 337(6095):727–730. doi:10.1126/science.1222483
26. Stefan CJ, Manford AG, Emr SD (2013) ER-PM connections: sites of information transfer and inter-organelle communication. Curr Opin Cell Biol 25(4):434–442. doi:10.1016/j.ceb.2013.02.020
27. Manford AG, Stefan CJ, Yuan HL, Macgurn JA, Emr SD (2012) ER-to-plasma membrane tethering proteins regulate cell signaling and ER morphology. Dev Cell 23(6):1129–1140. doi:10.1016/j.devcel.2012.11.004
28. Stefan CJ, Manford AG, Baird D, Yamada-Hanff J, Mao Y, Emr SD (2011) Osh proteins regulate phosphoinositide metabolism at ER-plasma membrane contact sites. Cell 144(3):389–401. doi:10.1016/j.cell.2010.12.034
29. Ling Y, Stefan CJ, Macgurn JA, Audhya A, Emr SD (2012) The dual PH domain protein Opy1 functions as a sensor and modulator of PtdIns(4,5)P(2) synthesis. EMBO J 31(13):2882–2894. doi:10.1038/emboj.2012.127
30. Gozani O, Karuman P, Jones DR, Ivanov D, Cha J, Lugovskoy AA, Baird CL, Zhu H, Field SJ, Lessnick SL, Villasenor J, Mehrotra B, Chen J, Rao VR, Brugge JS, Ferguson CG, Payrastre B, Myszka DG, Cantley LC, Wagner G, Divecha N, Prestwich GD, Yuan J (2003) The PHD finger of the chromatin-associated protein ING2 functions as a nuclear phosphoinositide receptor. Cell 114(1):99–111

31. Viaud J, Lagarrigue F, Ramel D, Allart S, Chicanne G, Ceccato L, Courilleau D, Xuereb JM, Pertz O, Payrastre B, Gaits-Iacovoni F (2014) Phosphatidylinositol 5-phosphate regulates invasion through binding and activation of Tiam1. Nat Commun 5:4080. doi:10.1038/ncomms5080
32. Viaud J, Boal F, Tronchere H, Gaits-Iacovoni F, Payrastre B (2014) Phosphatidylinositol 5-phosphate: a nuclear stress lipid and a tuner of membranes and cytoskeleton dynamics. Bioessays 36(3):260–272. doi:10.1002/bies.201300132
33. Ramel D, Lagarrigue F, Pons V, Mounier J, Dupuis-Coronas S, Chicanne G, Sansonetti PJ, Gaits-Iacovoni F, Tronchere H, Payrastre B (2011) Shigella flexneri infection generates the lipid PI5P to alter endocytosis and prevent termination of EGFR signaling. Sci Signal 4(191):ra61. doi:10.1126/scisignal.2001619
34. Guittard G, Gerard A, Dupuis-Coronas S, Tronchere H, Mortier E, Favre C, Olive D, Zimmermann P, Payrastre B, Nunes JA (2009) Cutting edge: Dok-1 and Dok-2 adaptor molecules are regulated by phosphatidylinositol 5-phosphate production in T cells. J Immunol 182(7):3974–3978. doi:10.4049/jimmunol.0804172
35. Vicinanza M, Korolchuk VI, Ashkenazi A, Puri C, Menzies FM, Clarke JH, Rubinsztein DC (2015) PI(5)P Regulates Autophagosome Biogenesis. Mol Cell 57(2):219–234. doi:10.1016/j.molcel.2014.12.007
36. Eugster A, Pecheur EI, Michel F, Winsor B, Letourneur F, Friant S (2004) Ent5p is required with Ent3p and Vps27p for ubiquitin-dependent protein sorting into the multivesicular body. Mol Biol Cell 15(7):3031–3041. doi:10.1091/mbc.E03-11-0793
37. Friant S, Pecheur EI, Eugster A, Michel F, Lefkir Y, Nourrisson D, Letourneur F (2003) Ent3p Is a PtdIns(3,5)P2 effector required for protein sorting to the multivesicular body. Dev Cell 5(3):499–511
38. Li X, Wang X, Zhang X, Zhao M, Tsang WL, Zhang Y, Yau RG, Weisman LS, Xu H (2013) Genetically encoded fluorescent probe to visualize intracellular phosphatidylinositol 3,5-bisphosphate localization and dynamics. Proc Natl Acad Sci U S A 110(52):21165–21170. doi:10.1073/pnas.1311864110
39. Zoncu R, Perera RM, Sebastian R, Nakatsu F, Chen H, Balla T, Ayala G, Toomre D, De Camilli PV (2007) Loss of endocytic clathrin-coated pits upon acute depletion of phosphatidylinositol 4,5-bisphosphate. Proc Natl Acad Sci U S A 104(10):3793–3798. doi:10.1073/pnas.0611733104
40. Simon ML, Platre MP, Assil S, van Wijk R, Chen WY, Chory J, Dreux M, Munnik T, Jaillais Y (2014) A multi-colour/multi-affinity marker set to visualize phosphoinositide dynamics in Arabidopsis. Plant J 77(2):322–337. doi:10.1111/tpj.12358
41. Schmid SL, Mettlen M (2013) Cell biology: lipid switches and traffic control. Nature 499(7457):161–162. doi:10.1038/nature12408
42. Suh BC, Inoue T, Meyer T, Hille B (2006) Rapid chemically induced changes of PtdIns(4,5)P2 gate KCNQ ion channels. Science 314(5804):1454–1457. doi:10.1126/science.1131163
43. Posor Y, Eichhorn-Gruenig M, Puchkov D, Schoneberg J, Ullrich A, Lampe A, Muller R, Zarbakhsh S, Gulluni F, Hirsch E, Krauss M, Schultz C, Schmoranzer J, Noe F, Haucke V (2013) Spatiotemporal control of endocytosis by phosphatidylinositol-3,4-bisphosphate. Nature 499(7457):233–237. doi:10.1038/nature12360
44. Uchida Y, Hasegawa J, Chinnapen D, Inoue T, Okazaki S, Kato R, Wakatsuki S, Misaki R, Koike M, Uchiyama Y, Iemura S, Natsume T, Kuwahara R, Nakagawa T, Nishikawa K, Mukai K, Miyoshi E, Taniguchi N, Sheff D, Lencer WI, Taguchi T, Arai H (2011) Intracellular phosphatidylserine is essential for retrograde membrane traffic through endosomes. Proc Natl Acad Sci U S A 108(38):15846–15851. doi:10.1073/pnas.1109101108
45. Varnai P, Balla T (2006) Live cell imaging of phosphoinositide dynamics with fluorescent protein domains. Biochim Biophys Acta 1761(8):957–967. doi:10.1016/j.bbalip.2006.03.019
46. Kutateladze TG (2010) Translation of the phosphoinositide code by PI effectors. Nat Chem Biol 6(7):507–513. doi:10.1038/nchembio.390
47. Moravcevic K, Mendrola JM, Schmitz KR, Wang YH, Slochower D, Janmey PA, Lemmon MA (2010) Kinase associated-1 domains drive MARK/PAR1 kinases to membrane targets by binding acidic phospholipids. Cell 143(6):966–977. doi:10.1016/j.cell.2010.11.028
48. Nishioka T, Frohman MA, Matsuda M, Kiyokawa E (2010) Heterogeneity of phosphatidic acid levels and distribution at the plasma membrane in living cells as visualized by a Foster resonance energy transfer (FRET) biosensor. J Biol Chem 285(46):35979–35987. doi:10.1074/jbc.M110.153007
49. Cicchetti G, Biernacki M, Farquharson J, Allen PG (2004) A ratiometric expressible FRET sensor for phosphoinositides displays a signal

change in highly dynamic membrane structures in fibroblasts. Biochemistry 43(7):1939–1949. doi:10.1021/bi035480w

50. van der Wal J, Habets R, Varnai P, Balla T, Jalink K (2001) Monitoring agonist-induced phospholipase C activation in live cells by fluorescence resonance energy transfer. J Biol Chem 276(18):15337–15344. doi:10.1074/jbc.M007194200
51. Sato M, Ueda Y, Takagi T, Umezawa Y (2003) Production of PtdInsP3 at endomembranes is triggered by receptor endocytosis. Nat Cell Biol 5(11):1016–1022. doi:10.1038/ncb1054
52. Niu Y, Zhang C, Sun Z, Hong Z, Li K, Sun D, Yang Y, Tian C, Gong W, Liu JJ (2013) PtdIns(4)P regulates retromer-motor interaction to facilitate dynein-cargo dissociation at the trans-Golgi network. Nat Cell Biol 15(4):417–429. doi:10.1038/ncb2710
53. Gillooly DJ, Morrow IC, Lindsay M, Gould R, Bryant NJ, Gaullier JM, Parton RG, Stenmark H (2000) Localization of phosphatidylinositol 3-phosphate in yeast and mammalian cells. EMBO J 19(17):4577–4588. doi:10.1093/emboj/19.17.4577
54. Yu JW, Mendrola JM, Audhya A, Singh S, Keleti D, DeWald DB, Murray D, Emr SD, Lemmon MA (2004) Genome-wide analysis of membrane targeting by S. cerevisiae pleckstrin homology domains. Mol Cell 13(5):677–688
55. Toth DJ, Toth JT, Gulyas G, Balla A, Balla T, Hunyady L, Varnai P (2012) Acute depletion of plasma membrane phosphatidylinositol 4,5-bisphosphate impairs specific steps in endocytosis of the G-protein-coupled receptor. J Cell Sci 125(Pt 9):2185–2197. doi:10.1242/jcs.097279
56. Heo WD, Inoue T, Park WS, Kim ML, Park BO, Wandless TJ, Meyer T (2006) PI(3,4,5)P3 and PI(4,5)P2 lipids target proteins with polybasic clusters to the plasma membrane. Science 314(5804):1458–1461. doi:10.1126/science.1134389
57. Giordano F, Saheki Y, Idevall-Hagren O, Colombo SF, Pirruccello M, Milosevic I, Gracheva EO, Bagriantsev SN, Borgese N, De Camilli P (2013) PI(4,5)P(2)-dependent and Ca(2+)-regulated ER-PM interactions mediated by the extended synaptotagmins. Cell 153(7):1494–1509. doi:10.1016/j.cell.2013.05.026
58. Idevall-Hagren O, Dickson EJ, Hille B, Toomre DK, De Camilli P (2012) Optogenetic control of phosphoinositide metabolism. Proc Natl Acad Sci U S A 109(35):E2316–E2323. doi:10.1073/pnas.1211305109
59. Hammond GR (2012) Membrane biology: making light work of lipids. Curr Biol 22(20):R869–R871. doi:10.1016/j.cub.2012.09.005
60. Kanai F, Liu H, Field SJ, Akbary H, Matsuo T, Brown GE, Cantley LC, Yaffe MB (2001) The PX domains of p47phox and p40phox bind to lipid products of PI(3)K. Nat Cell Biol 3(7):675–678. doi:10.1038/35083070
61. Ellson CD, Gobert-Gosse S, Anderson KE, Davidson K, Erdjument-Bromage H, Tempst P, Thuring JW, Cooper MA, Lim ZY, Holmes AB, Gaffney PR, Coadwell J, Chilvers ER, Hawkins PT, Stephens LR (2001) PtdIns(3)P regulates the neutrophil oxidase complex by binding to the PX domain of p40(phox). Nat Cell Biol 3(7):679–682. doi:10.1038/35083076
62. Safi A, Vandromme M, Caussanel S, Valdacci L, Baas D, Vidal M, Brun G, Schaeffer L, Goillot E (2004) Role for the pleckstrin homology domain-containing protein CKIP-1 in phosphatidylinositol 3-kinase-regulated muscle differentiation. Mol Cell Biol 24(3):1245–1255
63. Maffucci T, Brancaccio A, Piccolo E, Stein RC, Falasca M (2003) Insulin induces phosphatidylinositol-3-phosphate formation through TC10 activation. EMBO J 22(16):4178–4189. doi:10.1093/emboj/cdg402
64. Roy A, Levine TP (2004) Multiple pools of phosphatidylinositol 4-phosphate detected using the pleckstrin homology domain of Osh2p. J Biol Chem 279(43):44683–44689. doi:10.1074/jbc.M401583200
65. Sarkes D, Rameh LE (2010) A novel HPLC-based approach makes possible the spatial characterization of cellular PtdIns5P and other phosphoinositides. Biochem J 428(3):375–384. doi:10.1042/BJ20100129
66. Varnai P, Balla T (1998) Visualization of phosphoinositides that bind pleckstrin homology domains: calcium- and agonist-induced dynamic changes and relationship to myo-[3H]inositol-labeled phosphoinositide pools. J Cell Biol 143(2):501–510
67. Ben El Kadhi K, Roubinet C, Solinet S, Emery G, Carreno S (2011) The inositol 5-phosphatase dOCRL controls PI(4,5)P2 homeostasis and is necessary for cytokinesis. Curr Biol 21(12):1074–1079. doi:10.1016/j.cub.2011.05.030
68. Szentpetery Z, Balla A, Kim YJ, Lemmon MA, Balla T (2009) Live cell imaging with protein domains capable of recognizing phosphatidylinositol 4,5-bisphosphate; a comparative study. BMC Cell Biol 10:67. doi:10.1186/1471-2121-10-67
69. Santagata S, Boggon TJ, Baird CL, Gomez CA, Zhao J, Shan WS, Myszka DG, Shapiro L

(2001) G-protein signaling through tubby proteins. Science 292(5524):2041–2050. doi:10.1126/science.1061233

70. Dove SK, Piper RC, McEwen RK, Yu JW, King MC, Hughes DC, Thuring J, Holmes AB, Cooke FT, Michell RH, Parker PJ, Lemmon MA (2004) Svp1p defines a family of phosphatidylinositol 3,5-bisphosphate effectors. EMBO J 23(9):1922–1933. doi:10.1038/sj.emboj.7600203
71. Dowler S, Currie RA, Campbell DG, Deak M, Kular G, Downes CP, Alessi DR (2000) Identification of pleckstrin-homology-domain-containing proteins with novel phosphoinositide-binding specificities. Biochem J 351(Pt 1):19–31
72. Marshall AJ, Krahn AK, Ma K, Duronio V, Hou S (2002) TAPP1 and TAPP2 are targets of phosphatidylinositol 3-kinase signaling in B cells: sustained plasma membrane recruitment triggered by the B-cell antigen receptor. Mol Cell Biol 22(15):5479–5491
73. Varnai P, Rother KI, Balla T (1999) Phosphatidylinositol 3-kinase-dependent membrane association of the Bruton's tyrosine kinase pleckstrin homology domain visualized in single living cells. J Biol Chem 274(16): 10983–10989
74. Fairn GD, Hermansson M, Somerharju P, Grinstein S (2011) Phosphatidylserine is polarized and required for proper Cdc42 localization and for development of cell polarity. Nat Cell Biol 13(12):1424–1430. doi:10.1038/ncb2351
75. Yeung T, Heit B, Dubuisson JF, Fairn GD, Chiu B, Inman R, Kapus A, Swanson M, Grinstein S (2009) Contribution of phosphatidylserine to membrane surface charge and protein targeting during phagosome maturation. J Cell Biol 185(5):917–928. doi:10.1083/jcb.200903020
76. Kassas N, Tryoen-Toth P, Corrotte M, Thahouly T, Bader MF, Grant NJ, Vitale N (2012) Genetically encoded probes for phosphatidic acid. Methods Cell Biol 108:445–459. doi:10.1016/B978-0-12-386487-1.00020-1
77. Zhang F, Wang Z, Lu M, Yonekubo Y, Liang X, Zhang Y, Wu P, Zhou Y, Grinstein S, Hancock JF, Du G (2014) Temporal production of the signaling lipid phosphatidic acid by phospholipase D2 determines the output of extracellular signal-regulated kinase signaling in cancer cells. Mol Cell Biol 34(1):84–95. doi:10.1128/MCB.00987-13
78. Bohdanowicz M, Schlam D, Hermansson M, Rizzuti D, Fairn GD, Ueyama T, Somerharju P, Du G, Grinstein S (2013) Phosphatidic acid is required for the constitutive ruffling and macropinocytosis of phagocytes. Mol Biol Cell 24(11):1700–1712. doi:10.1091/mbc.E12-11-0789, S1701-1707
79. Antonescu CN, Aguet F, Danuser G, Schmid SL (2011) Phosphatidylinositol-(4,5)-bisphosphate regulates clathrin-coated pit initiation, stabilization, and size. Mol Biol Cell 22(14):2588–2600. doi:10.1091/mbc.E11-04-0362

Chapter 16

Analysis of Sphingolipid Synthesis and Transport by Metabolic Labeling of Cultured Cells with [^{3}H]Serine

Neale D. Ridgway

Abstract

Analysis of lipid biosynthesis by radioactive precursor incorporation provides information on metabolic rates and the identity of rate-limiting enzymes and transporters. The biosynthesis of sphingolipids in cultured cells is initiated in the endoplasmic reticulum (ER) by the formation of a sphingoid base from serine and palmitoyl-CoA. N-acylation of the sphingoid base produces ceramide, which is transported to the Golgi apparatus where phosphocholine or carbohydrate headgroups are added to form sphingomyelin (SM) and complex glycosphingolipids (GSLs), respectively. Herein is described a protocol to measure ceramide and SM biosynthesis in cultured cells based on [^{3}H]serine incorporation at the first step in the pathway. The method can be used to assay the effect of pharmacological and genetic manipulations on ceramide synthesis and transport to the Golgi apparatus.

Key words Sphingomyelin, Ceramide, Metabolic labeling, CHO cells, Thin-layer chromatography, Glucosylceramide

1 Introduction

Sphingolipid synthesis is initiated in the endoplasmic reticulum by the serine palmitoyltransferase (SPT)-catalyzed condensation of serine and palmitoyl-CoA to form 3-keto sphinganine [1] (Fig. 1). The 3-keto group of this intermediate is subsequently reduced to produce sphinganine, which is N-acylated to form dihydroceramide. A 4,5-trans double bond is introduced into dihydroceramide to form ceramide, the immediate precursor for the synthesis of SM, ceramide-1-phosphate, glucosylceramide (GlcCer), and galactosylceramide (GalCer). GlcCer and GalCer are the precursors for hundreds of complex (GSLs) that are synthesized in the Golgi apparatus by successive addition of carbohydrate moieties. Ceramide transfer protein (CERT) binds ceramide in the ER and transports it to the cytosolic surface of the *trans*-Golgi, where it is flipped to the luminal side of the membrane and converted to SM by the SM synthase 1 (SMS1) [2, 3]. GalCer synthesis occurs in

Mark G. Waugh (ed.), *Lipid Signaling Protocols*, Methods in Molecular Biology, vol. 1376,
DOI 10.1007/978-1-4939-3170-5_16,

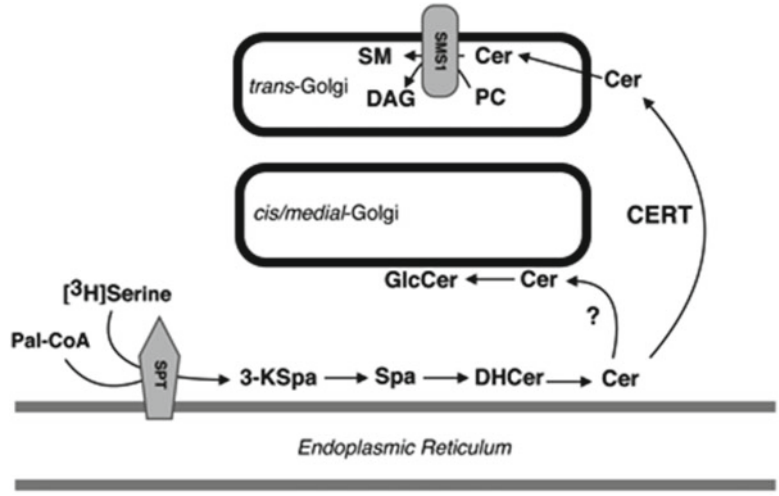

Fig. 1 Pathway for the synthesis of [^{3}H]serine-labeled sphingolipids in the ER and Golgi apparatus. Radioactive serine is incorporated at the first step in the pathway catalyzed by serine palmitoyltransferase (SPT). 3-Keto sphinganine is converted to ceramide on the cytosolic surface of the ER in a three-step reaction. Radioactive ceramide is transported to the *cis/medial*-Golgi for conversion to GlcCer or to SM synthase 1 (SMS1) located in the lumen of the *trans*-Golgi. Abbreviations used: *Cer* ceramide, *DHCer* dihydroceramide, *3-KSpa* 3-ketosphinganine, *Spa* sphinganine, *Pal-CoA* palmitoyl-CoA, *PC* phosphatidylcholine, *DAG* diacylglycerol

the ER, while GlcCer is synthesized on the luminal surface of the *cis/medial* Golgi apparatus after transport from the ER by a poorly understood mechanism.

The synthesis of SM is regulated by the activity of SPT at the level of substrate (serine and palmitoyl-CoA) availability [4], subunit composition [5], and end-product inhibition [6]. Ceramide transport from the ER to the *trans*-Golgi by CERT is also regulated and rate-limiting for SM synthesis under some conditions [3, 7]. CERT is a steroidogenic acute regulatory protein-related lipid transfer (START) protein family member characterized by a C-terminal ceramide binding domain, an N-terminal phosphatidylinositol 4-phosphate (PI-4P)-specific pleckstrin homology domain and an internal motif that binds to vesicle-associated membrane protein (VAMP)-associated protein (VAP) on the cytosolic surface of the ER. Interaction with PI-4P in the Golgi and VAP in the ER is proposed to facilitate unidirectional transfer of ceramide from the ER to the *trans*-Golgi.

Isotopically labeled precursors (sphingoid bases, serine or palmitate) have been used to monitor the synthesis and degradation of ceramide and SM in cultured cells [8]. These studies involve the continuous (pulse) or phased (pulse-chase) incubation of cultured cells with radioactive precursors, followed by analysis of precursor incorporation into lipid or water-soluble products. Isotopic

labeling offers an advantage over steady-state mass analysis by providing information on precursor flux through a biosynthetic pathway and the activity of individual enzymes/transporters. It should be noted, however, that determining the mass of the precursors and products in a lipid biosynthetic pathway is often necessary to fully interpret isotopic labeling experiments. Previously, we developed a short, continuous [^{3}H]serine-pulse protocol using Chinese hamster ovary (CHO) cells to specifically assay the activation of [^{3}H]SM synthesis in response to altered levels of cholesterol and oxysterol [9]. The protocol has been validated with respect to (1) substrate- and time-dependence and (2) incorporation of [^{3}H]serine at the SPT-catalyzed step and not secondarily into the acyl-CoA pool. Variations of this protocol have also been used to identify how pharmacological agents [10–12] and regulatory proteins affect SM synthesis [7, 13].

2 Materials

2.1 Pulse-Labeling of Cells with [^{3}H] Serine

1. Chinese hamster ovary (CHO) cells (ATCC CCL61): Other commonly used cultured cells have been adapted to this protocol, including HEK293, HeLa, and primary fibroblasts.
2. Medium A: Dulbecco's modified Eagle's Medium (DMEM) with 5 % (v/v) fetal bovine serum (FBS) and 33 μg/ml proline. Prewarm medium to 37 °C before adding to cells.
3. Medium B: Serine-free DMEM with 5 % (v/v) fetal bovine serum (FBS) and 33 μg/ml proline. Medium is pre-warm to 37 °C before adding to cells.
4. L-[^{3}H(G)]Serine (PerkinElmer): This serine isotope is uniformly labeled at non-exchangeable positions and is preferred due to low cost and high specific activity (1 μCi/ml, 20–40 mCi/mmol). Avoid using serine labeled at C_1 because decarboxylation occurs during the SPT reaction.
5. PBS: 10 mM sodium phosphate, pH 7.4, 150 mM NaCl.

2.2 Extraction and Isolation of [^{3}H] Serine-Labeled Phospholipids and Sphingolipids

1. Glass screw cap tubes (10–12 ml capacity): Screw cap tubes with solvent-resistant cap liners are required for solvent extraction of lipids from cell suspensions.
2. Ideal Upper Phase (IUP): Methanol–0.58 % NaCl–chloroform (45:47:3, v/v) can be added to tubes with a pump dispenser.
3. Nitrogen evaporating bath: Chloroform is removed from radioactive lipids extracts by evaporation under nitrogen in a 35 °C water bath. We use a 49-position Multivap Analytical Evaporator (Organomation).
4. Low speed centrifuge: Separation of chloroform and aqueous phases during lipid extraction requires a non-refrigerated

centrifugation equipped with high capacity swinging bucket rotor (for example, the Allegra 6 model from Beckman Coulter).

2.3 Thin-Layer Chromatography (TLC) Separation and Quantification of Lipids

1. TLC plates: Silica gel HL plates (20×20 cm, 250 μm thickness, Analtech). Plates are divided into 12 lanes using a pencil (not scored) and lipid extracts are applied in 1 cm zones within the lanes.
2. TLC developing solvent for phospholipids: Chloroform–methanol–acetic acid–water (60:40:4:1, v/v) (*see* **Note 1**).
3. TLC developing solvent for sphingolipid: Chloroform–methanol–water (65:25:4, v/v).
4. TLC standards: Phosphatidylserine (PS) (porcine brain, Avanti Polar Lipids), phosphatidylethanolamine (PE) (egg yolk, Avanti Polar Lipids), SM (egg yolk, Avanti Polar Lipids), and ceramide (porcine brain, Avanti Polar Lipids) standards are prepared as 1 mg/ml stocks in chloroform. A 1 mg/ml GlcCer (bovine buttermilk, Matreya) standard is prepared in chloroform–methanol (2:1, v/v). All standards were stored at −20 °C under nitrogen.
5. Scintillation cocktail: We use Ready Safe (Beckman Coulter) to quantify radioactivity in silica gel scrapings from TLC plates. Typically, TLC scrapings are collected in 2.5 ml of scintillation cocktail and allowed to set for 12 h to allow full release of radioactive lipids.

3 Methods

3.1 Pulse-Labeling of Cultured Cells with [^{3}H]Serine

1. CHO cells are seeded on 60 mm dishes in 3 ml of medium A and cultured in a 37 °C incubator with a 5 % CO_2 atmosphere. Cells are seeded at 400,000 cells/dish. Optimal incorporation of [^{3}H]serine into phospholipids and sphingolipids is obtained when the cells are 60–70 % confluent, which is typically 48 h after seeding. However, if cells are transfected or exposed to other treatments that could affect growth and viability, the seeding density or the culture period should be adjusted accordingly.
2. When CHO cells have reached optimal confluence, medium A is removed and replaced with 3 ml of medium B for 4 h (*see* **Note 2**).
3. After 4 h in medium B, 20 μl of [^{3}H]serine (20 μCi) is added directly to each dish of cells followed by gentle agitation to ensure mixing.
4. Cells are incubated with [^{3}H]serine for 2 h, the medium is aspirated and disposed of in accordance with local radiation licensing protocols. Each dish is rinsed with 2 ml of cold PBS.

3.2 Extraction and Isolation of [^{3}H] Serine-Labeled Phospholipids and Sphingolipids

1. After aspiration of the last PBS wash, add 1 ml of methanol–water (5:4, v/v) to each dish, collect the cells with a disposable plastic scraper and transfer the cell suspension to a screw cap tube.
2. Rinse the culture dish with 1 ml of methanol–water and combine with the primary cell suspension.
3. Sonicate the cell extract for 5 s with needle tip probe (30–40 W output) to break up cell aggregates, vortex, and remove a 200 µl aliquot to a 6 ml glass tube for protein analysis (*see* **step 5**, Subheading 3.3).
4. Add 6 ml of chloroform–methanol (1:2, v/v) to the sonicated cell suspension, cap each tube, and vortex for 5 s. Add 3 ml of 0.58 % NaCl, cap each tube, and vortex for 5 s. Centrifuge at 2000 × *g* for 5 min to separate the upper aqueous phase and the lower chloroform phase (there should be approximately 2 ml of chloroform phase). Carefully aspirate the upper aqueous phase and add 2 ml of IUP, cap the tube, and vortex for 5 s. Separate the phases by centrifugation at 2000 × *g* for 5 min and aspirate the upper phase. Add another 2 ml of IUP and repeat the extraction. It is important to remove as much IUP as possible from the chloroform phase.
5. Evaporate the chloroform from the radiolabeled lipid extract under nitrogen at 35 °C. This step should take 5–10 min; however, be certain that all chloroform and residual IUP is evaporated before continuing to the next step.
6. Dissolve the dried lipid extract in 1 ml of chloroform. Remove a 0.4 ml aliquot to a clean glass test tube, add phosphatidylserine (PS) and phosphatidylethanolamine (PE) standards (5 µg each) and evaporate under nitrogen at 35 °C (proceed to **step 1**, Subheading 3.3).
7. The remaining 0.6 ml of lipid extract (in a screw cap tube) is dried under nitrogen and subjected to base hydrolysis by the addition of 0.5 ml of 0.1 N KOH in methanol. The sample is incubated for 1 h at 37 °C, cooled for 5 min, and the hydrolysate is neutralized by addition of 0.1 ml of 0.5 N HCl (*see* **Note 3**).
8. SM, glucosylceramide and ceramide standards (5 µg each) are added to the neutralized lipid hydrolysate, followed by 3 ml of chloroform–methanol (2:1, v/v) and 2 ml of 0.58 % NaCl. Tubes are capped and vortexed for 5 s, and the aqueous and chloroform phases separated by centrifugation for 5 min at 2000 × *g*. Aspirate the upper aqueous phase and extract the lower chloroform phase twice with IUP as described in **step 4**, Subheading 3.2. Finally, the chloroform extract is dried under nitrogen at 35 °C (proceed to **step 2**, Subheading 3.3).

3.3 TLC Separation and Quantification of Lipids

1. The dried lipid extract containing the PS and PE standard is dissolved in 50 μl of chloroform and applied in a narrow 1 cm zone approximately 1 cm from the bottom of a TLC plate. The tube is rinsed with an additional 25 μl of chloroform, which is applied to the same zone. The TLC plate is placed in a tank containing the phospholipid developing solvent at a depth of approximately 0.5 cm and the solvent is allowed to migrate to within 2–3 cm from the top of the plate (run time is 40–60 min). After removal from the tank, solvents are evaporated from the TLC plate in a fume hood for 30–60 min.
2. The dried lipid extract containing the sphingolipids is applied to a TLC plate and developed exactly as described in **step 1**, Subheading 3.3 above, except that the sphingolipid developing solvent is used.
3. There are a number of methods for the non-destructive detection of phospholipid and sphingolipid on TLC plates. We expose each TLC plate to iodine vapor in a tank for 5–10 min and quickly mark the positions of the lipid standards. Alternatively, sphingolipids and phospholipids can be visualized by fluorography (Fig. 2). The plate is lightly sprayed with EnHance (surface autoradiography enhancer, PerkinElmer) in a fume hood, covered with plastic wrap and exposed to Kodak XAR film for 2–3 days at −70 °C. The exposed film is used as a template to mark the position of radioactive phospholipids and sphingolipids.
4. The bands corresponding to radioactive PS, PE, SM, ceramide and GlcCer are scraped onto 5 cm square weighing papers and carefully poured in 5 ml scintillation vials. Scintillation cocktail is added (2.5 ml) and radioactivity is quantified by scintillation counting in the tritium spectrum for 2 min.
5. Aliquots of the cell suspension that will be assayed for protein (Subheading 3.2, **step 3**) are allowed to evaporate in a fume hood overnight. Protein residues are dissolved in 0.1 ml of 0.1 N NaOH for 5–10 min at room temperature. Protein is quantified with an available colorimetric assay (Bradford or Lowry methods) using bovine serum albumin to generate a standard curve. The incorporation of [^{3}H]serine into PS, PE and sphingolipids is expressed relative to total cellular protein (i.e., DPM/mg protein).

4 Notes

1. The quantification of [^{3}H]serine incorporation into PS and PE provides a useful internal control for [^{3}H]serine uptake into cells and incorporation into an unrelated lipid biosynthetic pathway. PS synthase 1 and/or 2 catalyze the synthesis of PS

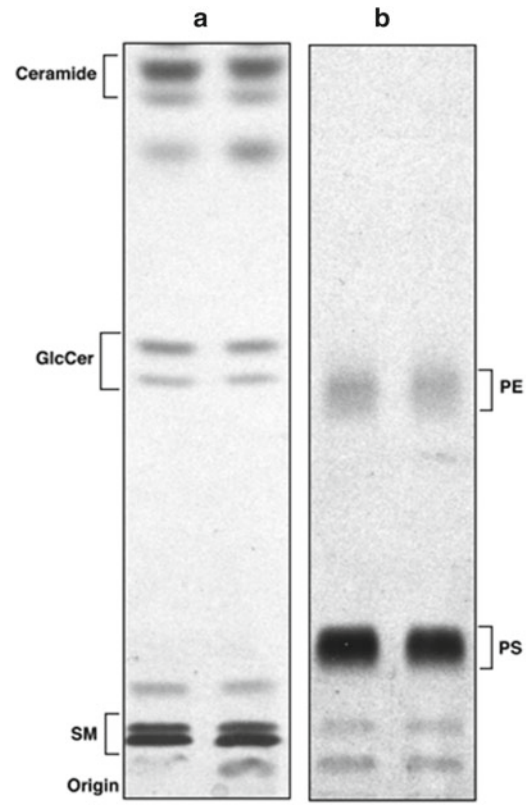

Fig. 2 Fluorogram of [^{3}H]serine-labeled PE, PS, and sphingolipids separated by TLC. *Panel* (**a**), lipid extracts that were subjected to base hydrolysis to remove glycerophospholipids were resolved by TLC, sprayed with EnHance and exposed to film for 3 days at −70 °C. The positions of radioactive SM, GlcCer, and ceramide coincided with authentic standards that were visualized with iodine vapor prior to fluorography. *Panel* (**b**), total lipid extracts were subject to TLC, sprayed with EnHance and exposed to film for 1 day at −70 °C. The positions of PE and PS coincide with authentic standards that were visualized with iodine vapor prior to fluorography

by headgroup exchange with PE and PC. PS is decarboxylated to PE by the mitochondrial PS decarboxylase. Be aware that an apparent increase in [^{3}H]PE occurs upon inhibition of ceramide synthesis due to increased [^{3}H]sphinganine degradation to phospho-[^{3}H]ethanolamine, which enters the CDP-ethanolamine pathway [11].

2. The addition of serine-free medium B has two purposes; depletion of cellular serine to enhance [^{3}H]serine incorporation into lipids, and to provide a 4 h window during which cells can be treated with agents that alter SM synthesis. For instance, we treat CHO cells with 25-hydroxycholesterol during this time to activate OSBP and CERT-dependent ceramide transport [7].

3. It is necessary to remove radioactive PE, PS, and other glycerolipids since these constitute >70 % of the radioactivity in the lipid extract and potentially interfere with separation and quantitation of the less abundant sphingolipids.

Acknowledgements

Our studies were supported by the Canadian Institutes of Health Research. Mark Charman assisted in editing of this manuscript.

References

1. Tidhar R, Futerman AH (2013) The complexity of sphingolipid biosynthesis in the endoplasmic reticulum. Biochim Biophys Acta 1833:2511–2518
2. Hanada K, Kumagai K, Tomishige N, Yamaji T (2009) CERT-mediated trafficking of ceramide. Biochim Biophys Acta 1791:684–691
3. Hanada K, Kumagai K, Yasuda S, Miura Y, Kawano M, Fukasawa M, Nishijima M (2003) Molecular machinery for non-vesicular trafficking of ceramide. Nature 426:803–809
4. Smith ER, Merrill AH Jr (1995) Differential roles of de novo sphingolipid biosynthesis and turnover in the "burst" of free sphingosine and sphinganine, and their 1-phosphates and N-acyl-derivatives, that occurs upon changing the medium of cells in culture. J Biol Chem 270:18749–18758
5. Lowther J, Naismith JH, Dunn TM, Campopiano DJ (2012) Structural, mechanistic and regulatory studies of serine palmitoyltransferase. Biochem Soc Trans 40:547–554
6. Siow DL, Wattenberg BW (2012) Mammalian ORMDL proteins mediate the feedback response in ceramide biosynthesis. J Biol Chem 287:40198–40204
7. Perry RJ, Ridgway ND (2006) Oxysterol-binding protein and vesicle-associated membrane protein-associated protein are required for sterol-dependent activation of the ceramide transport protein. Mol Biol Cell 17:2604–2616
8. Wang E, Norred WP, Bacon CW, Riley RT, Merrill AH (1991) Inhibition of sphingolipid biosynthesis by fumonisins-implications for diseases associated with Fusarium-Moniliforme. J Biol Chem 266:14486–14490
9. Ridgway ND (1995) 25-Hydroxycholesterol stimulates sphingomyelin synthesis in Chinese hamster ovary cells. J Lipid Res 36: 1345–1358
10. Perry RJ, Ridgway ND (2004) The role of de novo ceramide synthesis in the mechanism of action of the tricyclic xanthate D609. J Lipid Res 45:164–173
11. Badiani K, Byers DM, Cook HW, Ridgway ND (1996) Effect of fumonisin B1 on phosphatidylethanolamine biosynthesis in Chinese hamster ovary cells. Biochim Biophys Acta 1304:190–196
12. Burgett AW, Poulsen TB, Wangkanont K, Anderson DR, Kikuchi C, Shimada K, Okubo S, Fortner KC, Mimaki Y, Kuroda M, Murphy JP, Schwalb DJ, Petrella EC, Cornella-Taracido I, Schirle M, Tallarico JA, Shair MD (2011) Natural products reveal cancer cell dependence on oxysterol-binding proteins. Nat Chem Biol 7:639–647
13. Goto A, Liu X, Robinson CA, Ridgway ND (2012) Multisite phosphorylation of oxysterol-binding protein regulates sterol binding and activation of sphingomyelin synthesis. Mol Biol Cell 23:3624–3635

Chapter 17

Determination and Characterization of Tetraspanin-Associated Phosphoinositide-4 Kinases in Primary and Neoplastic Liver Cells

Krista Rombouts and Vinicio Carloni

Abstract

Accumulating evidence implicates phosphoinositide 4-phosphate as a regulatory molecule in its own right recruiting specific effector proteins to cellular membranes. Here, we describe biochemical and immunocytochemical methods to evaluate tetraspanin-associated phosphoinositide-4 kinases activity in primary human hepatic stellate cells (hHSC) and neoplastic hepatoblastoma cells.

Key words Thin layer chromatography, Tetraspanins, Tetraspanin-enriched microdomains, Human hepatic stellate cells, Density gradient centrifugation, Hepatocellular carcinoma cells

1 Introduction

Tetraspanins are transmembrane proteins defined by small and large outer loops, short N-terminal and C-terminal tails with four transmembrane domains. They form complexes termed tetraspanin-enriched microdomains (TEMs) by interacting with other tetraspanins and with a variety of transmembrane and cytosolic proteins that are required for their function. Although the structure of TEMs is similar to that of the lipid rafts, TEMs are evidently distinct from lipid rafts based on the absence of lipid raft-specific glycoproteins such as glycosylphosphatidylinositol-anchored proteins. Several tetraspanin molecules have been identified and implicated in the regulation of cell proliferation, cell migration and cell fusion [1–4]. The most important partners are integrins, particularly α3β1, α4β1, α6β1, and α6β4, intracellular associated heterotrimeric G proteins, proteases, immunoglobulin superfamily members and type II phosphoinositide-4 kinases (*PI4K2A* and its homologue *PI4K2B*) [5]. Type II phosphoinositide 4-kinase (PI4KII) is specifically associated

*These authors contributed equally to this work.

Mark G. Waugh (ed.), *Lipid Signaling Protocols*, Methods in Molecular Biology, vol. 1376,
DOI 10.1007/978-1-4939-3170-5_17,

with different tetraspanins such as CD81, CD9, CD63, and CD151 to create functional complexes [2]. PI4KII catalyzes the phosphorylation of phosphatidylinositol on the D-4 position of the inositol ring. The product of this reaction, phosphatidylinositol 4-phosphate (PI4-P) is a precursor in the synthesis of PI3,4P_2, PI4,5P_2, and PI3,4,5P_3, but PI4-P itself participates in signal transduction, membrane trafficking, and cytoskeletal reorganization.

2 Materials

Prepare all solutions by using ultrapure water (to be prepared by purifying deionized water to attain a sensitivity of 18 MΩ cm at 25 °C) and analytical grade reagents. Prepare and store all reagents at room temperature (unless indicated otherwise). Follow all disposal regulations when discarding waste materials.

1. *Hepatocellular carcinoma (HCC)complete culture medium:* human hepatoblastoma cell line HepG2 cultured in Eagle's Minimum Essential medium (EMEM), supplemented with GlutaMAX, 0.1 mM/L nonessential amino acids, 1.0 mM/L sodium pyruvate, and 10 % FBS.
2. *Human hepatic Stellate (hHSC)completeculture medium* (final volume 500 mL): 400 mL IMDM Iscove's Modified Dulbecco's Medium, 100 mL FBS fetal bovine serum, performance plus, US, 5 mL sodium pyruvate (100×), 5 mL EM-NEAA (100×), 5 mL antibiotics–antimycotics (100×), 5 mL L-GLUTAMINE (200 mM).
3. *PI4KII lysis buffer (final)*: 25 mM HEPES, pH 7.5 (*see* **Note 1**), 1 % CHAPS (*see* **Note 2**), 200 mM NaCl, 5 mM $MgCl_2$, 200 μM Na_3VO_4 (*see* **Note 3**), 2 mM NaF, 2 mM phenylmethylsulfonyl fluoride (PMSF).
4. *PI4KII reaction buffer (final)*: 20 mM HEPES, pH 7.5, 5 mM MgCl2, 0.3 % Triton X-100.
5. *Immunoprecipitation (IP) buffer (final)*: 50 mM Tris–HCl, pH 7.5, 0.5 M NaCl, 1 mM $CaCl_2$, 1 mM $MgCl_2$, 0.1 % Tween 20.

3 Methods

3.1 HCC Culture

HepG2 cells are cultured in serum-rich culture medium. Cells are cultured under standard conditions in a humidified incubator under 5 % CO_2 in air at 37 °C. Every 3 days the complete culture medium is changed and sub-confluent cells are trypsinized and passaged at a split ratio 1:3.

3.2 Human Hepatic Stellate Cell (hHSC) Isolation

Human HSCs were isolated from wedge sections of liver tissue, obtained from patients undergoing surgery in the Royal Free Hospital after giving informed consent (EC01.14-Royal Free). Cells were isolated according to Mederacke et al. [6] with modifications for non-cirrhotic human liver. Weigh the received human liver. All concentrations and volumes of the solutions described in this protocol are used for a wedge section of 10 g of human liver (non-cirrhotic). The principle of using the density gradient centrifugation to isolate HSCs from other hepatic cell types is based on the presence of intracellular vitamin A-containing lipid droplets in HSCs [7].

1. Preheat water bath at 37 °C and warm up the enzymatic digestion solution (*see* **Note 4**).
2. Remove liver and wash excessive blood away as much as possible with HBSS solution. Place extracted liver in a petri dish and homogenize with a sterile scalpel and scissor.
3. Transfer the homogenate in an autoclaved Erlenmeyer and add 100 mL of enzymatic digestion solution (*see* **Note 4**). Place in a shaking water bath, 37 °C for 30 min. Visually examine the process of digestion by analyzing the obtained cell suspension under the light microscope to assess the extent of digestion.
4. Filter the homogenate through a 100 μm nylon cell strainer.
5. Divide the obtained cell suspension in 4×50 mL conical centrifuge tubes, replenish with HBSS and centrifuge for 2 min at 4 °C, 500 rpm (50 × *g*). Discard the pellet which contains few hepatocytes.
6. Transfer the supernatant into 8 × 50 mL conical centrifuge tubes and fill up with HBSS then centrifuge for 7 min at 4 °C and 1500 rpm (427 × *g*). Discard the supernatant.
7. Collect and resuspend the cell pellet in 11.6 mL of gradient solution 1.
8. Prepare 4 × 15 mL conical centrifuge tubes for gradient density centrifugation: add 2.1 mL of gradient solution 2 to each conical centrifuge tube and add to this solution 2.9 mL of gradient solution 1 containing the cell suspension of **step 7**. Mix gently to form OptiPrep final concentration of 17 % to remove Kupffer cells or macrophages in general. At this point the final volume should be exactly 5 mL.
9. Layer an equal amount (5 mL) of gradient solution 3, very gently to create another gradient of OptiPrep 11.5 %, which after centrifugation contains a layer of human HSC.
10. Layer an additional 2 mL of gradient solution 1.
11. Centrifuge at 1400 × *g* for 17 min at 4 °C. It is very important to not use the centrifuge break nor accelerator.

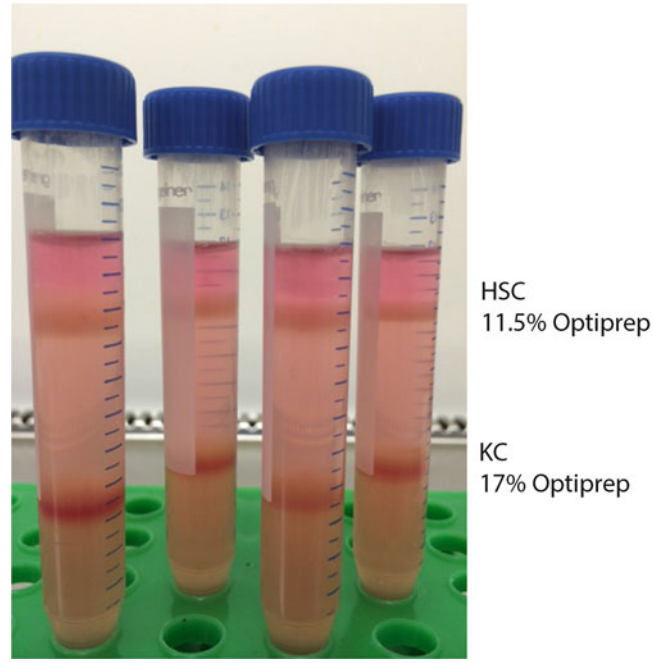

Fig. 1 Human hepatic stellate cells (hHSC) are isolated by employing an ex vivo enzymatic digestion of the liver tissue by enzymes such as collagenase, pronase, and DNase which allow the dissociation of the hepatic cells from the surrounding extracellular matrix (ECM). This is then followed by sequential centrifugation steps at different g force to separate the various cell types from the hHSC population. Next, a refined single step gradient centrifugation (OptiPrep 11.5–17 %) allows to select and to purify hepatic stellate cells

12. Aspirate with a 1 mL tip the hHSC layer (*see* Fig. 1) and resuspend in complete culture medium (*see*Subheading 2, **item 2**) followed by a centrifugation of 7 min at 427 × *g*.
13. Discard the supernatant and resuspend the cells in complete culture medium. Count the cells and establish viability by using trypan blue solution, then culture the cells according to the obtained yield (*see* Fig. 2).

3.3 Immunoprecipitation and Lipid Kinase Assay

1. Trypsinize the cells and culture the cells until ~70 % confluent
2. Put the cells in serum-free medium for 12 h.
3. Wash the cells with phosphate-buffered saline.
4. Lysate the cells with PI4KII lysis buffer at 4 °C, centrifuge, and measure protein concentrations in the supernatant

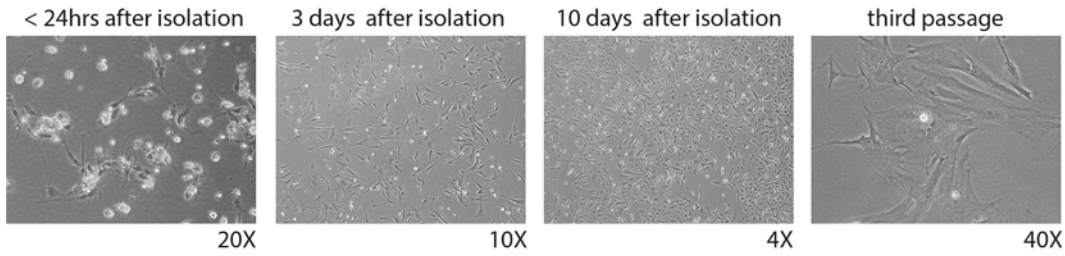

Fig. 2 Phase contrast images of HSCs in culture. Twenty four hours after isolation the freshly isolated hepatic stellate cells show prominent dendritic cytoplasmic processes, and the presence of lipid droplets. The HSC morphology gradually displays a slightly more myofibroblast-like phenotype during the subsequent days in culture. Images were taken after HSC isolation at <24 h, 3–10 days in culture and after the third passage. Magnification 4×, 10×, 20×, and 40×

3.4 Immunoprecipitation of Tetraspanin-Associated Phosphoinositide-4 Kinases

5. Carry out immunoprecipitations by using protein G Sepharose 4 Fast Flow. Protein G and protein A have different IgG binding specificities, dependent on the origin of the IgG. Compared to protein A, protein G binds more strongly antibodies from various species. For each antibody use 100 μl of protein G Sepharose 4 Fast Flow matrix.
6. Wash three times with ice-cold IP buffer
7. Add 300 μl of ice-cold IP buffer. Add antibodies 5–10 μg of anti-CD81 mAb, anti-CD63 rabbit, or nonimmune mouse IgG as a control, place on a rotator at 4 °C and incubate for a minimum of 30 min.
8. Wash protein G Sepharose-antibody complexes three times with ice-cold IP buffer.
9. Add lysate to each tube (500 μg to 1 mg of proteins). Be sure to add equal amount of proteins per tube/immunoprecipitation.
10. Bring total volume up to 300 μl with IP buffer. Try to not exceed 400 μl.
11. Incubate overnight on rotator at 4 °C.
12. Next day, spin down immune complexes and transfer supernatant to new tubes and store at −70 °C. Consider these aliquots as depleted lysates.
13. Wash immune complexes four times in lysis buffer and one time in 10 mM HEPES pH 7.5 plus 5 mM $MgCl_2$

3.5 Phosphoinositide Kinase Reactions

14. Perform reaction directly on immune complexes. Add the reaction mixture (50 μl total/tube), 20 μl water, 10 μl PI4KII reaction buffer, 5 μl ATP (50 μM final).
15. Start reactions adding 50 μg of L-α-phosphatidylinositol (*see* **Note 5**) and 10–15 μCi of ATP, [γ-^{32}P] (*see* **Note 6**), remember to store and dispose of radioactive and organic waste appropriately.

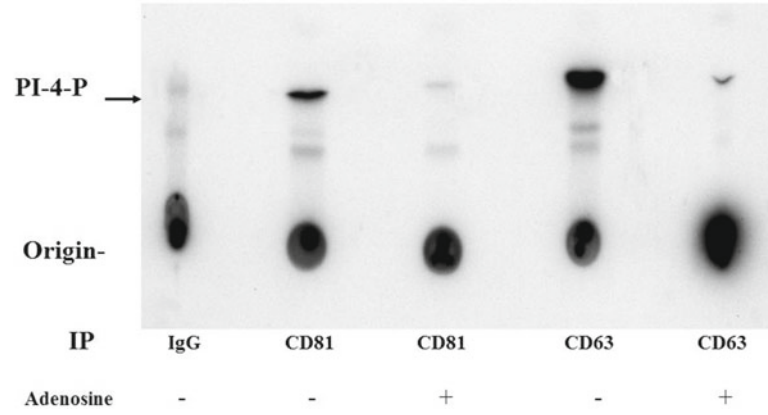

Fig. 3 Tetraspanin-associated phosphoinositide kinase activity. Huh7 cells are lysed and immunoprecipitated CD81 and CD63 are subjected to an in vitro phosphoinositide kinase assay in the absence or presence of adenosine. PI4-P is separated by thin layer chromatography

16. Carry out reactions for 5–10 min at room temperature
    Type II PI 4-kinases are not sensitive to wortmannin, but are inhibited by the nonspecific inhibitor adenosine, therefore perform a kinase reaction in the presence of the drug (200 μM/tube) as control (*see* Fig. 3) [8].
17. Prepare stop solution (1:1 MeOH–1 N HCl) and stop the reaction with 90 μl. Extract the organic layer twice with 100 μl $CHCl_3$ and vortex gently. Use elongated tips to withdraw the lower layer to a new tube. Combine the two organic layers and dry under nitrogen gas. Add 15 μl of 2:1 $CHCl_3$–MeOH solution to each tube, vortex and spin quickly.
18. Resolve the organic layer by thin layer chromatography (TLC) on potassium oxalate-treated silica gel 60 glass plates (*see* **Note 7**). Spot on TLC plate, no closer than 1 cm apart. Put plate in TLC tank filled to a depth of about 2 cm with developing buffer (120 ml chloroform–94 ml methanol–22.6 ml water–4 ml ammonium hydroxide), after running close to the top plate, lift up the plate, air-dry and expose with X-ray film. Cut out spots from TLC for counting radioactivity using scintillation counter [9, 10].

3.6 Intracellular Delivery of Phosphoinositides

The use of the carrier-cargo system to ferry fluorescent derivatives or native phosphoinositide polyphosphates (PIPs) into living cells provides a simple method to examine the action, localization, and metabolism of PIPs involved in signal transduction pathways in the context of changes in cell physiology. PIPs are crucial components for endocytic, exocytic, and Golgi vesicle movement, and in remodeling of the actin cytoskeleton [11–13].

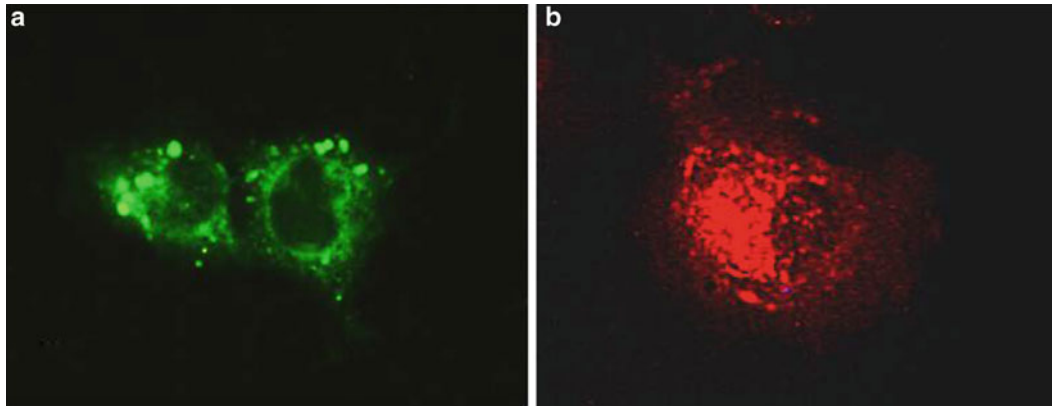

Fig. 4 Delivery and immunocytochemical detection of PI4-P into HepG2 cells. (**a**) Carrier-delivered BODIPY fluorescent-PI4-P in HepG2 cells. Image shown is recorded at 10 min after addition of the complex. The green fluorescing PI4-P can be seen in intracellular patterns consistent with its presence in the Golgi, cytoplasmic vesicles and the nuclear membrane. (**b**) HepG2 cells are fixed with 2.5 % paraformaldehyde and stained using saponin permeabilization. Anti-PI4-P antibody is applied to the cells. Anti-PI4-P antibody staining of the Golgi complex and cytoplasmic vesicles

1. Prepare freshly long-chain (di-C16) synthetic phosphatidylinositol 4-phosphate or BODIPY Fluorescent-PI4P at 300 μM in 150 mM NaCl, 4 mM KCl, and 20 mM HEPES pH 7.2 and resuspend by bath sonication.
2. Prepare polyamine carrier–PI4-P complexes following the Echelon Shuttle PI4-P kit guidelines..
3. Plate the cells on coverslips (10-mm diameter) for 12–24 h before employing delivery experiments with synthetic PI4-P or fluorescently tagged analogs.
4. Mount coverslips onto a glass bottom culture dish and add 20 μl of medium in the well and polyamine carrier–PI4-P complexes to the medium. The final concentrations are between 0.1 and 50 μM, but the optimal concentration for a given experimental system should be determined.
5. Collect optical sections after 10 min by using an inverted microscope and/or a laser scanning confocal microscope system with acquisition software (*see* Fig. 4a).

3.7 Immunofluorescence of Phosphoinositides (PIPs) in Cultured Cells

1. Discharge culture medium and fix cells by adding an equal volume of 2.5 % paraformaldehyde (*see* **Note 8**) for 10 min on ice.
2. Wash three times with Tris-buffered saline (TBS) (*see* **Note 9**).
3. Permabilize the cells with 0.5 % saponin on ice for 15 min.
4. Wash three times with TBS.
5. Block with 10 % Goat Serum in TBS either overnight at 4 °C or 30 min at 37 °C.

6. Add anti-PI4-P antibody diluted in TBS to the concentration suggested on the technical data sheet (use 200 μL per well in an 8-well chamber slide). Incubate for 60 min at 37 °C.
7. Wash 3 times with TBS-Goat Serum 1 %.
8. Add 200 μL /well biotinylated goat anti-mouse IgM (1:2000) or IgG (1:5000) in TBS. Incubate for 30 min at 37 °C.
9. Wash three times with TBS-Goat Serum 1 %.
10. Add Streptavidin-Alexa Fluor 488 at a dilution of 1:2000 in TBS. Incubate 200 μl/well for 30 min at 37 °C.
11. Rinse thoroughly with water.
12. Dry completely.
13. Seal with mounting media and coverslip. Store at 4 °C in the dark.
14. View with a confocal or fluorescence microscope (*see* Fig. 4b).

4 Notes

1. Add 11.91 g of HEPES to an appropriate beaker with about 80 mL of deionized water to the beaker. Add a stir bar to the beaker and leave it on a stir plate until completely dissolved (~1 min). Begin monitoring pH of the solution. It should be acidic (pH ~5). Add NaOH 10 N to increase the pH towards 7.5. If the pH is too high, lower it back to a pH of 7.5 by carefully adding HCl, while monitoring the pH. Once the pH of the solution is 7.5, add enough deionized water to raise the volume to 100 mL. Store at 4 °C for up to 2 months.
2. Sodium orthovanadate (activated), 200 mM. Dissolve 1.84 g of sodium orthovanadate in 45 ml purified water in a small beaker with a stir bar. Adjust the pH to 10 using either 1 N NaOH or 1 N HCl, with stirring. The starting pH of the sodium orthovanadate may vary with lots of the chemical. At pH 10, solution will be yellow. Boil solution until it turns colorless (approximately 10 min). All of the crystals should dissolve. Cool to room temperature. Readjust the pH to 10 and repeat **steps 3** and **4** until solution remains colorless and pH stabilizes at 10. Adjust the final volume to 50 ml with purified water. Store the activated sodium orthovanadate in 1-ml aliquots and freeze at –20 °C.
3. CHAPS, 3-[(3-Cholamidopropyl) dimethylammonio]-1-propanesulfonate is sulfobetaine derivative of cholic acid. This zwitterionic detergent is useful for membrane protein solubilization when it is important to maintain protein activity. Prepare a 10 % solution in water.

4. Prepare Stock solutions and Buffers to be used during human hepatic stellate cell isolation:

   Collagenase Type IV: Stock solution: 1 %—dissolve 0.1 g in 10 mL HBSS (without Ca^{+2}, Mg^{+2}), filter, aliquots can be stored at −20 °C.

   Pronase (protease): Stock solution: 5 %—dissolve 0.5 g in 10 mL HBSS (without Ca^{+2}, Mg^{+2}), filter, aliquots can be stored at −20 °C.

   Deoxyribonuclease I from bovine pancreas: Stock solution: 1 %—dissolve 0.1 g in 10 mL HBSS (without Ca^{+2}, Mg^{+2}), filter, aliquots can be stored at -20 °C.

   Bovine Serum Albumin (BSA): Stock solution: 10 % dissolve in HBSS—filter, aliquots can be stored at −20 °C.

   Enzymatic Digestion solution 1 (100 mL): HBSS (with Ca^{+2}, Mg^{+2}) add 1 mL Collagenase (0.01 % final), 1 mL Pronase (0.05 % final) and 0.1 mL DNase I (0.001 %).

   Gradient solution 1 (30 mL): 28.95 mL HBSS (without Ca^{+2}, Mg^{+2}) add 0.300 ml DNase I (0.001 % final), and 0.75 mL BSA (0.25 % final).

   Gradient solution 2 (21 mL): gradient solution 1 (7 mL) and add 14 mL of OptiPrep™ Density Gradient Medium final density gradient of 40 %.

   Gradient solution 3 (25 mL): 17.83 mL HBSS (without Ca^{+2}, Mg^{+2}) and add 7.17 mL of gradient solution 2 (final OptiPrep gradient of 11.5 %).

5. L-α-phosphatidylinositol, sodium salt.

   Use 4 μl of phosphatidylinositol, dry under nitrogen gas, and add 120 μl of deionized water. Seal the tube with Parafilm to avoid evaporation. Sonicate for 10 min for allowing micelle formation.

6. ATP, [γ-^{32}P]- 3000 Ci/mmol 10 mCi/ml . *Lipid kinase activity is expressed as counts/min within a defined area representing the PI 4-32P.*

7. Silica Gel 60 20 × 20 cm glass plates.

   TLC pretreatment solution: 2 % (w/v) potassium oxalate in methanol–water (40:60). Prepare fresh TLC pretreatment solution. Place plates in a TLC developing tank and add pretreatment solution. Run solvent, air-dry, and then activate plates at 100 °C for 1 h.

8. Paraformaldehyde fixation

   Heat a 2.5 % solution in calcium magnesium free PBS at 60 °C, add 2–4 drops of 10 N NaOH. When paraformaldehyde goes in solution, allow to cool at room temperature. Then adjust pH to 7.2 with HCl. Store for no longer than 1 week at 4 °C.

9. Tris-buffered saline (TBS)

   Dissolve the following salts in 800–900 ml of water. 8 g sodium chloride (136.8 mM final), 0.38 g potassium chloride (5.0 mM final), 0.1 g calcium chloride (anhydrous; 0.9 mM final). 0.1 g magnesium chloride hexahydrate (0.5 mM final), 0.1 g dibasic sodium phosphate (anhydrous; 0.7 mM final). Add 25 ml 1 M Tris–Cl, pH 7.4. Add water up to 1 l, distribute 100 ml aliquots into glass bottles, autoclave and store at room temperature.

References

1. Yáñez-Mó M, Barreiro O, Gordon-Alonso M, Sala-Valdés M, Sánchez-Madrid F (2009) Tetraspanin-enriched microdomains: a functional unit in cell plasma membranes. Trends Cell Biol 19:434–446
2. Yauch RL, Hemler ME (2000) Specific interactions among transmembrane 4 superfamily (TM4SF) proteins and phosphoinositide 4-kinase. Biochem J 351:629–637
3. Carloni V, Mazzocca A, Mello T, Galli A, Capaccioli S (2013) Cell fusion promotes chemoresistance in metastatic colon carcinoma. Oncogene 32:2649–2660
4. Mazzocca A, Carloni V, Sciammetta S, Cordella C, Pantaleo P, Caldini A, Gentilini P, Pinzani M (2002) Expression of transmembrane 4 superfamily (TM4SF) proteins and their role in hepatic stellate cell motility and wound healing migration. J Hepatol 37(3):322–330
5. Minogue S, Anderson JS, Waugh MG, dosSantos M, Corless S, Cramer R, Hsuan JJ (2001) Cloning of a human type II phosphatidylinositol 4-kinase reveals a novel lipid kinase family. J Biol Chem 276:16635–16640
6. Mederacke I, Dapito DH, Affò S, Uchinami H, Schwabe RF (2015) High-yield and high-purity isolation of hepatic stellate cells from normal and fibrotic mouse livers. Nat Protoc 10(2):305–315
7. Rombouts K (2015) Hepatic stellate cell culture models. IN: Stellate cells in health and disease. Gandhi CR, Pinzani M (eds), Academic press, NY, pp 15–27
8. Carloni V, Mazzocca A, Ravichandran KS (2004) Tetraspanin CD81 is linked to ERK/MAPKinase signaling by Shc in liver tumor cells. Oncogene 23:1566–1574
9. Touchstone JC (1995) Thin-layer chromatographic procedures for lipid separation. J Chromatogr B 671:169–195
10. Henderson RJ, Tocher DR (1992) Thin-layer chromatography. In: Hamilton RJ, Hamilton S (eds) Lipid analysis. A practical approach. IRL Press, Oxford, pp 65–111
11. Mazzocca A, Liotta F, Carloni V (2008) Tetraspanin CD81-regulated cell motility plays a critical role in intrahepatic metastasis of hepatocellular carcinoma. Gastroenterology 135:244–256
12. Ozaki S, DeWald DB, Shope JC, Chen J, Prestwich GD (2000) Intracellular delivery of phosphoinositides and inositol phosphates using polyamine carriers. PNAS 97:11286–11291
13. Weiner OD, Neilsen PO, Prestwich GD, Kirschner MW, Cantley LC, Bourne HR (2002) A PtdInsP(3)- and Rho GTPase-mediated positive feedback loop regulates neutrophil polarity. Nat Cell Biol 4:509–513

Chapter 18

Analysis of the Phosphoinositide Composition of Subcellular Membrane Fractions

Deborah A. Sarkes and Lucia E. Rameh

Abstract

Phosphoinositides play critical roles in the transduction of extracellular signals through the plasma membrane and also in endomembrane events important for vesicle trafficking and organelle function (Di Paolo and De Camilli, Nature 443(7112):651–657, 2006). The response triggered by these lipids is heavily dependent on the microenvironment in which they are found. HPLC analysis of labeled phosphoinositides allows quantification of the levels of each phosphoinositide species relative to their precursor, phosphatidylinositol. When combined with subcellular fractionation techniques, this strategy allows measurement of the relative phosphoinositide composition of each membrane fraction or organelle and determination of the microenvironment in which each species is enriched. Here, we describe the steps to separate and quantify total or localized phosphoinositides from cultured cells.

Key words Phosphoinositide, Subcellular fractionation, Metabolic labeling, Organelle

1 Introduction

Phosphatidylinositol and its seven phosphorylated phosphoinositide (PI) forms are interconnected by a network of kinases and phosphatases, which act in a dynamic balance to allow for the rapid initiation and termination of the PI signal in response to extracellular and intracellular cues [2]. Given that the cellular responses to activation/inhibition of PI-kinases and phosphatases depend not only on changes in the local concentration of the PI being formed, but also on changes in the local concentration of its precursors, precise measurement of the changes in all seven PIs within the cell is critical for full understanding of the outcome. High Performance Liquid Chromatography (HPLC) analysis of metabolically labeled phosphoinositides (PIs) has been the golden standard for quantitative measurements of cellular PI composition for many years. With the advancement in our understanding of the function of PIs in cells, new methodology for measuring cellular PIs have been developed. The discovery of PI-specific probes, for example,

Mark G. Waugh (ed.), *Lipid Signaling Protocols*, Methods in Molecular Biology, vol. 1376,
DOI 10.1007/978-1-4939-3170-5_18,

allowed for the detection of the subcellular localization of specific PIs in real-time [3]. The use of phospho-specific antibodies against proteins that are phosphorylated in a PI-dependent manner (as for phospho-Akt) became a popular method for quickly evaluating the activity of PI-kinases (e.g., PI 3-kinase) and the potential changes in the levels of PIs in cells. More recently, the development of PI-specific antibodies together with new methodology for staining PIs in situ added another valuable tool in the study of these lipids [4]. However, one major shortcoming of these techniques is the potential for generating false negative results. For example, certain subpopulations of PIs may not be accessible to PI probes and antibodies, or the local concentration and/or microenvironmental factors may prevent proper detection [5, 6]. HPLC analysis of PIs remains the most sensitive and the only technique that allows for a direct comparison between the levels of various PIs. However, this technique also has its own limitations. Unlike the in situ PI probes and antibodies, HPLC analysis of labeled PIs only gives a snapshot of the global cellular PI composition, with no spatial information. With this in mind, we developed a strategy for analyzing the subcellular PI composition, which combines two well-established techniques: subcellular fractionation of microsomal membranes and HPLC analysis of labeled PIs. Together these two techniques become a powerful tool for mapping the dynamic membrane distribution of all PIs within the cell and unraveling the coordinated function of these signaling molecules. Nonetheless, one has to keep in mind that for precise comparison of the levels of the various PI species, the metabolic labeling step needs to reach equilibrium. The subcellular fractionation methods described below have been developed by applying fundamental principles for organelle fractionation [7] and adapted from protocols used to isolate lipid binding proteins [8]. They have been optimized to reduce sample loss and minimize lipid dephosphorylation. Analysis of the subcellular distribution of PIs in HeLa and BTC6 cells using this strategy was previously reported [9]. For an overview of the procedures, refer to the workflow chart (Fig. 1).

2 Materials

1. Cells of interest and tissue culture reagents and facilities.
2. Tabletop ultracentrifuge and centrifuge tubes.
3. HPLC quaternary pump with degasser and autosampler (optional).
4. Strong anionic exchange columns (Agilent Zorbax SAX or Whatman Partisphere SAX).
5. Flow scintillation analyzer or β-counter and scintillation fluid.

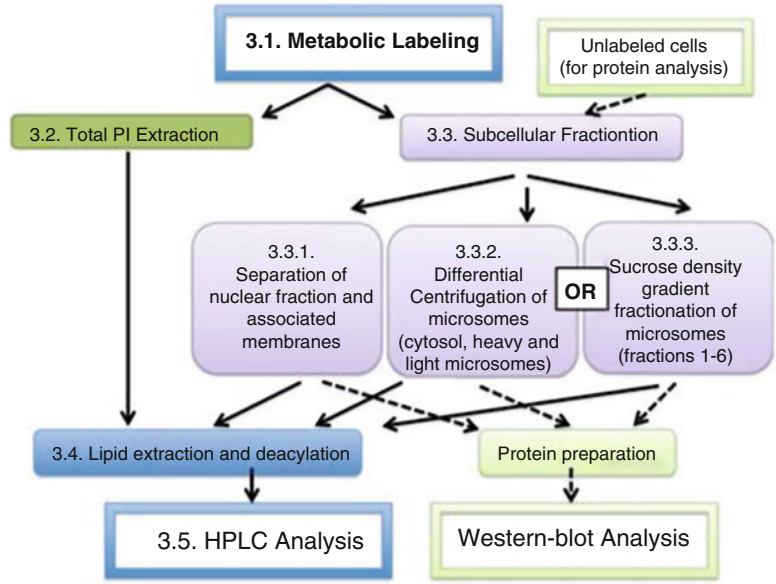

Fig. 1 Diagram depicting the workflow chart for the studies of the subcellular localization of PIs, as described in this chapter

6. Chemical fume hood.
7. Centrifugal evaporator.
8. Protective equipment for radioactivity and permit.

3 Methods

3.1 Labeling Cells with [^{3}H] Inositol

3.1.1 Materials

1. Inositol-free media.
2. L-glutamine 100×.
3. [^{3}H] inositol.
4. Treated tissue culture plates, 100 mm (P100).
5. Dialyzed fetal bovine serum (*see* **Note 1**).
6. Phosphate buffered saline (PBS).

3.1.2 Protocol

For tips for avoiding contamination of the area, *see* **Note 2**:

1. Seed a tissue culture plate with the cells of interest the day before the start of the labeling.
2. Rinse the cells with about 5 mL PBS and incubate them with inositol-free media for about 30 min (pre-labeling).
3. Add fresh inositol-free media (5 ml/P100) containing 1× (200 mM) L-glutamine, dialyzed serum (at the concentration in which your cells grow) and 10 μCi of [^{3}H] inositol per ml (*see* **Note 3**).

4. Culture cells in labeling medium for 24–72 h (*see* **Note 4**).

At this point, you can proceed to extract the total phosphoinositide content (as described in **steps 1** through **6** in Subheading 3.2), or use the labeled cells for subcellular fractionation (as described in Subheading 3.3).

3.2 Collection of Total PI Content

1. Rinse the cells in 5 ml PBS. After removing the PBS, keep the plate tilted for a few seconds and remove the last drop of PBS with a P1000 pipet tip (*see* **Note 5**).
2. Add 400 µl of 1 M HCl, then 400 µl of methanol.
3. Scrape the cells and transfer to a 1.5 ml microfuge tube (*see* **Note 6**) using a wide mouth P1000 pipet tip, clipped about 5 mm from the end (because the lysate will have a lot of white, insoluble material).

   Optional: add carrier lipids to the tube to which the lysate is being transferred (*see* **Note 7**).
4. Add 400 µl chloroform, vortex very well (*see* **Note 8**), centrifuge approximately 1 min in a microfuge at maximum speed (if using nanofuge, spin for at least 5 min) and collect bottom phase (organic phase) into a new microfuge tube (*see* **Note 9**). The white, insoluble material should make a thin line at the interface. Avoid this material when collecting the lipids.
5. To each tube containing the organic phase, add 400 µl of a mixture of freshly prepared methanol : 0.1 M EDTA pH 8.0 (10:9, v:v). Vortex very well, spin and collect the bottom phase into a new microfuge tube (*see* **Note 10**).
6. Evaporate the organic phase containing your lipids under a nitrogen stream and store the dried lipids at −80 °C until deacylation (Subheading 3.4.1).

3.3 Subcellular Fractionation

3.3.1 Materials

Cytosol buffer with phosphatase and protease inhibitors: 0.2 M sucrose; 25 mM HEPES, pH 7; 125 mM potassium acetate; 1 mM dithiothreitol; 1 mM sodium orthovanadate; 2 mg/ml sodium fluoride; 2 mg/ml β-glycerophosphate; 1 mM phenanthroline; 1 mM benzamidine, and protease inhibitor cocktail (*see* **Note 11**).

Sucrose solutions: using the cytosol buffer with phosphatase and protease inhibitors, make a 16 % (w:vol) sucrose solution (light) and a 64 % (w:vol) sucrose solution (heavy).

3.3.2 Protocol

1. Prepare cytosol buffer (25 ml for four 100 mm plates).
2. Turn on the tabletop ultracentrifuge and set temp to 4 °C.
3. Prechill the rotor in cold room.
4. Start with one 100 mm tissue culture dish, approximately 90–100 % confluent, containing cells labeled with [^{3}H]-inositol as in Subheading 3.1 (*see* **Note 12**).

5. Treat cells as required for your particular experiment. At the end of the treatment, place cells on ice.

   All steps below are conducted on ice with solutions at 4 °C.

6. Rinse plate 3 times with 5 ml PBS, removing excess in between washes (*see* **Note 13**).
7. Rinse twice with cytosol buffer plus inhibitors, 2 ml per plate.
8. Remove excess buffer by tilting the plate and aspirating remaining liquid with a pipet, without drying cells (*see* **Note 14**).
9. Scrape cells from plate: for optimal recovery, scrape the borders first and then tilt the plate towards you to scrape the center downward, letting the liquid flow to the bottom edge of the plate.
10. Transfer lysate to a microcentrifuge tube using a 29-gauge needle. Each plate of cells should yield about 150 μl of lysate. Pass cells through the needle about 6–12 times, avoiding creation of foam (*see* **Note 15**).
11. The percentage of cell lysis will vary from cell line to cell line and from experiment to experiment. If you are running a non-radioactive test for protein analysis, you can check for lysis at this point by mixing 5 μl of the lysate with 5 μl of Trypan Blue reagent and visualizing on a hemocytometer with an inverted phase contrast microscope.

    Optional: If lysis is less than 90 %, spin the lysate in a nanofuge for 1 min, transfer the supernatant to a new microcentrifuge tube and pass the concentrated pellet through the 29-gauge needle a few more times, returning the supernatant back gradually.

12. Centrifuge the lysates at approximately 100 × *g* for 10 min at 4 °C to pellet the nuclear fraction and associated membranes.
13. Remove the supernatant (post-nuclear fraction) carefully with clean pipet tip and transfer to new centrifuge tube.
14. Resuspend the nuclear fraction in 200 μl of cytosol buffer.

    Optional: pass the resuspended pellet through the same 29-Gauge needle 6–12 times and spin the tube at approximately 100 × *g* for 10 min to remove any remaining buffer. Remove supernatant and combine with the other supernatant, containing post-nuclear fraction.

15. Process the nuclear fraction by following Subheading 3.3.1 and process the post-nuclear supernatant by following either Subheading 3.3.2 (for separation of microsomal fraction through differential centrifugation) or Subheading 3.3.3 (for separation of microsomal fractions through sucrose density gradient) (*see* **Note 16**).

3.3.3 Separation of Membrane Associated with the Nucleus from the Nuclear Fraction

1. Resuspend the pellet in 200 µl of cytosol buffer and go through three freeze-thaw cycles (using dry ice and ethanol) to break remaining unbroken cells (*see* **Note 17**).
2. Spin at approximately 100 × *g* for 10 min in cold room. Remove supernatant (we usually save this fraction for analysis and label it Fraction X, *see* **Note 18**).
3. Resuspend the pellet with 200 µl of fresh cytosol buffer + 1 % Triton X-100.
4. Rock for 10 min in cold room and spin at 16,000 × *g* for 10 min in cold room.
5. Remove and save supernatant (this is the fraction containing the Triton-soluble membranes associated with the nucleus).
6. Resuspend the pellet in 200 µl of fresh cytosol buffer + 1 % Triton X-100 and save (this is the nuclear fraction).

3.3.4 Separation of Microsomal Fractions from Cytosol by Differential Centrifugation

1. If you opted to rinse the nuclear pellet as in **step 14** of Subheading 3.3 (above), combine the supernatant for each sample into one microcentrifuge tube.
2. Using a microfuge, spin the post-nuclear supernatant at 16,000 × *g* for 30 min.
3. Collect the supernatant and transfer to a thick-wall polycarbonate ultracentrifuge tube (11 × 34 mm). The pellet generated in **step 2** is the heavy microsomal fraction and should be resuspended in 200 µl of cytosol buffer containing 1 % Triton X-100 with protease and phosphatase inhibitors.
4. Balance and centrifuge the supernatant at 400,000 × *g* for 1 h on a tabletop ultracentrifuge with fixed angle rotor (we use Beckman TLA120.2).
5. Remove supernatant carefully and transfer to new tube (this is the cytosol fraction).
6. Add 200 µl of cytosol buffer containing 1 % Triton X-100 to pellet and let it soak for 45–60 min on ice (*see* **Note 19**). Resuspend by pipetting up and down and transfer to a new tube, making sure that nothing is left behind (this is the light microsomal fraction).

3.3.5 Sucrose Density Fractionation of the Microsomal Fractions

1. Prepare light (16 %) and heavy (64 %) sucrose solutions in cytosol buffer with protease and phosphatase inhibitors (4 ml of each is more than sufficient for four gradients).
2. Prepare nine microfuge tubes with mixtures of the two sucrose solutions, such that the first tube (solution A) has 10 % of the light sucrose and 90 % of the heavy sucrose solution, the second tube (solution B) has 20 % of light and 80 % of heavy, etc., increasing the ratio of the light to heavy solution by 10 % each time until you reach 90 % light and 10 % heavy sucrose solution (for solution I). Mix each tube well.

3. In a thick-wall polycarbonate centrifuge tube (11 × 34 mm), carefully overlay 100 µl of each sucrose solution, starting with the heaviest mixture (solution A) and ending with the 16 % sucrose solution alone, for the tenth layer.
4. Layer 200–250 µl of the post-nuclear supernatant on top of the discontinuous gradient, balance and spin at 250,000 × *g* for 4.5 h on a tabletop ultracentrifuge using a swinging bucket rotor (we use TLS55).
5. Collect 6 fractions of 200 µl each, starting from the top of the tube and going down, by placing the pipet tip just below the meniscus of the gradient and aspirating slowly as you move down with the meniscus (*see* **Note 20**). Fractions are labeled 1–6, 1 containing the lightest and 6 containing the heaviest organelles and cellular debris.

3.4 Lipid or Protein Extraction of Samples from Subcellular Fractionation Protocols (See Note 21)

If performing protein analysis of subcellular fractions from unlabeled cells, add 40 µl of 6× loading buffer containing reducing agent to all fractions and proceed to western-blot analysis, using conventional methods.

If performing PI analysis of labeled cells, proceed to **steps 1–4**, described below:

1. To each tube containing 200 µl of fractionated lysate, add 200 µl of 2 M HCl, 400 µl of methanol, and 400 µl of chloroform.

   Optional: add carrier lipids to the tube to which the lysate is being transferred (*see* **Note 22**).
2. Vortex the tube well, and then centrifuge approximately 1 min in a microfuge at maximum speed to separate the organic and aqueous phases. Collect the bottom organic phase containing lipids into a fresh microfuge tube, as in Subheading 3.2, **step** 7, for total lipids.
3. To each tube containing the organic phase, add 400 µl of a mixture of freshly prepared Methanol : 0.1 M EDTA pH 8.0 (10:9, v:v). Vortex very well, spin and collect the bottom phase into a new microfuge tube (*see* **Note 23**).
4. Evaporate the organic phase containing your lipids under a nitrogen stream and store the dried lipids at −80 °C until deacylation (Subheading 3.4.1).

3.4.1 Chemical Deacylation of the Lipids

1. Prepare fresh methylamine reagent in the chemical hood. For 10 ml (10 samples):

40 % methylamine in water	2.68 ml
H_2O	1.61 ml
Methanol	4.57 ml
n-butanol	1.14 ml

2. Prepare a vacuum pump inlet trap by filling the bottom of the trap with 50–100 ml of H_2SO_4 and surrounding it with dry ice to freeze the acid and avoid aspiration. Connect it to the centrifugal evaporator, in between the centrifuge and the condenser.
3. Add 1 ml methylamine reagent to each sample in a chemical fume hood.
4. Incubate samples at 53 °C for 50 min in well-sealed tubes. Cool samples to room temperature, quick spin to remove condensation, and dry them in the centrifugal evaporator. For proper set up of the centrifugal evaporator, *see* **Note 24**.
5. Store dried lipids at −80 °C until fatty acid extraction (Subheading 3.4.2).

3.4.2 Fatty Acid Extraction (See **Note 25***)*

1. Mix *n*-butanol, petroleum ether, and ethyl formate at 20:4:1 (v:v:v) (we call this "fatty acid extraction mix").
2. Label 2 sets of tubes per sample such that each set can be distinguished from each other and from the set of tubes already containing your sample.
3. Add 500 µl deionized H_2O and 500 µl fatty acid extraction mix to each deacylated, dried sample in the chemical fume hood. Vortex twice for at least 30 s and centrifuge for 1 min at top speed.
4. Remove the bottom (aqueous) layer with a P200 (*see* **Note 26**) and add it to the first set of tubes with 500 µl fatty acid extraction mix already in it. Vortex twice for at least 30 s and centrifuge for 1 min in a microfuge at top speed.
5. Extract the bottom (aqueous) layer using a P200 pipet tip and store in the empty set of labeled tubes.
6. Dry these samples by centrifugal evaporation (~2 h) and store at −80 °C.

3.5 HPLC Analysis of PIs

3.5.1 Preparing Samples for HPLC Injection

1. Resuspend samples in 100–120 µl H_2O.
2. Add the appropriate standards to the sample (*see* **Note 27**). Final volume should be about 120 µl.
3. Transfer to a microfuge spin filter and spin sample together with standards in a tabletop centrifuge, making sure to filter most of the sample volume.
4. If you have an automatic HPLC injector, transfer sample to a mini conical glass tube and insert into the HPLC sample holder, with all bubbles removed. You should have at least 110 µl.

3.5.2 Prepare the HPLC

1. For conventional method, install a 250 mm anionic exchange column. For PI-5-P separation, install two 250 mm anionic exchange columns in tandem (these must be Whatman Partisphere SAX columns).

2. Prepare 1 M ammonium phosphate dibasic pH 3.8 or 6.0, for conventional or PI-5-P separation methods, respectively. Use phosphoric acid to adjust the pH.
3. Fill reservoir for pump A with HPLC grade H_2O.
4. Fill reservoir for pump B with 1 M ammonium phosphate at appropriate pH.
5. Wash column as suggested by the vendor. We usually run H_2O followed by ammonium phosphate, then equilibrate with H_2O before running samples.
6. For conventional phosphoinositide separation, program the HPLC to run gradient A. For separation of PI-5-P from all other phosphoinositides, use gradient B:

Ammonium Phosphate pH 3.8, Gradient A

Step 1A. H_2O 5 min

Step 2A. Ammonium phosphate gradient from 0 to 15 % over 55 min

Step 3A. Isocratic 15 % ammonium phosphate for 15 min

Step 4A. Ammonium phosphate gradient from 15 to 65 % over 25 min

Step 5A. Isocratic 65 % ammonium phosphate for 5 min

Step 6A. H_2O for 15 min

Ammonium phosphate pH 6.0 (see Note 28), gradient B:

Step 1B. H_2O 5 min

Step 2B. Ammonium phosphate gradient from 0 to 1 % over 5 min

Step 3B. Ammonium phosphate gradient from 1 to 4 % over 60 min

Step 4B. Ammonium phosphate gradient from 4 to 15 % over 5 min

Step 5B. Isocratic 15 % ammonium phosphate for 20 min

Step 6B. Ammonium phosphate gradient from 15 to 65 % over 25 min

Step 7B. Isocratic 65 % ammonium phosphate for 5 min

Step 8B. H_2O for 15 min

3.5.3 Inject and Run HPLC

1. Using an automatic or manual injector, inject 100 μl of sample into the HPLC.
2. Run ammonium phosphate gradient A or B, described above, at 1 ml/min.
3. If using an online flow scintillation analyzer, use UltimaFlo AP (Perkin Elmer) as your scintillation cocktail, running at

5 ml/min. If using a 0.5 ml cell, set up detection for every 6 s (*see* **Note 29**).

4. If using a fraction collector, collect fractions as you desire and as frequently as possible. Mix them with scintillation fluid and measure the counts in a scintillation counter. This will need to be optimized for your own system to avoid losing fractions of interest.
5. Wash column with 65 % ammonium phosphate solution for 20 min followed by H_2O for 20 min.

3.5.4 Data Analysis

Using HPLC analysis software, identify and quantify the peaks equivalent to each phosphoinositide species. Enter the values in an excel spreadsheet, correct and normalize the data according to your particular application. At this point, you may have to correct for any loss that may have occurred during the process. For example, if you only load 50 % of the post-nuclear supernatant into the sucrose gradient, then the values from the sucrose gradient fractions need to be multiplied by 2. For analysis of fractionation data, we normalize the data two ways. First, we calculate the distribution of each species over the various fractions (*see* Fig. 2, Table B). Second, we calculate the distribution of all PI species within a particular fraction (*see* Fig. 2, Table C). By adding the total counts from each PI species and comparing the results with the expected relative amount of each PI in samples prepared without fractionation, you can determine whether there was any loss or gain of PIs due to dephosphorylation.

Based on our previous analysis, the bulk of the PIs will fractionate with the nuclear-associated membranes [9]. This fraction contains most of the endoplasmic reticulum (ER), where phosphatidylinositol is synthesized. The ER will also be present in the post-nuclear fractions and will be enriched in the heavy fractions of the density gradient (fractions 5 and 6) together with other heavy organelles, such as mitochondria and lysosomes. Plasma membrane derived microsomes will be enriched in fraction 4. Light organelles will be enriched in fractions 3 and 2 of the gradient. Fractions 1 and 2 will also contain cytosolic proteins. This pattern of distribution may vary from cell to cell.

4 Notes

1. Dialyzed serum can be purchased or prepared in the lab using a small pore dialysis bag and performing the dialysis at 4 °C overnight against PBS, to remove inositol from the serum.
2. Always use proper personal protective equipment, including gloves, lab coat, and appropriate shielding for isotope in use; use pipet tips with cotton plug when pipetting radioactive

TABLE A	PI-3-P	PI-4-P	PI-5-P	PI-3,5-P2	PI-3,4-P2	PI-4,5-P2	PIP3	total PIPs	PtdIns	total
Fx 1	1	2	3	4	5	6	7	28	100	128
Fx 2	2	3	4	5	6	7	8	35	101	136
Fx 3	3	4	5	6	7	8	9	42	102	144
Fx4	4	5	6	7	8	9	10	49	103	152
Fx5	5	6	7	8	9	10	11	56	104	160
Fx 6	6	7	8	9	10	11	12	63	105	168
Triton	7	8	9	10	11	12	13	70	106	176
Nuclear	8	9	10	11	12	13	14	77	107	184
Fx X	9	10	11	12	13	14	15	84	108	192
total	45	54	63	72	81	90	99	504	936	1440

TABLE B	PI-3-P	PI-4-P	PI-5-P	PI-3,5-P2	PI-3,4-P2	PI-4,5-P2	PIP3	total PIPs	PtdIns	total
Fx 1	0.01	0.02	0.03	0.04	0.05	0.06	0.07	0.28	1	1.28
Fx 2	0.01980198	0.02970297	0.03960396	0.04950495	0.05940594	0.06930693	0.07920792	0.34653465	1	1.34653465
Fx 3	0.02941176	0.03921569	0.04901961	0.05882353	0.06862745	0.07843137	0.08823529	0.41176471	1	1.41176471
Fx4	0.03883495	0.04854369	0.05825243	0.06796117	0.0776699	0.08737864	0.09708738	0.47572816	1	1.47572816
Fx5	0.04807692	0.05769231	0.06730769	0.07692308	0.08653846	0.09615385	0.10576923	0.53846154	1	1.53846154
Fx 6	0.05714286	0.06666667	0.07619048	0.08571429	0.0952381	0.1047619	0.11428571	0.6	1	1.6
Triton	0.06603774	0.0754717	0.08490566	0.09433962	0.10377358	0.11320755	0.12264151	0.66037736	1	1.66037736
Nuclear	0.07476636	0.08411215	0.09345794	0.10280374	0.11214953	0.12149533	0.13084112	0.71962617	1	1.71962617
Fx X	0.08333333	0.09259259	0.10185185	0.11111111	0.12037037	0.12962963	0.13888889	0.77777778	1	1.77777778
total	0.04807692	0.05769231	0.06730769	0.07692308	0.08653846	0.09615385	0.10576923	0.53846154	1	1.53846154

TABLE C	PI-3-P	PI-4-P	PI-5-P	PI-3,5-P2	PI-3,4-P2	PI-4,5-P2	PIP3	total PIPs	PtdIns	total
Fx 1	0.02222222	0.03703704	0.04761905	0.05555556	0.0617284	0.06666667	0.07070707	0.05555556	0.10683761	0.08888889
Fx 2	0.04444444	0.05555556	0.06349206	0.06944444	0.07407407	0.07777778	0.08080808	0.06944444	0.10790598	0.09444444
Fx 3	0.06666667	0.07407407	0.07936508	0.08333333	0.08641975	0.08888889	0.09090909	0.08333333	0.10897436	0.1
Fx4	0.08888889	0.09259259	0.0952381	0.09722222	0.09876543	0.1	0.1010101	0.09722222	0.11004274	0.10555556
Fx5	0.11111111	0.11111111	0.11111111	0.11111111	0.11111111	0.11111111	0.11111111	0.11111111	0.11111111	0.11111111
Fx 6	0.13333333	0.12962963	0.12698413	0.125	0.12345679	0.12222222	0.12121212	0.125	0.11217949	0.11666667
Triton	0.15555556	0.14814815	0.14285714	0.13888889	0.13580247	0.13333333	0.13131313	0.13888889	0.11324786	0.12222222
Nuclear	0.17777778	0.16666667	0.15873016	0.15277778	0.14814815	0.14444444	0.14141414	0.15277778	0.11431624	0.12777778
Fx X	0.2	0.18518519	0.17460317	0.16666667	0.16049383	0.15555556	0.15151515	0.16666667	0.11538462	0.13333333
total	1	1	1	1	1	1	1	1	1	1

Fig. 2 Example of an Excel spreadsheet for analyzing the data from the fractionation studies described within. *Table A* is the raw data. *Table B* is the PI composition of each fraction relative to phosphatidylinositol (PtdIns). *Table C* is the distribution of each PI through the fractions. The numbers shown are fictitious, not from an actual experiment. For example data refer to Sarkes and Rameh [9]

material. During incubation, place cells in a labeled box or tray, with shielding if necessary. Cover benches with absorbent paper pad. Use plastic bag for disposal of all solid consumables, and add absorbent material to container for liquid waste. Label area, waste container, and incubation box with radiation tape. Always check for spills by wipe testing the area when finished. Monitor with Geiger counter when appropriate.

3. Some commercial [^{3}H]-inositol comes dissolved in ethanol. If the final concentration of ethanol in the labeling medium is likely to harm your cells, you may choose to first evaporate the ethanol in a microfuge tube and resuspend the dried inositol in inositol-free media.
4. The ideal labeling period will depend on each cell line. If the cell line grows well in the labeling medium, it should incorporate the [^{3}H]-inositol into lipids in approximately 24–48 h (equilibrium). HeLa cells label well within 48 h. However, slow-growing cells may need to be labeled for 72 h or more,

assuming that they won't die in the labeling medium. In order to optimize labeling time, perform a test labeling.

5. It is important to remove all PBS to avoid diluting the HCl in the next step.
6. Use good quality microfuge tubes. Some brands don't seal well and will leak during vortexing.
7. This is especially important if you are starting with few cells, to avoid loss of the [^{3}H]-labeled lipids. You can use crude brain phosphoinositides or a mixture of any lipids available.
8. When "vortexing" radioactive materials dissolved in organic solvents, use a paper wipe around the tube to avoid spreading radioactivity to the area around the mixer, if leaking occurs. Always centrifuge the tubes before opening the cap to avoid contamination of the area.
9. When pipetting organic solvents, saturate the pipet tip first, to avoid dripping. When transferring chloroform from one tube to another, hold both tubes in one hand to shorten the distance between them and avoid sample loss and contamination of the work area.
10. At this point you can estimate the total counts obtained by measuring the cpm present in 1 μl of each sample using a scintillation counter and scintillation fluid. You should have at least 1,000,000 cpm total per sample.
11. Sodium orthovanadate, sodium fluoride and β-glycerophosphate are phosphatase inhibitors and are essential to the preservation of the phosphoinositide composition of the lysates during the fractionation. Other phosphatase inhibitors can be added to supplement these inhibitors.
12. Prior to using radioactive labeled cells, it is recommended to run through the protocol using unlabeled cells. This will allow for analysis of the distribution of organelle markers through western-blot and troubleshooting before conducting PI analysis.
13. Use plastic bag for disposal of all contaminated solid consumables, and add absorbent material to container for liquid waste.
14. Excess buffer is removed to reduce the total volume of the lysate to the minimum retained by the cell layer. The more concentrated the cells in the cytosol buffer, the higher the percentage of lysed cells after passage through the narrow needle.
15. Unlike other subcellular fractionation protocols, we avoid freezing and thawing at this stage, to avoid disrupting organelles. Passing the cells through a small needle will mechanically disrupt the cells without affecting the structure of most organelles. However, creation of foam may lead to protein denaturation and should be avoided.

16. Subheading 3.3.2 separates the microsomes based on size to isolate heavy microsomes from light microsomes and from cytosol. This is a faster fractionation protocol and suitable for quickly isolating small cytosolic vesicles such as Golgi-derived vesicles (COPI and COPII-containing vesicles) from other organelles and plasma membrane, and from nucleus and nuclear-associated membranes. Subheading 3.3.3 is more time consuming, but allows for separation of dense organelles, such as mitochondria and lysosome, from lighter organelles, such as smooth ER and Golgi. Subheading 3.3.3 also allows for separation of plasma membrane-derived microsomes from the other organelles.
17. By freezing and thawing the lysates several times, you should achieve 100 % lysis. Thus, this step allows removal of any contaminating post-nuclear material from unbroken cells.
18. Fraction X may contain a mixture of organelles. It will contain, for example, the microsomes from the leftover unbroken cells. We save and analyze this fraction to ensure that no material was lost at the end of the protocol.
19. You can also freeze the resuspended pellet overnight.
20. After centrifugation, the total volume may decrease such that the last fraction may have less than 200 μl. Be sure to record the volume of the last fraction for normalization during data analysis. If you loaded more than 200 μl of lysate on top of the gradient, you should collect 250 μl (or your actual load volume) as your first fraction.
21. We recommend running the procedure for protein extraction and western-blot analysis prior to any lipid analysis to confirm the separation of various organelles using antibodies against proteins markers. We also recommend checking the density of the collected fractions using a refractometer. When performing protein extraction for western-blot and density measurements, cells should not be labeled with [^{3}H]-inositol.
22. This is especially important if you are starting with few cells, to avoid loss of the [^{3}H]-labeled lipids. You can use crude brain phosphoinositides from Sigma or a mixture of any lipids available.
23. At this point you can estimate the total counts obtained by measuring the cpm present in 1 μl of each sample using a scintillation counter and scintillation fluid.
24. Make sure a dry ice H_2SO_4 trap is properly fixed to the centrifugal evaporator, to allow circulation of the vapors from the samples into the trap, without aspiration of the acid into the pump. After 2 h have passed, remove the H_2SO_4 trap and continue until lipids are dry. Avoid overnight usage of the

centrifugal evaporator. Monitor the increasing volume of the sulfuric acid/methylamine reagent mixture and empty when necessary to prevent contamination of your samples or aspiration by the pump. Store H_2SO_4 trap in a chemical fume hood and dispose of waste properly.

25. We are interested in the PI head group only. This step is to clean the sample from the fatty acid chains and from any remaining lipids and thus avoid clogging the HPLC column.
26. Using a P200 gives better control and prevents sample loss and contamination of work area. Do not use P1000 pipet tips, they are too large for 1.5 ml microcentrifuge tubes containing 1 ml sample and the mixture will spill over the tube.
27. PI-4-P and PI-4,5-P_2 peaks are easy to identify, as they are the most abundant PIs in cells. Therefore, we don't need standards for these lipids. We use [^{32}P] labeled standards to identify the peaks corresponding to the less abundant PIs. For example, we prepare [^{32}P]-labeled PI-3-P, PI-3,4-P_2, PI-3,5-P_2, and PI-3,4,5-P_3 using baculovirus-expressed PI3-kinase and the appropriate precursor as substrate.
28. We found that using ammonium phosphate pH 6.0 makes the PI-4-P and PI-5-P peaks narrower and helps avoid overlapping bases. However, with this method we sometimes loose good separation of PI-3,4-P_2 from PI-4,5-P_2.
29. In order to cut on the volume of scintillation fluid used per sample, we often opt to start detection after 45 min into the gradient, just before PI-3-P elutes. This can only be done if you opt to use the total counts, rather than the PI counts, for normalization.

Acknowledgements

This work was supported by the NIH-NIDDK grant # RO1-DK63219-06 (L.E.R.). The content does not necessarily reflect the position or the policy of the United States Government, and no official endorsement should be inferred.

References

1. Di Paolo G, De Camilli P (2006) Phosphoinositides in cell regulation and membrane dynamics. Nature 443(7112):651–657
2. De Matteis MA, Godi A (2004) PI-loting membrane traffic. Nat Cell Biol 6(6):487–492
3. Downes CP, Gray A, Lucocq JM (2005) Probing phosphoinositide functions in signaling and membrane trafficking. Trends Cell Biol 15(5):259–268
4. Hammond GR, Schiavo G, Irvine RF (2009) Immunocytochemical techniques reveal multiple, distinct cellular pools of PtdIns4P and PtdIns(4,5)P(2). Biochem J 422(1): 23–35
5. Balla T (2005) Inositol-lipid binding motifs: signal integrators through protein-lipid and protein-protein interactions. J Cell Sci 118(Pt 10):2093–2104

6. Carlton JG, Cullen PJ (2005) Coincidence detection in phosphoinositide signaling. Trends Cell Biol 15(10):540–547
7. Higgins JA, Graham JM (1997) Membrane analysis. The introduction to biotechniques. Bios Scientific Publishers, New York
8. Patki V, Virbasius J, Lane WS, Toh BH, Shpetner HS, Corvera S (1997) Identification of an early endosomal protein regulated by phosphatidylinositol 3-kinase. Proc Natl Acad Sci U S A 94(14):7326–7330
9. Sarkes D, Rameh LE (2010) A novel HPLC-based approach makes possible the spatial characterization of cellular PtdIns5P and other phosphoinositides. Biochem J 428(3):375–384

Chapter 19

Single-Molecule Imaging of Signal Transduction via GPI-Anchored Receptors

Kenichi G.N. Suzuki

Abstract

Lipid rafts have been drawing extensive attention as a signaling platform. To investigate molecular interactions in lipid rafts, we often need to observe molecules in the plasma membranes of living cells because chemical fixation and subsequent immunostaining with divalent or multivalent antibodies may change the location of the target molecules. In this chapter, we describe how to examine dynamics of raft-associated glycosylphosphatidylinositol (GPI)-anchored receptors and interactions of the receptors with downstream signaling molecules by single-particle tracking or single-molecule imaging techniques.

Key words Single-particle tracking, Single-molecule imaging, GPI-anchored protein, Rafts, Colocalization, Temporal confinement, Src family kinase, PLCγ, IP_3, Calcium

1 Introduction

Lipid rafts in cell plasma membranes have been drawing extensive attention as a platform where glycosylphosphatidylinositol (GPI)-anchored receptors, glycosphingolipids, cholesterol, and lipid-anchored signaling molecules such as Src family kinases and G-proteins are assembled and activated [1]. Lipid rafts have been defined operationally in terms of their detergent-resistant insolubility in cold Triton X-100 treatment [2]. However, Triton X-100 induces domain formation in lipid raft mixtures [3], and a more recent study showed that Triton X-100 induced phase separation in the previously homogeneous membrane of giant unilamellar vesicles of erythrocyte membrane lipids [4], which further complicates the definition of lipid rafts. Although characterization by detergent insolubility is still useful and may help us to predict the association preference of specific membrane molecules to rafts, we should keep in mind that the insoluble fraction is created by the detergent treatment.

Mark G. Waugh (ed.), *Lipid Signaling Protocols*, Methods in Molecular Biology, vol. 1376,
DOI 10.1007/978-1-4939-3170-5_19,

To examine the location of raft-associated molecules in plasma membranes, immunoelectron and immunofluorescence microscopy is frequently used. These methods usually contain a fixation step using 1–4 % paraformaldehyde. However, lipid-anchored proteins such as GPI-anchored proteins and Src family kinases are easily cross-linked by antibodies even after the fixation procedure [5]. For example, about half of GPI-anchored proteins, in which the ecto-protein domain is Halo-tagged, are still mobile and easily cross-linked by antibodies even after fixation with 4 % paraformaldehyde for 90 min [5]. Tanaka et al. found that 80 % of lipid-anchored proteins could be fixed after treating cells with 4 % paraformaldehyde and 0.2 % glutaraldehyde at 25 °C for 30 min or longer, yet up to 20 % of the molecules could still be cross-linked by antibodies. Tanaka et al. recommended that for fluorescence microscopy, it would be better to observe live cells using fluorescent protein-conjugated molecules or monovalent fluorescent probes.

Obviating the limitations incurred through fixation steps, single-molecule imaging is a powerful tool to observe molecular events that transiently or only rarely occur. In particular, dual-color observation of two different kinds of single molecules allows us to observe molecular interactions within plasma membranes. For example, dual-color single-molecule imaging revealed that the GPI-anchored receptor CD59 formed transient (~160 ms) homodimers, which are induced by ecto-protein domain interactions and stabilized by raft-lipid interactions [6]. Upon ligation, CD59 formed stable homooligomers, which repeatedly underwent stimulation-induced Temporal Arrest of LateraL diffusion (STALL) [7, 8], which is induced by the activity of Src family kinase and binding of actin filament [9, 10] and stabilized by cholesterol. Just before STALL periods, lipid-anchored signaling molecules such as G-protein (Gαi2) and Src family kinase (Lyn) were transiently (0.1–0.2 s) recruited to the stable CD59 homooligomers [7], and the activation of these signaling molecules further induced the transient (~0.25 s) recruitment of PLCγ2 to STALL sites. PLCγ2 molecules produced 20–50 IP_3 molecules during each recruitment period, inducing the intracellular Ca^{2+} response [8]. The pulse-like signaling of PLCγ2 may easily maintain a stable level in the overall signaling activity [11].

As evidenced by the aforementioned study, single-molecule imaging provides very useful information on signal transduction occurring in rafts of plasma membranes. In this chapter, we describe protocols to induce signal transduction by stimulating CD59 with 40-nm gold particles or fluorescent latex beads coated with anti-CD59 IgG antibody, or by providing CD59 ligand to cells. Furthermore, we also explain how the dynamic behavior of CD59,

especially the STALL events in plasma membranes, are correlated with the downstream signaling events such as recruitment of Gαi2, Lyn, and PLCγ2, IP_3 production, and intracellular Ca^{2+} mobilization. The methodology described here would be also applicable to the study of signaling mediated by other GPI-anchored receptors within rafts.

2 Materials

2.1 Preparation of Gold Particles and Latex Beads for Stimulating CD59

1. Gold particles: 40 nm in diameter.
2. Yellow-green or dark-red latex beads: 40 nm in diameter.
3. Washing buffer: Carbowax 20 M in 2 mM phosphate buffer (pH 7.2). Prepare 2 mM phosphate buffer (pH 7.2) by mixing 1/15 M KH_2PO_4 with 1/15 M Na_2HPO_4, adjusting the pH to 7.2, and diluting the mixture with Milli-Q water. Filter 2 mM phosphate buffer with a 0.22 μm filter to remove contaminants which induce aggregation of gold particles and latex beads.
4. Observation buffer: Carbowax 20 M in Hanks' balanced salt solution buffered with 2 mM PIPES, pH 7.2. Filter HBSS with a 0.22 μm filter as well.

2.2 Drug Treatments

1. Partial cholesterol depletion: 4 mM methyl-β-cyclodextrin (MβCD) in HBSS.
2. Partial actin depolymerization: 50 nM latrunculin B in HBSS.
3. Inhibition of activity of Src family kinases: 10 μM PP2 in HBSS.
4. Inhibition of activity of Gαi2: 1.7 nM pertussis toxin in HBSS.

2.3 Labeling of Halo7-Tagged Signaling Molecules with Fluorophores

1. Prepare commercially available rhodamine G110 (R110) or tetramethylrhodamine (TMR)-conjugated ligand for the Halo7 tag.
2. Prepare 50 nM fluorescent ligand solution in cell culture medium.

2.4 cDNA Construction of Vectors for the Expression of Tagged Signaling Molecules

1. Vector: Epstein-Barr virus (EBV)-based episomal vector pOsTet15T3, which carries the components of the tetracycline-regulated expression system, including the transactivator (rtTA2-M2) and the TetO sequence (a Tet-on vector) [6, 12].
2. Subcloning of tagged signaling molecule fusion proteins: Insert cDNA sequences that encode monomeric GFP (A206K) or Halo7 tags for expression of N- or C-terminal tagged signaling molecules.

3 Methods

3.1 Preparation of Gold Particles Coated with Antibodies Directed Against GPI-Anchored Receptors

1. Centrifuge at 100 × *g* for 10 min to remove clumped particles.
2. Mix a fivefold minimal protecting amount (MPA) of IgG antibody directed against the GPI-anchored receptor of interest, such as CD59, with the gold particles (40 nm in diameter). In the specific case of anti-CD59 IgG, the MPA is 2.5 μg/ml (*see* **Note 1**).
3. Incubate the mixture of the antibody and the gold particles on a slowly tumbling shaker at room temperature for 60 min.
4. Stabilize the gold particles by addition of Carbowax 20 M to a final concentration of 0.03 % and resume incubation for an additional 15 min.
5. Wash the gold particles by sedimentation (17,400 × *g* for 10 min) and resuspension in 0.03 % Carbowax 20 M in 2 mM phosphate washing buffer 3 times and then resuspend them in HBSS containing 0.03 % Carbowax 20 M (Observation buffer). Use the gold particles within 6 h.

3.2 Preparation of Gold Particles Coated with the Fab Fragment of Antibodies Directed Against GPI-Anchored Receptors

1. Centrifuge at 100 × *g* for 10 min to remove clumped particles
2. Mix small amounts of the Fab fragment of IgG antibody against the GPI-anchored receptor of interest with 40-nm gold particles (*see* **Note 2**). In the specific case of the Fab fragment of anti-CD59 IgG antibody, the final concentration of the Fab fragment in the mixture is one third of the MPA, or 0.8 μg/ml.
3. Incubate the mixture of the Fab fragment and gold particles on a slowly tumbling shaker at room temperature for 60 min. Stabilize and wash the Fab-coated gold particle mixture as described above in the preparation of the IgG-coated gold particle mixture (*see* **Note 3**).

3.3 Preparation of 40-nm Yellow-Green or Dark-Red Fluorescent Latex Beads Coated with Antibodies Directed Against GPI-Anchored Receptors

1. Centrifuge at 2400 × *g* for 10 min to remove clumped particles.
2. Mix 6 μl of the 40-nm (diameter) yellow-green or dark-red fluorescent latex beads with 1 μl (2.1 mg/ml) of IgG antibody against GPI-anchored receptors, as well as 3 μl (1.25 mg/ml) of nonspecific IgG antibody, and adjust the total volume to 200 μl with 2 mM phosphate buffer (*see* **Note 4**).
3. Incubate the mixture on a slowly tumbling shaker at 4 °C for 4 h. Stabilize the beads by adding Carbowax 20 M to a final concentration of 0.02 % and resume incubation for 15 min.
4. Washing by alternate sedimentation (100,000 × *g* for 15 min) and resuspension in 0.02 % Carbowax 20 M in 2 mM phosphate washing buffer for 3 times and then resuspend the beads in HBSS containing 0.02 % Carbowax 20 M (Observation buffer). Use the beads within 8 h.

3.4 Stimulation of Cells with Antibody-Coated 40-nm Gold Particles or 40-nm Yellow-Green or Dark-Red Fluorescent Latex Beads

1. Trypsinize ECV304 (T24) cells cultivated in a 6-cm dish, seed the cells on coverslips (4×10^3 cells/coverslip), and grow the cells for 18–30 h before each experiment. Use cells at about the same level of confluency (~10 %) for every experiment because the diffusion coefficient of ECV304 (T24) cell membranes depends on the confluency level (the macroscopic diffusion coefficient for CD59 was twofold larger in the membranes of confluent cells).
2. Add 40-nm IgG-coated gold particles or 40-nm IgG-coated yellow-green or dark-red fluorescent latex beads to the cells at a final concentration of 1.8×10^{10} particles/ml. This optimal concentration is sufficiently high enough to induce robust intracellular signaling responses yet sufficiently low enough not to interfere with the single-particle tracking, which may be disrupted if two particles on the cell surface come into close proximity with one another. The 40-nm IgG-coated gold particles or 40-nm IgG-coated fluorescent latex beads cross-link about 3–6 CD59 molecules (Fig. 1). Cross-linking of CD59 induces signaling events that are very similar to those initiated by the addition of the ligand C8 [7, 8, 13].
3. In case of CD59 stimulation with C8, add a mixture of 40-nm Fab fragment-coated gold particles to the cells at a final concentration of 1.8×10^{10} particles/ml, 8.3 μg/ml of free Fab fragment (which is not bound to gold particles, *see* **Note 5**), and C8 of a cytolytic membrane attack complex unit of 1000 (Fig. 1).

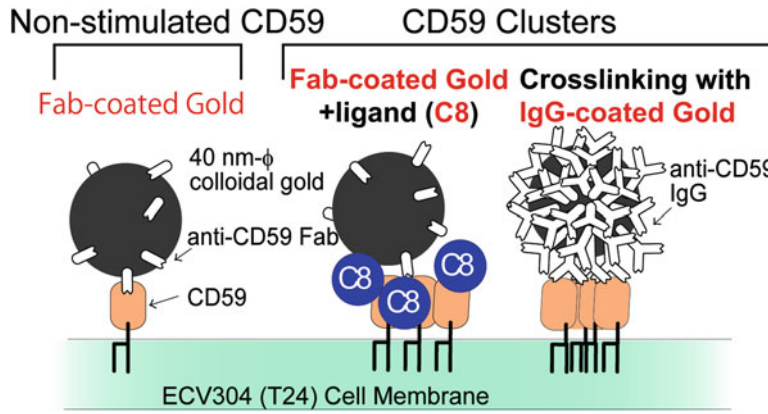

Fig. 1 Gold particles or fluorescent latex beads to induce CD59 clustering. Non-stimulated CD59 is observed with 40-nm diameter gold particles coated with small amounts of anti-CD59 Fab fragments (Fab-coated Gold). To inhibit multivalent binding, free Fab fragment should be included in the observation buffer. To observe CD59 upon stimulation, CD59 is first tagged with a Fab-coated gold particle and then the ligand (C8) is added, or CD59 is cross-linked by 40-nm gold particles or latex beads conjugated with anti-CD59 IgG antibody (IgG-coated Gold, IgG-coated Bead) [7]

3.5 Single-Particle Tracking of Gold Particles and Fluorescent Latex Beads and Detection of Stimulation-Induced Temporal Arrest of LateraL Diffusion (STALL)

1. For single-particle tracking of the gold particles, observe the particles attached to the apical/dorsal membrane at 33-ms resolution (video rate), using a microscope equipped with a 100× 1.4 NA objective lens and a CCD camera [14, 15].
2. For single-fluorescent particle tracking of the latex beads, observe the beads attached to the apical/dorsal membrane at 33-ms resolution (video rate), using objective lens-type, TIRF microscope equipped with a 100× 1.49 NA objective lens and an image intensifier coupled with a sCMOS camera. Use oblique angle illumination to observe the beads on the apical membrane.
3. Estimate the accuracy of the position determinations for stationary probes from the standard deviations of the determined coordinates of the probes fixed on poly-L-lysine-coated coverslips immersed in a 10 % polyacrylamide gel (*see* **Note 6**).
4. Detect STALL events of the 40-nm gold particles or the 40-nm fluorescent latex beads recorded at a video rate (33-ms resolution) for a period of 10 s [16] (*see* **Note 7**). The length of the trajectories for the analysis has no influence on the estimated parameters, as long as it is >5 s.
5. Observe the STALL events of the gold particles or the beads after cholesterol depletion with 4 mM MβCD treatment (30 min), actin depolymerization with 50 nM latrunculin B (10 min), inhibition of Src family kinase with 10 μM PP2 (5 min), or inhibition of Gαi2 with 1.7 nM pertussis toxin (22 h).

3.6 Observation of IP_3 Production in Relation to STALL Events

1. Transfect ECV304 (T24) cells with cDNA (vector; pEGFP) encoding the PH domain of PLCδ fused to GFP at the C-terminus [17] in a 6-cm dish. The PH domain binds to both IP_3, which is located in the cytoplasm, and PIP_2, which is located on the inner leaflet of the plasma membrane. Upon binding to CD59, PLCγ hydrolyzes membrane-bound PIP_2 to generate IP_3, and thus the cytoplasmic IP_3 concentration increases.
2. Cultivate the transfected cells in Ham's F12 medium supplemented with 10 % (v/v) FBS for 24 h. After cultivation, trypsinize the transfected cells, seed the cells on a glass-based dish (4×10^3 cells/dish), and grow the cells for 18–30 h before each experiment.
3. Wash the cells with HBSS twice and then cover the washed cells with fresh HBSS.
4. Add 40-nm IgG-coated gold particles or 40-nm dark-red fluorescent latex beads to the cells to a final concentration of 1.8×10^{10} particles/ml.
5. Observe the distribution of the PH-GFP fusion protein with a fluorescence microscope equipped with a spinning-disc confocal scanner system. Detect the relative increase of the fluores-

cence signal of PH-GFP in the cytoplasm versus that in the plasma membrane [8, 18].

6. Observe the distribution of PH-GFP after cholesterol depletion, actin depolymerization, inhibition of Src family kinase, or inhibition of Gαi2, and examine correlation between occurrences of STALL events and IP_3 signaling.

3.7 Fluorescence Imaging of Ca^{2+} Mobilization in Living Cells in Relation to STALL Events

1. Incubate ECV304 (T24) cells in HBSS containing 5 μM fluo-8 AM for 30 min.
2. Wash cells twice with HBSS and incubate with the IgG—coated gold particles or Fab-coated gold particles and C8, or with the IgG-coated dark-red beads.
3. Obtain fluorescence images of fluo-8 by epi-fluorescence microscopy.
4. Observe Ca^{2+} mobilization after cholesterol depletion, actin depolymerization, inhibition of Src family kinase, or inhibition of Gαi2, and examine correlation between occurrences of STALL events and Ca^{2+} response.

3.8 Expression and Fluorescent Labeling of Signaling Molecules in Cell Membranes for Dual-Color Observations

1. Transfect ECV304 (T24) cells with cDNA (vector; pOsTet15T3) encoding signaling molecules (e.g., Gαi2, Src family kinase, PLCγ2) tagged with monomeric GFP (A206K) or Halo7 in a 6-cm dish.
2. Culture the transfected cells in Ham's F12 medium supplemented with 10 % (v/v) FBS for 24 h. Trypsinize the transfected cells, seed the cells on coverslips or glass-based dishes (4×10^3 cells/coverslip), and grow the cells for 18–30 h before each experiment.
3. For observation of signaling molecules tagged with Halo7, incubate cells with Halo7 fluorescent ligand in the cell culture medium. Specifically, incubate cells with Halo7 ligand conjugated with 50 nM TMR for 15 min or 50 nM R110 for more than 120 min at 37 °C and 5 % CO_2 (*see* **Note 8**). Wash the cells with the cell culture medium 3 times, and incubate the cells in the cell culture medium at 37 °C and 5 % CO_2 for 30 min.
4. Wash the cells with cell culture medium twice, and add HBSS to the coverslips or the glass-based dishes for single-molecule observation.

3.9 Simultaneous Dual-Color Observation of CD59 Clusters Underneath 40-nm Fluorescent Latex Beads and Signaling Molecules

1. Using TIRF microscopy, simultaneously observe ECV304 (T24) cells expressing low amounts of signaling molecules (e.g., Gαi2, Src family kinase, PLCγ2) conjugated with fluorophores via Halo7 or mGFP fusion tags and 40-nm fluorescent beads which crosslink CD59 on the plasma membranes (*see* **Note 9**). For detailed instructions regarding TIRF microscopy, *see* ref. 12. Use dark-red or yellow-green beads when signaling molecules are labeled with R110 or TMR, respectively.

2. Define colocalization of a fluorescent signaling molecule and a fluorescent bead (a CD59 cluster) when they become located within 240 nm of each other [12]. The probability of finding two molecules located at exactly the same coordinates within a distance x in the images increases with an increase in x, and with the localization precision of single particles, the probability of finding these bound particles within 240 nm is greater than 99 %.
3. Examine the relationship between the timing of colocalization of signaling molecules with CD59 and that of STALL events of CD59 clusters (*see* **Note 10**).

4 Notes

1. The concentration of IgG antibody should be optimized. When the concentration of IgG antibody on the gold particles is too high, the IgG antibody tends to release from the gold particles after the preparation, then bind to the target proteins in the plasma membranes. This interferes with the ability of the gold particles to cross-link the proteins and trigger signal transduction.
2. We do not use 40-nm fluorescent latex beads that are coated with Fab fragments of IgG antibody to monovalently label GPI-anchored receptors.
3. We optimized the concentration of Carbowax to maximize the signal-transducing activity of the Fab fragment. It is usually easier to prepare gold particles coated with the Fab fragments from a monoclonal antibody rather than from a polyclonal antibody, since gold particles coated with the Fab fragment of a polyclonal antibody sometimes tend to aggregate.
4. Nonspecific IgG antibodies are mixed with antibodies against GPI-anchored receptors to decrease the number of GPI-anchored receptors bound to the beads. Extensively cross-linked GPI-anchored receptors tend to be immobilized, while liganded GPI-anchored receptors diffuse slowly (diffusion coefficient is ~0.02 $\mu m^2/s$), with 3–6 receptors in a typical cluster [7]. Therefore, we aimed to cluster 3–6 receptors underneath each of the IgG-coated gold particles.
5. Free Fab fragments should be added with Fab-coated gold particles to inhibit multivalent binding of the gold particles to CD59.
6. For the ATTO488, ATTO594, TMR, Cy3, and ATTO647N probes recorded at a video rate, the localization precisions of single molecules are ±17, ±12, ±17, ±17, and ±14 nm, respectively.

7. The temporal confinement of GPI-anchored clusters can be also detected by the method developed by Sahl et al. [19].
8. The incubation period of cells with R110 should be longer than that with TMR because TMR penetrates through plasma membranes more easily than R110. The density of the fluorescent spots should be lower than 2 molecules/μm² because higher spot densities interfere with tracking of the single molecules. If the density of the fluorescent spots is too high, decrease the dye concentration.
9. For dual-color observation of CD59 clusters and single signaling molecules, 40-nm yellow-green or dark-red fluorescent latex beads are used because gold particles give signals that cannot be separated from the fluorescence signals [7, 8].
10. Periods of colocalization between CD59 clusters and signaling molecules (e.g., Gαi2, Lyn, and PLCγ2) are very short (0.1–0.2 s). Furthermore, STALL behavior of CD59 clusters also transiently occurs (~0.6 s). Single molecules of Gαi2 were recruited to CD59 clusters just before the STALL events, while single molecules of Lyn randomly recruited to the clusters. Interestingly, single molecules of PLCγ2 were recruited only during the STALL events, as shown in Fig. 2.

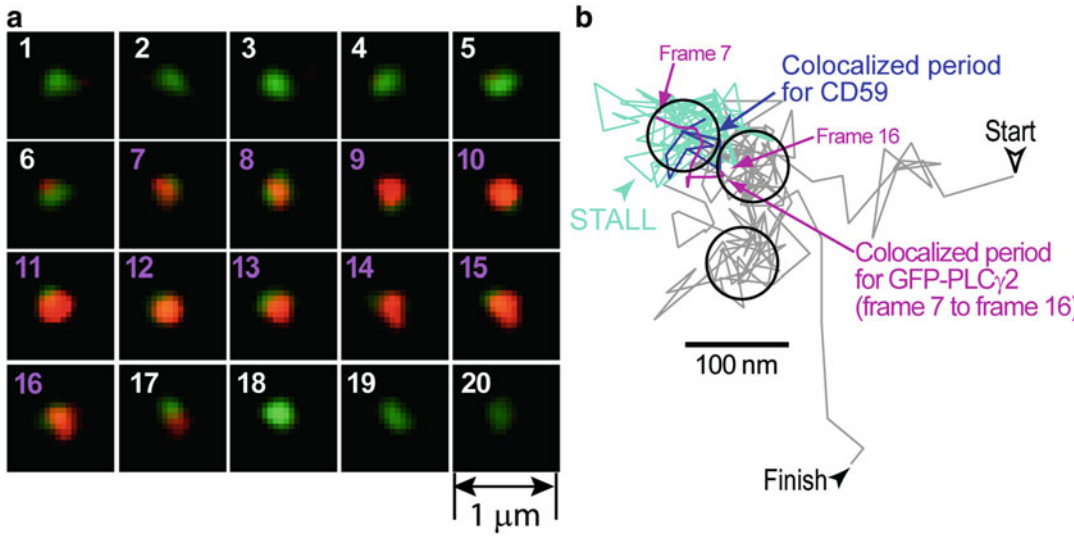

Fig. 2 Simultaneous observation of GFP-PLCγ2 and CD59 clusters (IgG-Bead). (**a**) An image sequence of simultaneous observation of a CD59 cluster and a single molecule of GFP-PLCγ2. They are colocalized from frame 7 to 16, which are within a STALL period. GFP-PLCγ2 suddenly appears and then returns to the cytoplasm [8]. (**b**) A typical trajectory of a CD59 cluster, which includes 3 STALL periods (*three circles*). During one of the STALL periods (indicated by a *circle* in the *top-left*) a GFP-PLCγ2 molecule is recruited to the CD59 cluster. The colocalization period is included within the STALL period

Acknowledgement

This work was supported in part by Grants-in-Aid for Specific Research (B) (No. 24370055) and by Innovative Areas (No. 2311002) from the Ministry of Education, Culture, Sports, Science, and Technology of Japan.

References

1. Simons K, Ikonen E (1997) Functional rafts in cell membranes. Nature 387:569–572
2. Brown DA, Rose JK (1992) Sorting of GPI-anchored proteins to glycolipid-enriched membrane subdomains during transport to the apical cell surface. Cell 68:533–544
3. Heerklotz H (2002) Triton promotes domain formation in lipid raft mixtures. Biophys J 83:2693–2701
4. Casadei BR, Domingues CC, de Paula E, Riske KA (2014) Direct visualization of the action of Triton X-100 on giant vesicles of erythrocyte membrane lipids. Biophys J 106:2417–2425
5. Tanaka KAK, Suzuki KGN, Shirai YM, Shibutani ST, Miyahara MSH, Tsuboi H et al (2010) Membrane molecules mobile even after chemical fixation. Nat Methods 7:865–866
6. Suzuki KGN, Kasai RS, Hirosawa KM, Nemoto YL, Ishibashi M, Miwa Y et al (2012) Transient GPI-anchored homodimer rafts are units for raft organization and function. Nat Chem Biol 8:774–783
7. Suzuki KGN, Fujiwara TK, Sanematsu F, Iino R, Edidin M, Kusumi A (2007) GPI-anchored receptor clusters transiently recruit Lyn and Gα for temporary cluster immobilization and Lyn activation: single-molecule tracking study 1. J Cell Biol 177:717–730
8. Suzuki KGN, Fujiwara TK, Edidin M, Kusumi A (2007) Dynamic recruitment of phospholipase Cγ at transiently immobilized GPI-anchored receptor clusters induces IP_3-Ca^{2+} signaling: single-molecule tracking study 2. J Cell Biol 177:731–742
9. Suzuki K, Sterba RE, Sheetz MP (2000) Outer membrane monolayer domains from two-dimensional surface scanning resistance measurements. Biophys J 79:448–459
10. Suzuki K, Sheetz MP (2001) Binding of cross-linking glycosylphosphatidylinositol-anchored proteins to discrete actin-associated sites and cholesterol-dependent domains. Biophys J 81:2181–2189
11. Suzuki KGN (2012) Lipid rafts generate digital-like signal transduction in cell plasma membranes. Biotechnol J 7:753–761
12. Suzuki KGN, Kasai RS, Fujiwara TK, Kusumi A (2013) Single-molecule imaging of receptor-receptor interactions. Methods Cell Biol 117:373–390
13. Murray EW, Robbins SM (1998) Antibody cross-linking of the glycosylphosphatidylinositol-linked protein CD59 on hematopoietic cells induces signaling pathways resembling activation by complement. J Biol Chem 273:25279–25284
14. Suzuki K, Ritchie K, Kajikawa E, Fujiwara T, Kusumi A (2005) Rapid hop diffusion of a G-protein-coupled receptor in the plasma membrane as revealed by single-molecule techniques. Biophys J 88:3659–3680
15. Fujiwara T, Ritchie K, Murakoshi H, Jacobson K, Kusumi A (2002) Phospholipids undergo hop diffusion in compartmentalized cell membrane. J Cell Biol 157:1071–1081
16. Simson R, Sheets ED, Jacobson K (1995) Detection of temporary lateral confinement of membrane proteins using single-particle tracking analysis. Biophys J 69:989–993
17. Hirose K, Kadowaki S, Tanabe M, Takeshima H, Iino M (1999) Spatiotemporal dynamics of inositol 1,4,5-triphosphate that underlies complex Ca^{2+} mobilization patterns. Science 284:1527–1530
18. Raucher D, Sheetz MP (2001) Phospholipase C activation by anesthetics decreases membrane-cytoskeleton adhesion. J Cell Sci 114:3759–3766
19. Sahl SJ, Leutenegger M, Hilbert M, Hell SW, Eggeling C (2010) Fast molecular tracking maps nanoscale dynamics of plasma membrane lipids. Proc Natl Acad Sci U S A 107:6829–6834

Chapter 20

Measuring Phosphatidylinositol Generation on Biological Membranes

Mark G. Waugh

Abstract

Phosphatidylinositol (PI) is a phospholipid molecule required for the generation of seven different phosphoinositide lipids which have a diverse range of signaling and trafficking functions. The precise mechanism of phosphatidylinositol supply during receptor activated signaling and the cellular compartmentation of the synthetic process are still incompletely understood and remain controversial despite several decades of research in this area. The synthesis of phosphatidylinositol requires the activity of an enzyme called phosphatidylinositol synthase, also known as CDIPT, which catalyzes a reversible headgroup exchange reaction on its substrate liponucleotide CDP-diacylglycerol resulting in the incorporation of inositol to generate phosphatidylinositol and the release of CMP. This protocol describes a method for locating PI synthase activity in isolated, intact biological membranes and vesicles.

Key words Phosphatidylinositol, CDIPT, Lipid, Endoplasmic reticulum

1 Introduction

The enzyme phosphatidylinositol (PI) synthase (also known as CDIPT or CDP-diacylglycerol--inositol 3-phosphatidyltransferase) [1–3] catalyzes the reversible exchange of inositol for CMP on CDP-DAG [4] resulting in the production of the phospholipid PI which is the crucial upstream precursor for the subsequent kinase- and phosphatase-catalyzed generation of signaling lipids such as PI(4,5)P_2, P(3,4,5)P_3 and PI5P. Eukaryotes express a single PI synthase enzyme [5] which localizes mainly to the endoplasmic reticulum (ER) [6] but pools of the enzyme have also been reported on trafficking vesicles [7] as well as at the plasma membrane [8–10]. The cellular targeting of this enzyme has generated a lot of interest since it is still not clear, despite several decades of research, how a primarily ER-localized enzyme can sense and replenish pools of PI that are depleted following receptor-stimulated phospholipase C activation [11]. Different experimental models have suggested that either PI is transported via transfer

Mark G. Waugh (ed.), *Lipid Signaling Protocols*, Methods in Molecular Biology, vol. 1376,
DOI 10.1007/978-1-4939-3170-5_20,

proteins and presented to PI kinases on other membranes or that PI resynthesis occurs in specialized, low-density vesicles that can traffic to the plasma membrane [7, 12, 13]. Another possible explanation is that specialised ER domains contact the plasma membrane and that lipid transfer can occur across these protein-mediated interorganelle contact sites [6].

There are some indications that PI synthase may be dysfunctional in disease. Increased PI synthase expression has been associated with oral cancer [14] and recent insights gained from studies on zebrafish have linked ablated expression of the enzyme with the development of hepatic steatosis [15] and inflammation of the intestinal mucosa [15]. Additionally in zebrafish, PI synthase expression in the eye is required to maintain particular cell populations [16] including photoreceptor and lens epithelial cells; loss-of-function mutations in this enzyme give rise to the opaque lens or cataract phenotype in this organism [16].

Despite some progress in understanding the physiological and pathological roles of the enzyme there is still a dearth of knowledge concerning how, or even if, PI synthase is regulated and how its activity integrates into the phosphoinositide synthetic pathways known to be important for receptor signaling and intracellular trafficking. The protocol described herein describes a method for assessing PI synthesis on intact membrane vesicles isolated under detergent-free conditions using sucrose density gradients [17, 18]. However, the assay works well with all types of membrane preparations. This method has an advantage in that it allows for an assessment of PI synthase activity in its endogenous membrane environment where potential lipid and protein regulators of the enzyme may reside or be recruited to and this approach has previously been very useful for uncovering the mechanisms regulating PI 4-kinase IIα activity [19–21]. This protocol involves isolating membrane enriched for PI synthase activity and then monitoring the incorporation of radiolabeled inositol into membrane associated CDP-DAG to form [^{3}H]PI which can then be detected and measured by liquid scintillation counting.

The membrane isolation step in this procedure takes about a day to complete while the assay and downstream analyses usually occurs on the following day, although membrane samples can also be frozen and analyzed on a later date.

2 Materials

The water used for making up buffers is highly purified and deionized. Personal protective equipment and access to a fume hood are necessary for preparing the lipid extraction and chromatography buffers requiring the use of solvents and strong acids. Radioactive inositol is used as substrate for the phosphatidylinositol synthase

reaction and most institutions will have policies in place covering the use of unsealed radioisotopes that may have to be taken into consideration when setting up these experiments.

2.1 Membrane Isolation Materials

1. Phosphate-buffered saline (PBS) with Ca^{2+} and Mg^{2+}, pH 7.4. This should be pre-chilled on ice for at least 30 min before commencing the experiment.
2. TE buffer: 1 mM EGTA, 1 mM EDTA, 10 mM Tris–HCl, pH 7.4.
3. Carbonate buffer: 100 mM Na_2CO_3, pH 11.0 and 1 protease inhibitor tablet (Complete™ Roche) added per 10 ml. This buffer is used for cell lysis; it is freshly prepared before each experiment and placed on ice about 30 min before starting the cell harvesting step.
4. Sucrose solutions of varying densities: These are required for membrane isolation on discontinuous sucrose density gradients. These prepared by adding the desired weight of sucrose to the 50 ml falcon tubes and topping up to 10 ml with TE buffer. The sucrose concentrations required are 80 % w/v, 35 % w/v, and 5 % w/v of sucrose dissolved in TE buffer (Please *see* **Note 1**).
5. A probe ultrasonicator for the cell disruption step. In our laboratory we use a Sonics vibracell ultrasonics processor.
6. 12 ml polycarbonate ultracentrifuge tubes.
7. A supply of ice.
8. Access to a swing-out rotor such and ultracentrifuge, for example an SW41 Ti Beckman rotor and Beckman Coulter Optima™ LE80-K ultracentrifuge.
9. Liquid scintillation counter.
10. Solvent-resistant scintillation vials.
11. Bench-top vortexer.
12. 50 ml polypropylene conical tubes.
13. 5 ml polystyrene round-bottomed tubes.

2.2 PI Synthase Assay Reagents

1. Assay buffer: 20 mM Tris–HCl pH 7.4, 20 mM $MgCl_2$, 1 mM EGTA and 1 mM CTP containing 1–2 μCi/tube [^{3}H] myo-inositol ([^{3}H] myo-inositol with a specific activity of >60 Ci/mmol can be purchased from Perkin Elmer). This is usually prepared just before use, although stock solutions of 10 mM unlabeled CTP can be stored immediately after preparation for up to a month at –20 °C. A high concentration of unlabeled CTP is included to enable the liponucleotide substrate CDP-DAG to be produced by membrane-associated CDP-DAG synthase activity from endogenous phosphatidic acid.

2. Chloroform.
3. HCl 1 M.
4. Lipid organic extraction buffer: This consists of chloroform:methanol:1 M HCl prepared in the ratio 60:36:4 and methanol:HCl 1:1. The ratios refer to the volume of each component of the buffer and it is important they be added in the order listed and with constant mixing. Usually 100 ml of this buffer is prepared as it can be stored for up to a week at room temperature in a glass bottle with a glass stopper.

3 Isolation of a Low Buoyant Density Membrane Preparation

1. Cells such as A431 or Hela care grown on 100 mm tissue culture dishes. For this preparation at least one confluent plate of cells is required but up to six plates can be combined per ultracentrifugation tube.
2. Place cell culture dish on a tray of ice.
3. Rapidly aspirate off all of the culture medium.
4. Wash the cell monolayer twice with 20 ml of ice-cold PBS making sure that the PBS is completely removed at the end of each wash.
5. Add 2 ml of carbonate buffer to lyse the cells. Agitate the plate to ensure that the entire cell monolayers come into contact with the carbonate buffer.
6. Using a plastic cell lifter scrape all the cells from the culture dish into the carbonate buffer. If more than one dish cells is to be used, this 2 ml carbonate cell lysate can be kept on ice and used to harvest cells from subsequent dishes. This latter technique concentrates the amount of membrane present facilitating easier downstream detection of enzyme activity.
7. The cell lysate (2 ml) is transferred to a 5 ml polystyrene round-bottomed tube. These lysates are usually viscous due to nuclear lysis and the release of DNA. The 5 ml tube is then stood securely in the middle of a 200 ml plastic beaker that has been half-filled with ice.
8. The carbonate cell lysate is disrupted by sonication by 6×5-s blasts at an amplitude setting of 40, using a Sonics vibracell ultrasonics processor in pulsed mode or equivalent settings when using another apparatus. The sonication probe is placed approximately halfway down the tube in the middle of the cell lysate to minimize foaming. If a small amount of foaming does occur it tends to subside in minutes and does not have a noticeable negative impact to on subsequent analyses. Adjust the sample volume if necessary to 2 ml with TE buffer.

9. Add the sonicated cell lysate to the bottom of a 12 ml polycarbonate ultracentrifuge tube. Add 2 ml of 80 % sucrose w/v solution by pipetting directly into the sonicated cell lysate and not down the side of the tube. Pipette up and down slowly several times to mix thoroughly.
10. Layer on 4 ml of 35 % w/v sucrose solution, 1 ml at a time using a pipette. It is very important to add the sucrose slowly and to avoid mixing with the 40 % sucrose layer at the bottom of the tube.
11. Add 4 ml of 5 % w/v sucrose solution slowly on top of the 35 % sucrose w/v layer. It is important that the ultracentrifuge tube is filled to within with 5 mm of the top; otherwise the tube may collapse inwards during the ultracentrifugation step. As the tubes must be balanced for ultracentrifugation another ultracentrifuge tube should be filled in an identical manner with either another sonicated cell sample or 2 ml of carbonate buffer and the gradient prepared exactly as detailed here for the sample-containing tube.
12. Carefully transfer the sample-containing tube to the swing-out rotor bucket and centrifuge for a minimum of 4 h but usually overnight 4 °C at 175,000 × *g*.
13. After centrifugation has ceased, the ultracentrifuge tubes are removed and placed securely and vertically in an ice bucket. A turbid white or opaque membrane band situated between the 5 and 35 % sucrose layers can sometimes be visible at this point in the preparation.
14. To harvest the subcellular fractions a 1 ml pipette is used to slowly decant off 12 × 1 ml fractions beginning at the top of the sucrose gradient. Note that the volume of the ultracentrifuge tubes tends to be slightly greater than 12 ml which means that fraction 12, the last to be collected, will often be more than 1 ml in volume (please *see* **Note 2**).
15. The fractions that contain ER-derived low buoyant density membranes enriched for PI synthase activity usually peak in fractions 5 and 6 of the gradient which corresponds to the interface between the 5 and 35 % w/v sucrose layers (Fig. 1). The subcellular fractions can be used immediately or alternatively they can be aliquoted and stored for later use at −20 °C. Note that these membranes also contain low-buoyant density membrane fragments from other cellular membrane and organelles (please *see* **Note 3**).

3.1 PI Synthase Assay

1. Initiate the PI synthase assay by gently mixing equal volumes of membrane sample (50 µl) with 50 µl assay buffer in a 1.5 ml polypropylene microcentrifuge tube.
2. Incubate the reaction at 37 °C for 30 min.

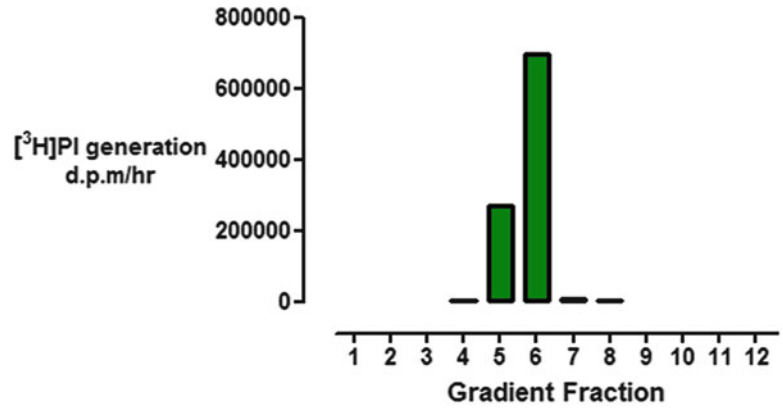

Fig. 1 Typical distribution of [^{3}H]PI generation activity in the sucrose density gradient fractions. The peak activity is located at the interface of the 5 and 35 % w/v sucrose layers which correspond to gradient fractions 5 and 6

3. Terminate reaction by the addition of 100 μl of chloroform:methanol:1 M HCl (60:36:4).
4. Centrifuge tubes for 2000 r.p.m. for 10 s to aid phase separation.
5. Remove 50 μl from the lower organic phase which contains the phosphatidylinositol product to a fresh tube. Unincorporated [^{3}H]-inositol should partition into the top aqueous phase.
6. Add 100 μl of methanol:HCl.
7. Centrifuge tubes for 2,000 r.p.m. for 10 s to repeat phase separation step. This is done to minimize carryover of any free radiolabeled inositol into the organic phase.
8. Remove 30 μl of the organic lower chloroform phase and remove to a solvent resistant scintillation vial.
9. Allow to dry in a fume hood. As only a small organic sample volume is present it only takes a few minutes for the chloroform to evaporate.
10. Add scintillation fluid, close the vial securely, and vortex to resuspend lipid.
11. Determine the amount of [^{3}H]PI present using a scintillation counter.

4 Notes

1. It can be difficult to prepare the 80 % w/v sucrose solution which for example involves dissolving 8 g of sucrose in TE buffer to give a final volume of 10 ml. This solubility issue can be overcome by adding the sucrose to 50 ml polypropylene conical

tube and then topping up with TE buffer to the 10 ml mark on the tube. The tube is then placed horizontally on a rocking platform with gentle movement for about 15 min during which time the sucrose will slowly dissolve.

2. The sucrose density profile of the gradients can be measured using a refractometer and by converting the refractive index measurements obtained to sucrose concentrations using standard Blix tables. Often experimental variability in these types of preparations is due to differences in the gradient sucrose density profile.
3. As well as ER membranes, fractions 5 and 6 also contain low-buoyant-density membrane vesicles enriched for lipid raft proteins such as caveolin. The presence of ER membranes can be confirmed by western blotting for calnexin—an ER-resident protein or for phosphatidylinositol synthase. Western blotting for phosphatidylinositol synthase also facilitates an estimate of the apparent specific activity of the enzyme in each subcellular fraction by relating the mass of enzyme present to the rate of [^{3}H]PI generation. A more accurate determination of the enzymatic properties requires detergent solubilization of the membranes and the addition of CDP-DAG substrate the assay buffer in order to offset potential liponucleotide substrate variations and limitations in the different gradient fractions. For these purposes the PI synthase assay buffer needs to be modified by the addition of 0.3 % v/v TX-100 detergent and 0.4 mM CDP-DAG [22]. The liponucleotide substrate is prepared by dissolving the CDP-DAG in chloroform which is then evaporated off under a steady stream of nitrogen. H_2O is added to a final concentration of 4 mM and the CDP-DAG is then dispersed into solution by probe sonication.

Acknowledgements

MGW acknowledges financial support from the Royal Free Charity.

References

1. Antonsson B (1997) Phosphatidylinositol synthase from mammalian tissues. Biochim Biophys Acta 1348:179–186
2. Antonsson BE (1994) Purification and characterization of phosphatidylinositol synthase from human placenta. Biochem J 297(Pt 3):517–522
3. Monaco ME, Feldman M, Kleinberg DL (1994) Identification of rat liver phosphatidylinositol synthase as a 21 kDa protein. Biochem J 304(Pt 1):301–305
4. Cubitt AB, Gershengorn MC (1990) CMP activates reversal of phosphatidylinositol synthase and base exchange by distinct mechanisms in rat pituitary GH3 cells. Biochem J 272:813–816
5. Lykidis A, Jackson PD, Rock CO, Jackowski S (1997) The role of CDP-diacylglycerol synthetase and phosphatidylinositol synthase activity levels in the regulation of cellular phosphatidylinositol content. J Biol Chem 272: 33402–33409

6. Waugh MG, Minogue S, Clayton EL, Hsuan JJ (2011) CDP-diacylglycerol phospholipid synthesis in detergent-soluble, non-raft, membrane microdomains of the endoplasmic reticulum. J Lipid Res 52:2148–2158
7. Kim YJ, Guzman-Hernandez ML, Balla T (2011) A highly dynamic ER-derived phosphatidylinositol-synthesizing organelle supplies phosphoinositides to cellular membranes. Dev Cell 21:813–824
8. Imai A, Gershengorn MC (1987) Regulation by phosphatidylinositol of rat pituitary plasma membrane and endoplasmic reticulum phosphatidylinositol synthase activities. A mechanism for activation of phosphoinositide resynthesis during cell stimulation. J Biol Chem 262:6457–6459
9. Imai A, Gershengorn MC (1987) Independent phosphatidylinositol synthesis in pituitary plasma membrane and endoplasmic reticulum. Nature 325:726–728
10. Piatti E, Piacentini MP, Fraternale D, Bucchini A, Mangani F, Accorsi A (1999) myo-[3H]-inositol loaded erythrocytes and white ghosts: two models to investigate the phosphatidylinositol synthesis in human red cells. Biochimie 81:1011–1014
11. Claro E, Wallace MA, Fain JN (1992) Concerted CMP-dependent [3H]inositol labeling of phosphoinositides and agonist activation of phospholipase C in rat brain cortical membranes. J Neurochem 58:2155–2161
12. Sillence DJ, Downes CP (1993) Subcellular distribution of agonist-stimulated phosphatidylinositol synthesis in 1321 N1 astrocytoma cells. Biochem J 290(Pt 2):381–387
13. Vaziri C, Downes CP, Macfarlane SC (1993) Direct labelling of hormone-sensitive phosphoinositides by a plasma-membrane-associated PtdIns synthase in turkey erythrocytes. Biochem J 294(Pt 3):793–799
14. Kaur J, Sawhney M, Dattagupta S, Shukla NK, Srivastava A, Ralhan R (2010) Clinical significance of phosphatidyl inositol synthase overexpression in oral cancer. BMC Cancer 10:168
15. Thakur PC, Davison JM, Stuckenholz C, Lu L, Bahary N (2014) Dysregulated phosphatidylinositol signaling promotes endoplasmic-reticulum-stress-mediated intestinal mucosal injury and inflammation in zebrafish. Dis Model Mech 7:93–106
16. Murphy TR, Vihtelic TS, Ile KE, Watson CT, Willer GB, Gregg RG, Bankaitis VA, Hyde DR (2011) Phosphatidylinositol synthase is required for lens structural integrity and photoreceptor cell survival in the zebrafish eye. Exp Eye Res 93:460–474
17. Waugh MG, Hsuan JJ (2009) Preparation of membrane rafts. Methods Mol Biol 462: 403–414
18. Waugh MG, Lawson D, Tan SK, Hsuan JJ (1998) Phosphatidylinositol 4-phosphate synthesis in immunoisolated caveolae-like vesicles and low buoyant density non-caveolar membranes. J Biol Chem 273:17115–17121
19. Waugh MG, Chu KM, Clayton EL, Minogue S, Hsuan JJ (2011) Detergent-free isolation and characterization of cholesterol-rich membrane domains from trans-Golgi network vesicles. J Lipid Res 52:582–589
20. Waugh MG, Minogue S, Blumenkrantz D, Anderson JS, Hsuan JJ (2003) Identification and characterization of differentially active pools of type IIalpha phosphatidylinositol 4-kinase activity in unstimulated A431 cells. Biochem J 376:497–503
21. Minogue S, Chu KM, Westover EJ, Covey DF, Hsuan JJ, Waugh MG (2010) Relationship between phosphatidylinositol 4-phosphate synthesis, membrane organization, and lateral diffusion of PI4KIIalpha at the trans-Golgi network. J Lipid Res 51:2314–2324
22. Carman GM, Fischl AS (1992) Phosphatidylinositol synthase from yeast. Methods Enzymol 209:305–312

Chapter 21

Assay for CDP-Diacylglycerol Generation by CDS in Membrane Fractions

Mark G. Waugh

Abstract

CDP-DAG is a liponucleotide formed by the condensation of CTP with the phospholipid phosphatidic acid in a reaction catalyzed by CDP-DAG synthase (CDS). CDP-DAG is required for the synthesis of phosphatidylinositol; the parent molecule whence all seven phosphoinositides including the signaling molecules PI4P, PI(4,5)P_2, and PI(3,4,5)P_3 are derived. This protocol describes a highly sensitive radiometric assay to detect the generation of CDP-DAG on isolated biological membrane fractions.

Key words CDP-DAG, CDS, Liponucleotide, Assay, Endoplasmic reticulum, Membrane

1 Introduction

Cytidine-diphosphate diacylglycerol (CDP-DAG) is a liponucleotide generated on endoplasmic reticulum membranes [1, 2] by the enzyme CDP-DAG synthase (CDS) [3] which is also known as CDP-DAG synthetase or phosphatidate cytidylyltransferase. CDS catalyzes the condensation of CTP with phosphatidic acid (PA) to form CDP-DAG. This reaction is important for lipid signaling via the receptor-activated phospholipase C and phosphoinositide 3-kinase pathways as the enzyme phosphatidylinositol synthase requires a supply of CDP-DAG to provide the acyl chains used in the production of phosphatidylinositol. In this way CDS activity is required for the resynthesis of phosphatidylinositol and therefore PI(4,5)P_2 required for receptor-stimulated phospholipase C signaling [4]. However, the mechanism through which CDS activity replenishes signalling pools of phosphoinositides is unclear and another report has demonstrated that the overexpression of recombinant CDS in mammalian cells, even in combination with phosphatidylinositol synthase, does not result in an increase in cellular phosphatidylinositol levels [5].

Mark G. Waugh (ed.), *Lipid Signaling Protocols*, Methods in Molecular Biology, vol. 1376,
DOI 10.1007/978-1-4939-3170-5_21,

There are two isoforms of CDS expressed in mammalian cells CDS1 and CDS2 [5–8]. These enzymes both localize to domains of the endoplasmic reticulum and some of these may be closely juxtaposed to the plasma membrane where receptor-stimulated phosphoinositide signaling is initiated [9]. Very recently an enzyme called Tam41 has been identified in Saccharomyces cerevisiae that appears to account for CDP-DAG generation in the mitochondria [1]. While the reactions catalyzed by both CDS enzymes result in the generation of the same CDP-DAG end product, a recent publication has suggested that CDS1 is less restricted in terms of acyl chain preference for its phosphatidic acid substrate than CDS2, and also that both isoforms are negatively regulated by their anionic downstream phosphoinositide products such as $PI(4,5)P_2$ [2].

CDS enzymes are tightly membrane-associated and found across both eukaryotic [10–12] and prokaryotic phylae [3]. The crystal structure of a CDS enzyme from the thermophilic bacterium *Thermotoga maritima* has recently been described [1] and this work has revealed the existence of a funnel-shaped structural feature that enables this enzyme to simultaneously interact with its membrane associated lipid substrate PA and hydrophilic CTP molecules in order to catalyze their condensation to form CDP-DAG.

The assay described here has been designed to detect the generation of CDP-DAG by CDS1 on endoplasmic reticulum membranes using endogenous membrane-associated PA as the lipid substrate. This method monitors the incorporation of radiolabeled CDP into CDP-DAG from α^{32}P-CTP. It is possible to use [^{3}H]-labeled CTP as a low-energy β-emitting substrate (as for example as in ref. 13) but the inclusion of CTP labeled on the α-position with ^{32}P allows for more rapid and sensitive detection of the liponucleotide reaction product. The subcellular fractionation step to isolate membrane fractions enriched for the endoplasmic reticulum typically takes about a day, including an overnight ultracentrifugation step. The radiometric assay is based on the technique originally described by Mok and colleagues [13]. This assay usually takes about 2–3 h to perform and the subsequent separation, detection, and quantification of the radiolabeled CDP-DAG usually takes place over the ensuing 24 h.

2 Materials

Where indicated the H_2O used is highly purified and deionized. This protocol requires the use of strong acids and solvents which require appropriate working practices and areas for safe handling.

Radioactive CTP is used in this method. Most jurisdictions have strict legislation regarding the safe storage, use, and disposal of radioisotopes and this should be taken into account when planning these experiments. All reagents are analytical grade.

2.1 Membrane Isolation Materials

1. Phosphate-buffered saline (PBS) with Ca^{2+} and Mg^{2+}, pH 7.4.
2. TE buffer: 1 mM EGTA, 1 mM EDTA, 10 mM Tris–HCl, pH 7.4.
3. Homogenization buffer: 0.25 M sucrose, 10 mM EGTA, 10 mM EDTA, 10 mM Tris–HCl, pH 7.4, plus 1 protease inhibitor tablet (Roche) per 10 ml.
4. Sucrose solutions of varying densities: These are prepared by adding the desired weight of sucrose to the 50 ml falcon tubes and topping up to 10 ml with TE buffer (Please *see* **Note 1**).
5. 12 ml polycarbonate ultracentrifuge tubes.
6. Access to a swing-out rotor such and ultracentrifuge, for example an SW41 Ti Beckman rotor and Beckman Coulter Optima™ LE80-K ultracentrifuge.

2.2 CDS Assay Reagents

1. Assay buffer: 20 mM Tris–HCl pH 7.4, 40 mM $MgCl_2$, 2 mM EGTA, and 1 mM CTP containing 20 μCi/ml [α^{32}P]CTP (can be purchased from Perkin Elmer). This is usually prepared just before use, although stock solutions of 10 mM unlabeled CTP can be stored immediately after preparation for up to a month at –20 °C.
2. Chloroform.
3. HCl 1 M.
4. Phase extraction reagents: Chloroform:methanol:1 M HCl in the ratio 60:36:4 and methanol:HCl 1:1. The ratios refer to the volume of each component and the reagents should be added in the order listed and with constant mixing.

2.3 Thin-Layer Chromatography Components

1. Thin-layer chromatography (TLC) plates: Silica plates with lane divisions for example Merck Silica60, glass plates without fluorescence indicator are usually used.
2. Oxalate buffer: 1 % w/v potassium oxalate, 20 % v/v methanol, and 1 mM EDTA. This buffer is used for activating TLC plates.
3. TLC acidic resolving buffer: 65:35 propan-1-ol:2 M acetic acid and 1 % 5 M H_3PO_4. This buffer contains highly volatile solvents and should be handled in a fume cabinet.
4. Glass tank for developing TLC plates.
5. Unlabeled, purified CDP-DAG standard. This can be purchased pre-dissolved in chloroform from Avanti Polar lipids.

3 Methods

3.1 Membrane Isolation

1. Adherent mammalian cells such as A431, Cos-7, or Hela cells are cultured at 37 °C in a humidified incubator at 10 % CO_2. Cells are grown in DMEM supplemented with stabilized glutamate, 10 % fetal calf serum, 50 i.u./ml penicillin, and 50 μg/ml streptomycin. For this method 2–4 confluent 150 mm dishes of cells are required.
2. Cell monolayers are harvested by placing the culture dish on a tray of ice; aspirating the cell culture medium and then rinsing the monolayer twice with 30 ml ice-cold PBS.
3. The PBS is removed and 15 ml of ice-cold TE buffer is added for 1 min to induce osmotic swelling. This buffer is quickly removed and replaced with 1 ml of ice-cold homogenization buffer into which the cells are scraped using a plastic cell lifter (please *see* **Note 2**).
4. The cell suspension is removed to a manually operated loose-fitting 2 ml capacity Dounce homogenizer and disrupted by 15 strokes.
5. A post-nuclear supernatant (PNS) is obtained by centrifuging the disrupted cell homogenate at 1,000 × *g* for 5 min in a cooled bench-top centrifuge to pellet unbroken cells and nuclei.
6. The PNS is removed, taking care not to disturb the nuclear pellet fraction and adjusted to 2 ml with homogenization buffer and stored on ice.
7. A 10 ml 20—60 % w/v sucrose gradient is prepared in a 12 ml polycarbonate ultracentrifuge tube by adding 2 ml of 60 % w/v sucrose slowly to the bottom of the tube and then layering on slowly and without mixing 2 ml of 55 % w/v sucrose, 2 ml of 45 % sucrose, 2 ml of 40 % sucrose, 1 ml of 30 % sucrose, and 1 ml of 20 % w/v sucrose (please *see* **Note 3**).
8. The PNS is added to the top of the sucrose gradient and the tube is topped up to the top if necessary with homogenization buffer.
9. The gradient is subjected to a minimum of 4 h but usually overnight ultracentrifugation at 175,000 × *g* using an SW41 Ti swing-out rotor.
10. When centrifugation has stopped the ultracentrifuge tube is slowly removed from the rotor and placed vertically in ice or held securely using a clamp or retort stand.
11. 1 ml gradient fractions are carefully and slowly removed using a 1 ml pipette and by following the meniscus. The gradient fractions can be used immediately or stored at –20 °C for up to

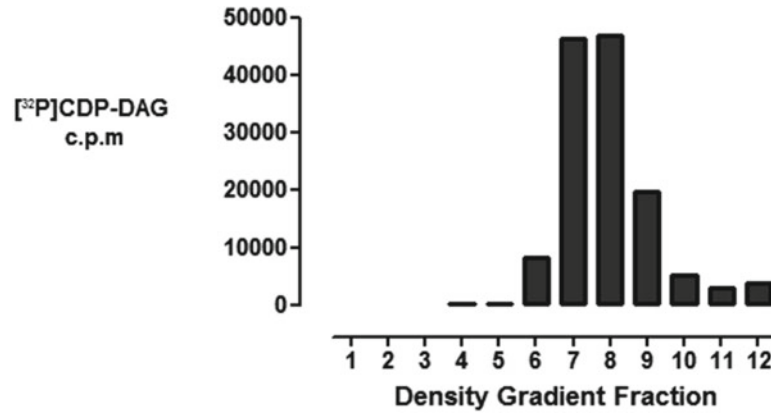

Fig. 1 A typical distribution of [^{32}P]CDP-DAG in the sucrose density gradient fractions. Note that Fraction 1 refers to the first fraction and least dense fraction collected from the top of the ultracentrifuge tube. Fraction 12 is the densest fraction and is located at the bottom of the ultracentrifuge tube. [^{32}P]CDP-DAG peaks in a broad region in the middle of the sucrose density gradient which corresponds to the location of membranes from the endoplasmic reticulum

a year with no noticeable loss in activity as long as there are no repeated cycles of thawing and freezing. The endoplasmic reticulum fraction usually bands between gradient fractions 6 and 9 of the sucrose gradient (Fig. 1) corresponding to a sucrose density of 1.2–1.23 g/ml (please *see* **Note 4**).

3.2 CDS Assay to Detect CDP-DAG Generation

1. To detect CDS activity using endogenous membrane-associated PA as substrate, remove a 50 µl aliquot of membrane sample from the gradient fraction of interest and add to a 1.5 ml non-coated microcentrifuge tube.
2. Add 50 µl of assay buffer and leave for 30 min at room temperature.
3. Stop the reaction by the addition of 100 µl of chloroform:methanol:1 M HCl (60:36:4).
4. Shut the lid of the microcentrifuge tube securely and vortex briefly to mix the phases.

   Spin the tube for 20 s at 1000×*g* at room temperature in a bench-top microfuge.
5. Remove 35 µl of the lower organic phase which contains the CDP-DAG lipid and add to a fresh tube.
6. Add 100 µl of methanol:HCl 1:1. Shut the lid of the tube and vortex briefly gain.
7. Spin the microcentrifuge tube for 20 s at 1000×*g* at room temperature in a bench-top centrifuge.
8. Remove 20 µl from the lower solvent phase. This fraction contains the radiolabeled CDP-DAG (please *see* **Note 5**).

3.3 Separation of the Reaction Products by Thin-Layer Chromatography

1. Activation of TLC plates. This step is necessary to remove ions that could potentially chelate and interfere with the mobility of the CDP-DAG during TLC. Silica 60 TLC plates (Whatman) are dipped for a few seconds in oxalate buffer and then dried in an oven set at 118 °C for 20 min.
2. Using a small-bore pipette tip spot 1 μl aliquots of the solvent-extracted lipid reaction products and CDP-DAG standard on the loading area/origin at a position estimated to be well above the mobile phase. The volume of sample to be loaded can be increased by allowing each spot to dry and by repeating the application step.
3. Place the plate in the TLC tank already containing 1 cm of TLC resolving buffer and permit to develop for at least 5 h or until such time that a minimum of three quarters of the plate has been developed
   Remove the plate from the TLC tank and evaporate residual organic solvent by standing upright supported in a fume hood or more rapidly by using an electric hair dryer. If desired, the position of the unlabeled CDP-DAG standard can be visualized at this point by primulin staining (please *see* **Note 6**). However, in our experience this assay only ever results in a single, mobile radioactive lipid band in each lane following TLC.
4. Wrap the plate securely in cling film or saran wrap and tape to the inside of an X-ray cassette.
   Expose to X-ray film and overlay the TLC plate with the developed film to locate the position of the radioactive CDP-DAG spots
5. Cut the spots out by first wetting the TLC lanes with a small stream of deionized water using a plastic bottle. This softens the silica strips and renders them easier to detach from the plate. The wetted area of interest can subsequently be removed by using a razor blade to slowly scrape along the TLC lane whilst all the time maintaining contact with the backing glass.
6. Place the sample containing the radioactive liponucleotide product into a scintillation vial and count by Cerenkov counting (please *see* **Note 7**) using a scintillation counter.

4 Notes

1. As an example, a 50 % w/v sucrose solution consists of 5 g of sucrose added to a 50 ml tube which is then topped up top 10 ml with TE buffer. The use of the wide 50 ml tube allows for a greater surface area for the sucrose to dissolve and this is

further facilitated by placing the tube horizontally on a rotating or rocking platform.

2. The cell swelling step can be omitted if preferred but usually this leads to an increase in size of the p1000 nuclear fraction suggesting that cell disruption is not as effective under such conditions.
3. It is not absolutely necessary to partially isolate endoplasmic reticulum membranes prior to assaying for CDS activity. The assay works has also been shown to work well with on cell lysates, immunoisolated vesicles, and detergent-resistant membrane fractions [9].
4. It can be useful to western blot the gradient fractions in order to identify the position of the endoplasmic reticulum protein calnexin and also the CDS1 enzyme. Antibodies directed against both proteins that are suitable for this purpose are commercially available [9]. The sucrose concentrations of the gradient can be determined using a handheld refractometer such as the Leica AR200 model and by converting refractive index values to sucrose densities using linear regression and standard conversion tables.
5. The volume of the chloroform CDP-DAG fraction can be further reduced if desired using a continuous very slow stream of liquid nitrogen in a fume hood. This step permits concentration of the reaction products when the dried down lipids are subsequently resuspended in a smaller chloroform volume.
6. Primulin solutions at a concentration of 50 mg/ml dissolved in a solution of acetone:H_2O at ratio of 8:1 can be used to detect phospholipids and neutral lipids. The primulin solution is sprayed as a thin film on the surface of the TLC which is then dried. The position of the primulin-bound lipids can then be visualized under a UV light source [14].
7. TLC plates can also be imaged using phosphorimaging technologies such as the Typhoon 9400 phosphorimager (GE Healthcare) that is used in our laboratory. This method of detection has many advantages including greater sensitivity leading to shorter exposure times and also the elimination of the spot cutting and scintillation counting steps. The detection of radiolabel incorporation is also more accurate and sensitive than for X-ray film-based techniques.

Acknowledgements

MGW acknowledges financial support from the Royal Free Charity.

References

1. Tamura Y, Harada Y, Nishikawa S, Yamano K, Kamiya M, Shiota T, Kuroda T, Kuge O, Sesaki H, Imai K, Tomii K, Endo T (2013) Tam41 is a CDP-diacylglycerol synthase required for cardiolipin biosynthesis in mitochondria. Cell Metab 17:709–718
2. D'Souza K, Kim YJ, Balla T, Epand RM (2014) Distinct properties of the two isoforms of CDP-diacylglycerol synthase. Biochemistry 53(47):7358–7367
3. Heacock AM, Agranoff BW (1997) CDP-diacylglycerol synthase from mammalian tissues. Biochim Biophys Acta 1348:166–172
4. Pan W, Pham VN, Stratman AN, Castranova D, Kamei M, Kidd KR, Lo BD, Shaw KM, Torres-Vazquez J, Mikelis CM, Gutkind JS, Davis GE, Weinstein BM (2012) CDP-diacylglycerol synthetase-controlled phosphoinositide availability limits VEGFA signaling and vascular morphogenesis. Blood 120:489–498
5. Lykidis A, Jackson PD, Rock CO, Jackowski S (1997) The role of CDP-diacylglycerol synthetase and phosphatidylinositol synthase activity levels in the regulation of cellular phosphatidylinositol content. J Biol Chem 272:33402–33409
6. Weeks R, Dowhan W, Shen H, Balantac N, Meengs B, Nudelman E, Leung DW (1997) Isolation and expression of an isoform of human CDP-diacylglycerol synthase cDNA. DNA Cell Biol 16:281–289
7. Saito S, Goto K, Tonosaki A, Kondo H (1997) Gene cloning and characterization of CDP-diacylglycerol synthase from rat brain. J Biol Chem 272:9503–9509
8. Halford S, Dulai KS, Daw SC, Fitzgibbon J, Hunt DM (1998) Isolation and chromosomal localization of two human CDP-diacylglycerol synthase (CDS) genes. Genomics 54:140–144
9. Waugh MG, Minogue S, Clayton EL, Hsuan JJ (2011) CDP-diacylglycerol phospholipid synthesis in detergent-soluble, non-raft, membrane microdomains of the endoplasmic reticulum. J Lipid Res 52:2148–2158
10. Kinney AJ, Carman GM (1990) Enzymes of phosphoinositide synthesis in secretory vesicles destined for the plasma membrane in *Saccharomyces cerevisiae*. J Bacteriol 172:4115–4117
11. Wu L, Niemeyer B, Colley N, Socolich M, Zuker CS (1995) Regulation of PLC-mediated signalling in vivo by CDP-diacylglycerol synthase. Nature 373:216–222
12. Liu Y, Wang W, Shui G, Huang X (2014) CDP-diacylglycerol synthetase coordinates cell growth and fat storage through phosphatidylinositol metabolism and the insulin pathway. PLoS Genet 10:e1004172
13. Mok AY, McDougall GE, McMurray WC (1992) CDP-diacylglycerol synthesis in rat liver mitochondria. FEBS Lett 312:236–240
14. White T, Bursten S, Federighi D, Lewis RA, Nudelman E (1998) High-resolution separation and quantification of neutral lipid and phospholipid species in mammalian cells and sera by multi-one-dimensional thin-layer chromatography. Anal Biochem 258:109–117

INDEX

Mark G. Waugh (ed.), *Lipid Signaling Protocols*, Methods in Molecular Biology, vol. 1376,
DOI 10.1007/978-1-4939-3170-5, © Springer Science+Business Media New York 2016

K

L

M

O

P

R

S

T